Cu CONTAINING MIXED METAL OXIDES AND THEIR APPLICATIONS IN RED-OX AND ACID-BASE CATALYZED REACTIONS

A thesis submitted to the

UNIVERSITY OF PUNE

for the degree of

DOCTOR OF PHILOSOPHY

(in Chemistry)

BY

A. SATYANARAYANA REDDY

CATALYSIS DIVISION

NATIONAL CHEMICAL LABORATORY

PUNE- 411008

INDIA

APRIL2007

Dedicated to My Mother

CERTIFICATE

Certified that the work incorporated in the thesis**, "Cu Containing Mixed Metal Oxides and their Applications in Red-Ox and Acid-Base Catalyzed Reactions"** submitted by **Mr. A. Satyanarayana Reddy,** for the Degree of **Doctor of Philosophy,** was carried out by the candidate under my supervision in the Catalysis Division, National Chemical Laboratory, Pune - 411008, India. Materials obtained from other sources have been duly acknowledged in the thesis**.**

Dr. C.V.V. Satyanarayana

(Research Supervisor)

ACKNOWLEDGEMENTS…

It gives me great pleasure to express my heartfelt gratitude to my research supervisor, Dr. Satyanarayana Chilukuri, for his unending support and invaluable guidance throughout the period of this investigation. I sincerely thank him for the care and affection that I received from him in the entire period.

I take this opportunity to express my deepest sense of gratitude towards Dr. B. S Rao for his timely help, constant support and valuable guidance.

I also sincerely thank Dr. C. S. Gopinath for his help during my research in conducting the XPS and valuable suggestions and fruitful discussions. I express my gratitude to him.

I am very much grateful to Dr. Rajiv Kumar, Head, Catalysis and Inorganic Chemistry Division, NCL, who is very kind and generous and the help I received from him is gratefully acknowledged

I express my gratitude to Dr. S. Siva Sankar and Dr. A.V. Ramaswamy, former HOD's of the Catalysis Division for their support and help during the period of my research work.

I also thank Dr. S. P. Mirajkar and Ms. Violet Samuel for their cooperation and valuable support during the entire period. I have to acknowledge the friendly and cooperative attitude of all scientists and staff of our Division. I would like to thank Dr. A. P. Singh, Dr. S. B. Halligudi, Dr. D. Srinivas, Dr. Veda Ramaswamy, Dr. Manikandan, Dr. Dongare, S. Umbarkar, Ms. Agashe, Mrs. Nalini Jacob, Dr. Belhekar, Dr. Awate, Mr. S. C. Jha for their valuable help and cooperation given to me in completing my research work successfully. I am also grateful to Mr. A. B. Gaikwad (CMC, NCL) for his generous help in carrying out my research studies.

I also thank Mr. V. V. Bokade, Dr. P.A. Joy, Dr. Vijayamohanan, Dr. Murali Sastry, Dr. T. Raja, Dr. Selvaraj, Dr. R. A. Shaikh, Mr. Purushothaman, for their help on various occasions. I would like to acknowledge the help recieved from Mr. Madhu, Mr. Milind and Mr. Katti.

I sincerely thank my labmates, Sachin, Shivanand, Shiju, Thomas, Anjali, Anil, Ganesh, Pradeep, Sivaram, Upendra, Koteswarrao, Rituraj, Atul, Sebastian, Sharanappa,

Santosh Bhat, Roshan, Prasanth, Praful, for their friendly help and kind cooperation during the period of my work. I also thank all my friends in the division and in NCL for their help and support in one way or other, which made my work much easier. I specially thank all my telugu friends, many of them are abroad now, for their love, support and help. They made my life in NCL enjoyble and lively.

I would like to thank all my teachers at various teachers for the love and encouragement that I received from them. I would like to acknowledge specially my teachers at B.Sc level, who really created interest in Chemistry in me. I take this occasion to thank all my classmates till M.Sc course whose cooperative attitude helped me very much. Also I thank all well wishers and friends whose names are not mentioned here.

I specially thank my professors, in the Department of Chemistry, University of Pune, who really shaped my curiosity towards research. I take this opportunity to express my gratitude to Prof. S. B. Padye, Dr. V. D. Kelkar, Dr. S. Y. Rane, Dr. A. K. Nikumbh, Dr. A. S. Kumbhar and Prof. B. S. M. Rao. I also thank my M. Sc friends Ram Reddy, Raghuram, Pramod and Praveena, who really made my life memorable in pune.

I am sure that this work would not have completed successfully with out the support of my near and dear friends and well-wishers at various stages of my life. I thank Nagamalleswara Reddy, Srinivasa reddy, Koti Reddy, Surender Reddy, Ramchander and K.V.

I would like to thank Dr. S. Sivaram, Director, NCL and Dr. P. Ratnasamy (former Director, NCL) for allowing me to carryout the research work at NCL. I thank UGC, New Delhi, India, for the financial support in the form of junior and senior research fellowships.

Words are not enough to express my love and gratitude to my family members. It is their love, blessings and prayers that helped me throughout my life. I am very much indebted to them. I specially thank my wife, Satyavathi for her cooperation while writing this thesis.

Above all, I thank God for his blessings, for forgiving my mistakes, for leading me in the right path and for being there whenever I needed.

Satyanarayana Reddy

ABBREVIATIONS

BE	**Binding energy**
CT	**Charge transfer**
DRS	**Diffuse reflectance spectroscopy**
DTA	**Differential thermal analysis**
DTG	**Differential thermogravimetry**
FID	**Flame Ionization detector**
FTIR	**Fourier Transform Infrared**
FWHM	**Full width at half maximum**
GHSV	**Gas hourly space velocity**
I.D.	**Internal diameter**
ICP-AES	**Inductively coupled plasma atomic emission spectroscopy**
PXRD	**Powder X-ray diffraction**
SEM	**Scanning electron microscopy**
TCD	**Thermal conductivity detector**
TG	**Thermogravimetry**
TOS	**Time on stream**
TPD	**Temperature programmed desorption**
TPR	**Temperature programmed reduction**
WHSV	**Weight hourly space velocity**
XPS	**X-ray photoelectron spectroscopy**

CONTENTS

1 INTRODUCTION

SECTION-C: CHARACTERIZATION OF CATALYSTS: RESULTS AND DISCUSSION

CHAPTER 1

Introduction

1. INTRODUCTION

Catalysis is one of the most fascinating areas in applied science. Catalysis is applied to produce pharmaceuticals, petrochemicals, specialty chemicals and fine chemicals in economical way leading to fewer by-products. In addition to the production of fuels most efficiently, catalysis helps in the removal of pollutants that are released from various sources such as thermal power stations, automobiles and bulk chemical industries. Catalysis is involved everywhere, including many of the processes in our body. Berzelius coined the term catalyst in 1836 to refer a substance that increases the rate of a chemical reaction without being itself consumed [1]. Berzelius's definition highlights the fact that, at the beginning at least, the focus in catalysis was on enhancing reaction rates. The modern definition for catalyst is "a substance that increases the rate of a chemical reaction towards equilibrium while retaining its form at the end of process". In general, catalysts are categorized as heterogeneous, homogeneous and enzymatic. Catalysis, that takes place on surface i.e., heterogeneous catalysis is of great importance to chemical industry. Homogeneous catalysis, despite its drawbacks like poor thermal stability, separation problems and short catalyst life, still has advantages such as better selectivity, highest activity and reproducibility.

1.1. Heterogeneous catalysis

Faraday was one of the first scientists, who studied heterogeneous catalysis to examine the ability of platinum to facilitate oxidation reactions during early 19^{th} century. Later on, catalysts have been developed for reactions such as hydrogenation, dehydrogenation, alkylation, isomerization and polymerization. Advent of these processes revolutionized the chemical industry. Cracking of long chain hydrocarbons to smaller chain hydrocarbons is critical for fueling automobiles. The catalytic processing of crude oil to fuels and other petrochemical products continued to impact the society and lifestyles during the 1900's. In the 21st century, it is difficult to imagine the world that does not use the fruits of heterogeneous catalysis. The demand for better selective catalysts is only increasing as environmental and economic concerns necessitate the development of more

efficient catalyst materials. One issue of chemical reviews was devoted to addressing various issues involved in the practice of heterogeneous catalysis [2].

In heterogeneous catalysis, the reacting species are usually held on to the surface of a catalyst by a physical attraction called adsorption, where the reaction takes place. Adsorption may be relatively weak (physical adsorption) or may have strength comparable to the strengths of chemical bonds (chemisorption). In either case, adsorption is generally not uniform across a solid surface. Adsorption and therefore catalysis, occurs primarily at certain favorable locations called active sites. Among catalytic reactions, performing a reaction under heterogeneous catalytic conditions has several advantages such as elimination of inorganic salt formation, easy regenerability, non-toxicity, easy handling, safe storage and long catalyst life. Heterogeneous catalysts are also inexpensive, easily separable from reaction mixture by filtration or centrifugation and tolerate a wide range of temperatures and pressures. Above all, most of them can be easily and safely disposed off.

Despite all these benefits, heterogeneous catalysts are not popular among organic chemists, e.g. the average chemist in an organic chemical laboratory uses zeolites only as molecular sieves for drying solvents. This situation is slowly changing due to the commercial availability of a wide variety of catalysts and polymeric (functionalized) materials as supports for catalysts.

1.2. Classification of heterogeneous catalysts

Most of the catalysts used in large scale are porous inorganic solids. These catalysts may contain active species, promoters and supports. The resultant activity and selectivity would be a combined effect of the various components present in the active catalyst. Catalytic reaction takes place when one or more of the reactants chemisorbed on the surface and get reacted. The activity and selectivity of a catalyst depends strongly on the structure of the surface. Preparation of various types of catalysts has been more of an art than science. In the literature, many reports on catalyst preparation omit important details thus making it difficult to reproduce them. As a result, development of catalysis as a qualitative science got hindered. However, the art is slowly developing into science and there are now many examples of catalysts that are thoroughly described. Depending on the nature and form of an active component, the catalysts can be classified as follows.

1.2.1. Bulk metal catalysts

Metals are among the most important and widely used industrial catalysts as they catalyze wide variety of reactions [1]. Preparation and characterization of unsupported metals are reviewed [3]. Introduction of a second metal may improve the properties of the resultant catalytic system. Relatively, the high densities of skeletal catalysts provide excellent settling characteristics compared to supported catalysts when used in slurry phase reactors.

1.2.2. Supported metal catalysts

Multiphase catalysts are non-uniform solids at the molecular or crystalline level and usually consist of an active phase dispersed on a carrier support. Metals used in industrial catalysis are often expensive and hence they are predominantly used in a highly dispersed form on high surface area porous supports (e.g. metal oxides, zeolites, carbon or polymers). Naphtha reforming catalyst, which is rhenium-platinum supported on γ-Al_2O_3 is a classic example of this kind [4].

1.2.3. Metal oxides

Bulk oxide catalysts in pure or mixed form are either amorphous or polycrystalline materials. There are two characteristics of metal oxides that distinguish them from metals. The first one is the absence of metal bonds and the second characteristic is non-zerovalent metal. Three key concepts that describe oxides are (i) coordination environment of surface atoms (ii) redox properties of the oxides and (iii) oxidation state of metal at the surface. Metal oxides are widely used as catalysts as well as catalyst supports. Metal oxide surfaces are more complex in their structure and are highly heterogeneous. Metal oxide surfaces exhibit both basic and acidic characters, based on their composition, which is important for some reactions in catalysis. For example, silica-alumina catalyst is used for cracking of petroleum and bismuth molybdate for ammoxidation of propylene to give acrylonitrile. Rhenium oxide (Re_2O_7) supported on alumina is used for olefin metathesis.

Single and multicomponent transition metal oxides exist in many different crystallographic forms [5]. Metal oxides are generally belonging to one of the structural

classes of corundum, rock salt, wurzite, spinel, perovskite and rutile structures [6]. The corundum, the rutile and the spinel structures are made up of layers of close packed oxygen ions. When these oxide layers are stacked on top of the other in ABABAB sequence, the resulting structure is called hexagonal close packing (h.c.p) and it forms the basis for the corundum and the rutile structures. If the sequence of the layers is ABCABCABC then the resulting structure is called cubic close packing (c.c.p) and it forms the basis for the spinel structure.

The spinel structure is named after the mineral spinel ($MgAl_2O_4$) and the general composition is AB_2O_4. It is essentially cubic, with the O^{2-} ions forming an f.c.c. lattice. The cations occupy 1/8 of the tetrahedral sites and 1/2 of the octahedral sites and there are 32 O-ions in the unit cell. There are two types of cubic building units inside a big f.c.c. O-ion lattice, filling all 8 octants. The spinel structure is very flexible with respect to the cations it can incorporate. In a tetrahedral site the interstitial is in the center of tetrahedra formed by four lattice atoms. An octahedral position for an (interstitial) atom is the space in the interstices between 6 regular atoms that form octahedra.

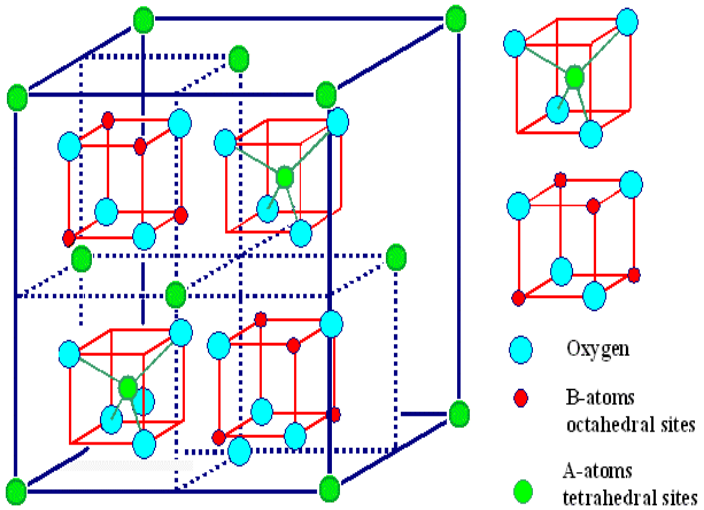

AB_2O_4 spinel structure

1.2.4. Zeolites

These are a class of minerals containing aluminum oxide and silicon oxide tetrahedral called aluminosilicates. These are formed, when Al^{3+} replaces some of the Si^{4+}

cations in silicates. For each Si^{4+} ion replaced by an Al^{3+}, the charge must be balanced by having other positive ions such as Na^{+}, K^{+}, and Ca^{2+} ions. Active sites in some of the important industrial catalytic reactions based on zeolites in the petrochemical industry reported [7]. The zeolites are unique for their molecular sieving characteristics, which are a consequence of their narrow uniform pores [8]. Catalytic processes have been developed to take advantage of these properties of zeolites. Among the chemical reactions that are catalyzed by zeolites, medium pore HZSM-5 has many applications.

1.2.5. Molecular catalysts on supports

Modified inorganic solids or polymer supports with catalytically active groups or molecules are used as industrial catalysts in some reactions. For example, ion exchange resin is used for methyl-t-butyl ether (MTBE) synthesis from methanol and isobutylene and synthesis of bisphenol-A from phenol and acetone [9]. Surfaces of inorganic solids can be functionalized with active catalyst groups just as organic polymers.

1.3. Transition metal oxides

Transition metal oxides are technologically important materials that have found many applications in chemical and electrochemical processes and also in electronic industry as conductors and superconductors. Among these applications, the use of transition metal oxides as catalysts is the most technologically advanced and commercially important. The activity of oxides is mainly due to partially coordinated surface atoms, redox nature and average oxidation state of metal on the surface. Surface coordination environment can be controlled by the choice of crystal plane exposed and by the preparation procedure for materials. Specification of redox properties is largely a matter of the choice of oxide. Some of the important chemical processes that make use of transition metal oxides as catalysts are selective oxidations, ammoxidations, dehydrogenation reactions etc. [10]. It is quite possible that transition metal oxides will occupy an important position as catalysts in chemical processes like amination, alkylation, aldol condensation and carbonylation. In addition to being used as catalysts, transition metals are also important as supports and promoters.

1.3.1. Surface chemistry of metal oxides

The surface composition of metal oxides is determined by the surface anion to cation ratio and oxidation states of surface cations as it depends on the stoichiometry of the oxide and the orientation of the exposed crystal planes. Non-stoichiometry often arises from preferential removal of surface oxide leading to reduction of the surface by pretreatment of the samples. For mixed metal oxides, in addition to surface anion to cation ratio, the ratio of the different cations is also of interest. In this case, the cation ratio at the surface and the bulk depends on the surface tension of the individual oxides and the bulk strain of the solid solution due to mismatch of the ionic sizes or coordination symmetry. Sometimes, the chemisorbed species may lower the surface energy of solid inducing surface aggregation of the component that binds more strongly with the adsorbate. Formation of surface compound that is different from the bulk is also possible in presence of adsorbate that has different oxidation states.

The formal oxidation state of transition metal for example can range from unity in Cu_2O to eight in OsO_4. Since, ionic nature at the surface affects the oxide properties including the surface electric field gradient, the surface electrostatic potential and the mode of surface relaxation, knowledge of its magnitude is important. The ionic character results in the presence of a strong electric field that point outward from the oxide surface. The separation of cations and anions results in a strongly modulated electronic potential on the oxide surface. These effects lead to the common phenomenon of heterolytic dissociative adsorption of molecules. The true ionic charges in many transition metal oxides are less than those predicted from formal oxidation state. The ionic character influences the striking probability and the orientation of polar molecule in a particular direction.

1.3.2. Coordinative unsaturation at surface

In most transition metal oxides, the oxygen anions in the bulk form close packed layers and the metal cations occupy holes among the anions. Since, in the bulk, the cations in the holes are densely packed by anions, these cations are saturated. Where as metal surfaces that are formed by cleavage of metal oxide bonds leave cations with fewer number

of nearest oxide neighbors than the corresponding ions in the bulk. In most instances, coordinative unsaturated sites are responsible for chemisorption and binding of molecules at the surface. Indeed this explains very well a variety of phenomena including poisoning of a surface, competitive adsorption and the common requirement of heating of an oxide to remove adsorbed water.

1.3.3. Acid-base properties of metal oxides

The exposed cations and anions on oxide surfaces have been described as acid-base pairs [11]. In metal oxide systems, oxide ions act as Brønsted or Lewis base sites and metal cations as Lewis acid sites. Hydroxyl groups bound at certain oxide surfaces may exhibit considerable Brønsted acidity. Strong Brønsted acidity usually arises in mixed oxides rather than pure oxides, due to charge imbalance and/or coordination changes caused by incorporation of a second cation type. Exposed coordinatively unsaturated cations may act as acceptors for free electron pairs of adsorbed species.

The strength of the acid sites on metal oxides depends on the charge and size of the cations, both of which may vary with the oxidation number of the cation. In general, according to the concept of hard and soft acids, cations of higher oxidation are harder. For cations in the same group and of the same oxidation state, those in later period are softer. Harder cations are smaller and polarizable. This will adsorb or bind hard bases stronger than soft or polarisable bases. Surface hydroxyl groups may act as Brønsted acid sites, which may dissociate to protonate-adsorbed bases. The resultant conjugate acid and bases are stabilized on the surface by electrostatic interaction with each other and with oxide. The compiled list of studies of organic molecules on a single crystal oxide includes examples on various crystal planes of MgO, ZnO, SnO_2, TiO_2, V_2O_5, NiO, MoO_3 and Cu_2O [12] and organic reactions on well-defined surfaces of metal oxides [13]. Kung and coworkers studied the surface coordination vacancy required for surface cations in acid-base reactions [14]. The low index planes of majority of oxides do in fact expose surface cations with at least one coordination vacancy along with surface anions. Thus one may expect such surfaces to be active for dissociative adsorption of Bronsted acids.

1.3.4. Red-ox properties of metal oxides

In catalytic oxidation, oxide catalysts have to undergo oxidation-reduction cycles. In selective oxidation reactions, gaseous oxygen reacts with substrate to form oxygenates or water. In oxidation reactions, the introduction of oxidant into reactant molecule takes place in two ways. (i) The electrons may be transferred to adsorbed oxygen to form the species like O^-, O_2^{2-} and O^{2-}, which on the incorporation of oxygen in to a product molecule and its subsequent desorption, return to the solid; (ii) Direct incorporation of lattice oxygen of the oxide in to product molecule, while, the site of adsorption of oxide and incorporated lattice oxide into the molecule may be different. The migration of oxide ion between these two sites would occur; which is referred to as Van Krevelan mechanism. This mechanism, that involves lattice oxide ions, leads to cause some changes in local structure on the surface of oxide. The cations in metal oxides that undergo redox cycle would change the local cation-anion ratio in the solid. The oxide catalysts must be able to accommodate these changes reversibly and easily. Some of the important factors that influence the redox cycle during the oxidation reactions are metal-oxygen bond strength, presence of cation vacancies, ability to form shear structures, optimal density of active oxygen, acid base properties, electron binding energy of lattice oxygen and the crystallographic plane [15]. This thesis is mainly aimed to prepare mixed metal oxide catalysts and exploit them for their acid-base and redox properties in chemical reactions.

1.4. Preparation of metal oxides

Different protocols are commonly employed for the preparation of metal oxides, which involve a sequence of complex processes that impart advantages and disadvantages for catalytic applications. The properties of good catalysts are determined based on the activity and selectivity to produce desired product, and their thermal and mechanical stability under reaction conditions. Excellent reviews on catalyst preparation are available [16,17] some of the most commonly used methods are described below.

1.4.1. Co-precipitation

In the preparation of multicomponent systems, the composition of precipitate significantly depends on the differences in the solubility's of the components of interest and the chemistry that occurred during the processes. Sequential precipitation of compounds occurs if a large difference in the solubility products of compounds is involved. Well-defined homogeneous chemical compounds would form if solubility products of resultant components were close enough. This route is preferred when better mixing of the catalysts are desired. The formation of precipitates results by physical (change of temperature or solvent or solvent evaporation) or chemical transformation (presence of base or acid or complexing agent) of homogeneous precursor solution. Formation of solid from solution results from two elementary processes i.e., nucleation and growth or agglomeration of particles

1.4.2. Sol-gel method

The sol-gel method is a homogeneous process, which results in a continuous transformation of solution into a hydrated solid precursor (hydrogel). Sol-gel methods have been recognized for their versatility, which allows control of the texture, composition, homogeneity and structural properties of the finished solids. The applications of catalysts prepared by the sol-gel method were reviewed [18]. The method is based on the hydrolysis and gelation (for instance by controlled addition of water) of alkoxides or other reactive compounds in alcoholic solution [19,20]. The chemistry of the processes, that occur during the formation of porous structure are controlled by changing of various parameters during preparation, such as pH, solvent and amount of water added for reaction.

Hydrolysis (hydroxylation) of the metal alkoxides

$$M\text{-}OR + H_2O \rightarrow M\text{-}OH + R\text{-}OH \quad (M = \text{metal or Si; } R = \text{alkyl})$$

Olation (condensation with formation of hydroxy bridges)

$$M\text{-}OH + M\text{-}OHX \rightarrow M\text{-}OH\text{-}M + X\text{-}OH \ (X = H \text{ or } R)$$

Oxolation (condensation with formation of oxygen bridges)

$$M\text{-}OH + M\text{-}OX \rightarrow M\text{-}O\text{-}M + X\text{-}OH \ (X = H \text{ or } R)$$

1.4.3. Ceramic method

In the high-temperature ceramic method, formation of mixed oxide phase results from heating intimate mixture of individual oxides at temperatures high enough to allow inter diffusion and solid state reactions [21]. This method has the advantage of the extreme simplicity. A major shortcoming of the ceramic method is the lack of homogeneity, because of very slow rates of the solid-state reaction between the precursor oxides. The high temperatures (1300 K or above) that is required to complete solid-state reactions between oxides generally lead to a drastic decrease in surface area of the resulting material by sintering. This severely confines the use of the ceramic method for the preparation of catalysts. To overcome this problem, precursor compounds, such as carbonates and oxalates that decompose at lower temperature have been used instead of the corresponding oxides.

1.4.4. Impregnation method

Preparation of impregnated catalysts usually involves filling of porous support with solution of active catalyst components followed by removing the solvent and activating the catalyst [22]. The impregnation solution may be simple aqueous solution of metal precursors.

Dry Impregnation: In this method, the amount of solution to be added is exactly calculated to fill the pores of the support completely. The solution may be sprayed onto the support and usually is absorbed quickly because of the capillary action. Hydro treating catalysts containing transition metals on alumina are examples of this method [23].

Pore volume filling or wet Impregnation: For the catalysts with extremely small pore structures, it may be difficult to fill the support completely with impregnating solution with dry method. In this case, the bare support is placed in a suitable vessel, the air is withdrawn and metal solution is added to cover the support while it is under vacuum. Air or some other gas is then admitted to the vessel, which forces the liquid in to the pores and the excess liquid is drained out and heated. Depending on the nature of the finished catalyst, the impregnated support may or may not be calcined further.

1.4.5. Deposition precipitation method

The addition of precipitating agent to a well dispersed suspension of the support in a solution of the active metal salt results in the precipitation of the active metal precursor onto the surface of the support provided there is a sufficiently strong interaction between the support and the precipitating compound. The precipitate must be kept as homogeneous as possible. One way of accomplishing is the slow addition of the precipitant into a well-stirred suspension of the support and the solution of the active component. Another way of obtaining a nearly homogeneous precipitate involves aqueous hydrolysis of urea to liberate the base required for precipitation. After isolation, the supported precipitate is washed, dried and usually calcined to produce a supported catalyst. Precipitation-deposition can be used to produce catalysts with a variety of supports such as silica, alumina, magnesia, titania, thoria, zinc oxide and chromia.

1.5. Acid-base catalysis on solid catalysts

Insoluble acid-base catalysts are preferable to homogeneous catalysts to facilitate product separation and easy catalyst recovery. Solid acid catalysts are being used in various processes of petroleum refining and are presently being studied intensively in both academic and applied fields for use in a variety of reactions. Solid base catalysts are also gaining increasing recognition as potential catalysts. Acidic, basic or acid-base bifunctional catalysts are promising not only with respect to acid and/or base-catalyzed reactions but some of these oxide materials have applications as adsorbents, sensors, ceramics, etc. A large number of industrial processes such as alkylation, isomerization, dehydration and condensation, amination, cracking, etherification, aromatization hydration, hydrocracking, MTG/MTO, oligomerization and polymerization exploit acid-base catalysts. A larger number of catalysts such as zeolites, oxides, complex oxides, ion-exchange resins and phosphates, clays are being employed for the above stated industrial processes. Tanabe et al. reported a detailed review on industrial processes based on acid-base catalysts [24].

1.5.1. Solid acid catalysts

Aluminum chloride is widely used as an efficient homogeneous acid catalyst for the liquid phase Friedel-Crafts alkylation and acylation using alkyl halides, acyl halides, carboxylic acids and anhydrides. Environmental concerns and regulations necessitate the development of new, efficient and selective solid catalysts. A review was devoted to the use of solid catalysts for Friedel-Crafts reactions to replace conventional problematic homogeneous catalysts, using Nafian–H, zeolites montmorillonite clay, SiO_2-Al_2O_3, sulfate doped metal oxides, and heteropolyacids [25]. Acidic ion exchange resins are often employed as catalysts but their use is limited due to their less thermal stability [26]. The aim in any catalytic conversion is to avoid or minimize waste production, which means 100% selectivity and zero percent by-products. Alkylation reactions are good examples for acid catalyzed reactions. A number of acid catalyzed alkylation reactions are being operated commercially that include production of ethyl benzene [27], cumene from propylene and benzene [28], linear alkyl benzenes [29], alkylated gasoline [30], methyl amines [31], t-butyl amine from isobutene with ammonia [32], cyclohexanol by hydration of cyclohexene [33] and thiocompounds by thiolation of alcohols etc. [32]

1.5.2. Solid base catalysts

Base catalyzed reactions have been studied to a lesser extent as compared to acid-catalyzed reactions in heterogeneous systems. In contrast to the extensive studies the heterogeneous acidic catalysts, fewer efforts have been made to study the heterogeneous basic catalysts. Pines et al. reported the first study of heterogeneous basic catalyst, sodium metal dispersed on alumina acted as an effective catalyst for double bond migration of alkenes [34]. Hattori et al. reviewed the types of heterogeneous basic catalysts [35]. Except for non-oxide catalysts, the basic sites are believed to be surface oxygen atoms. Oxygen atom existing on any materials may act as basic sites because any oxygen atom would be able to interact with a proton. The examples of heterogeneous base-catalyzed reactions include 1-Butene isomerization to 2-butenes over MgO [36], dehydrogenation of alcohols to aldehydes or ketones [37], olefin hydrogenation on ZnO and MgO [38,39], amination by addition of primary or secondary amine to conjugated dienes [40], Meervein-Ponndorf-

Verley reduction [41], alkylation [42] and aldol addition (or condensation) [43]. In addition, named reactions like Tischenko reaction for dimerization of aldehydes to form esters [44], Michael additions by KF supported on alumina [45], Wittig-Horner Reaction and Knoevenagel condensations [46] are well known base catalyzed heterogeneous reactions. Phenol methylation with methanol to produce 2,6-xylenol over MgO was developed by General Electric [47] and side chain alkylation of cumene with ethylene to form t-amyl benzene over a super base, K/KOH/γ-alumina [48]. Many base catalyzed heterogeneous reactions are reported in the literature [24].

1.5.3. Acid-Base bifunctional catalysts

A number of reactions have been investigated that are catalyzed by the simultaneous co-operation of both acidic and basic sites [49]. In this case, high catalytic activity and selectivity and long life is exhibited if the acid-base pair site is suitably oriented to the acidic and basic groups of a reactant molecule. Phenol methylation with methanol over MgO and hydrogenation of olefins on ZnO and MgO are typical examples for bifunctional catalysis. NaOH treated ZrO_2 for the production of vinylcyclohexane by dehydration of 1-cyclohexyl ethanol [50] and production of ethyleneimine [51] are the commercial processes of this category. For the industrial application of bifunctional catalysis many commercial processes have been developed [24].

1.6. Red-ox catalysis

Catalytic oxidation reactions are of prime importance at industrial level. The concept of oxidation involves oxygen or metal ion, which oxidizes the starting material in a two-electron transfer reaction followed by deoxidization of the reduced species. The catalytic properties in oxidation reactions involve redox mechanism between reactant molecules and surface active sites as suggested by Mars and van Krevelen in 1953 [52]. This mechanism necessitates the catalyst to contain a redox couple (transition metal ions) and should exhibit high electric conductivity to favor electron transfer as well as high lattice oxygen anion mobility with in the material to ensure the re-oxidation of the reduced catalyst.

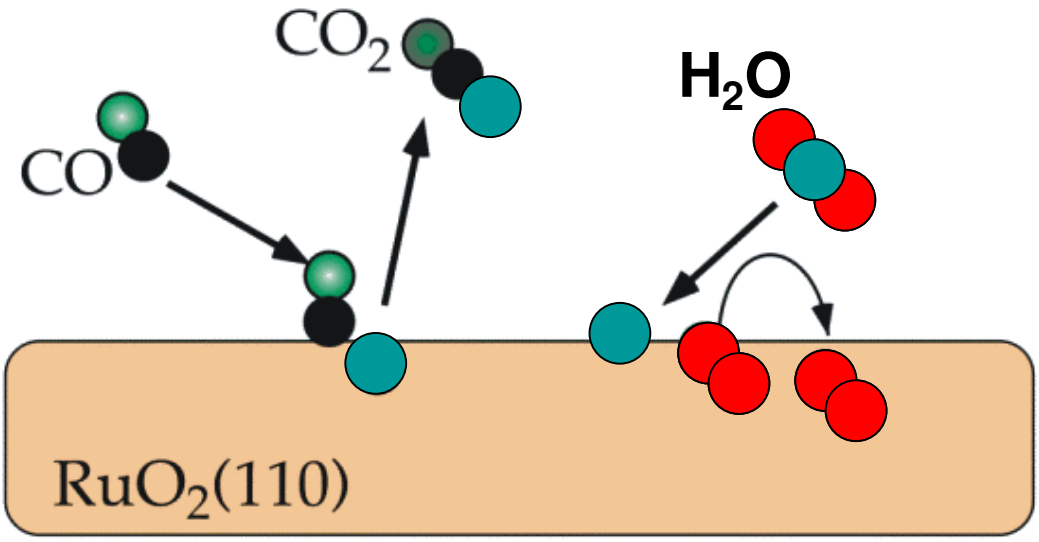

Scheme 1. Mars and van Krevelen Mechanism in oxidation reactions

According to Mars and van Krevelen the solid oxidizes the substrate directly and not by molecular oxygen of the gaseous phase. The oxygen that was introduced into the substrate originates from the lattice of metal oxide. The role of such oxygen is to regenerate or maintain the oxidized state of the catalyst. The mechanism involves the presence of two types of distinct sites: an active site, which oxidizes the substrate and another site active for oxygen reduction. An adequate structure of the material should also facilitate transfer of both electrons and oxygen species transfer. Depending on the nature, oxidation state of the metal ion and its environment (coordinative structure), metal oxygen bonds may be more or less polarized and therefore the oxygen ion may exhibit electrophilic or nucleophilic properties. The strength of the metal oxygen bond will also play a determining role in the selectivity of oxidation reactions. Reducibility of the cations is obviously important as well and should be related to the redox potential of the metal ion involved in the reaction. Many catalysts and reactions of this kind have been investigated and processes are being operated on industrial scale. For example, large-scale selective oxidation processes based on heterogeneous catalysts are ethylene epoxidation [53] and epoxidation of propylene on Ti silicalite [54]. Oxidation or oxidative dehydrogenation of alkanes and alkenes of important industrial processes involving the heterogeneous catalysts

are listed [55]. Selective oxidation of benzene to maleic anhydride, o-xylene to pthalic anhydride and butane to maleic anhydride were reported over vanadium-based catalysts [56,57]. Oxidative dehydrogenation of alcohols to aldehydes, ketones and carboxylic acids is another important class of reactions [56,58]. Ammoxidation of propylene to yield acrylonitrile is the most important commercial reaction that was invented by SOHIO (now BP-America) [59]. Many other processes based on redox catalysts were investigated and commercialized [60].

1.7. Acid-base and red-ox reactions on oxide catalysts

1.7.1. Phenol methylation

Alkyl phenols are important intermediates in the chemical industry for a variety of products. Application of phenolic compounds includes the drug intermediates for the manufacture of pharmaceuticals, dyes and antioxidants etc. The major markets are nonionic detergents, phenolic resins, polymer additives, and agrochemicals [61,62]. Alkyl phenols can be synthesized using a number of methods including alkylation of phenol catalyzed by different catalysts, hydroxylation of an alkylbenzene and dehydrogenation of an alkyl cyclohexanol or ring closure of an appropriately substituted acyclic compound. The choice of approach depends on the target alkylphenol, availability of raw materials and cost of manufacturing. The technique generally used to synthesize alkyl phenols is Friedel-Crafts alkylation. Alkyl phenols containing C_3 to C_{12} alkyl groups are generally synthesized by alkylating phenols through acid catalysis using sulphuric acid, phosphoric acid, BF_3 and aluminum chloride. Sufonated polystyrene ion exchange resins were found to be better as solid catalysts in this regard [63].

Monomethyl phenol (cresol) and dimethyl phenol (xylenol) are generally produced by the reaction of phenol with methanol using acidic as well as basic catalysts. In the absence of acid catalysts, ortho products are obtained predominantly. The commercial process to produce 2,6-xylenol is phenol methylation with methanol in a fixed bed flow reactor at 723-873 K over MgO catalyst [64]. Asashi chemical industry introduced an improved catalytic methylation of phenol process with a silica supported iron-vanadium catalyst employing fluidized bed reactor [65]. Its high activity allows the process to be

operated at low temperatures in the range of 573-623 K. In the presence of acid catalysts such as silica alumina, HZSM-5 and USY, *o*- and *p*- cresols are formed under kinetically controlled reaction conditions. Since, the thermodynamically favored *meta*-isomer of cresol is absent, the products formed in this case are attributed to electrophilic substitution of alkyl group at the *ortho* or *para* positions preferentially. Considerable numbers of reports appeared for methylation of phenol over MgO, Al_2O_3 and TiO_2 [66-68]. Metal oxides containing one of the components as Fe_2O_3 [69], V_2O_5 [70] and hydrotalcites [71] and various other oxide systems were also reported for phenol methylation [72-75].

A thorough literature survey reveals that phenol methylation over both modified and unmodified zeolites mostly result in a mixture of methylated products (both O- and C-methylation), of which anisole is the predominant product and these catalysts are less selective for 2,6-xylenol, the most sought after methylated phenol. The poor selectivity of ortho alkyl phenols, especially 2,6-xylenol is attributed to the pore constraints and fast deactivation due to coking. Hence, industrial chemists found metal oxide catalysts to be promising for high 2,6-xylenol selectivity by phenol methylation. Metal oxides either alone or in combination with other oxides are thus far superior for selective formation of 2,6-xylenol. Oxide catalysts studied for this reaction are MgO, Al_2O_3, TiO_2 and Fe_2O_3, which mostly contained components like Mn^{2+}, Cu^{2+}, Co^{2+}, Ni^{2+}, V^{5+}, Cr^{3+},Ti^{4+}, SiO_2, phosphates and Ce^{4+} etc, as second component. Oxides based on MgO and Al_2O_3 are two classic examples and have been widely employed for phenol methylation. These two oxides are different in their acid-base properties as MgO is basic and Al_2O_3 is acidic in nature. Their acid-base properties considerably influence the product distribution. Interestingly, incorporation of titania into MgO increased the basicity, initially of the resultant mixed oxide. However, maximum phenol conversion and ortho selectivity was obtained when the molar ratio is 1:1 of the oxides [68]. The activity on this system was attributed to the considerable amount of both acid and base sites. In case of Al_2O_3, the basicity monotonously increased with the presence of ZnO reaching a maximum basicity when Al_2O_3 to ZnO is 1:1, but 100% ortho selectivity was observed on Al_2O_3-ZnO (1:9) [67]. The activity was attributed to the presence of weakly acidic sites (active sites), which do not interact, with the pi-electrons of benzene ring of phenolate formed on the catalyst surface [76,77]. Considerable amount of anisole and p-cresol was also observed along with

ortho alkylated products on pure alumina against predominant ortho alkylation over MgO. This is due to the difference in nature of mode of interaction of phenol molecule on these surfaces due to the difference in their acid-base properties. Hence, it is anticipated that addition of any oxide component over MgO or Al_2O_3 modifies their acid-base properties and accordingly product selectivity. Phenol methylation reaction on MgO-CuO [78], MgO-MnO and MgO-Mn_2O_3 [79] was reported. In the US patent 4933 509 granted to G.E, it claims 92.7% conversion with 76.9% selectivity to 2,6-xylenol over MgO catalyst and through another US patent 4661638, it claims that the conversion could be improved to about 97.0% by promoting MgO with Mn oxide. This demonstrates that MgO is most favorable in the synthesis of 2,6-xylenol as compared to other catalysts that are used in the methylation of phenol.

Balsama et al. reported the formation anisole and cresols in alkylation of phenol with methanol over zeolites [74]. They also correlated the selectivity of o- and p-cresol with surface acidity of the material, indicating that the strongly acidic catalysts promoted ring alkylation. Similarly, vanadia-chromia catalysts with variation of vanadia content showed increase in acidity that in turn led to preferential C-alkylation of phenol with methanol. Another example for acid catalysts is V_2O_5/TiO_2; with the increase of vanadia content, selectivity to 2,6-xylenol is also enhanced [70]. This reaction on borate zirconia also produced selective C-methylation and the activity was attributed to weak and medium acid sites [80].

Recently, a systematic study of phenol methylation over ferrites has been carried out from this laboratory. The work on aromatic ring methylation of pyridine, N-alkylation of aniline with $(Zn/Ni)_{1-x}Co_xFe_2O_4$ [81] and phenol methylation on $CuFe_2O_4$ and $CoFe_2O_4$ [69,82] revealed the catalytic effectiveness of ferrospinels and the possibility of tuning the catalyst composition towards specific alkylation reaction. The main focus of this study was to understand the surface structural properties of oxide catalysts during the course of reaction and the role of various components present in the system in addition to the acid-base properties. Robust structural features of the ferrospinels enabled them to withstand harsh reducing atmosphere even under the reduction of Fe^{3+} to Fe^{2+} [83] and the original state can be regained by simple oxidation. This demonstrates that Fe^{3+} can be shunted between Td and Oh sites by varying the concentration of other cations. This leads to

changes in acid–base properties and cation distribution of the spinel lattice and hence both in catalytic activity and product selectivity. In Cu-Co-Fe spinel catalysts, copper species are active for methylation and cobalt catalyzes the hydrogenation of carbon species and decreases the coke deposition [83].

In spite of these studies, there is no clear picture of the influence of the acidic and basic properties of these oxide catalysts on the alkylation of phenol with methanol. However, most of the reports in the literature are in agreement with bi-functional mechanism of phenol methylation over metal oxides having comparable acid-base sites with required strengths to obtain high 2,6-xylenol selectivity. Though there is substantial work carried out on this subject, literature data is scattered and in many cases in the form of patents, moreover various reported conclusions are controversial and contradictory.

1.7.2. Water gas shift reaction

The water gas shift reaction (WGSR) plays a crucial role in many important processes such as methanol synthesis, methanol steam reforming for industrial H_2, ammonia synthesis and coal gasification, as well as in H_2 production for fuel cells. Water gas shift is an old and established technology that is finding new applications in fuel cell (FC) technology, biomass gasification and coal processing; which are receiving renewed interest due to an envisaged shift to hydrogen energy based economy.

Fuel cell based energy promises to be an efficient and clean alternative to fuel combustion for primary power generation, both for stationary and mobile applications. Fuel cells are much more efficient than internal combustion engine and produce virtually no CO, HC or NO_x and a reduced content of CO_2. They operate on the basic principle of direct conversion of chemical energy into electrical energy, avoiding the mechanical steps and thermodynamic limitations of traditional combustion energy generation cycles. Hydrogen gas is electrochemically oxidized to hydrogen ions at the anode which pass through a proton conductive membrane to the cathode where they combine with electrochemically reduced O_2 (from the air) producing H_2O. The electrons flow through the external circuit that provides power. The hydrogen may be provided to the fuel cell in pure form (compressed gas etc.) or it may be generated on site from hydrocarbons using a fuel processor.

Fuel processing is the most convenient method of supplying hydrogen in the absence of a suitable transportation and infrastructure for hydrogen. Fuel processors generate hydrogen from hydrocarbons (i.e. natural gas) by either steam reforming or autothermal reforming. This reforming step generates a gas which contains 8–12% CO besides hydrogen and CO_2. This CO must be converted with the help of steam to CO_2 and hydrogen via the water gas shift (WGS) reaction before a final clean up step can reduce the CO content to <50 ppm for use by a PEM fuel cell. Such low CO levels are needed at the fuel cell anode to efficiently carry out the electrochemical oxidation of hydrogen. WGS reaction is as follows,

$CO\,(g) + H_2O\,(g) \leftrightarrow CO_2\,(g) + H_2\,(g)$ $\Delta H = -41.2$ kJ/mol, $\Delta G = -28.6$ kJ/mol

Water gas shift is a reversible, exothermic reaction that is thermodynamically unfavorable at elevated temperatures. Since it is an exothermic reaction, higher CO removal is favored at lower temperature. On the other hand, from the viewpoint of kinetics, the reactant gases are not active enough to reach the chemical equilibrium at lower temperatures. Therefore, there exists an optimum temperature for WGSR; in general, the optimum temperature is between 473 and 553 K. In addition, CO_2 in the reformate gas mixture suppresses WGS according to Le Chatlier's principle.

Due to the moderate exothermicity, the reaction is industrially achieved in two steps namely, the high temperature shift (HTS) at 623-723 K and the low temperature shift (LTS) at 453-303 K, the Fe-Cr and Cu-Zn based catalysts are, respectively, used in most of the industrial ammonia plants [84]. Even though these catalysts have been optimized for many years, they are not suitable for use in stationary or automotive fuel processors. The lengthy and tedious reduction procedure associated with commercial Cu-Zn catalysts as well as the pyrophoricity of the active catalyst is not acceptable. Several catalysts have been investigated for WGS reaction, both base metals as well as precious metal catalysts on various supports. A number of recent studies have focused on precious metal catalysts [85,86], especially ceria-supported catalysts [87]. There are considerable number of reports on platinum, rhodium and gold catalysts [88]. The potential enhancement of catalytic activity by using rhenium as a promoter for ceria supported platinum catalysts were reported [89]. Gold has been regarded as a potentially useful system when it is highly dispersed on a suitable support for low temperature water gas shift reaction [90]. High

catalytic activity for WGS reaction was found for the first time using Au/Fe_2O_3 at low-temperature [91]. Gold supported on well crystalline titania and zirconia enables the preparation of highly active catalysts in the reaction [92]. It has been established that gold supported on titanium oxide manifests higher catalytic activity in the WGS reaction in comparison with other catalysts such as Au/Fe_2O_3, Au/Co_3O_4 [91,93], Au/ZnO and Au/Al_2O_3 [94]. Amorphous zirconia, titania and mixed oxides (Fe_2O_3–ZnO and Fe_2O_3–ZrO_2) have also been used as supports for gold catalysts in WGS reaction [93,94]. Transition metal exchanged zeolites were investigated as potential catalysts for this reaction [95]. Cobalt-molybdate has proved to be good water gas shift catalysts, and has been extensively studied in the literature [96].

The most promising catalyst and widely accepted for the low temperature WGS reaction is Cu supported on $ZnO\text{-}Al_2O_3$ based mixed oxide [97]. The copper based low temperature shift catalysts usually have zinc oxide as well as Cr_2O_3 to act as a structural stabilizer and promoter. The composition of a typical catalyst is as follows in the oxidized state, ZnO:0.24 Cr_2O_3:0.24 CuO, with 2 to 5% of Mn, Al and Mg oxides [98]. Supported copper catalysts were also proved to be potential alternatives to precious metal catalysts for this reaction [99]. It is well known that the catalytically active site for WGS reaction is metallic copper (Cu^o). Therefore, the formation of highly dispersed Cu particles would result in the enhancement of catalytic activity. However, Yureva et al. claimed that metallic copper was not the active ingredient of the catalyst and believed that the active sites were copper ions in the lattice of copper-chromite [100]. The copper–ceria catalysts were found to perform exceptionally well in WGS reaction [101]. They have claimed that copper–ceria catalysts are more stable than Cu-Zn catalysts and at least as active as the precious metal ceria catalysts. Both metallic copper and oxygen vacancies in ceria were proposed to involve in the generation of active sites for the WGS reaction [84,102]. A comparative study of Cu, Ag, Au, on ceria also has been reported [103]. Copper, as a promoter was also reported on Au-ZnO catalysts with variation of Cu to Zn ratio.

Three classes of WGSR catalysts, e.g. $Fe_2O_3\text{-}Cr_2O_3$, $CuO\text{-}ZnO\text{-}Al_2O_3$ and $Co\text{-}MoO_3\text{-}Al_2O_3$ have been commercialized world over after continuous research efforts during the past 80 years. The developments on water gas shift catalysts were reviewed [104].

1.8. Importance of copper in catalyzed reactions

Copper, one of the most widely used metals in the history of civilization while also has various industrial applications. It has been the most active transition metal oxide used extensively to catalyze variety of organic reactions. Copper-chromite catalysts have been used for years in various industrial processes such as the partial hydrogenation of vegetable oils and fatty acids as well as the decomposition or dehydration of alcohols [105]. The utilization of these catalysts in hydrogenation reactions for their capability to selectively hydrogenate carbonyl bonds while leaving unsaturated C=C bonds untouched is well known. The mechanistic studies on copper-chromite catalysts reveal that Cu^{1+} is the active species in various hydrogenation reactions [106]. The copper-zinc-aluminum oxide catalysts are used in many industrial processes, including the low-pressure methanol synthesis [107], CO low-temperature shift reaction [84], dehydration/dehydrogenation of alcohols [105] and for the production of hydrogen from oxidative steam reforming of methanol [108]. In addition, copper based catalysts are also employed in the decomposition of N_2O to N_2 and the selective catalytic reduction of nitrogen oxides by hydrocarbons [109].

Despite the superior activity of copper catalysts for several chemical reactions, its utility is often limited due to rapid deactivation and poor mechanical stability under reaction conditions. One of the probable reasons for deactivation of copper catalyst is its sintering as a result of low melting point. Thus, instead of bulk copper, the supported copper catalyst has become the focus of current research and searching for appropriate support is extremely important for distributing copper particles to avoid or at least, retard the occurrence of sintering. A catalyst support may also serve as an active species in some reacting systems, in addition to playing the role of an inert material for increasing the degree of metal dispersion, promoting thermal stability and modifying mechanical properties.

1.8.1. Copper-manganese oxides

Copper-manganese oxide catalysts are used as oxidation catalysts, their possible use as replacement for precious metals [110] is being probed. It is known that amorphous $CuMn_2O_4$, hopcalites are powerful oxidation catalysts, which can catalyze near room

temperature the oxidation of Co to CO_2 and at high temperature (473-773 K) the combustion of several organic compounds [111]. It has also been reported that in the reduced state, Cu-Mn mixed oxides are active catalysts for the methanol synthesis from $CO/CO_2/H_2$ mixture [112]. Copper manganese oxides have generally been observed to lose activity for CO oxidation at temperature above 773 K when crystallization of the spinel occurs [113]. However, crystalline Cu_1MnO_4 has been shown to be an active catalyst for CO oxidation at lower temperatures [114]. In addition, copper manganese oxides were also catalysts for the oxidation of ammonia and other gas species [115]. Recently, copper manganese oxides supported on activated carbon were reported as efficient catalysts for the oxidation of p-cresol [116]. A study of cobalt manganese oxide, copper manganese oxide and iron manganese oxide catalysts for the water-gas shift reaction has been reported [117]. Hausmannite, Mn_3O_4 exhibit a normal spinel in a cubic form containing Mn^{2+} in tetrahedral sites and Mn^{3+} in octahedral sites. A series of manganites of the general composition AMn_2O_4 with A = Cd, Mg, Co, Fe, Cu or Ni, were found to be spinel type. A spinel is described as a unit cell of 32 oxygens in 'A' sites with tetrahedral coordination, and 16 metal ions in 'B' sites with octahedral coordination with the oxygen. The structure and oxidation states of the components of copper manganite are difficult to determine. The ionization state of copper in copper-manganite is Cu^{1+}, which is different from that of the other isomorphous compounds such as $CuFe_2O_4$, $CuCrO_4$ where it is Cu^{2+}. In addition Mn is generally present as Mn^{3+} where as in $CuMn_2O_4$; it is likely to be Mn^{4+}. The structure of copper manganite found to be distorted from the ideal cubic symmetry. The distortion has been attributed to an ordering and formation of directed bonds by the cations, Cu^{2+} and Mn^{3+}. Orgel and Dunitz [118] have ascribed the distortion to the Jahn-Teller distortion. It has been suggested that electron transfer between two different valance states of both copper and manganese with in the spinel lattice be related to the extremely high oxidation activity. Zinc-manganites show a normal cation distribution and are tetragonally distorted. The distortion is caused by Jahn-Teller (JT) distortion of Mn^{3+}, located on the B-sites of the oxygen sublattice. Zn^{2+} with filled outermost electronic shell is not JT active and has a strong preference for the A sites. Cobalt-zinc-manganites and copper zinc-manganites showed a good activity and selectivity to N_2 and CO_2 for the reduction of NO by hydrocarbons in the absence of oxygen. The active species in zinc and copper-zinc-

manganites are Mn^{3+} as well as Cu^{2+} for the NO reduction. It is generally accepted that an enhancement of the Cu^{+} and Mn^{4+} concentrations is resulting in the deactivation of these catalyst materials.

1.9. Scope and objectives of the thesis

Phenol methylation and WGSR are industrially important reactions. A large number of catalysts have been reported for both phenol methylation and water gas shift reaction. Transition metal oxide catalysts are known to exhibit acid-base and redox properties. Hence, the prime aim of this thesis is to exploit these properties of copper and/or manganese containing catalysts. It is well known that phenol methylation is an acid-base catalyzed reaction and water gas shift, a redox reaction. A large number of patents and publications that deal with phenol methylation reaction show that there is still demand for new catalysts for concentration of 2,6-xylenol. Most of the catalytic systems studied for phenol methylation using methanol demonstrate poor selectivity towards 2,6-xylenol formation and rapid deactivation of the catalysts [111]. Ferrite catalysts have been reported to be promising catalysts for phenol methylation. However, the activity and 2,6-xylenol selectivity of the catalysts need to be improved further. Deactivation of these catalysts was attributed to the reduction of active species i.e Cu^{2+} in Cu-Co-Fe catalysts, which is mainly due to the reduction atmosphere during the reaction. It is therefore, necessary to develop a catalyst with long life along with superior activity for phenol methylation. MgO promoted with Mn^{2+} showed considerable improvement in the activity and 2,6-xylenol selectivity. Mn_3O_4 has been found to be highly selective towards 2,6-xylenol. Exceptional red-ox properties of manganese-based catalysts that are active in oxidation reactions are well acknowledged. It is expected that this property could unravel the deactivation of catalysts due to the prevailing reduction atmosphere during phenol methylation. In the continuing quest for new spinel catalysts, that offers better phenol methylation activity and stability. The objectives of this thesis are

- To develop Cu based catalysts that offer high phenol conversion and 2,6-xylenol selectivity,
- To investigate structural changes after the reaction and correlate the structural properties to catalytic activity and reasons for deactivation.

Owing to the renewed interest of water gas shift reaction in the production of H_2 for fuel cells, redox properties of copper based catalysts were also studied in the WGSR for this thesis. Since, commercial water gas shift catalysts are not suitable for fuel cell applications, as they require careful activation procedure and are also pyrophoric, it is necessary to develop cost effective highly active robust catalysts. Recently, copper manganese spinel like catalysts were reported to offer better activity compared to commercial Cu-Zn catalysts for WGS reaction. In this thesis, copper-manganite and copper-zinc-manganite with variation in their composition were comprehensively investigated for water gas shift reaction. The objectives set for in the development of better WGS catalysts are,

- To synthesize novel copper containing catalysts water gas shift reaction
- Correlation of redox properties of catalysts with their activity by various techniques.

The following objectives were kept in mind during the execution of this study.

- Preparation of Cu containing catalysts in combination with Mn, Zn-oxides with variable composition through co-precipitation.
- Characterization of the catalysts by various physico-chemical methods and techniques such as X-ray diffraction, SEM, BET surface area by N_2 sorption, FTIR, UV-visible spectroscopy, temperature programmed reduction, TG-DTA, SEM and XPS.
- Evaluation of the catalytic activity of the above described catalyst systems for phenol methylation and water gas shift activity and the study of the effect of variables like compositional variation, reaction temperature and space velocity etc.
- Investigation of the spent catalysts using different characterization techniques such as IR, UV-visible, XRD and XPS.
- Correlation of the catalytic activity with the acid-base and/or redox properties to arrive at the structure-activity relationship.

This thesis describes the preparation, characterization and catalytic activity of Cu-Mn, Cu-Zn-Mn spinel type catalysts. The chosen reactions for evaluation of catalysts are phenol methylation using methanol and water gas shift reaction using simulated reformate

gas mixture that are close in composition to reformats that are used in industry. The thesis has been divided into five chapters.

Chapter 1 gives a general introduction to heterogeneous catalysis with particular emphasis on transition metal oxide catalysts and their applications in acid-base and redox reactions. This chapter also presents an introduction to phenol methylation and water gas shift reaction. A review of the relevant literature to date in these areas is incorporated. At the end, the aim and objectives of the thesis is outlined.

Chapter 2 is divided into three sections. Section-A deals with various methods of preparation of catalytic materials. Section-B describes the theoretical background and experimental procedures of different characterization techniques employed in this study. The techniques such as powder XRD, N_2 sorption for BET surface area, UV-visible and IR spectroscopy, TPD, TPR, XPS, thermal analysis and SEM etc. are described. Section-C deals with the characterization results and discussion of freshly calcined Cu-Mn, Zn-Mn and Cu-Zn-Mn catalysts.

Chapter 3 presents the catalytic activity data of phenol methylation using methanol over Cu-Mn catalysts in vapor phase using down flow reactor. The influence of various parameters such as catalyst composition, reaction temperature, space velocity and reactant feed ratio on the activity and selectivity is reported. The structure-activity correlation based on the investigations of Cu-Mn series fresh and spent catalysts after phenol methylation is discussed.

This chapter also describes the evaluation of Zn-Mn and Cu-Zn-Mn catalysts for phenol methylation. The effect of various reaction parameters such as reaction temperature, space velocity and phenol to methanol mole ratio, on phenol conversion and 2,6-xylenol selectivity are reported and discussed. The correlation between the structure and activity of the catalysts based on the characterization of fresh and spent catalysts is also discussed in this chapter.

Chapter 4 deals with the WGS activity of Cu-Mn and Cu-Zn-Mn catalysts. Effect of various reaction parameters such as temperature, space velocity and influence of CO_2 in the feed stream were investigated. Structure activity relationship is discussed based on the characterization results obtained for fresh and spent catalysts using techniques like XRD, TPR and XPS etc. It also contains characterization results of Cu catalysts supported on

mixed oxides and their activity in WGS reaction. The supported Cu catalysts were characterized by XRD, Cu dispersion, BET surface area (by N_2 sorption), FTIR, UV-visible spectroscopy and TPR.

Chapter 5 summarizes the conclusions arrived at based on the above studies and also sums up the entire study. At the end of the thesis, suggestions were given for further research to be carried out in order to develop robust catalysts for phenol methylation and WGSR processes, so that they can be deployed immediately in industry.

1.10. References

[1] A.P. Kieboom, J. Moulijn, P.W.N.M. van Leeuwen, R.A. van Santen, in: R.A. van Santen et al. (Eds.), Catalysis: An Integrated Approach, Stud. Surf. Sci. Catal., second ed., Elsevier, Amsterdam, 1999, Chap.1.

[2] S.M. George, Chem. Rev. 95 (3) (1995) 475.

[3] S.C. Davis and K.J. Klabunde, Chem. Rev. 82 (1982) 153.

[4] C.L. Pieck, M.B. Gonzalez, J.M. Parera, Appl. Catal. A 205 (2001) 305.

[5] C.N.R. Rao, B. Raveau, Transition Metal Oxides: Structure, Properties and Synthesis of Ceramic Oxides, second edn., Wiley-VCH, New York, 1998, p. 373.

[6] Z.L. Wang, Z.C. Kang, Functional and Smart Materials: Structural Evolution and Structure Analysis, Springer, 1998.

[7] W.O. Haag, R.M. Lago, P.B. Weisz, Nature, 309 (1984) 589.

[8] R. Szostak, Molecular Sieves, second ed., Blackie Academic & Professional, London, 1998.

[9]. H. Widdecke, in: D.C. Sherrington, P. Hodge (Eds.), Synthesis and Separations Using Functional Polymers, John Wiley & Sons, 1988, p. 149.

[10] H.H. Kung, Transition Metal Oxides: Surface Chemistry and Catalysis, Elsevier, Amsterdam, 1989.

[11] R.L. Burwell Jr., G.L Haller, K.C. Taylor, J.F. Read, Adv. Synth. Catal. 29 (1969) 1.

[12] V.E. Henrich, P.A. Cox, The Surface Science of Metal Oxides, Cambridge University Press, Cambridge, 1994.

[13] M.A. Barteau, Chem. Rev. 96 (4) (1996) 1413.

[14] W.H. Cheng, S. Akhter, H.H. Kung, J. Catal. 82 (1983) 341.

[15] R.A. Sheldon, R.A. Van Santen, Catalytic Oxidation: Principles and Applications, World Scientific, 1995, 53.

[16] J.A. Schwarz, C. Contescu, A. Contescu, Chem. Rev. 95 (3) (1995) 477.

[17] G. Ertl, H. Knozinger, J. Weitkamp, Handbook of Heterogeneous Catalysis, Weinheim, VCH, vol. 1, 1997, p. 49.

[18] H.D. Gesser, P.C. Goswami, Chem. Rev. 89 (1989) 765.

[19] C.J. Brinker, G.W. Sherer, Sol-Gel Science, Academic Press, San Diego, 1990.

[20] L.L. Hench, J.K. West, Chem. Rev. 90 (1990) 33.

[21] U. Schubert, N. Hüsing, Synthesis of Inorganic Materials, second. ed., Wiley-VCH, 2005, p. 5.

[22] R.L. Augustine, Heterogeneous Catalysis for the Synthetic Chemist, Marcel Dekker, NewYork, (1996) p. 277.

[23] S.Y. Lee, R. Aris, Catal. Rev. Sci. Eng. 27 (1985) 207.

[24] K. Tanabe, W. F. Hoelderich, Appl. Catal. A 181 (1999) 399.

[25] G. Sartori, R. Maggi, Chem. Rev. 106 (2006) 1077.

[26] J.N. Armor, Appl. Catal. 78 (1991) 141.

[27] S. Bhatia, Zeolite Catalysis: Principles and Applications, CRC Press, Boca Raton, F1, 1990.

[28] A. Hernandez-Robinson, S. Ram, C.M. Smith, Proceedings of Worldwide Solid Acid Process Conference 1993, Houston, TX, 1993.

[29] J.L.G. de Almeida, M. Dufaux, Y.B. Taarit, C. Naccache, JAOCS 71, (7) (1994) 675.

[30] L.F. Albright, K.E. Kranz, K.R. Masters, Ind. Eng. Chem. Res. 32 (1993) 2991.

[31] M. Misono, N. Nojiri, Appl. Catal. 64 (1990) 1.

[32] A. Chauvel, B. Delmon, W.F. Holderich, Appl. Catal. A 115 (1994) 173.

[33] C. Forguy, T. Arretz, Stud. Surf. Sci. Catal. 41 (1988) 91

[34] H, Pines, J.A.Vesely, V.N. Ipatieff, J. Am. Chem. Soc. 77 (1955) 347

[35] H. Hattori, Chem. Rev. 95 (1995) 537.

[36] H. Hattori, Stud. Surf. Sci. Catal. 78 (1993) 35.

[37] A.J. Lundeen, R. Van Hoozer, J. Org. Chem. 32 (1967) 3386.

[38] R.J. Kokes, A.L. Dent, Adv. Catal. 22 (1972) 1.

[39] H. Hattori, Y. Tanaka, K. Tanabe, J. Am. Chem. Soc. 98 (1976) 4652.

[40] Y. Kakuno, H. Hattori, J. Catal. 85 (1984) 509.

[41] M. Shibagaki, K. Takahashi, H. Matsushita, Bull. Chem. Soc. Jpn. 61 (1988) 3283.

[42] T. Yashima, K. Sato, T. Hayasaka, N. Hara, J. Catal. 26 (1972) 303.

[43] G. Zhang, H. Hattori, K. Tanabe, Appl. Catal. 36 (1988) 189.

[44] K. Tanabe, K. Saito, J. Catal. 35 (1974) 247.

[45] J. Yamawaki, T. Kawate, T. Ando, T. Hanafusa, Bull. Chem. Soc. Jpn. 56 (1983) 1885.

[46] A. Corma, V. Fornes, R.H. Martin-Aranda, H. Garcia, J. Primo, Appl. Catal. 59 (1990) 237.

[47] K. Tanabe, T. Nishizaki, in: F.C. Tompkins (Eds.) Procedings of the Sixth International Congress on Catalysis, vol. 2, 1977, p. 863.

[48] K. Tanabe, H. Hattori, T. Yamaguchi, T. Tanaka, Kodansha, (Eds.), Acid-Base Catalysis, VCH, Weinheim, 1989.

[49] G. Suzukamo, M. Fukao, M. Minobe, Chem. Lett. (1987) 585.

[50] K. Takahsahi, T. Hibi, Y. Higashio, M. Araki, Shokubai Catalysis, 35 (1993) 12.

[51] M. Ueshima, Y. Shimazaki, K. Ariyoshi, H. Yano, H. Tsuneki, Proceedings of the Tenth International Congress on Catalysis, Budapest, 1992, p. 2447.

[52] J. Mars, D.W. van Krevelen, Chem. Eng. Sci. 3 (1953) 41

[53] R.A. van Santen, H.C.P.E. Kuipers, Adv. Catal. 35 (1987) 265.

[54] J.H.P. vander Pol, J.H.C. van Hoof, Appl. Catal. A 92 (1992) 93.

[55] G. Ertl, H. Knozinger, J. Weitcamp (Eds.), Hand Book of Heterogeneous Catalysis, VCH, Weinheim, vol. 5, 1997, p. 2254.

[56] P. Mars, D. W. van Krevelen, Chem. Eng. Sci. Special Suppl. 3 (1954) 41.

[57] C.T. Au, W.D. Zhang, H.L. Wan, Catal. Lett. 37 (3-4) (1996) 241.

[58] I. E.Wachs, R.J. Madix, J. Catal. 53 (1978) 208.

[59] J. L. Callahan, R. W. Foreman, F. Veatch, Process for the Oxidation of Olefins, U.S. Patent 2941007, 1960.

[60] R. Dowbenko, in: J.I. Kroschwit, M. Houl-Grant (Eds.), Kirk–Othmer Encyclopedia of Chemical Technology, vol. 2, fouth ed., 1999, p. 106.

[61] H. Fiege, in: W. Gerhartz (Eds), Ullman's Encyclopedia of Industrial Chemistry, vol. A8, fifth ed., VCH, Weinheim, 1987, p.25.

[62] W. Keim, in: Ullman's Encyclopedia of Industrial Chemistry, vol. A1, VCH, Weinheim, 1985, p. 48.

[63] S.B. Hamilton, US Patent 3446856, 1969.

[64] K. Takahashi, H. Murotani, Jpn. Patent H05–286880, 1994.

[65] H. Nikajima, F. Nomura, S. Iszwa, US patent 3855318, 1974.

[66] S. Sato, K. Koizumi, F. Nozaki, J. Catal.178 (1998) 264.

[67] K. Tanabe, K. Shimazu, H. Hattori, K. Shimazu, J. Catal. 57 (1979) 35.

[68] K. Tanabe, H. Hattori, T. Sumiyoshi, K. Tamaru and T. Kondo, J. Catal. 53 (1978) 1.

[69] T. Kotanigawa, Bull. Chem. Soc. Jpn. 47 (1974) 950.

[70] K.V.R. Chary, K. Ramesh, G. Vidyasagar, V. Venkata Rao, J. Mol. Catal. A: Chem 198 (2003) 195.

[71] S. Velu, C.S. Swamy, Appl. Catal. A 145(1996)141.

[72] T.M. Jyothi, S. Sugunan, K. Sreekumar, M.B. Talwar, B.S. Rao, Ind. J. Chem. Tech. 7 (2000) 155.

[73] T.G. Lin, L.W. Ho, A.N. Ko, Y.J. Perng, US Patent 4876398, 1989.

[74] S. Balsama, P. Beltrame, P.L. Beltrame, P. Carniti, L. Forni, G. Zuretti, Appl. Catal. 13 (1984) 161.

[75]. T. Kotanigawa, M. Yamamoto, K. Shimokawa, Y. Yoshida, Bull. Chem. Soc. Jpn. 44 (1971) 1961.

[76] N. Nozaki, I. Kimura, Bull. Chem. Soc. Jpn. 50 (1977) 614.

[77] H. Grabowska, W. Kaczmarczyk, J. Wrzyszez, Appl. Catal. 47 (1989) 351

[78] J.G. Bennett, G.R. Chambers, European Patent, 127833, 1984.

[79] T. G. Lin, L. W. Ho, A. N. Ko, Y. J. Perng, US Patent 4876398, 1989.

[80] K.M. Malshe, P.T. Patil, S.B. Umbarkar, M.K. Dongare, J. Mol. Catal A Chem. 212 (2004) 337.

[81] K. Sreekumar, T. Mathew, S. P. Mirajkar, S. Sugunan and B. S. Rao, Appl. Catal. A 201 (2000) L1.

[82] B. S. Rao, T. Mathew, N. R. Shiju and R. Vetrivel, Indian Patent filed.

[83] Thomas paper

[84] X. Wang, J.A. Rodriguez, J.C. Hanson, D. Gamarra, A. Martinez Arias, M. Fernandez Garcya, J. Phys. Chem. B 110 (2006) 428.

[85] T. Tabakova, F. Boccuzzi, M. Manzoli, J.W. Sobczak, V. Idakiev, D. Andreeva Appl. Catal. A 298 (2006) 127.

[86] C.L. Thomas, Catalytic Processes and Proven Catalysts, Academic Press, New York, 1970.

[87] W. Deng, M. Flytzani-Stephanopoulos, Angew. Chem. Int. Edn**.,** 45 (2006) 2285.

[88] R. Radhakrishnan, R.R. Willigan, Z. Dardas, T.H. Vanderspurt, AIChE 52 (5) (2006) 1888.

[89] R. Radhakrishnan, R.R. Willigan, Z. Dardas, T.H. Vanderspurt, Appl. Catal. B: Environ.l 66 (1-2) (2006) 23.

[90] W. Deng, J. De Jesus, H. Saltsburg, M. Flytzani-Stephanopoulos, Appl. Catal. A 291 (2005) 126.

[91] B.A.A. Silberova, G. Mul, M. Makkee, J.A. Moulijn, J. Cata. 243 (2006) 171

[92] V. Idakiev, T. Tabakova, A. Naydenov, Z-Y. Yuan, B-L. Su, Appl. Catal. B: Environ. 63 (3-4) (2006) 178.

[93] M. Haruta, S. Tsubota, T. Kobayashi, H. Kageyama, M. Genet and B. Delmon. J. Catal. 144 (1993) 175.

[94] H. Jinming, Z. Qi, Z. Yuanhui, W. Kemei, L. Xingyi, Catal. Lett. 102 (1-2) (2005) 99.

[95] T.R.O. De Souza, S.M. De Oliveira Brito, H.M.C. Andrade, Appl. Catal. A 178 (1999) 7.

[96] R. Hakkarainen, T. Salmit, L. Keiskir, Appl. Catal. A 99 (1993) 195.

[97] M.V. Twigg, Catalyst Handbook, second ed., Wolf Scientific Texts, London, 1989.

[98] Y. Cai, S.L. Davies, J.P. Wagner, US Patent 7064097, 2006.

[99] R.K. Pati, I.C. Lee, D. Chu, S. Hou, O. Akhuemankhan, S.H. Ehrman, ACS National Meeting Book of Abstracts 229 (1) (2005) FUEL-111.

[100] M.V. Twigg, M.S. Spencer, Appl. Catal. A 212, (2001) 161.

[101] Y. Li, Q. Fu, M. Flytzani-Stephanopoulos, Appl. Catal. B 27 (2000) 179.

[102] X. Qi, M. Flytzani-Stephanopoulos,Ind. Eng. Che. Res. 43 (2004) 3055.

[103] H.L. Lian, M.J. Jia, W.C. Pan, W.X. Zhang, D.Z. Jiang, Chem. Res. Chin. Univer. 22 (1) (2006) 99.

[104] Q. Liu, Q. Zhang, W. Ma, R. He, L. Kou, Z. Mou, Progr. Chemistry 17 (3) (2005) 389.

[105] R.M. Rioux, M.A. Vannice, J. Catal. 216 (2003) 362.

[106] R. Rao, A. Dandekar, R.T.K. Baker, M.A. Vannice, J. Catal. 171 (1997) 406.

[107] Q. Sun, Stud. Surf. Sci. Catal.147 (2004) 397.

[108] G. Busca, U. Costantino, F. Marmottini, T. Montanari, P. Patrono, F. Pinzari, G. Ramis, Appl. Catal. A 310 (1-2) (2006) 70.

[109] S.W. Hedges, H.W. Pennline, Int. J. Environ. Pollution 17 (1-2) (2002) 44.

[110] M.R. Morales, B.P. Barbero, L.E. Cadus, Appl. Catal. B: Environ. 67 (2006) 229.

[111] S. Veprek, D.L. Cocke, S. Kehl, H.R. Oswald, J. Catal. 100 (1986) 201.

[112] G.C. Chichen, K.C. Waugh, D.A. Whan, Appl. Catal. 25 (1986) 201.

[113] S.B. Kanungo, J. Catal. 58 (1979) 419.

[114] G.M. Schwab and S.B. Kanungo, Z. Phys. Chem. NF. 107 (1977) 109.

[115] A. Wollner, F. Lange, H. Schmelz and H. Knozinger, Appl. Catal. A 94 (1993) 181.

[116] F. Wang, Guan-yu Yang, W.Zhang, Wen-hai Wu, J.Xu, Chem. Comm. 10 (2003) 1172.

[117] Y. Tanaka, T. Takeguchi, R. Kikuchi, K. Eguchi, Appl. Catal. A 279 (2005) 59.

[118] L. E. Orgel, J. D. Dunitz, Nature 179 (1957) 462.

CHAPTER 2

PREPARATION AND CHARACTERIZATION OF THE CATALYSTS

SECTION A - PREPARATION AND EVALUATION OF THE CATALYSTS

2.1. Preparation of the catalysts

2.1.1. Introduction

Optimization of catalyst performance was given higher importance in the past, while less attention was paid to problems concerning catalyst preparation. It is known that catalysis research is facing two problems viz., (i) "Materials gap" that describes the discrepancy between a commercial catalyst material that is often too complex to be successfully characterized and model (single crystal) catalysts that are often not good at achieving good product rates (ii) "Pressure gap" that exists in real systems and model systems, as the surface investigations are commonly performed under UHV conditions, while commercial processes are carried out at ambient or high pressure. As a result, information on reaction mechanisms or the "real structure" under reaction conditions is very limited.

A major task in catalyst preparation is to produce highly defective metastable material. In this regard co-precipitation meets many requirements that ensure high reproducibility compared to other preparation methods. This can be achieved by monitoring each step during the precipitation process.

A preparation method should allow precise control of the phase composition of a mixed oxide catalyst, crystallite size, crystallanity and morphology of the active phase. Subsequent drying process as well as further activation procedures needs to be well understood. The low synthesis temperatures often lead to formation of oxides with amorphous or metastable phases. Hence, in this study, co-precipitation of metal cations at 353 K was employed for catalyst preparation. The Cu based metal oxide spinel catalysts were prepared and characterized by various physico-chemical methods such as X-ray powder diffraction, AAS, BET surface area, UV-visible, IR spectroscopy, TPD, TPR, TG-DTA, SEM and XPS etc. The theory and experimental procedures of various characterization techniques are briefly described in the following section. Characterization results of the catalysts, obtained by various techniques along with detailed discussion are presented in this chapter. This chapter is divided into three sections, i.e., section-A describes the preparation of catalysts, section-B describes theory behind various

characterization techniques used in this study along with the experimental procedure used and section-C deals with the results and discussion of characterization of mixed oxide spinel catalysts.

2.1.2. Copper-manganese oxides spinels

In this study, a series of copper-manganese mixed oxides, $Cu_xMn_{3-x}O_4$ (x = 0.25, 0.5, 0.75 and 1.0) were prepared from aqueous solutions of $Cu(CH_3COO)_2.H_2O$ (Loba Chemie Pvt. Ltd., India, GR) and $Mn(CH_3COO)_2.4H_2O$ (Merck, India) by co-precipitation using KOH (Merck, India) solution as alkali. Ratnasamy et al. has reported a similar preparation method [1]. In a typical synthesis, for obtaining 7 g of $Cu_xMn_{3-x}O_4$ (x = 0.25) mixed oxide, stoichiometric quantities of premixed (0.1 M) solutions of Mn and Cu acetates (20.40 g and 1.52 g) were prepared in double distilled water. This solution was precipitated using 0.25 M KOH. Both alkali and salt solutions were mixed simultaneously, by drop wise addition, under vigorous stirring at 353 K in a 2 L five necked round bottom flask. The cations were precipitated in the form of their hydroxides. The pH of the gel was monitored continuously and adjusted to 10.5, followed by its digestion at 353 K for 12 h. The precipitate thus obtained was separated by filtration, followed by washing with demineralized water until the pH of the filtrate was ~7.5. The absence of potassium ions was determined by atomic absorption spectroscopy (AAS, Varian Spectr SF-220). The precipitated cake was dried at 383 K for 12 h followed by calcination at 773 K in air. These samples are designated as CM_x, where 'x' denotes the fraction of copper used for the synthesis of $Cu_xMn_{3-x}O_4$.

2.1.3. Zinc-manganese and copper-zinc-manganese oxides spinels

Zinc-manganese oxide spinels ($Zn_xMn_{3-x}O_4$) with variation of zinc content (x = 0.25, 0.5, 0.75 and 1.0) were also prepared by co-precipitation as mentioned above using aqueous solutions of $Zn(CH_3COO)_2.2H_2O$ (s.d. fine-chem. ltd., India), $Mn(CH_3COO)_2.4H_2O$ (Merck, India) and aqueous KOH. These catalysts are designated here after as $ZM_{0.25}$, $ZM_{0.5}$, $ZM_{0.75}$ and $ZM_{1.0}$ where 'x' denotes the fraction of zinc (0.25, 0.5, 0.75 and 1.0) in the general spinel formula, $Zn_xMn_{3-x}O_4$. Copper-zinc-manganese oxide spinel

catalysts with variation of metal contents were similarly prepared by co-precipitation. Catalysts containing Cu: Zn: Mn in the atomic ratios of (i) 36:18:46 (ii) 35:35:30 (iii) 18:36:46 were designated as CZM1, CZM2 and CZM3, respectively. All the above-mentioned copper containing catalysts were tested for phenol methylation and water gas shift (WGS) reaction. While zinc-manganite spinel catalysts were tested for acid-base catalyzed phenol methylation reaction. All the catalysts used in this study were calcined at 773 K, unless stated otherwise.

2.2. Evaluation of catalytic activity

2.2.1 Phenol methylation: Copper-manganese oxide catalysts were evaluated in a vertical, down flow, fixed bed glass reactor positioned in a two zone split furnace (Geomechanique, France). A schematic diagram of the reaction setup is shown in Fig.2.0.

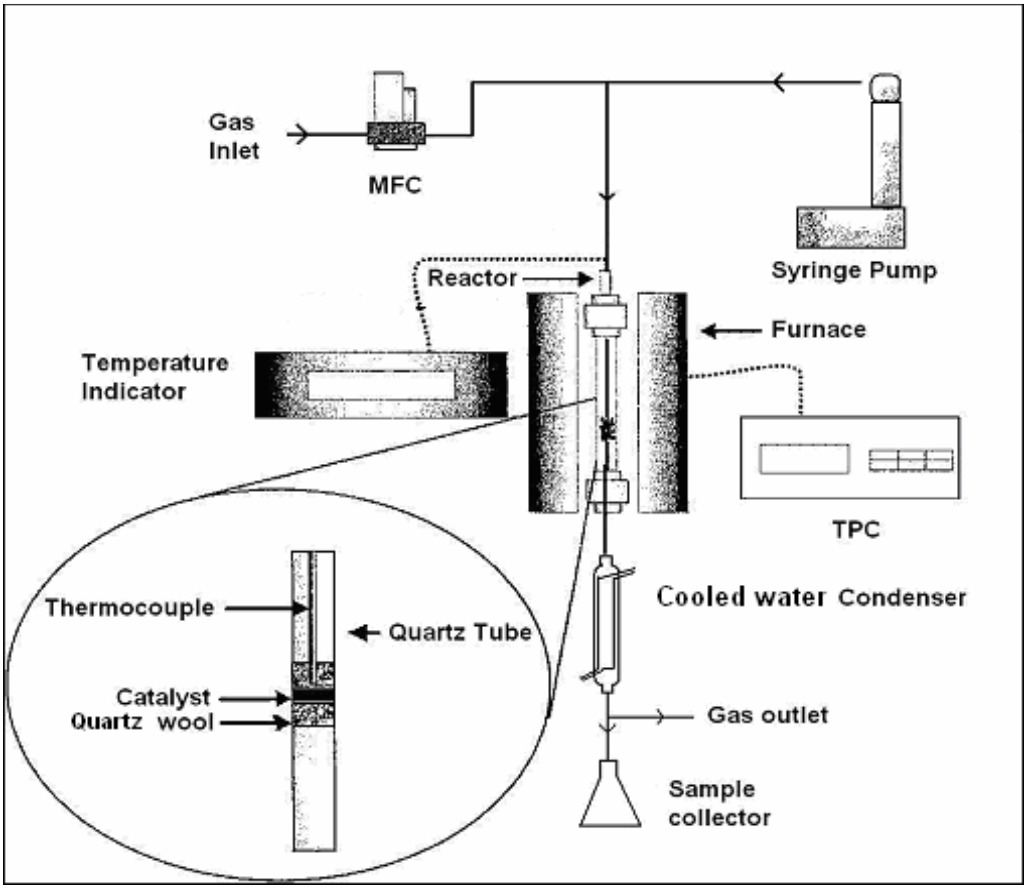

Fig.2.0. *Schematic of the reactor set-up used for the catalyst evaluation. (MFC: Mass Flow Controller, TPC: Temperature Programmer Controller)*

The phenol methylation reaction was carried out at atmospheric pressure in the 623 - 748 K temperature range, using 2 g of catalyst (particles 10-20 mesh). The temperature of the catalyst bed was continuously monitored with the help of a Cr-Al thermocouple. Prior to the reaction, catalyst was activated in dry airflow at 773 K followed by cooling it to the reaction temperature in nitrogen flow. The liquid reactant mixture containing phenol and methanol was fed to the reactor using a high precision (ISCO model 500D) syringe pump, at a constant flow rate dictated by WHSV. The reactant mixture was preheated and evaporated in the upper part of the reactor before the vapors reach the catalyst bed. The reaction was carried out under nitrogen flow (20 mL). The product mixture was cooled using chilled water condenser and collected in a gas-liquid separator.

Analysis of the liquid product mixture was carried out, at regular intervals, using a gas chromatograph (HP 6890N) equipped with BP-5 capillary column (50 m, 0.32 mm id, 1 μ film thickness) and FID. All the products were identified using pure authentic compounds (Aldrich). Whereas, the gaseous products were analyzed by online gas chromatograph (Chemito1000) equipped with TCD and spherocorb column (1/8", 8 feet). The response of FID for different components in the product mixture was determined by using a mixture containing authentic standard compounds. The performance of catalysts in phenol methylation reaction has been is defined as follows,

$$\text{Phenol conversion (mole \%)} = (C_{phenol\ in} - C_{phenol\ out} / C_{\text{phenol } in}) \times 100$$

$$\text{Product selectivity (mole \%)} = (C_{\text{desired product}} / C_{\text{alkyl phenols}}) \times 100$$

where 'C' denotes the concentration and the subscripts, "in" and "out", the respective concentrations in the feed and outlet product. Selectivity was mainly concerned with alkyl phenols such as *o*-cresol, 2,6-xylenol and mesitol.

2.2.2. Water gas shift reaction: All copper containing catalysts were tested for their catalytic activity in water gas shift reaction. A micro reactor unit (BTRS Jr., Autoclave Engineers, USA) was used for this purpose at atmospheric pressure. About 0.5 cc of catalyst was initially calcined in air at 673 K and subsequently reduced at 623 K in 10% H_2 in N_2 stream for 4 h prior to the WGS reaction. The activity was compared in the temperature range of 473 to 673 K at various space velocities (GHSV = 5000-50000 h^{-1}). Composition of the wet gas mixture used for this study contains 24% H_2, 6% CO, 9% CO_2,

21% N_2 and 40% H_2O), which is representative of reformate that is produced by ATR based reformer. The gas flows were accurately controlled by means of thermal mass flow controllers (Hi Tech, Bronkhorst, The Netherlands). The required amount of water was supplied using a high precision syringe pump (ISCO 500D) that was vaporized in a preheater and is mixed with the feed gas stream. The reaction was also carried out in the absence of CO_2 (30% H_2, 6% CO, and 24% N_2 and 40% H_2O) to study the effect of CO_2 on the activity. Composition of the gas mixture at the outlet of WGS reactor was analyzed by on-line gas chromatograph (Chemito 1000, India) equipped with TCD. A spherocorb packed column (8 feet, 1/8" dia) was used that gave baseline separation of H_2, N_2, CO and CO_2. Carbon monoxide conversion was determined as;

$$\text{CO conversion (\%)} = [(C_{CO\ in} - C_{CO\ out})/ C_{CO\ in}] \times 100$$

SECTION B- CATALYST CHARECTERIZATION TECHNIQUES: THEORY AND EXPERMENTAL PROCEDURES

2.3. Introduction

The science of heterogeneous catalysis is a subject, which is intimately intertwined with that of the fundamentals of surface science. Monitoring the atomic events occurring on catalyst surfaces therefore is crucial for a full understanding of the working mechanism of a given catalytic reaction. This monitoring includes identification and characterization of the active centers, observation of reaction intermediates, activation processes of reactants as well as mobility of species at the catalyst surfaces. This demands probing of surfaces at the atomic level, where non-conventional powerful spectroscopic tools can play a major role. Though substantial progress has been made in this direction, a deeper insight into the atomic structure of catalyst surfaces is far more complex and still offers demanding challenges for further investigation.

The characterization of solid catalyst is necessary to develope a new catalyst. However, the catalyst characterization requires specific techniques for the determination of each of the property. Some of the catalyst characterization techniques for solid catalysts are mentioned and discussed. The general techniques are ammonia temperature-programmed desorption, Infrared spectroscopy, ammonia IR-TPD, Laser Raman spectroscopy, Solid state nuclear magnetic resonance, Thermogravimetry, X-ray photoelectron spectroscopy (namely ESCA), Nitrogen adsorption, Temperature-programmed reduction, CO adsorption, Inductively-couples plasma (ICP) emission spectroscopy, X-ray diffraction, Scanning electron microscopy, X-ray absorption fine structure and test reactions.

Advent of advanced spectroscopic techniques provide opportunity to investigate the changes occurring on the surface of solid catalyst during the course of reaction, which gives in depth knowledge of chemical processes under more realistic conditions.

2.3.1. BET Surface area

The most common method of measuring surface area of catalytic materials is that based on the theory developed by Brunauer, Emmett and Teller (BET) in 1938 considering the multilayer adsorption. Surface area and porosity form important characteristics of a catalyst that influence its activity and utility of many catalysts. Hence, it is important to determine and optimize them accurately. Knowledge of porosity and surface area of a catalyst is also important for understanding the catalyst structure, its formation and potential applications it has as catalyst. The most commonly used technique for determining surface area is the so-called BET method, which has some limitations. Its assumptions are (i) adsorption energy remains constant from zero coverage to full coverage for the primary layer of the adsorbate and each of the layers above; (ii) there is no inter molecular interaction, though they attract and retain molecules striking them from the gas phase (iii) enthalpy of adsorption is the same for any layer other than the first (iv) a new layer can be initiated before the one under formation is completed. The Brunauer-Emmett-Teller (BET) equation [2] is:

$$p/V(p_0-p) = 1/cV_m + [(c-1)/cV_m]\ (p/p_0) \qquad (2.1)$$

where p is adsorption equilibrium pressure, p_0 is saturation vapor pressure of the adsorbate at the experimental temperature, V is volume of gas adsorbed at pressure p, V_m is volume of adsorbate required for monolayer coverage and c, a constant that is related to the heat of adsorption and liquefaction. A linear relationship between p/V (p_o/p) and p/p_o is required to obtain the quantity of nitrogen adsorbed. This linear portion of the curve is restricted to a limited portion of the isotherm, generally between 0.05-0.30. The monolayer volume, V_m is given by 1/(S+I), where S is the slope and is equal to $(c-1)/cVm$ and I is the intercept on Y-axis and is equal to $1/cVm$. The surface area of the catalyst (S_{BET}) is related to Vm, by the equation,

$$S_{BET} = (Vm/22414)\ N_a\ \sigma \qquad (2.2)$$

where N_a is Avogadro number and σ is mean cross sectional area covered by one adsorbate molecule. The σ value generally accepted for N_2 is 0.162 nm^2.

The BET surface areas (S_{BET}) of the samples reported in this study were measured by nitrogen adsorption method at 77 K using a NOVA-1200 (Quantachrome) unit. Prior to

N_2 adsorption, the samples were evacuated for 3 h at a residual pressure of 2×10^{-3} Torr at 573 K. The isotherms were analyzed following the usual convention in the relative pressure region, P/P_0 = 0.05 to 0.3.

2.3.2. Powder X-ray diffraction

Powder X-ray diffraction technique is commonly used for structural elicidation of solid materials and to e crystallite sizes. The most widespread use of this technique is in the identification of crystalline phases of solids [3]. The XRD method involves interaction of incident monochromatized X-rays with the atoms of a periodic lattice. Each crystalline material produces its own diffraction pattern. Both position (value of the scattering angle θ) and intensity of the lines are characteristic of a particular phase and the pattern thus provides fingerprint of the material. The spacing between two (hkl) planes'd' is related to the diffraction angle 2θ by the Bragg's law:

$$n\lambda = 2\,d\sin\theta;\ n = 1,2,3,\ldots. \qquad (2.3)$$

λ is the wavelength of X-ray beam (like Cu Kα or Mo Kα source), d is spacing between the planes and θ is the diffraction angle.

A rule of thumb is that a phase present in quantities lower than 5% by weight is usually not detected by XRD. Crystalline solids show a series of sharp peaks, where as amorphous materials (liquids, glasses etc.) produce broad peaks. Powder XRD can be used to determine the crystallinity by comparing the integrated intensity of the background pattern to that of the sharp peaks. From the diffraction line broadening, it is possible to determine average crystallite size by Debye-Scherrer equation [4],

$$D_{hkl} = k\lambda/\beta\cos\theta \qquad (2.4)$$

where k = 0.8-0.9 (constant usually 0.9), λ-wavelength of the incident radiation (λ_{Cu} = 1.54056 Å), β is full width at half maximum of peak (FWHM) in radians or β = half-width (degree) Π/180, θ is the diffraction angle.

Powder X-ray diffraction patterns of the catalysts reported in this thesis were obtained on a Rigaku Geigerflex diffractometer with a monochromatic CuK_α radiation (λ = 0.15406 nm, 40 kV, 30 mA). Samples were scanned in the 2θ range 10 to 80^o at a step size of 0.02.

2.3.3. DRS UV-visible spectroscopy

Diffuse reflectance spectroscopy is a suitable technique for studying heterogeneous catalysts [5], as both d-d and charge transfer transitions of metal ions can be probed. Diffusion reflectance spectroscopy is a technique based on the interaction of light in the ultraviolet (UV), visible (VIS) and near infrared (NIR) regions with the sample. In a DRS spectrum the ratio of the light scattered from infinitely thick layer and the scattered light from an ideal non-absorbing reference sample is measured as a function of the wavelength λ. The illumination of powdered samples by incident radiation leads to diffuse illumination. The incident radiation can undergo partial absorption and scattering. The basic equation for the description of diffuse reflectance is the radiation transfer equation [6].

$$-dI/k\rho\, dS = I - (j/k) \qquad (2.5)$$

Where *I* is the incident light intensity of a given wavelength, *dI/dS* is the change of the intensity with the path length *dS, ρ* is the density of the medium, *k* is an attenuation coefficient corresponding with the total radiation loss due to absorption and scattering, j is the scattering function. If the sample is infinitely thick, the diffuse reflection of the sample (Rα) is related to apparent absorption (K) and apparent scattering coefficient (S) *via* the Kubelka-Munk function [6].

$$F(R_\alpha) = (1 - R_\alpha)^2 / 2R_\alpha = K/S \qquad (2.6)$$

K and S are characteristic of the material under investigation. DRS are particularly a suitable technique for studying the transition metal ions because it measures both their d-d transitions and charge transfer bands. Excellent reviews are available to give a background of DRS technique [5-7]

For this study, the DRS UV-visible spectra were recorded on Shimadzu UV-2550 spectrophotometer in diffuse reflectance mode in the 200–800 nm range, at room temperature.

2.3.4. Infrared spectroscopy

Infrared spectroscopy is the most common form of vibrational spectroscopy and is based on the excitation of vibrations in molecules or in solid lattices by the absorption of photons, which occurs if there is a change in dipole moment during the vibration. The intensity of the infrared band is proportional to the change in dipole moment. A variety of IR techniques have been used to get information on the surface chemistry of different solids. With respect to the characterization of metal oxide catalysts two techniques predominate i.e., either transmission/absorption mode or the diffuse reflectance techniques [5,8-11]. In the first case, the sample typically consists of 10-100 mg of catalyst, pressed into a self-supporting disc of approximately 1 to 2 cm diameter and a few tenths of a millimeter thickness. Diffuse reflectance (DRIFT) measurements are generally carried out by depositing the sample on a sample holder, which avoids the tedious preparation of wafers. This technique is especially useful for strongly scattering or absorbing samples. The infrared absorption spectrum is described by Kubelka Munk function [6].

Fourier transform-infrared spectra of the catalysts reported in this study were recorded (on Shimadzu 8300 FTIR) at ambient conditions. The spectra were recorded using circular discs obtained by pressing a mixture of catalyst sample with KBr.

2.3.5. Thermal analysis

Thermal analysis is nothing but measurement of changes in physical or chemical properties of materials as a function of temperature, usually heating or cooling at a uniform rate. (i) Thermogravimetric analysis measures weight loss or gain during programmed heating of sample (ii) Differential thermal analysis measures temperature difference (ΔT) between a sample and reference material during heating (iii) Differential scanning calorimetry (DSC), measures the differential heat flow between a sample and reference material during heating.

Thermogravimetric analysis is a technique that permits the continuous monitoring of weight of a sample as a function of temperature when it is heated at a desired heating rate [12,13]. The major applications of this technique include materials characterization through their characteristic decomposition patterns, study of degradation mechanisms and

kinetics, prediction of lifetime (stability) at desirable time and temperature for a particular environment e.g., screening of additives (stabilizers, flame retardants and plasticizers, etc.).

DTA can be used to detect the physical or chemical changes in a material that accompany by absorption or desorption of heat [12,13]. DSC provides similar information but, unlike DTA, can quantify the thermal events. Many of the physical or chemical changes are associated with heat absorption (endothermic) or release of heat (exothermic). DTA measures the differential temperature between an inert reference and the sample upon heating or cooling at a particular rate or under isothermal conditions. Applications of DTA and DSC include evaluation of phase transformations (glass transition, melting, solidification, etc.), decomposition, thermal and mechanical histories.

In the present work, thermogravimetry and differential thermal analysis measurements of the as synthesised samples were performed using a Perkin Elmer instrument, model Diamond TG/DTA analyzer equipped using a control and data acquisiton system. All the analyses were carried out in air (80 mL/min) at a heating rate of 10 K/min using about 10 mg sample. The reference material was α-alumina powder.

2.3.6. Temperature programmed desorption

Temperature programmed desorption of simple bases on solid oxides is a popular method to estimate their acidity [14-16]. TPD analysis determines the number, type and strength of active sites available on the surface of a catalyst carried out by measuring of the amount of gas desorbed at various temperatures. Falconer and Schwarz have reviewed the applications of temperature programmed desorption [17]. Programmed desorption is carried out by raising the temperature linearly with time in presence of a steady stream of inert carrier gas. When the heat overcomes the activation energy, the bond between the adsorbate and adsorbent breaks and the adsorbed species is desorbed. If active species of different strengths are present, desorption of adsorbate species takes place at different temperatures. The concentration of desorbed species at different temperatures yields the number and strength of active sites. Surface spectroscopic studies are typically conducted in conjunction with thermo-chemical techniques to provide information about the nature of adsorbed species. The common probe molecules for determination of acidity are ammonia,

pyridine, methylamine, dimethyl amine, trimethyl amine, n-butyl amine etc. The size of a probe molecule may affect accessibility to the reactive sites and influence the rate of diffusion in TPD experiments. Acidic probe molecules such as carbon dioxide and sulfur dioxide are ideal gases that are commonly used to study basicity of solid acids.

TPD results of carbon dioxide and ammonia reported in this study were obtained using a Micromeritics AutoChem 2910 unit. The samples (200-300 mg) were pre-treated in helium at 773 K before the adsorption of probe gas (10% CO_2 or 10% NH_3 in helium). During desorption experiment, the samples were heated in helium flow (40 mL/min) at a temperature ramp of 10 K/min. The concentration of CO_2 or NH_3 desorbed from the samples was estimated from the area under the peak after taking the thermal conductivity detector response into consideration.

2.3.7. Temperature programmed reduction

In temperature-programmed reduction, a reducible catalyst is exposed to a flow of a reducing gas mixture (few volume percent hydrogen in Argon) while the sample temperature is linearly increased. It is possible to determine the total amount of hydrogen consumed and the average oxidation state of the solid after reduction. It also helps in determining reduction temperature that might help in deciding the operating temperature for a given catalytic reaction. An important aspect of TPR technique is that the sample does not require any special characteristics other than containing reducible metals. Several review articles have been devoted in the past to describe the significance of TPR technique in catalyst characterization [18,19].

TPR results reported in this thesis were obtained using Micromeritics AutoChem 2910 unit. Prior to programmed reduction, the samples were pretreated in high purity (99.98%) argon (20 mL/min) at 773 K for 3 h. After cooling to ambient, argon was replaced with 5% H_2 in argon mixture and the catalyst was heated to 1073 K at a heating rate of 10 K/min. The flow rate of H_2-Ar mixture used for this study was 40 mL/min. The water produced during the reduction step was condensed and collected in a cold trap immersed in slurry of isopropanol-liquid nitrogen mixture.

2.3.8. Copper metal dispersion

The mild oxidizing property of N_2O is generally exploited for the determination of surface area of copper metal that is dispersed or exposed to the surface in a copper based mixed oxide. Adsorptive decomposition of N_2O is generally used to determine the extent of the reaction of N_2O with surface copper [20,21]. The analysis is based on reactive chemisorption of nitrous oxide on reduced metallic copper surfaces. The amount of decomposed gas can be quantified by measuring nitrogen as the reaction product or by performing a subsequent TPR measurement. To avoid bulk oxidation of copper, a proper choice of reaction temperature and contact time is crucial. It is generally acknowledged that oxidation of subsurface layers can be anticipated above 363 K. For the determination of copper surface area; dissociation of nitrous oxide on metallic copper was considered as follows,

$$N_2O\ (g) + 2\ Cu_s \rightarrow N_2\ (g) + (Cu\text{-}O\text{-}Cu)_s \qquad (2.7)$$

Dispersion, metal surface area and crystallite sizes of copper catalysts used in this study were determined by temperature programmed reduction of oxidized surfaces (s-TPR). Thus copper surface area, percent dispersion and Cu crystallite size were calculated by hydrogen consumed determined by *s*-TPR. The catalysts were pretreated in a helium flow (40 mL/min) and heated at 673 K for 30 min. Subsequently; the catalysts were reduced in a flow of 5% H_2-Ar mixture, while raising the temperature at a heating rate of 10 K/min to 673 K. The reduced sample was cooled to room temperature and temperature programmed oxidation was carried out using 5%N_2O in helium (30 mL/min) at 343 K. Reduction of the subsurface oxide was performed through TPR, raising the temperature up to 673 K.

Dispersion of copper is defined as the ratio of Cu exposed at the surface determined by N_2O decomposition to the total Cu present (determined by ICP) in the system. Cu metal surface area and average particle size were calculated as reported by Gervasini et al [22].

2.3.9. Surface analysis by XPS

XPS is one of the most frequently used techniques in catalysis. It yields information on the elemental composition, the oxidation state of elements and in favorable

cases the dispersion of one phase over another. XPS is based on the photoelectric effect, in this technique, sample surface is irradiated with X rays and the emitted photoelectrons are measured. When an atom absorbs a photon of energy hν, a core or valence electron with binding energy E_b is ejected with kinetic energy E_k:

$$E_k = h\nu - E_b - \varphi \quad (2.8)$$

where h is Planck's constant, ν is the frequency of the exciting radiation, E_b is the binding energy of the photoelectron relative to the Fermi level of the sample and φ is the work function of the spectrometer. XPS (also referred by the acronym ESCA, electron spectroscopy for chemical analysis) entails emission from both core and valence electrons of the solid, the stimulating X-ray sources being usually Al Kα (1486.6 eV) or Mg Kα (1253.6 eV). The XPS spectrum is usually a plot of the intensity of photoelectrons versus binding energy.

Since the electrons whose energies are analyzed in XPS arise from a depth of no greater than about 5 nm, the technique is highly surface specific. A set of binding energies is characteristic for an element and hence XPS can be used to analyze the composition of samples, considering the area of the peak and cross section for photoemission. Binding energies are not only element specific but contain chemical information like oxidation state, because the energy levels of core electrons depend slightly on the chemical state of the atom. Chemical shifts are typically in the range of 0-3 eV [23].

An experimental problem in XPS is that electrically insulating samples may charge during measurement, as photoelectrons leave the sample. Due to the positive charge on the sample, all XPS peaks in the spectrum shift by the same amount to higher binding energies. Calibration for this effect is generally done by using C 1s binding energy (284.9 eV) from carbon contamination, which presents on most of the catalysts [24-28].

Auger Electron Spectroscopy: It is an electron spectroscopic method that uses a beam of electrons to knock electrons out of inner-shell orbitals. Auger electrons are ejected to conserve energy when electrons in higher shells fill the vacancy created by photoemission in the inner shell. These Auger electrons have energies characteristic of the emitting atom due to the characteristic energy-level structure of that element.

In the present study, X-ray Photoelectron spectra were acquired on a VG Microtech Multilab ESCA 3000 spectrometer using a non-monochromatized Mg Kα X-ray source (hν

= 1253.6 eV) on '*in situ*' scraped fresh catalyst pellets at room temperature. Selected spectra were recorded with Al Kα X-ray (hν = 1486.6 eV) also to eliminate the overlap between different Auger and core levels. Base pressure in the analysis chamber was maintained at 3-6 x 10-10 Torr range. The energy resolution of the spectrometer was determined from the full width at half maximum of metallic gold and the value obtained is better than 0.8 eV for Mg Kα radiation and 1.1 eV for Al Kα radiation respectively, at a pass energy of 20 eV.

2.3.10. Scanning electron microscopy

The primary use of SEM is to study the surface topography and morphology of solids. Any solid material may be studied by this technique. Electrically conductive materials can be examined directly, while nonconductive materials may require a thin conductive coating of gold or carbon to prevent electrical charging of the specimen. Broad coverage on electron microscopic methods that can provide information about heterogeneous catalysts was reviewed [29-31]. Electromagnetic lenses focus electron beam passing through an evacuated column onto the specimen surface. The beam is then raster over the specimen in synchrony with the beam of a cathode ray display screen. The secondary electrons emitted from the sample are then used to modulate the brightness of the cathode ray display screen, thereby forming the image.

The external surface morphology of catalysts in this study by SEM images was obtained on a Leica Stereoscan-440 scanning electron microscope equipped with a Phoenix EDX attachment. Prior to the analysis, all samples were coated with gold.

SECTION C - CHARACTERIZATION OF CATALYSTS: RESULTS AND DISCUSSION

2.4. Copper-manganese oxides spinels

Copper-manganese based spinel type catalysts were characterized by various physico-chemical techniques such as BET surface area, XRD, UV-Visible, FTIR, TG-DTA, TPD, TPR, SEM and XPS. All these techniques have been described in the above section. In addition, copper metal dispersion was determined by reduction-oxidation cycle using N_2O as oxidant.

2.4.1. Catalyst composition and structural characterization

Table 2.1 summarizes the metal content (wt%), crystallite sizes, crystalline phases and BET surface area of various copper-manganese oxide spinel catalysts.

Table 2.1. Chemical *composition, crystallite sizes, crystalline phases and surface areas of various Cu-Mn based spinel ($Cu_xMn_{3-x}O_4$) catalysts after calcination at 773 K.*

Catalyst	Metal concentration (wt%)[a] Mn	Cu	Crystallite size (nm)	Crystalline phases	SBET (m^2/g)
CM_0	66.40 (72.05)[b]	-	20.92 (20.83)[c]	Mn_3O_4,Mn_5O_8	21(20)[c]
$CM_{0.25}$	55.85 (64.43)	6.00 (6.87)[b]	14.04 (15.23)	Mn_3O_4,Mn_5O_8 Mn_2O_3	17(16)
$CM_{0.5}$	57.03 (58.94)	12.26 (13.61)	18.59 (25.73)	Mn_3O_4,Mn_5O_8, Mn_2O_3	36(25)
$CM_{0.75}$	52.98 (52.57)	18.78 (20.24)	16.74 (22.24)	$Cu_{1.5}Mn_{1.5}O_4$, Mn_5O_8,	44(28)
$CM_{1.0}$	43.75 (46.30)	23.00 (26.74)	15.97 (38.25)	$Cu_{1.5}Mn_{1.5}O_4$, Mn_5O_8,	33(22)

[a]Chemical analysis values obtained by AAS analysis, [b]expected metal content in parenthesis, [c]for spent catalysts after phenol methylation.

The metal contents in these samples were analyzed by bulk chemical method (AAS) and are in good agreement with the input metal content values (given in parenthesis) used for their preparation. Surface area values of the catalysts were reasonably high, but did not follow any particular trend, catalysts with higher content of copper in

general had relatively high surface areas. Surface areas of CM_0 and $CM_{0.25}$ are relatively lower compared to other catalysts but they remained same even after phenol methylation reaction. While in other case there was reduction in the surface area values after phenol methylation.

Crystallite sizes of the fresh and spent catalysts calculated using Debye-Sherrer equation are summarized in Table 2.1. The crystallite sizes are in the range of 14-20 nm for fresh samples. Addition of copper in to hausmannite (Mn_3O_4) structure showed considerable influence on surface area, crystalline phase and crystallite size. The influence of Cu content is more evident at higher concentrations. Gradual transformation of tetragonal hausmannite into cubic $Cu_{1.5}Mn_{1.5}O_4$ phase was observed with increase of copper content.

2.4.2. Powder X-ray diffraction

X-ray diffraction patterns of fresh Cu-Mn spinel catalysts are presented in Fig.2.1. Pure manganese oxide (CM_0) showed characteristic diffraction peaks of hausmannite phase (Mn_3O_4, JCPDS file no.24-734), a normal spinel system, after calcination in air at 773 K. The characteristic peaks of hausmannite remain unchanged even after the addition of copper up to $x \leq 0.5$ in $Cu_xMn_{3-x}O_4$, indicating that incorporation of copper did not alter the tetragonal structure. Diffraction peaks due to copper oxide were not found in these samples including higher copper containing (26 wt%, $CM_{1.0}$) sample. However, a minor manganese oxide phase, Mn_5O_8 (JCPDS file no.39-1218) was detected in all catalysts. The diffraction lines at (2θ) 21.6, 47.8 and 66.2 were assigned to Mn_5O_8. In addition to this, small content of Mn_2O_3 (JCPDS file no.10-0069) corresponding to diffraction peak at 33.01^o was detected for low copper containing catalysts (x = 0.25 and 0.5).

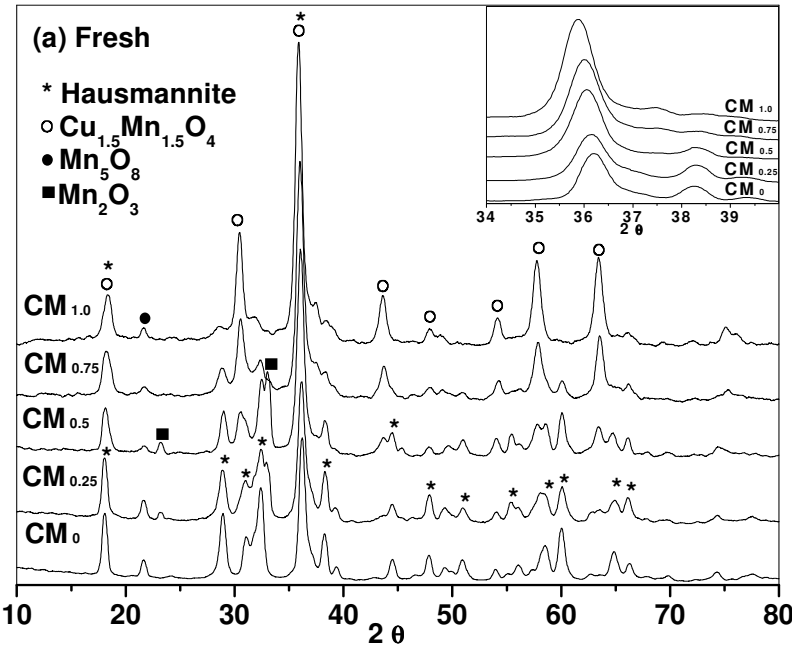

Fig.2.1. *X-ray diffraction pattern of fresh copper-manganese spinel type catalysts after calcination at 773 K.*

Though the hausmannite structure did not alter with incorporation of copper initially (for $x \leq 0.25$), further increase of copper ($x \geq 0.75$), induced transformation of tetragonal phase into cubic spinel phase [32]. The diffraction patterns obtained for these high Cu containing samples ($CM_{0.75}$ and $CM_{1.0}$) are characteristic of $Cu_{1.5}Mn_{1.5}O_4$ phase (JCPDS file no.35-1171). These results suggest that copper ions are either in hausmannite or $Cu_{1.5}Mn_{1.5}O_4$ lattice. Absence of diffraction peaks due to copper oxide reveals the formation of solid solution of copper-manganese mixed oxide. The shift in the diffraction peak ($2\theta = 36^o$) to low angles may be seen from Fig.2.1 (given as inset). This shift shows that the manganese ions of hausmannite lattice were replaced by copper ions. Cell parameters were calculated using PDP11 software. The cell parameters (a = 5.73, c = 9.41 for CM_0; a = 5.74, c = 9.40 for $CM_{0.25}$ and a = 5.75, c = 9.38 Å for $CM_{0.5}$) obtained for these catalysts suggest distorted tetragonal phase. Whereas, unit cell parameters (a = 8.26 and 8.28 Å) for $CM_{0.75}$ and $CM_{1.0}$ reveal formation of cubic structure. Therefore, it appears that phase transformation was induced at higher concentration of copper. Thermodynamic and crystallographic data of metal ions doped Mn_3O_4 samples has been reported in detail [33]. It was stated that gradual transformation of tetragonal into cubic form (decrease in 'c'

and increase in 'a' value) with increasing copper content is apparent, which is attributed to John Teller ion, Cu^{2+}. The cation arrangements in the structure of $Cu_xMn_{3-x}O_4$ were described elsewhere [33,34]. However, phase transformation may also occur because of the disproportionation of Mn^{3+} ions into Mn^{2+} and Mn^{4+} at high temperatures. The decrease in the c/a ratio of tetragonal phase may be attributed to the change in cation distribution of John Teller ions such as Mn^{3+} (d^4) and Cu^{2+} (d^9) [35].

The transformation of distorted tetragonal spinel in to cubic spinel has been reported and claimed that phase transformation occurs in presence of various dopants (like Cd, Mg, Ni, Cu, Co, Fe) and as a function of temperatures [36]. This phase transformation was mainly attributed to the presence of two John-Teller ions (Cu^{2+} and Mn^{3+}) in $Cu_xMn_{3-x}O_4$. Therefore, phase transformation observed from our samples is attributed to Mn^{3+} in octahedral sites, which is compensated by Cu^{2+} in tetrahedral sites of hausmannite structure resulting in cubic spinel structure. According to both ligand field and crystal field theories, the most likely cation distribution has been reported by several authors [33,37,38] using diverse techniques that indicate predominantly the presence of Cu^{+}, $Cu^{2+}$and Mn^{2+} ions at A sites and Cu^{2+}, Mn^{3+} and Mn^{4+} ions at B sites in the spinel structure.

2.4.3. Diffuse reflectance UV-visible spectroscopy

Fig.2.2 presents UV-visible absorption spectra obtained for copper-manganese oxide catalysts. Assigning the absorption bands to individual metal ions is rather cumbersome. Since, Mn_3O_4 is a normal spinel, the Mn^{2+} and Mn^{3+} cations are expected to be present in tetrahedral and octahedral sites, respectively.

The charge transfer (CT) continuous bands for hausmannite have been reported [39] at about 230 and 305 nm that are assigned to $O^{2-} \rightarrow Mn^{2+}$ and $O^{2-} \rightarrow Mn^{3+}$ transitions, respectively. Whereas, the absorption band in the visible region was attributed to highly symmetric, single spin allowed *d-d* transition of Mn^{3+} in octahedral environment, which is expected at about 500 nm [40]. However, a distortion of the octahedral co-ordination sphere can give rise to a different splitting of *d* levels and so other *d-d* transitions can occur [41,42]. Interpretation of the DRS spectra of hausmannite that contain dopants is complex because of random cation distribution. Mn^{2+} (d^5) *d-d* transitions are expected to be weak in

both octahedral and tetrahedral sites, since they are, in principle, both spin as well as orbitally forbidden [43].

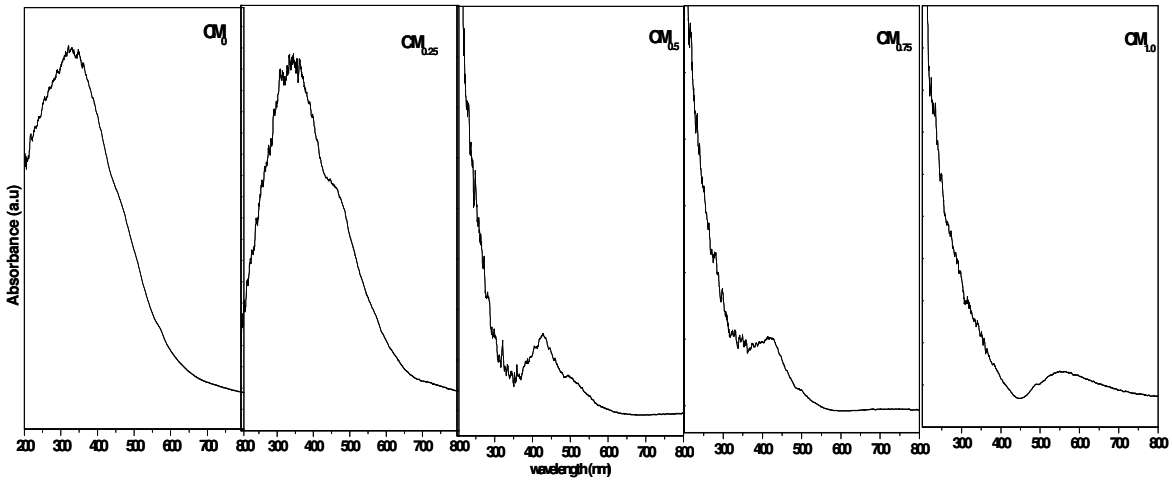

Fig.2.2. *DRS UV–visible spectra of copper-manganese oxide spinel type catalysts calcined at 773 K.*

The electronic spectra of CM_0 and $CM_{0.25}$ display a continuous absorption band in the UV and visible region with the main band centered at 330-340 nm with a shoulder at 460 nm. These spectra are fully consistent with those reported in the literature for hausmannite [39]. Hence, unresolved absorption bands that are seen in the visible region of our samples may be attributed to distorted *d-d* transitions originating from Mn^{3+} [39,44-47]. No bands in the region of 800 nm were observed that could be attributed to *d-d* transitions of Cu^{2+} in the octahedral environment [48,49]. However, the catalysts with $x \geq 0.5$ show very distinguishable DRS spectra. These spectra show a shift in the UV region band to lower wavelengths and presence of low intense band in the visible region around 430 and 500 nm for catalysts with x = 0.5, 0.75 and 1.0, respectively. The shift in the UV region may be due to the replacement of $Cu^{2+/1+}$ ions in the tetrahedral sites. Presence of copper in the structure induces redox equilibrium amongst the constituent ions, $Cu^{2+} + Mn^{3+} \rightarrow Cu^{1+} + Mn^{4+}$. The reduction in the intensity of the band in the visible region may be due to the reduction of number of Mn^{3+} ions in octahedral sites.

2.4.4. Infrared spectroscopy

FTIR spectra of fresh catalysts are shown in Fig.2.3. The skeletal vibrations of pure manganese sample (CM_0) and also the sample with less copper content ($CM_{0.25}$) show bands at 429, 516 and 628 cm^{-1}, which are characteristic of hausmannite [39,46-53].

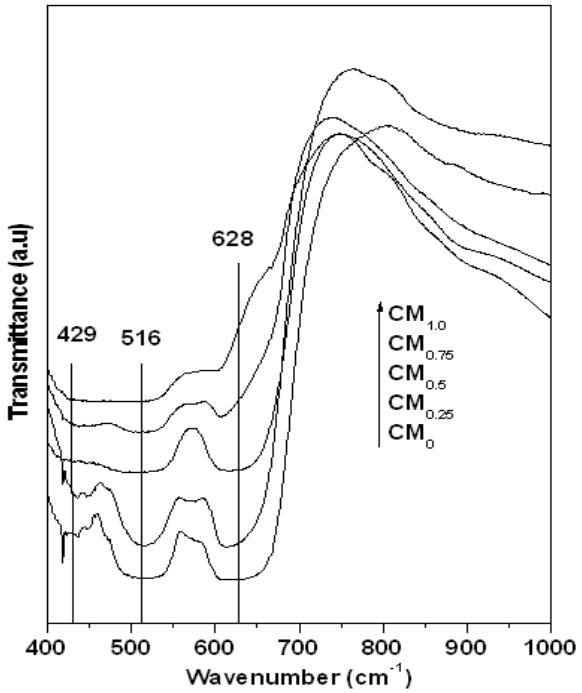

Fig.2.3. *FT IR spectra of copper-manganese oxide catalysts calcined at 773 K.*

The effect of copper is especially evident for samples with $x \geq 0.5$ resulting in disappearance of bands at 429 and 516 cm^{-1}. In addition, the intensity of the band at 628 cm^{-1} was found to decrease as a function of copper. It is therefore, the copper content influences the skeletal vibrations of mixed oxide catalysts. These bands have been assigned in the literature to octahedral MnO_6 at 450–550 cm^{-1} [50]. It can be postulated that differences in charge and covalency between copper and manganese ions is sufficiently great. IR spectra further support the phase transformation from tetragonal to cubic structure with increasing copper content that was observed by powder XRD. Thus IR and UV-visible spectra corroborate the XRD results discussed earlier.

2.4.5. Thermal analysis

The thermal analysis results (TG-DTG) during decomposition of the metal hydroxide precursors were obtained in presence of nitrogen. All the samples exhibited similar decomposition behavior. The initial weight losses due to loss of water ≤2.5-wt% (Table 2.2) were observed for all the precursors. The thermograms pertaining to decomposition of hydroxide precursors showed mainly two weight losses below 600 K, they are in the temperature range of 350-370 K and 470-520 K, corresponding to loss of physisorbed water and dehydration of metal oxyhydroxide, respectively, which are presented in Fig.2.4 (a)-(e).

Table 2.2. *Thermal analysis results of copper-manganese oxide spinels in nitrogen*

Catalyst	Weight loss (wt%)			
	300-600 K	**600-1000 K**	**1000-1273 K**	**Total wt loss**
CM_0	1.84	4.18	5.22	11.24
$CM_{0.25}$	1.82	2.64	0.67	5.13
$CM_{0.5}$	1.93	2.34	0.95	5.22
$CM_{0.75}$	2.38	3.28	2.26	7.92
$CM_{1.0}$	2.0	2.28	1.02	5.30

Further loss of weight was observed for these samples in the temperature range of 600-1000 K. The weight loss at this stage may be attributed to transformation of Mn_3O_4 (hausmannite phase) along with mixture of partially reduced oxides i.e. Mn_2O_3 or MnO (23,24). Transformation of α-Mn_3O_4 to β-Mn_3O_4 cannot be attributed to this, as this transformation does not involve any weight loss. The weight loss was higher (4.18%) in case of pure manganese compared with Cu substituted spinels (≤ 2.64 % for x ≥0.25). The XRD of these samples obtained after heating at 773 K in N_2 were identified as hausmannite spinel phase. An additional weight loss observed at 1070 K in the case of CM_0 may be due to phase transformation of Mn_3O_4 from tetragonal to cubic phase [54].

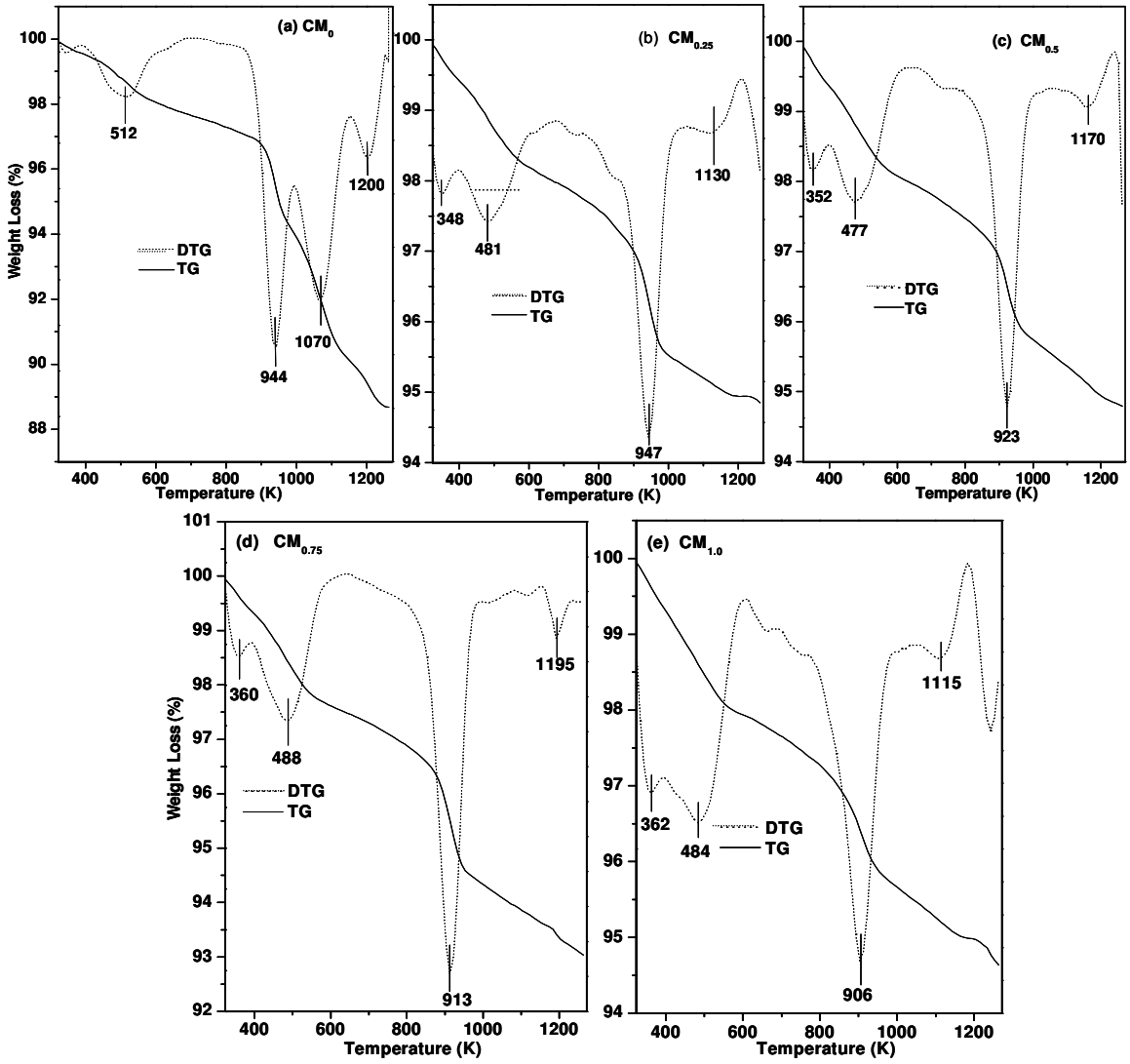

Fig.2.4. *TG-DTA analysis of copper-manganite spinel catalysts (a) CM_0 (b) $CM_{0.25}$ (c) $CM_{0.5}$ (d) $CM_{0.75}$ (e) $CM_{1.0}$*

However, this peak is shifted to high temperatures on incorporation of copper in to the hausmannite structure [55]. Pure manganese oxide (CM_0) showed higher total weight loss (11.2%) when compared to other catalysts (<8%) of the series. The total weight loss is 7.9-wt% for samples $CM_{0.75}$, while other samples showed ~5-wt%. A high temperature above 1100 K may be due to phase transformation from tetragonal to cubic form [54,56]. The DTG peak at 944 K obtained for CM_0 remains same even after substitution of small amount of copper (x = 0.25): however, this peak has continuously shifted to lower temperatures on further increasing the copper content. It may be noted here that hausmannite structure was retained only at lower copper contents in the samples. It is

therefore, inferred that the catalysts containing copper content hindered the decomposition or phase transformation. There were two temperature maxima in high temperature regions of DTG belonging to CM_0, while only one DTG peak at about 906-947 K was observed for all other Cu substituted phases. The high temperature weight loss with maxima at 1040 K is mostly subdued for all copper containing samples. The total weight loss for CM_0 is higher when compared to all copper containing samples. A large amount of vacancies may form after incorporation of copper on the surface of the mixed oxides surfaces as reported by Yongnian et.al [57].

2.4.6. Temperature programmed desorption

TPD results of CO_2 and NH_3 for fresh catalysts after calcination at 773 K are presented in Table 2.3 and Fig.2.5. The chosen probe molecules, ammonia for acidity and carbon dioxide for basicity estimation are the most suitable to determine the acid-base properties of solid catalysts.

Table 2.3. *Results of TPD of carbon dioxide and ammonia on copper manganese oxide catalysts*

Catalyst	Total CO_2 desorbed (mmol)/g	Total NH_3 desorbed (mmol/g)
CM_0	0.0312	0.276
$CM_{0.25}$	0.06	0.139
$CM_{0.5}$	0.056	0.114
$CM_{0.75}$	0.076	0.10
$CM_{1.0}$	0.072	0.11

It may be seen from the results that CO_2 is completely desorbed below 573 K, giving two desorption peaks centered at about 437 and 527 K for CM_0 and $CM_{0.25}$ catalysts (Fig.2.5a). These peaks suggest the presence of two kinds of adsorption sites for CO_2 at the catalyst surface, which may be attributed to weak and moderately strong basicity.

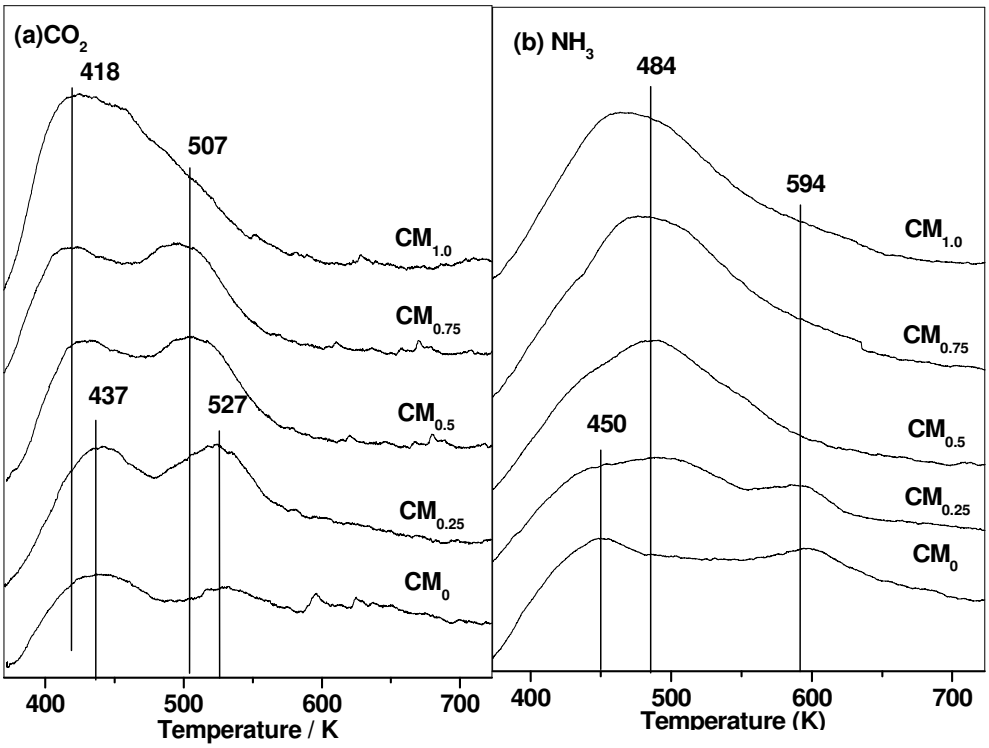

Fig.2.5. *Temperature programmed desorption of (a) CO_2 and (b) NH_3 on copper-manganese spinel oxide catalysts*

For catalysts with higher concentration of copper ($x \geq 0.5$), desorption maxima shifts towards lower temperatures, indicating relatively weaker basicity for samples with $x \geq 0.5$.

TPD of ammonia results over these catalysts is also presented in Fig.2.5b. Deconvolution of these spectra, particularly for CM_0 and $CM_{0.25}$ showed three peaks with peak maxima at 450, 484 and 594 K, indicating the presence of acid sites of varied strength. The high temperature desorption peak at 594 K was not present for copper rich catalysts ($x \geq 0.5$). However, total acidity obtained from TPD of ammonia has increased with increasing copper content. One should also note that desorption of ammonia may not always necessarily reflect the true acid site strength/density because of the limitations of this technique. For example, TPD of ammonia on CaO shows desorption peak, which is mainly due to dissociation of ammonia by the sample, despite the material being highly basic nature. Hence, in this study we are mainly considering the TPD results for the comparison of the acidity or basicity of a series of copper–manganese catalysts as function of copper content. In fact, the idea is to correlate surface acidity/basicity obtained from these results with catalytic activity.

Acidity and basisity of relatively higher strength for catalysts with x = 0 or 0.25 can be related with the crystalline structure of the samples. Catalysts with higher copper (x > 0.25), exhibit cubic phases, where as other samples formed distorted tetragonal phases. Hence, change of composition of metal ions on the surface, i.e. Mn/Cu or Cu^{2+}/Cu^{1+} ratio may have influenced with the increase of copper content in the samples with $x \geq 0.5$. Hence, structural changes and the heterogeneity on the surface of the catalysts are responsible for variation of acid-base properties for these catalysts.

2.4.7. Temperature programmed reduction

TPR profiles of freshly calcined samples are presented in Fig.2.6. The pure manganese oxide sample, Mn_3O_4 (CM_0) showed two reduction peaks with temperature maxima (T_{max}) at 565 and 705 K. These peaks can be safely assigned to the reduction of surface and bulk Mn^{3+} to Mn^{2+} ions, respectively, as the sample contains only Mn^{3+} as reducible ions. This assignment is based on the fact that hausmannite forms a normal spinel with Mn^{2+} ions in tetrahedral and Mn^{3+} in octahedral sites [57]. Further reduction of Mn^{2+} ions is not thermodynamically feasible under the experimental conditions. Incorporation of copper into hausmannite significantly enhanced the reducibility of the catalysts with reduction temperature of the peaks shifting to lower temperature.

Table 2.4. *Hydrogen consumption and T_{max} values obtained from TPR of copper-manganese oxide catalysts calcined at 773 K*

Catalyst	T_{max2} (K)	H_2 consumption (mmol)	T_{max1} (K)	H_2 consumption (mmol)
CM_0	565	1.47	705	3.97
$CM_{0.25}$	437	0.225	541	6.15
$CM_{0.5}$	444	0.25	522	6.29
$CM_{0.75}$	427	0.361	529	7.04
$CM_{1.0}$	446	0.41	538	8.08

The T_{max} of the main reduction peak (~530 K) of copper substituted samples is at higher temperature than T_{max} usually observed for pure CuO (~500 K) [46], but lower than that of bulk Mn_3O_4 (~700 K). Powder XRD pattern obtained after TPR experiment, revealed the formation of MnO and Cu. Reduction in peak width (FWHM) for the high

copper containing samples ($x \geq 0.5$) reveals the influence of $Cu^{2+/1+}$ which enhances the reducibility of Mn^{3+}. A shift in the position of main peak was observed for the samples up to x = 0.5 towards lower temperatures, thereafter it has shifted marginally to higher temperatures for catalysts, $x > 0.5$. This shift in the T_{max} may be attributed to the change of phase, as observed by XRD (Fig.2.1). The low temperature peak at about 446 K for all copper containing samples was found to increase in the intensity with the copper content. This peak, therefore, may be due to reduction of Cu^{2+} ions to copper metal. However, not much shift in the T_{max} of this peak was observed with increase of copper content [47-51]. The shift in the reduction of high remperature peak of pure manganese with copper is mainly attributed to the intimate coordination of copper ions in the lattice. Since, Cu and Mn ions are surrounded by each other in the lattice the reduction occurred at intermediate temperature compared to the reduction of individual metal oxides.

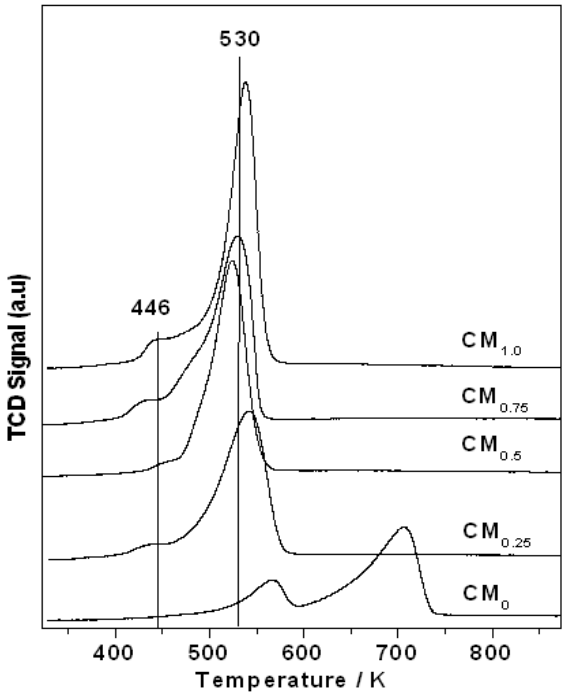

Fig.2.6. *TPR profiles of copper-manganese oxide catalysts calcined at 773 K.*

2.4.8. Copper dispersion and particle size

Copper metal dispersion was calculated from H_2 uptakes determined by the TPR analysis after surface oxidation of reduced catalysts using 5% N_2O in helium according to

the report by Gervasini et al. [47]. Copper dispersion values for the catalysts are presented in Table 2.5. It is seen that the catalysts with lower copper i.e. $CM_{0.25}$ showed better dispersion, which is close to 54%.

Table 2.5. *Surface properties of copper manganese oxide catalysts derived from N_2O decomposition*

Catalyst	Copper content (wt%)	Cu dispersion D_{Cu}	Copper metal area (m^2/g Cu)	Cu particle size (nm)
CM_0	---	---	--	--
$CM_{0.25}$	6.0	54	349	1.9
$CM_{0.5}$	12.2	27	176	3.8
$CM_{0.75}$	18.8	17	107	6.3
$CM_{1.0}$	23.0	16	101	6.7

The dispersion decreased with increasing copper content in the catalyst. Surface copper area and average particle sizes are also in good agreement with the dispersion data. It is generally known that with increase in metal content aggregation of the particles takes place to form larger crystallites [58]. Hence, reduction in the dispersion and enhancement in the particle size has occurred. The higher Cu^o surface area associated with $CM_{0.25}$ may be due to the interaction generated between Cu and Mn species. Effect of copper content showed a considerable decrease in the surface area upto x = 0.5, thereafter not much change was observed for samples with x >0.5, despite raise in the copper content by about 6 wt%. This decrease may be due to larger copper metal particles formed after reduction [59,60].

2.4.9. Scanning electron microscopy

The SEM images of various copper-manganite catalysts are illustrated in Fig.2.7. Based on SEM images of theses catalysts, no noticeable changes were observed in the morphology of oxides even after incorporation of copper up to $x \leq 0.5$. Fig.2.7d shows some small needle like structures for sample $CM_{0.75}$, which became very prominent in Fig.2.7e for $CM_{1.0}$. Moreover, larger particles were seen in case of pure manganese oxide, while particle sizes are reduced in case of copper rich samples i.e.100 nm [61].

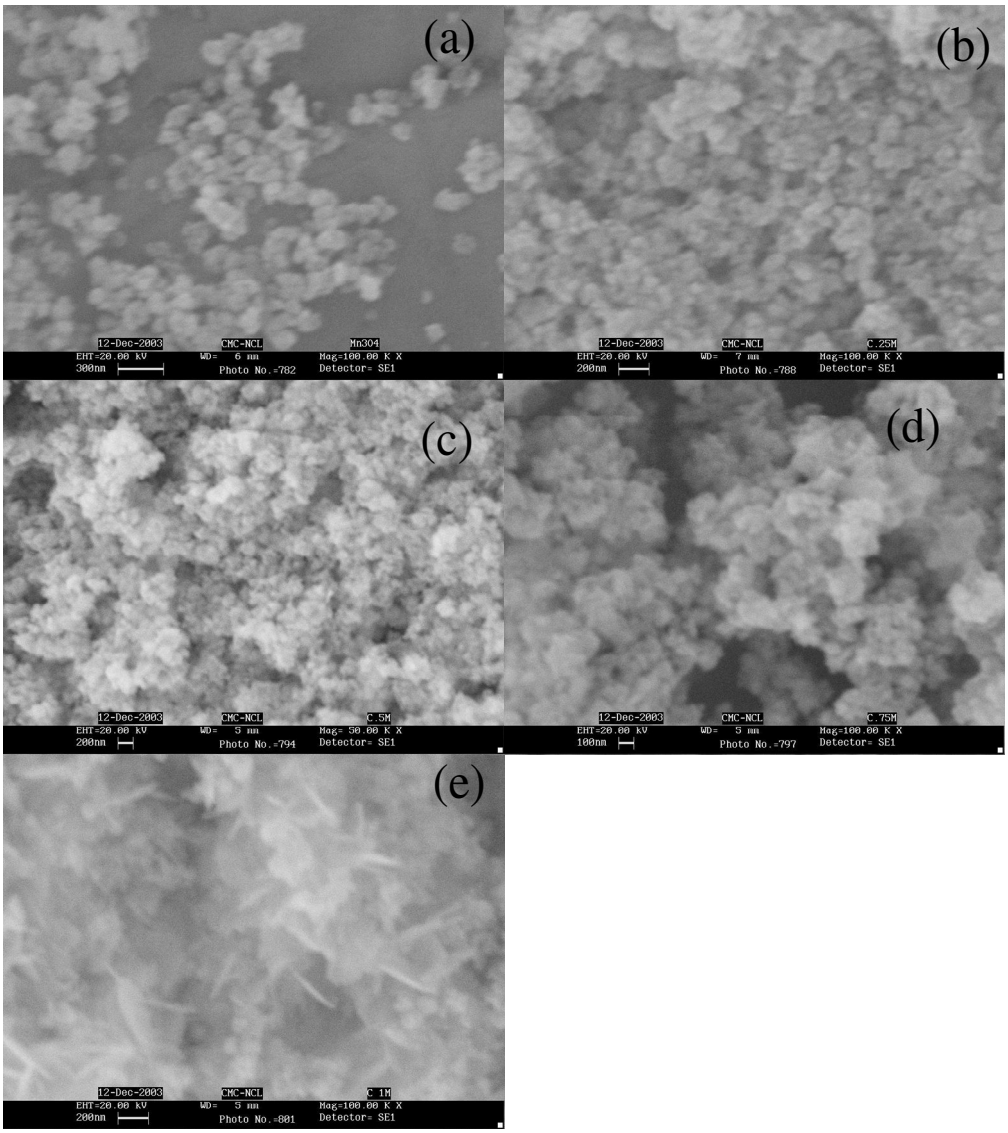

Fig.2.7. *SEM images of copper- manganese oxide catalysts (a) CM_0 (b) $CM_{0.25}$ (c) $CM_{0.5}$ (d) $CM_{0.75}$ (e) $CM_{1.0}$ after calcinations at 773 K.*

2.4.10. X- ray photoemission spectroscopy

Surface characterization of fresh and spent catalysts (CM_0, $CM_{0.25}$ and $CM_{1.0}$) was carried out by XPS and X-ray initiated Auger electron spectroscopy (XAES).

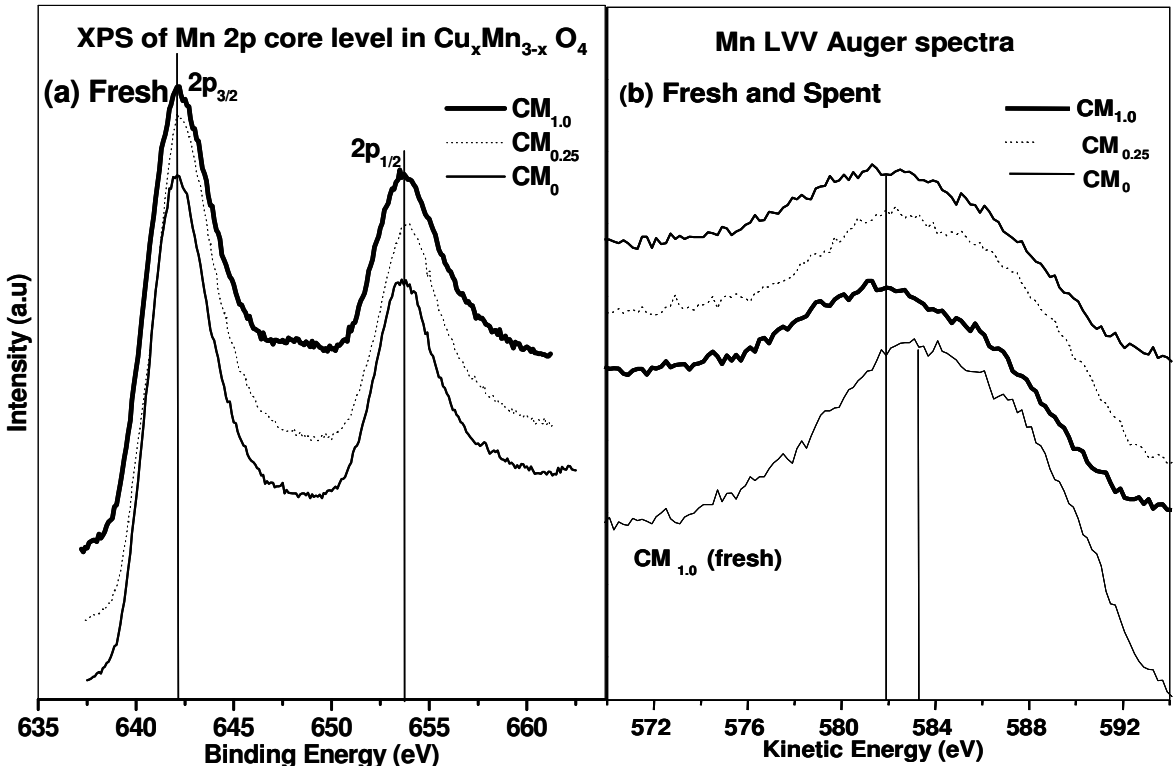

Fig.2.8. *Mn 2p photoemission spectra of (a) fresh, (b) Mn LVV of fresh and spent $Cu_xMn_{3-x}O_4$ catalysts. Spent catalysts are obtained after 4 h of phenol methylation reaction at T = 673 K.*

Mn 2p core level and Mn-LVV Auger transitions: Mn 2p photoemission spectra of fresh catalysts along with Mn-LVV Auger transitions are shown in Fig.2.8. A binding energy value at of 642.1 ± 0.1 eV with ΔE of 11.4 ± 0.1 eV was observed for all the catalysts indicating the oxidation state of Mn to be 3+. These binding energy values for Mn $2p_{3/2}$ are in good agreement with those reported [62,63]. Hausmannite has a spinel structure that contains both Mn^{2+} and Mn^{3+} ions. Oku et al. reported that it is difficult to distinguish between the oxidation states of Mn in Mn_3O_4 using XPS [64]. Allen et al. has reported that the BE values of $2p_{3/2}$ peak for the manganese cations in MnO, Mn_3O_4, Mn_2O_3 and MnO_2 as 640.9, 641.7, 641.8 and 642.4, respectively [65]. Mn 2p peaks of spent catalysts are at 641.1, 641.4 and 641.4 eV for CM_0, $CM_{0.25}$ and $CM_{1.0}$, respectively. Mn-LVV Auger

spectra of fresh $CM_{1.0}$ and spent CM_0, $CM_{0.25}$, $CM_{1.0}$ catalysts are shown in Fig.2.8b. Mn-LVV spectra of fresh catalysts are similar; hence only $CM_{1.0}$ spectrum is given in Fig.2.8b to show the changes from fresh to spent catalysts. A broad Auger transition is observed between 576 to 592 eV for all the samples. The shift in energy to lower KE is observed for spent catalysts compared to fresh catalyst ($CM_{1.0}$). The spectra from spent CM_0 and $CM_{0.25}$ are identical.

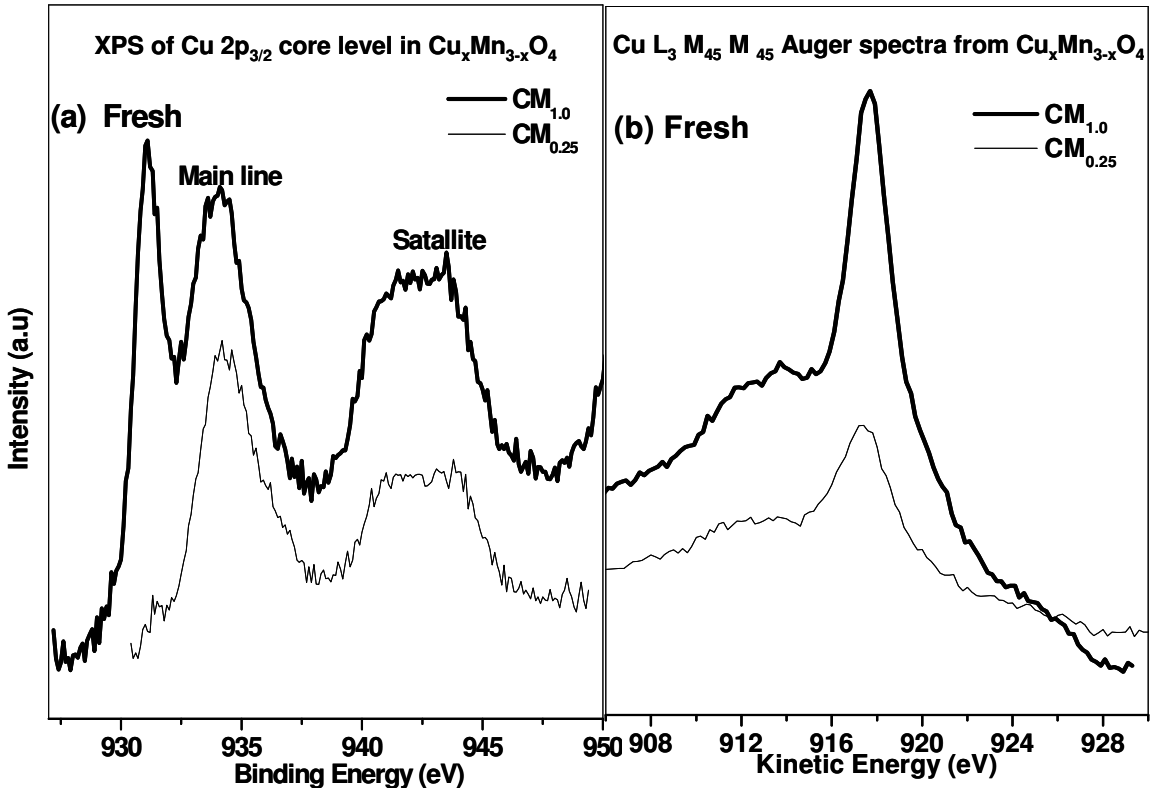

Fig.2.9. *(a) Cu 2p core level XPS spectra and (b) X-ray initiated Augur electron spectra (XAES) from Cu-$M_3M_{45}M_{45}$ of fresh $Cu_xMn_{3-x}O_4$ catalysts*

Cu 2p core level: XPS spectra of Cu $2p_{3/2}$ core level for fresh $CM_{0.25}$ and $CM_{1.0}$ catalysts are shown in Fig.2.9a. A main peak at 934.1 ± 0.1 eV for the fresh catalysts with satellite peak around 942 ± 0.1 eV was observed for $CM_{0.25}$ as well as $CM_{1.0}$. Their FWHM values were found to be 2.56 and 3.25 eV, respectively. The B.E of Cu $2p_{3/2}$ peak in CuO is reported to be about 933.6 eV [62,63], with a shake up satellite between 940 and 945 eV. The B.E values of our samples are in good agreement with those reported. Where as for $CM_{1.0}$, an additional peak at lower binding energy value of 931.0 eV was seen with another

strong peak at 934.1 eV. The former peak indicates the presence of Cu^{1+}/Cu^{o} species. The $2p_{3/2}$ peak of Cu^{1+} in Cu_2O is reported to be at 932.2 ± 0.3 eV [66], but for Mn containing oxides the same is expected at around 931 eV [67]. These experimental observations are in good agreement with the formation of Cu^{1+} and Mn^{4+} as a result of reduction-oxidation equilibrium $Cu^{2+} + Mn^{3+} \rightarrow Cu^{1+} + Mn^{4+}$, which is expected on copper substitution [66]. XPS of spent $CM_{0.25}$ catalysts gave a single peak for Cu 2p at 932.5 eV with FWHM of 1.2 eV without any satellite peaks. Similarly, $CM_{1.0}$ shows only one peak at 932 eV with FWHM of 1.4 eV. Though the B.E. value of this peak is close to Cu^{1+}, we presume it to be copper metal based on the powder XRD results. However, in this study the main Cu 2p peak at 931.2 eV from $CM_{1.0}$ could be assigned to Cu^{1+}, which does not show any satellite peak. However, metallic copper (Cu^{o}) also exhibit similar B.E values as that of Cu^{1+}, and hence identification of oxidation states is rather difficult merely from XPS of Cu 2p.

Cu-$L_3M_{45}M_{45}$: Auger electron transition, that modifies Auger parameter α', distinguishes the different oxidation states of Cu in the same or related compounds [62,68]. The Cu-$L_3M_{45}M_{45}$ Auger spectra of fresh catalysts are shown in Fig.2.9b. It can be seen that the $CM_{0.25}$ catalyst gave the Cu-$L_3M_{45}M_{45}$ line at a K.E of 917.3 eV. Further increase in copper content of the sample shifts the peak to 917.7 eV. For pure CuO, this peak is reported at 917.6 eV [62,68]. The values of α' determined for fresh $CM_{0.25}$ and $CM_{1.0}$ catalysts are 1851.4 and 1851.6, which are very close to that observed for CuO (1851.5). The additional value of α' = 1848.7 eV obtained for $CM_{1.0}$ from the low B.E $Cu2p_{3/2}$ peak supports the presence of Cu^{1+}.

Valence band photoemission: XPS spectra of the valence band (VB) region obtained from fresh catalysts are shown in Fig.2.10. The main VB observed below 9 eV has contributions from 3d orbitals of Cu and Mn. At *hv* = 1253.6 employed in these experiments, the photoionisation cross-section (σ) value (Cu 3d = 0.021, Mn 3d = 0.0026 and O 2p = 0.0005 Mb) [67] is the dominant factor in determining the spectral intensity.

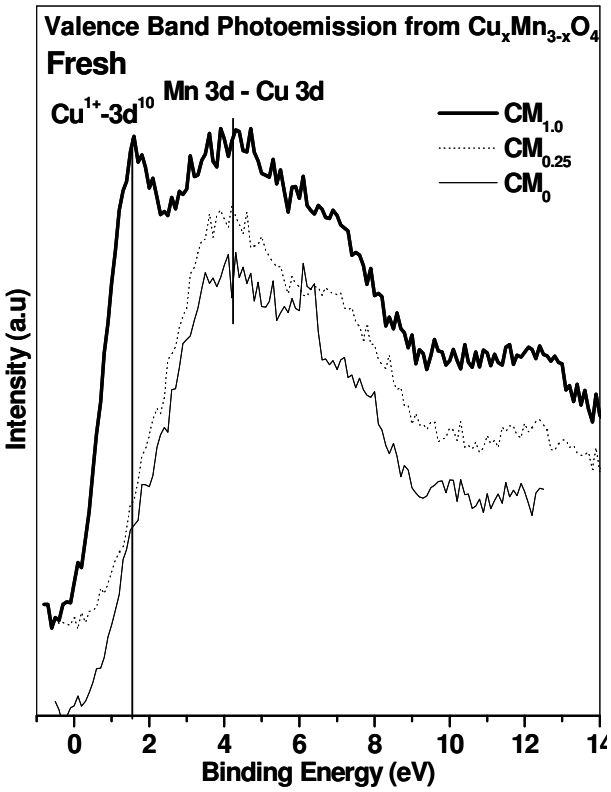

Fig.2.10. *Valence band XPS spectra of fresh and spent copper manganese oxide catalysts*

The above data suggests that the contribution from O 2p is negligible. Similarly, Cu 3d should largly contribute to the VB intensity. The VB assignments are straightforward from the intensity and the B.E of the bands. High intensity VB observed on CM_0 at 4 eV is due to Mn 3d bands. The intensity of VB increases with increase in copper content along with a new peak at 2 eV and satellite around 12 eV. These observations clearly suggest that the new features are from Cu 3d bands. The band at low BE (2 eV) is attributed to Cu-$3d^{10}$ band [68]. An overlapping of Mn 3d and Cu 3d is observed around 4 eV for fresh catalysts. The intensity variation observed with an increase of copper content is mostly due to the high σ of the Cu 3d bands. Comparatively low intensity features observed between 6 and 8 eV is attributed to O 2p bands.

2.5. Zinc-manganese oxide spinels

2.5.1. Catalyst composition and structural characterization

Zinc-manganese oxide spinel catalysts were prepared by co-precipitation. Their bulk metal compositions were determined by chemical analysis (AAS) after dissolving them in aquaregia. The analysis results match with the input concentrations used for the preparation. Crystalline phases, unit cell parameters, BET surface area and crystallite sizes of the catalysts are also summarized in Table 2.6.

Table 2.6. *BET surface areas and structural properties of zinc-manganese oxide spinel catalysts after calcination at 773 K*

Catalyst	Composition	Crystalline phases	Crystallite size (nm)	Cell parameters a and c (A^o)	S_{BET} (m^2/g)
ZM_0	Mn_3O_4	Mn_3O_4, Mn_5O_8	21	5.73, 9.41	21 (20) [s]
$ZM_{0.25}$	$Zn_{0.25}Mn_{2.75}O_4$	Mn_3O_4 or $ZnMn_2O_4$, Mn_5O_8	16	5.70, 9.29	37 (28)
$ZM_{0.5}$	$Zn_{0.5}Mn_{2.5}O_4$	Mn_3O_4 or $ZnMn_2O_4$	16	5.70, 9.26	35 (30)
$ZM_{0.75}$	$Zn_{0.75}Mn_{2.25}O_4$	Mn_3O_4 or $ZnMn_2O_4$	17	5.69, 9.20	28 (24)
$ZM_{1.0}$	$Zn_{1.0}Mn_2O_4$	$ZnMn_2O_4$	20	5.67, 9.17	25 (20)

[s] *surface areas of spent catalysts after phenol methylation at 723 K for 4 h.*

It may be seen that the incorporation of zinc enhanced the surface area initially up to $x \leq 0.5$, while further increase in zinc content led to a reduction in the surface area. The crystallites have small sizes with low Zn contents ($x \leq 0.5$) but increased thereafter. These results are in consistent with surface area measurements. After phenol methylation at 623 K for 4 h), all the catalysts showed reduction in the surface area compared with the fresh catalysts, followed by increase in the crystallite size. All the catalysts contain spinel type mixed oxide (Mn_3O_4 or $ZnMn_2O_4$) as major phase with tetragonal structure, while Mn_5O_8 was found as minor phase. As was reported, hausmannite has distorted tetragonal spinel structure at room temperature [36].

2.5.2. Powder X-ray diffraction

X-ray diffraction patterns of $Zn_xMn_{3-x}O_4$, with various zinc concentrations (x = 0 to 1.0) are shown in Fig.2.11. Diffraction peaks characteristic of hausmannite or hetaerolite ($ZnMn_2O_4$) are found. All the catalysts consist of hausmannite as a major phase, but with the increasing amount of zinc a shift in the peak position to higher angles (2θ) was observed as shown in the inset of Fig.2.11. It is rather difficult to assign these peaks entirely either to Mn_3O_4 or $ZnMn_2O_4$ (JCPDS file no. 24-1133). In any case, both the phases belong to same hausmannite group. Peaks corresponding to ZnO were not seen for any of the samples. But, apart from hausmannite Mn_5O_8 (JCPDS file no.39-1218) in small quantities was observed in case of ZM_0 and $ZM_{0.25}$. Crystallographic distortions in hausmannite, after introduction of other cations in Mn_3O_4 have been reported [69-71]. $Zn_xMn_{3-x}O_4$ was reported to be found to be highly stable in air [72] for 'x' in the range $0 \leq x \leq 1.48$. The structure of $Zn_xMn_{3-x}O_4$ was reported earlier [73]. The present results indicate that pure solid solution of zinc-manganese oxide was formed at all compositions. The samples exhibit distorted tetragonal hausmannite phase. The unit cell parameters observed (Table 2.6) reveal a decrease in the unit cell volume (reduction in 'a' and 'c' values). $ZnMn_2O_4$ was reported as a normal spinel [36,74] with a tetragonal structure at ambient temperature. Unlike in the case of copper manganites, the phase transformation from tetragonal to cubic was not observed at increased concentrations of zinc in zinc-manganites. However, the phase transformation also usually depends on the temperature. For example, hausmannite when heated to about 1423 K, Mn^{3+} ions concentration goes down with simultaneous increase in Mn^{2+} and Mn^{4+} ions resulting a change of structure to cubic phase. The cation distribution reported for $ZnMn_2O_4$ has Zn^{2+} in tetrahedral sites preferentially, which was determined by various techniques [67].

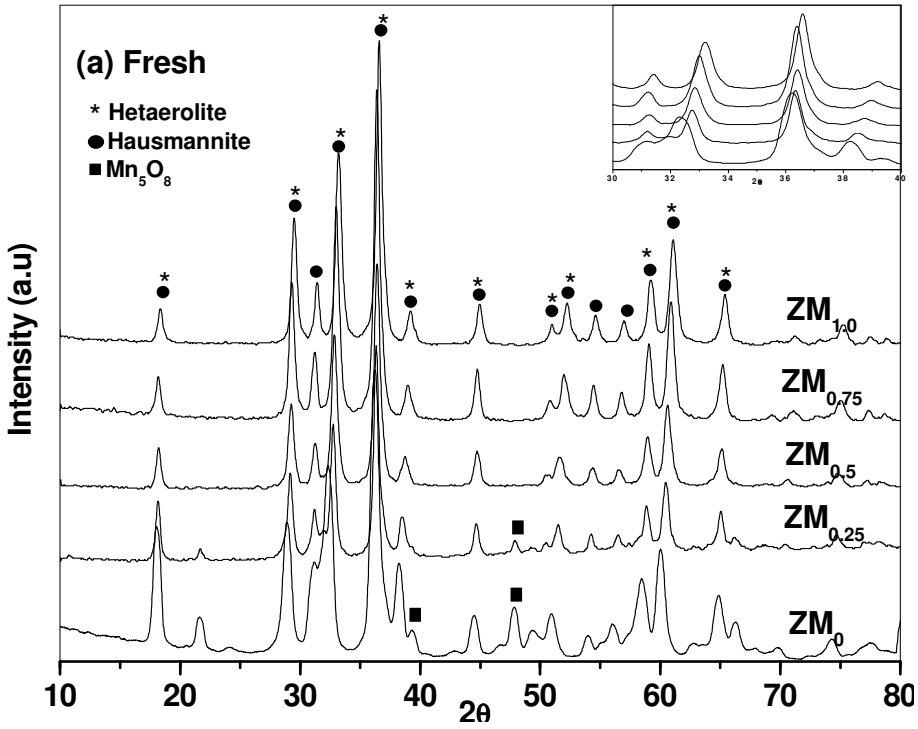

Fig. 2.11. *X-ray diffraction patterns of zinc-manganese oxide catalysts calcined at 773 K.*

2.5.3. UV-visible spectroscopy

Fig.2.12 presents UV-visible spectra of ZM_x samples. The electronic spectrum of pure manganese oxide with continuous absorption band due to charge transfer in the range of 230-305 nm and absorption in the visible region is due to d-d transitions are in good agreement with that reported for hausmannite [39,40]. Introduction of zinc in the hausmannite initially (x = 0.25) showed a shift in the absorption band to about 470 nm, which may be attributed to *d-d* transition of octahedral Mn^{3+} [40]. The absorption band in the visible region was reported to be due to single spin allowed *d-d* transition of Mn^{3+} in octahedral environment, which is expected at about 500 nm [40]. Where as, further increase in the zinc content does not show much change in the electronic spectra as was observed for copper-manganese oxides [70]. This could be attributed to substitution of Zn^{2+} in tetrahedral sites preferentially, where as in case of copper-manganites redox equilibrium between Cu^{2+} and Mn^{3+} led to the formation of Mn^{4+} ions. Hence, assignment of these bands to individual metal ions is difficult, but distribution of Zn^{2+} and Mn^{2+} in tetrahedral sites and Mn^{3+} ions in octahedral sites was reported [36]. Charge transfer continuous band obtained for pure manganese oxide in UV region may be ascribed to O^{2-}

→ $Mn^{2+}$and O^{2-} → Mn^{3+} transitions and in the visible region (500 nm) to d-d transitions of octahedral Mn^{3+} ions [48-50]. $ZnMn_2O_4$ is a normal spinel with tetragonal structure, similar to hausmannite (Mn_3O_4) [72]. It is clear that after introducing Zn^{2+} ions, spectra show distinguishable bands at at 290 nm ($ZM_{0.5\text{-}1.0}$) and 400 nm ($ZM_{0.25}$). The charge transfer band due to Zn^{2+} ions in ZnO appears at 375 nm [36]. From the UV results, it appears that charge transfer band due to Zn^{2+} ions in tetrahedral sites show a red shift. No noticeable effect in the position of absorption band was observed due to CT band or *d-d* transition due to Mn^{3+} ions.

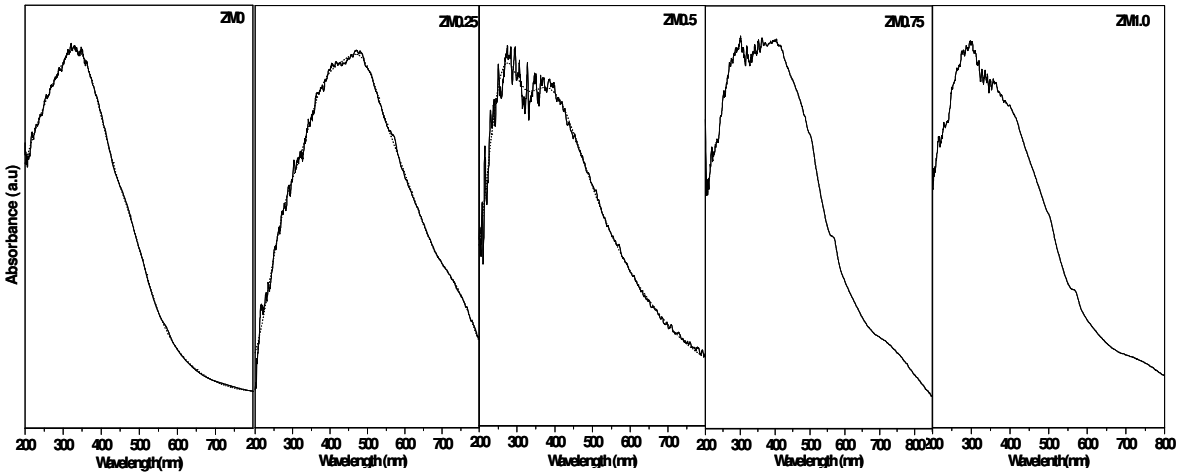

Fig. 2.12. *UV-Visible spectra of zinc manganese oxide spinel catalysts calcined at 773 K.*

2.5.4. FTIR spectroscopy

The FTIR spectra obtained for zinc-manganese oxides are presented in Fig.2.13. Three absorption bands characteristic of hausmannite structure of the pure manganite were observed. The bands centered at 431, 515 and 635 cm^{-1}, were observed for all the samples, which are akin to hausmannite as reported by Milella et al. [40]. It is to be noted that incorporation of zinc show gradual shift in the band positions to higher wave numbers, indicating that basic skeletal vibrations were influenced due to presence of zinc. It is therefore, as discussed above, Zn^{2+} ions may be occupying tetrahedral sites in the hausmannite lattice. Three bands at 431, 515 and 635 cm^{-1} are prominent for pure manganese oxide, while the low energy band disappeared gradually for zinc rich catalysts.

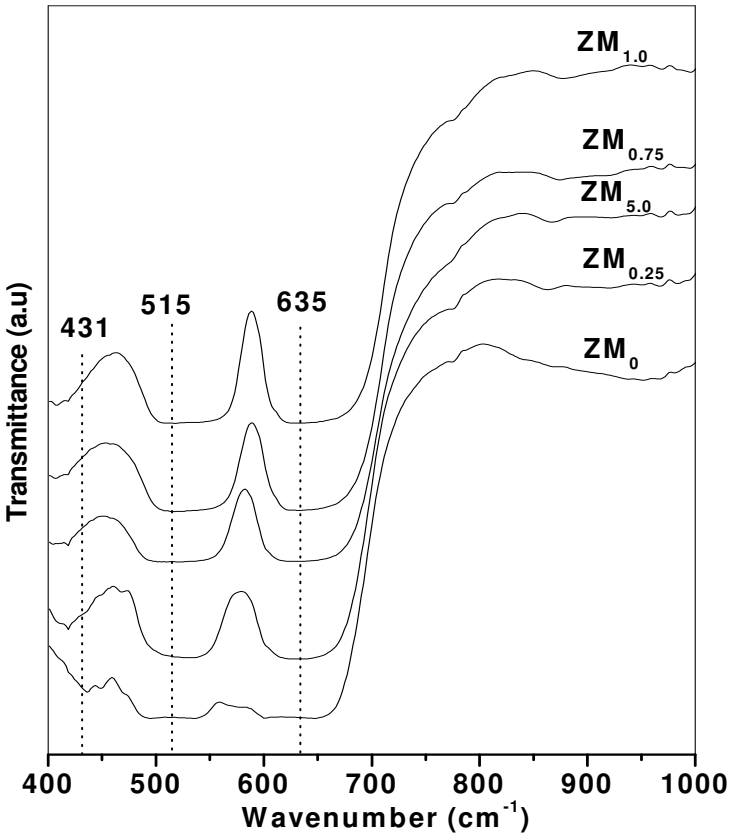

Fig.2.13. *FTIR spectra of fresh zinc manganese oxide catalysts calcined at 773 K.*

There were no additional bands observed due to zinc oxide or other manganese oxide phases. IR spectra further supports the result observed by UV-visible and XRD that demonstrate the presence of Zn^{2+} ions in tetrahedral sites while retaining the distorted tetragonal hausmannite structure even after the incorporation of higher zinc contents.

2.5.5. Temperature programmed desorption

It is known that metal oxides exhibit both acidity and basicity, which depends on the nature of the cation and its location. Quantitative determination of desorbed molecues were obtained after deconvolution of TPD peaks and presented in Table 2.7. TPD results of ammonia and carbon dioxide of zinc manganites that probes their acid-base character. Desorption of CO_2 occurs below 523 K with peak maxima at about 438 K for ZM_0, $ZM_{0.25}$ and $ZM_{0.5}$ catalysts.

Table 2.7. *Results of TPD of NH_3 and CO_2 on zinc- manganese oxide catalysts*

Catalyst	Total CO_2 desorbed (mmol/g)	NH_3 desorbtion Temp (K)	NH_3 desorbed (mmol/g)		Total NH_3 desorbed (mmol/g)
			T_{max1}	T_{max2}	
ZM_0	0.031	448, 595	0.188	0.088	0.276
$ZM_{0.25}$	0.021	451, 583	0.069	0.04	0.11
$ZM_{0.5}$	0.03	454, 554	0.076	0.24	0.10
$ZM_{0.75}$	0.02	451,556	0.053	0.018	0.072
$ZM_{1.0}$	0.01	454	0.09	--	0.09

Fig.2.14a demonstrate that there is only one kind of adsorption site for CO_2 at the surface, which may be assigned to weak basicity. The samples with higher concentration of zinc ($x \geq 0.75$), showed desorption at slightly lower temperatures representing further decrease in the basic strength of these catalysts. TPD of NH_3 results on these catalysts are presented in Fig.2.14b.

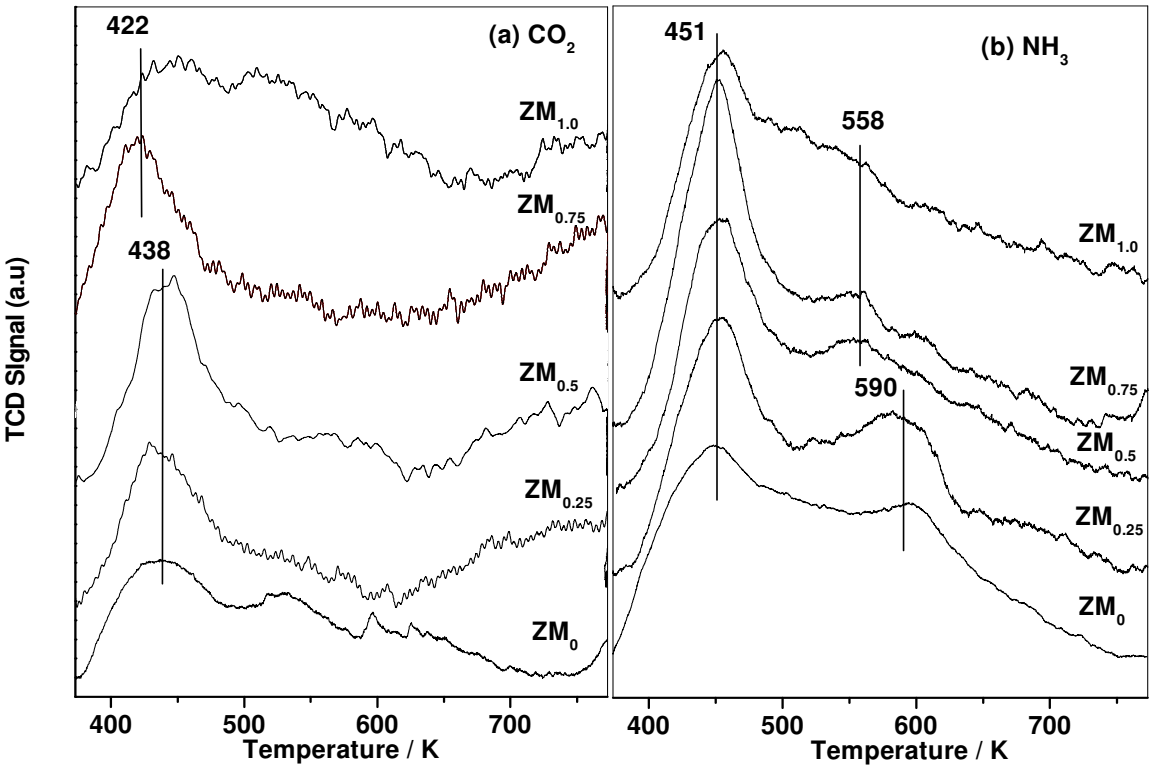

Fig.2.14. *Temperatures programmed desorption of (a) CO_2 and (b) NH_3 on zinc manganese spinel catalysts calcined at 773 K.*

ZM_0 and $ZM_{0.25}$ catalysts show ammonia desorption at two-temperatures centered at 451 and 590 K, signifying that they are associated with two kinds of acid sites of different strengths. But, the desorption peak appeared at 590 K shifted to lower temperature with increasing zinc concentration, demonstrating the presence of relatively very weaker acidity on these samples. However, not much shift was found in the low temperature desorption position. The total weak acidity was found to increase gradually with increasing zinc content.

From these results, it is interpreted that $ZM_{0.25}$ shows relatively stronger acidity (high T_{max} of TPD NH_3) along with some basicity. The addition of a small fraction (x = 0.25) of zinc helped in the generation of relatively higher acidity. According to Jacob et al. [73] this may be attributed to heterogeneous surface with Zn^{2+}/Mn^{2+}or Mn^{3+} ratio. A fall in the acidity of the catalysts with increasing concentration of zinc is observed (Table.2.7). No particular trend was observed in regard to the total carbon dioxide desorbed obtained by TPD of CO_2. It is known that a particular balance in the acidity and basicity of required strength is necessary for catalysts to offer better performance and selectivity towards desired product in acid-base catalyzed reactions.

2.5.6. Temperature programmed reduction

The T_{max} and the amount of hydrogen consumption obtained by TPR study are given in Table 2.8. TPR results show two reduction peaks corresponding to Mn^{3+} species for pure manganese oxide. These peaks (T_{max}) appeared at 565 K and 705 K for ZM_0 and $ZM_{0.25}$ catalysts, which are ascribed to the reduction of surface and bulk Mn^{3+} ions of hausmannite.

Table 2.8. *Results of hydrogen consumption by TPR of zinc-manganese oxide catalysts*

Catalyst	**T_{max} (K)**	**H_2 consumption (mmol/g)**	**T_{max} (K)**	**H_2 consumption (mmol/g)**
ZM_0	565	1.47	705	3.97
$ZM_{0.25}$	571	0.435	735	1.97
$ZM_{0.5}$	---	--	735	1.87
$ZM_{0.75}$	---	--	732	1.65
$ZM_{1.0}$	---	---	750	1.73

Reduction profiles obtained for the zinc-manganese oxide spinels after calcination at 773 K are presented in Fig.2.15. Catalysts with higher zinc ($x \geq 0.5$) were reduced in a single step showing only the high temperature reduction (430 K). From these results, it may be concluded that the amount of zinc in hausmannite did not affect the reducibility of surface Mn^{3+} ions with low concentrations of zinc ($x = 0.25$). The high temperature reduction peak did not show any shift with increase of zinc up to $x \leq 0.75$, but $ZM_{1.0}$ showed little shift to higher temperature. The disappearance of lower reduction peak with $x > 0.25$ may be due to decrease in the Mn^{3+}/Zn^{2+} ratio at the suface. It is to be noted that presence of non-reducible zinc ions did not influence the reduciblility of Mn^{3+} ions unlike copper ions in Cu-Mn oxide catalysts.

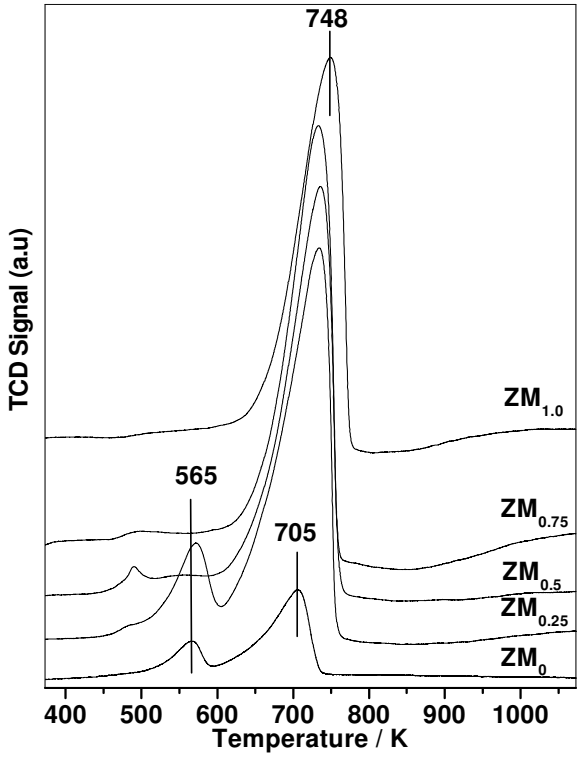

Fig.2.15. *TPR profiles of zinc-manganese oxide catalysts calcined at 773 K.*

The reduced phases obtained after TPR experiment were found to be MnO (manganosite) and ZnO (zincite). Formation of MnO was also qualitatively suggested by the color of the powder from black to brown. The shift towards high temperature in the

T_{max} of main peak in case of $ZM_{1.0}$ is probably due to the stabilization of Mn^{3+} ions in spinel by Zn^{2+} ions.

2.5.7. Scanning electron microscopy

The SEM images of various calcined zinc-manganite catalysts are shown in Fig.2.16. By comparing these images, we have found that the spinel oxide surface structure has not been changed markedly with the variation of zinc concentration. The SEM images predominantly show agglomerates of particles without definite shape. These images are found be a mixture of small and large aggregates. The aggregates of $ZM_{0.75}$ seemed to be relatively smaller than the other catalysts.

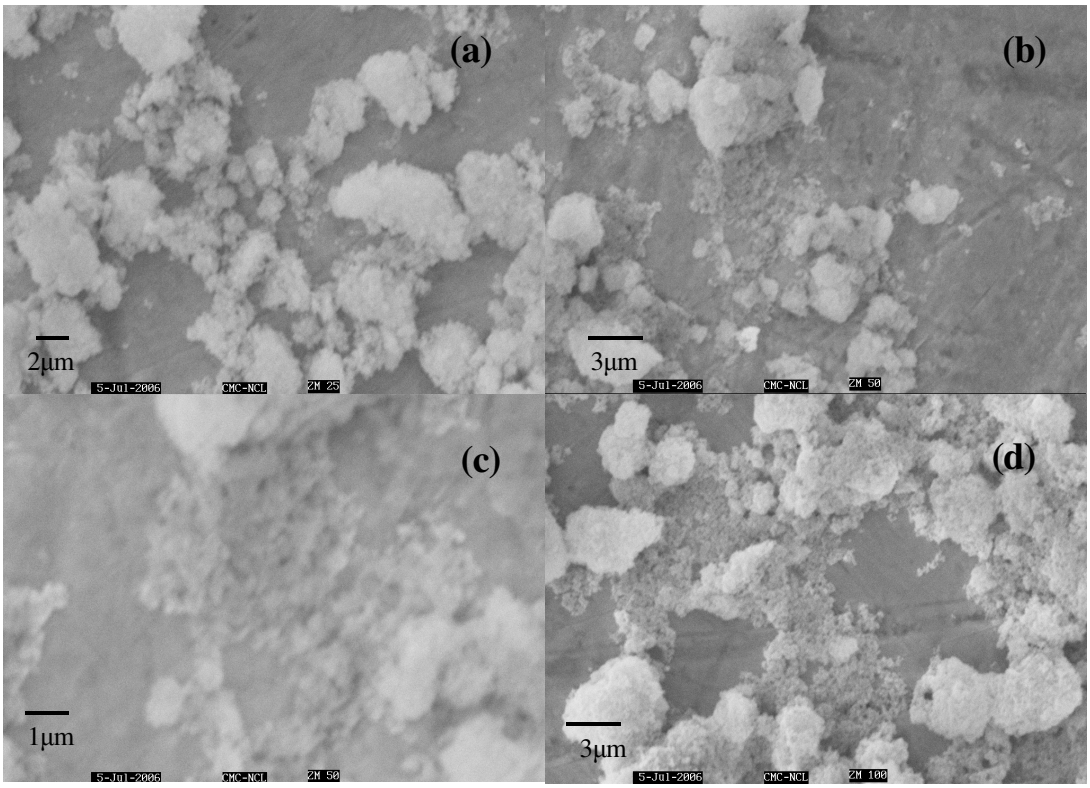

***Fig. 2.16**. SEM images of the fresh $Zn_xMn_{3-x}O_4$ catalysts (a) $ZM_{0.25}$ (b) $ZM_{0.5}$ (c) $ZM_{0.75}$ (d) $ZM_{1.0}$*

2.6. Copper-Zinc-Manganese Oxide spinels

2.6.1. Catalyst composition and structural characterization

Catalyst composition, specific surface area and crystalline phases of copper-zinc-manganese oxides obtained after calcination at 773 K are reported in Table 2.9. Catalyst composition significantly influenced the surface areas of these oxides. The catalyst with equal molar concentration of metals in the mixed oxide ($Cu_{1.0}Zn_{1.0}Mn_{1.0}O_4$) showed high surface area values. The CZM1 and CZM2 samples were crystallized mostly as cubic ($Cu_{1.5}Mn_{1.5}O_4$) phase, while CZM3 has tetragonal $ZnMn_2O_4$ as the major phase. All the three samples contain Mn_2O_3 as minor phase. The XRD patterns (Fig.2.17) indicate that there are no peaks that correspond to single oxides such as CuO and ZnO. Hence, it appears that the solid solution was formed by the isomorphous substitution of Zn^{2+} and Cu^{2+} ions in the tetrahedral sites of the spinel lattice (tetrahedral ionic radii of Cu^{2+} and Zn^{2+} are 0.57 and 0.60 A^o) [67]. Hence, based on the previous XRD data (Fig.2.1 and 2.11), it is interpreted that Cu^{2+}/Zn^{2+} have substituted Mn^{2+} ions in hausmannite lattice until it attains the composition of MMn_2O_4 ($M \leq 1$, M = Cu or Zn) reached. On further increasing the M, it may substitute Mn^{3+} in octahedral sites, resulting in the formation of Mn^{2+} and Mn^{4+} [67]. However, due to d^{10} electronic configuration, the Zn^{2+} cations are highly stabilized in the tetrahedral sites of spinel structure [33].

Table 2.9. *Physico-chemical properties of copper zinc manganese oxide catalysts*

Catalyst	Composition	Crystalline phases	Crystallite sizes (nm)	BET surface area (m^2/g)
CZM1	$Cu_{1.0}Zn_{0.5}Mn_{1.5}O_4$	$Cu_{1.5}Mn_{1.5}O_4$, Mn_2O_3	11	35
CZM2	$Cu_{1.0}Zn_{1.0}Mn_{1.0}O_4$	$Cu_{1.5}Mn_{1.5}O_4$, Mn_2O_3	12	61
CZM3	$Cu_{0.5}Zn_{1.0}Mn_{1.5}O_4$	$ZnMn_2O_4$, Mn_2O_3	21	35

X-ray powder pattern of the catalysts show that high Cu containing samples contain $Cu_{1.5}Mn_{1.5}O_4$ phase while CZM3 with lower Cu was found to be in hausmannite ($ZnMn_2O_4$) phase. However, all the catalysts showed diffraction lines that belong to

Mn_2O_3. No additional diffraction peaks that can be assigned to individual copper or zinc oxides were observed. This observation may be due to formation of solid solution is incorporation of Cu^{1+}/Cu^{2+} and Zn^{2+} ions into spinel lattice with high content of zinc or copper. XRD results suggest that when the concentration of Cu decreased in the composition, $ZnMn_2O_4$ spinel phase was predominant. It has been reported that Cu and Zn have a preference for tetrahedral sites and the degree of inversion in $CuMn_2O_4$ and $ZnMn_2O_4$ is only 10% [33]. Catalysts with equal proportions of copper and zinc gave cubic spinel structure due to red-ox equilibrium present among constituent metal ions. Therefore, it may be stated that copper ion concentration determines the crystalline phase. Though considerable content of copper is present in CZM3, it formed distorted tetragonal hausmannite phase, due to the preference of Zn^{2+} ions for tetrahedral sites at ambient conditions. Hence, increase in the concentration of Zn^{2+} did not induce phase transformation (Fig.2.11). This may be due to the high preference of Zn^{2+} ion for tetrahedral sites in a spinel than Cu^{2+}. Hence, it may be concluded that substitution of copper induces significant phase transformation compared to zinc, which may be attributed to John Teller effect of Cu^{2+} ions (section 2.4.2)**.**

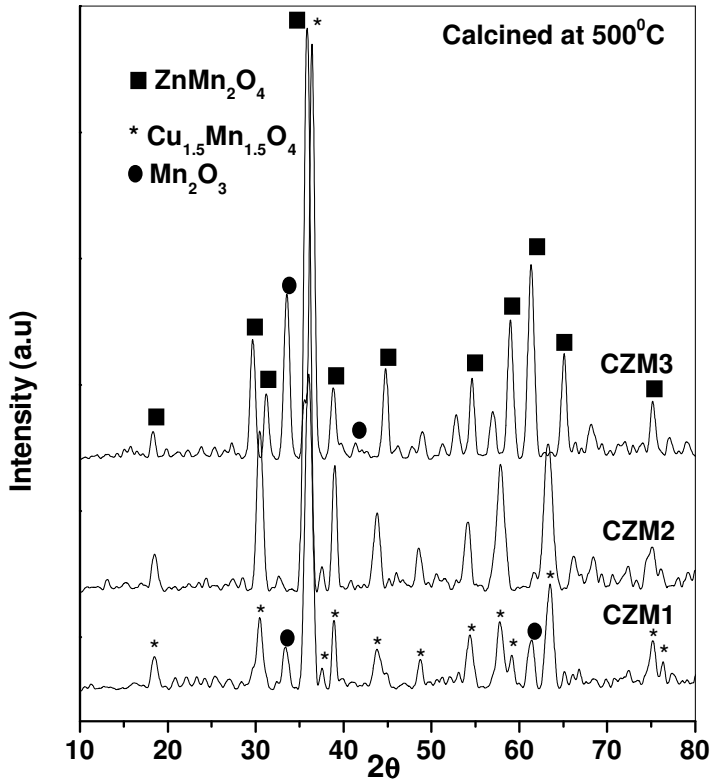

Fig.2.17. *XRD of calcined copper-zinc-manganese spinel type mixed oxides*

2.6.2. Copper dispersion and particles size

The results of copper surface area, its dispersion and average crystallite sizes in various Cu-Zn-Mn-O spinel samples, determined by nitrous oxide decomposition, have been summarized in Table 2.10.

Table 2.10. *Copper dispersion, metal surface area and average crystallite size of copper zinc manganese oxide catalysts calcined at 773 K.*

Catalyst	Copper content (wt%)	Cu dispersion D_{Cu}	Copper metal surface area (m^2/g Cu)	Cu crystallite size (nm)
CZM1	23.2	16	106	6.3
CZM2	22.8	17	107	6.2
CZM3	12.1	52	180	3.7

The copper surface area values varied from 106 to 180 m^2/g and the copper dispersion from 16 to 52%. While the average Cu crystallite size varies from 6.3 to 3.7 nm, which was expected, as dispersion is a function of copper content. However, not much variation was observed between CZM1 and CZM2, as the copper contents were almost same. This may also be attributed to the formation of identical crystalline phases. Crystallite sizes of the dispersed copper of CZM_x samples are in full agreement with the dispersion and surface area values. The N_2O decomposition results suggest that higher copper containing samples have dense copper species; in other words more intimate coordination with neighboring Mn or Zn ions. However, the copper may also be present in the bulk when copper in the samples is higher. In addition to this, the phases may also determine the Cu dispersion and crystallite sizes. In case of CZM3, the copper dispersion was found to be relatively high with smaller crystallite sizes. The major crystalline phase in case of CZM3 was $ZnMn_2O_4$, without the presence of characteristic CuO peaks. Hence, it is believed that copper was highly distributed in $ZnMn_2O_4$ lattice without inducing any structural changes in the tetragonal spinel unlike copper rich manganites (section 2.4.2).

2.6.3. Thermal analysis

Thermal analysis (TG, DTG and DTA) of Cu-Zn-Mn hydroxide precursors obtained in nitrogen flow is presented in Fig.2.18.

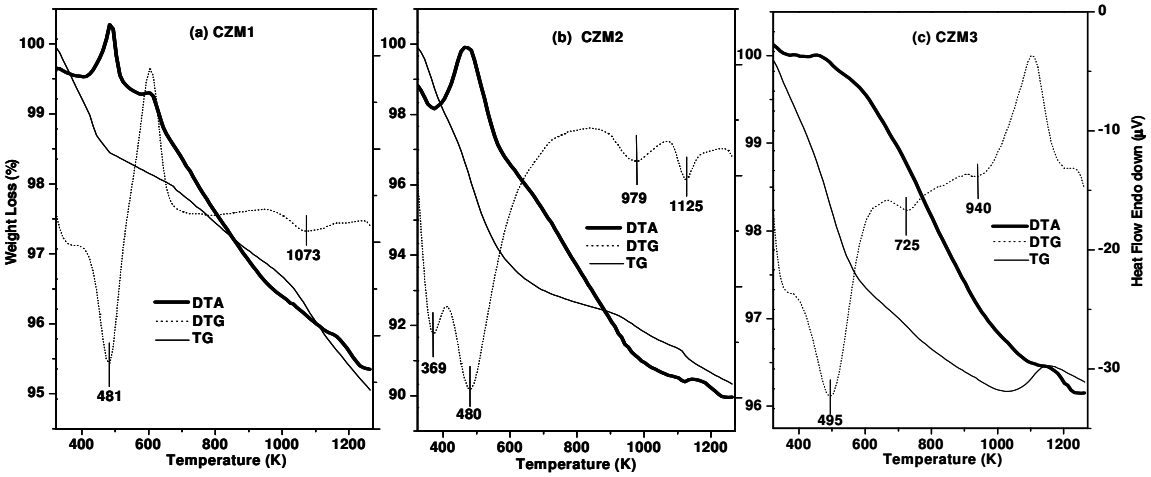

Fig.2.18. *TG-DTA analysis of copper-zinc-manganese spinel catalysts (a) CZM1 (b) CZM2 (c) CZM3*

The thermograms of the samples show two weights lose below 573K. These weight losses occurred at about 365 and 485 K corresponding to removal of physisorbed water and dehydration of metal hydroxides, respectively. The associated weight losses below 673 K are 2, 7 and 3% for CZM1, CZM2 and CZM3 samples, respectively. While the total weight losses observed on heting uptor 1273 K in air are 5, 9.5 and 3.5 wt% occurred for CZM1, CZM2 and CZM3, respectively. The DTA shows exothermic peak corresponding to weight losses due to water removal as expected for this process [54]. Unlike in case of CM_x series decomposition at high temperatures is not observed (absence of DTG peak at about 950 K). It is therefore inferred that presence of zinc in the spinel hindered the decomposition and increased the thermal stability of zinc rich manganites samples as was reported [54,57].

2.6.4. Temperature programmed desorption

TPD of ammonia profiles that through light on acidity of Cu-Zn-Mn oxide catalysts are presented in Fig.2.19. Desorption of NH_3 occurred in the temperature range of 373 to 573 K. From the deconvolution of these spectra the NH_3 desorbed at low temperatures centered at about ~450 K (T_{max}) and this is attributed to weak acidity. However, desorption peaks were rather broad in nature. No considerable shift in low temperature desorption peak maximum (T_{max}~ 450 K) was observed with variation in catalyst composition. CZM2 catalyst shows clearly two peak maxima with a higher temperature peak at about 552 K, which can be attributed to the presence of moderate acidity on this sample.

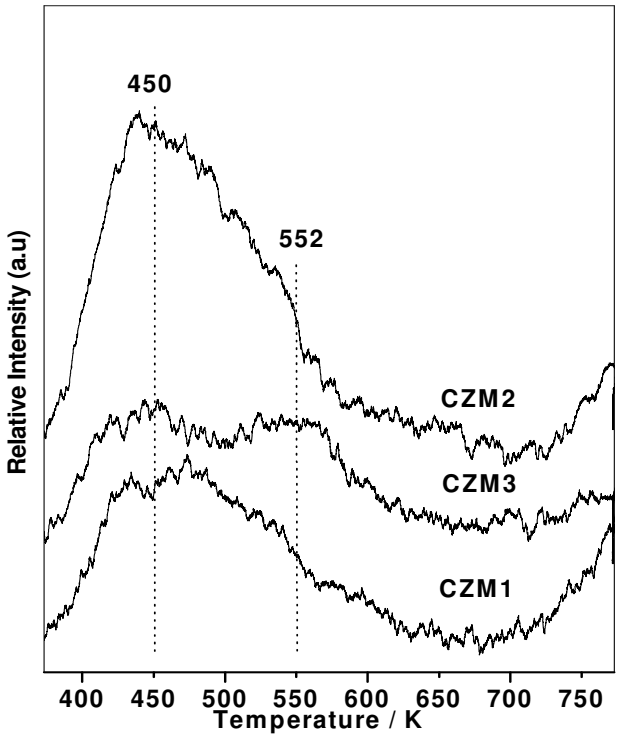

Fig.2.19. *Temperature programmed desorption of NH_3 on copper-zinc-manganese oxide catalysts calcined at 773 K.*

Based on the relative peak intensities as well as quantitative estimation of desorbed ammonia, it was observed that CZM2 has acid sites with higher strength compared to other catalysts. A quantitative approach is adopted for comparison of relative acidity of the catalysts, as exact determination of acid sites is not possible. Further from the acidity

profiles, no clear distinction of the peak maxima can be seen, that can provide information related to the strength/density of acid sites. The acidity of the catalysts is influenced by catalyst composition, and the catalyst containing equal atomic percentages of metals (i.e. Cu and Zn in CZM2) show higher total acidity as well as relatively stronger acidity (T_{max} = 552 K). The total concentration of ammonia desorbed due to weak and moderate acidity is given in Table 2.11.

Table 2.11. *NH_3 desorbed during temperature programmed desorption of ammonia on Cu-Zn-Mn-O catalysts calcined at 773 K.*

Catalyst	T_{max} (K)	Total NH_3 desorbed (mmol/g)
CZM1	450, 552	0.12
CZM2	450, 552	0.224
CZM3	~450, ~530	0.053

An increase in the acidity of CZM2 compared to other catalysts may be due to appropriate concentration of $Cu^{2+/1+}$, Zn^{2+} or Mn^{3+} in it. In addition, surface concentrations of each of the metal ions also determine the acid-base character of the catalyst.

2.6.5. Temperature programmed reduction

Hydrogen consumption during TPR of copper-zinc-manganese oxide catalysts is presented in Table 2.12.

Table 2.12. *H_2 consumption obtained from TPR of coppe-zin-manganese oxide catalysts*

Catalyst	T_{max1} (K)	H_2 consumption (mmol/g)	T_{max2} (K)	H_2 consumption (mmol/g)
CZM 1	470	0.238	610	12.41
CZM 2	461	0.418	568	8.81
CZM 3	468	---	553	7.90

A quantitative approach based on total hydrogen consumption as well as relative ease of reduction is employed for comparison of catalysts for the determination of

reducibility. The XRD of catalysts after TPR study showed formation of Cu metal, ZnO and MnO. It was observed that the intensity of low temperature shoulder decreased with decreasing copper content (Fig.2.20).

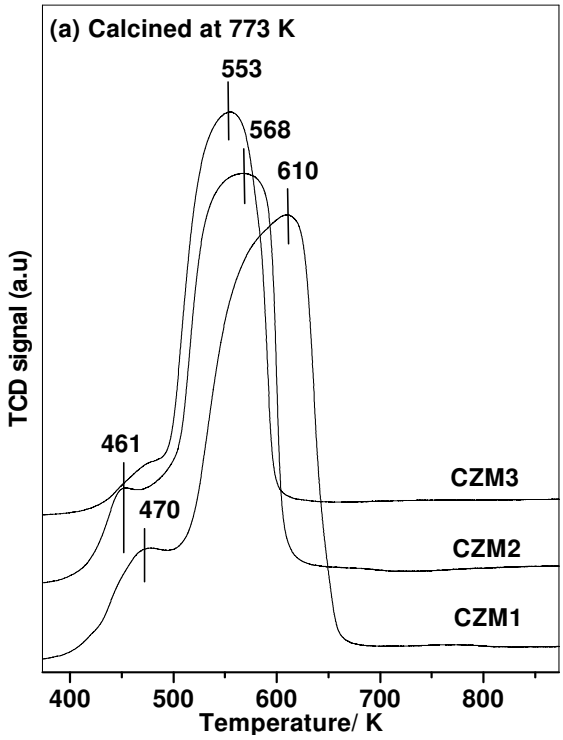

Fig.2.20*. TPR profiles of copper zinc manganese oxide catalysts*

Therefore, this peak can be assigned to surface copper species. The broad main reduction peak can be assigned to both bulk copper ions as well as manganese ions of $Cu_{1.5}Mn_{1.5}O_4$ phase. The low temperature shift of main reduction peak (T_{max}) reveals the important role of concentrations of constituent ions in the sample. TPR shows a broad intense reduction peak (with a shoulder at lower temperatures) below 700 K, for all the catalysts. These catalysts, after calcination at 773 K showed temperature maxima at 610, 568 and 553 K for CZM1, CZM2 and CZM3 catalysts, respectively. These catalysts showed a broad shoulder in the range of 450 and 480 K. A shift in the T_{max} of main reduction peak is found as a function of catalyst composition. Similarly, these catalysts after calcinations at 993 K showed the main reduction peak centered at 589, 621 and 644 K for CZM1, CZM2 and CZM3, respectively as well as low temperature shoulder centered at 487 K. However, these catalysts showed a shift in the T_{max} towards higher temperatures. It is noted that

reduction peaks are rather broad compared to Cu-Mn or Zn-Mn oxide catalysts (Fig.2.6 and 2.15). This observation may be due to different environments reducible ions surrounded by other constituent ions.

2.6.7. X-ray photoemission spectroscopy

Cu 2p core level and Cu-LMM spectra: Cu 2p photoemission spectra and XAES of calcined CZM_x catalysts are presented in Fig.2.21. These spectra from Cu $2p_{3/2}$ exhibited the main line at 933.7 ± 0.1 eV while the FWHM values are 3.2, 2.9 and 3.2 ± 0.1 eV for CZM1, CZM2 and CZM3, respectively (Fig2.21a).

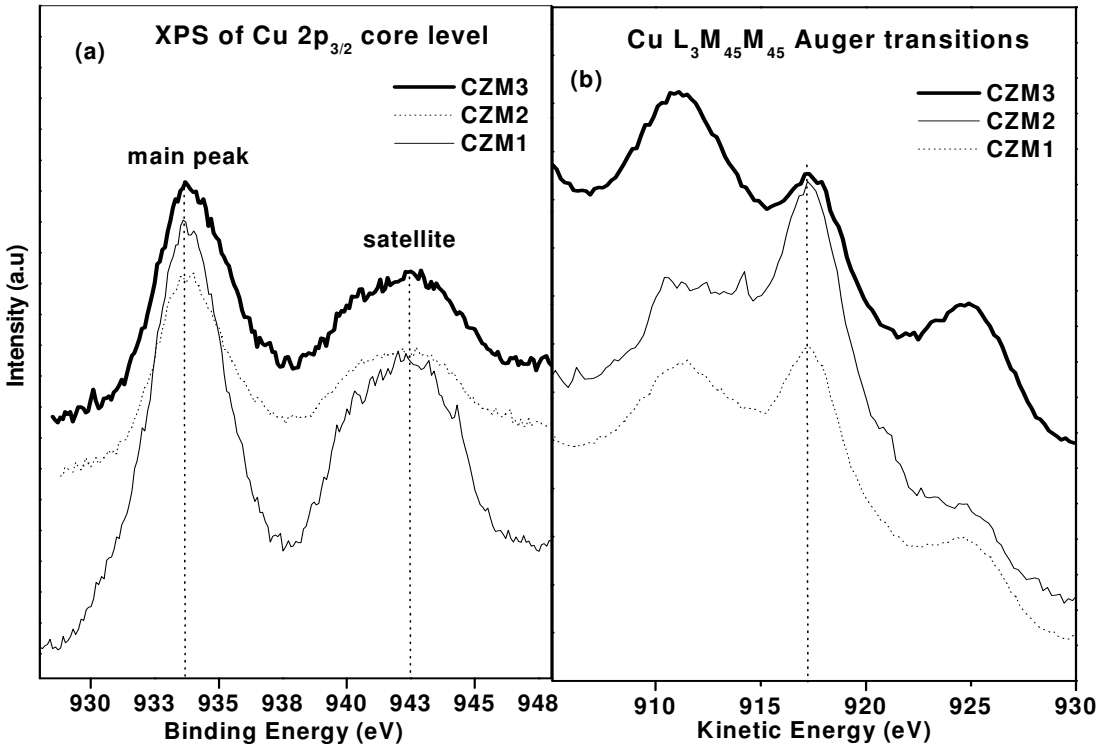

Fig.2.21. *(a) Cu2p core level XPS spectra and (b) Auger electron spectra from Cu-LMM of calcined Cu-Zn-Mn spinel catalysts*

This value of 933.7 ± 0.1 eV for all the samples reveals that the concentration of zinc did not influence markedly the surrounding electron density of Cu. However, the concentration of zinc influenced the FWHM values. The good satellite intensity observed at about 941.5 ± 0.1 eV; indicate the existence of Cu^{2+} ions. There are no peaks observed due to Cu^{1+} ions at lower BE values as observed for high copper containing samples

(Fig.2.9). However, some amount of Cu^{1+} at the surface cannot be ruled out due to broad nature the peaks. The Cu-LMM Auger spectra of these catalysts are presented in Fig.2.21b, which exhibited LMM line at KE of 917.3 ± 0.1 eV corresponding to CuO.

The Mn 2p and Zn 2p core levels: The photoemission spectra of Mn 2p and Zn2p are presented in Fig.2.22. All the catalysts exhibited binding energy values of 642.2 ± 0.1 eV with ΔE of 11.5 ± 0.1 eV. Though these BE values are in good agreement with the hausmannite structure, it is very difficult to distinguish and differentiate the various oxidation states of Mn like Mn^{2+}, Mn^{3+} and Mn^{4+} in these samples. The BE values of Zn 2p core level for all the three samples was calculated at 1021.1 ± 0.1 eV, while FWHM values are 2.3, 2.3 and 2.5 ± 0.1 eV for CZM1, CZM2 and CZM3, respectively. This value is very close to the BE of ZnO (1022 eV) [75]. There is noticeable increase in the FWHM in case of CZM3, which may be due to the possible contribution of Zn^{2+} in $ZnMn_2O_4$.

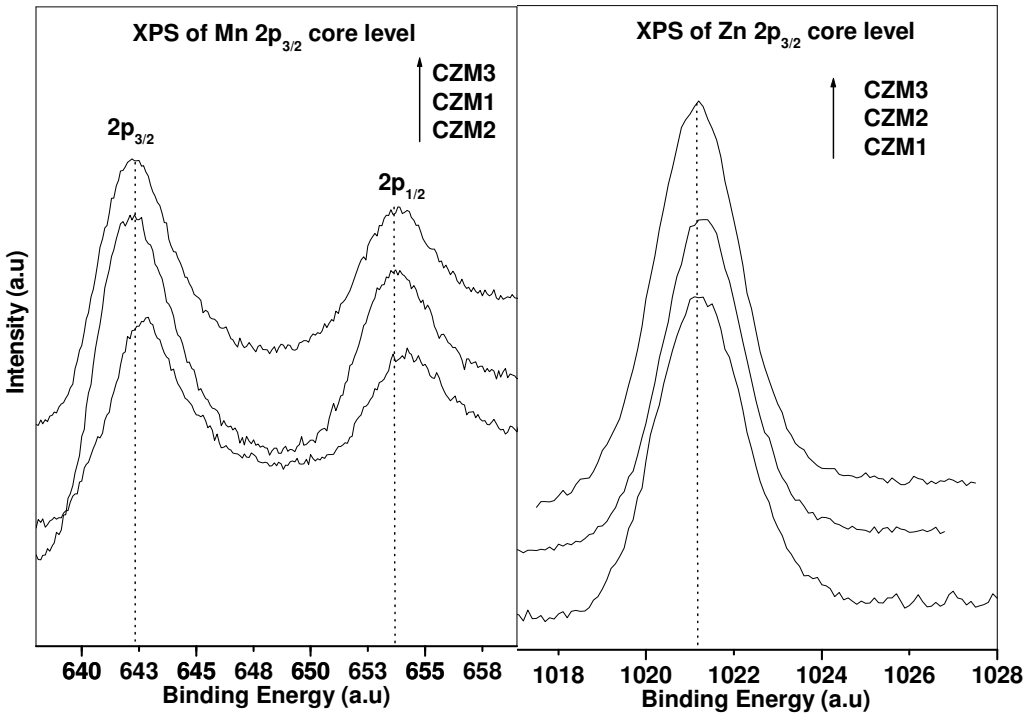

Fig.2.22. *(a) Mn2p and (b) Zn2p core level XPS spectra of calcined Cu-Zn-Mn spinel catalysts*

The valance band photoemission: XPS spectra of valance band (VB) region obtained for calcined CZM catalysts are shown in Fig.2.23.

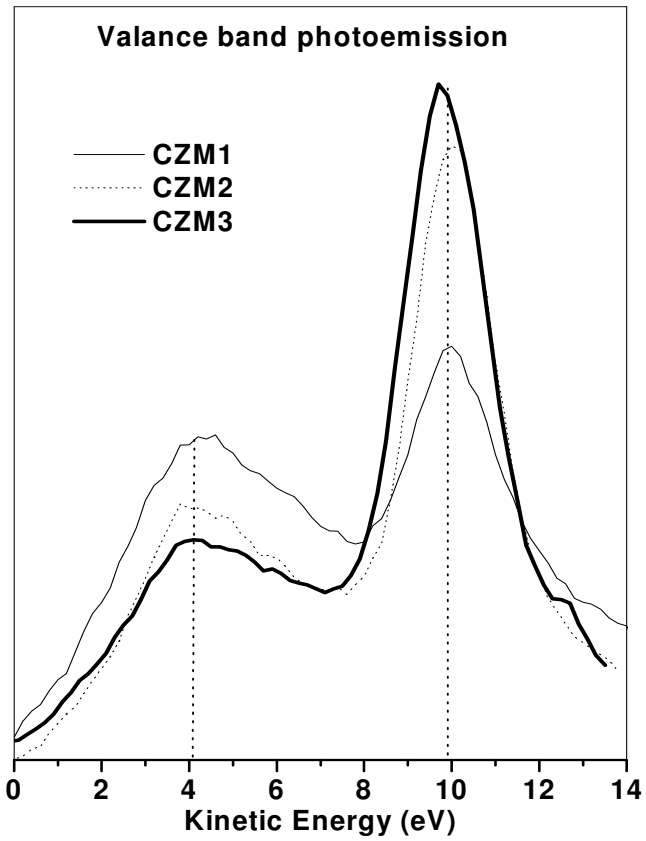

Fig.2.23. *Valance band spectra of calcined Cu-Zn-Mn spinel catalysts*

The main VB observed below 8 eV has contributions from 3d orbitals of Cu, and Mn. At the hν = 1253.6 eV used in these experiments, the photoionization cross-section (σ) value (Cu 3d = 0.021, Mn = 0.0026, and O 2p = 0.0005 Mb). The above data suggests that the contribution from O 2p was negligible. Similarly, Cu 3d should make significant contributions to the VB. The intensity of VB around 4 eV is due to Cu 3d and Mn 3d bands. It is seen that the intensity of this band is high with higher concentration of Cu. The band at 10 eV is assigned to Zn 3d, which marginally shifted to lower BE (for CMZ1). These points suggest that the changes in VB were significant with the concentration of copper and zinc.

2.6.7. Scanning electron spectroscopy

To study the influence of catalyst composition on the morphology of particles, SEM was employed to examine the general features of calcined catalysts and presented in Fig.2.24. There is a clear distinction in the morphology of the catalysts. CZM1 showed the larger aggregates of particles with out uniform size or shape. When the amount of zinc was increased to that of copper (wt %), the needle like structures are formed. Needle like morphology was also found for $CM_{1.0}$. Careful examination of SEM image for CZM3 shows a mixture of needles and shapeless crystallite aggregates. The needle like structures generally offers higher surface area, which is true in this case. Hence, SEM images of the catalysts clearly demonstrate the effect of catalyst composition on morphology change.

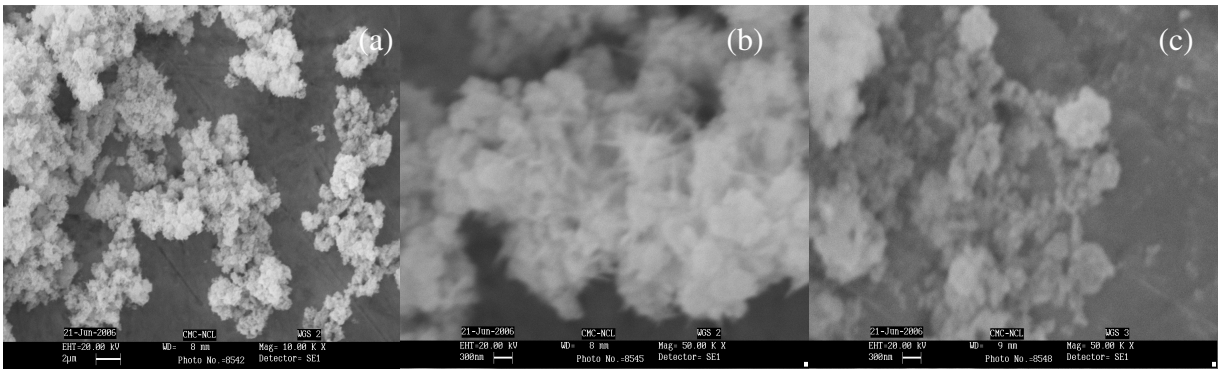

Fig.2.24. *SEM images of copper-zinc-manganese mixed oxide catalysts (A) CZM1 (B) CZM2 (C) CZM3 calcined at 773 K.*

2.7. References

[1] P. Ratnasamy, D. Srinivas, C.V.V. Satyanarayana, P. Manikandan, R.S. Senthil Kumaran, M. Sachin, V.N. Shetti, J. Catal. 221 (2004) 455.

[2] S. Brunauer, P.H. Emmett, E. Teller, J. Am. Chem. Soc. 60 (1938) 309.

[3] B. Imelik, in: B. Imelik, J.C. Vedrine, (Eds.), Catalyst Characterization: Physical Techniques for Solid Materials, Plenum Press, 1994, Chap.15.

[4] J.M. Thomas, W.J. Thomas, Principles and Practice of Heterogeneous catalysis, VCH, Weinheim, 1997.

[5] W.N. Delgass, G.L. Haller, R. Kellerman, J.H. Lunsford, Spectroscopy in Heterogeneous Catalysis, Academic Press, New York, 1979, Chap. 4.

[6] B.M. Weckhuysen, R.A. Schoonheydt, Catal. Today 49 (1999) 441.

[7] R. A. Schoonheydt, in: F. Delanny, (Eds.), Diffuse Reflectance Spectroscopy: Characterization of Heterogeneous Catalysts, Marcel Dekker Inc., 1984, p. 125

[8] J.L.G. Fierro, in: J.L.G. Fierro, (Eds.), Spectroscopic Characterization of Heterogeneous Catalysis, Part B, Elsevier, Amsterdam, 1990, p. 67.

[9] G. Coudurier, F. Lefebvre, in: B. Imelik, J.C. Vedrine (Eds.), Catalyst Characterization: Physical Techniques for Solid Materials, Plenum Press, New York, (1994) p.11.

[10] H. Knozinger, in: H.H. Brongersma, R.A. van Santen, (Eds.), Fundamental Aspects of Heterogeneous Catalysis Studied by Particle Beams, Plenum Press, New York, 1991, p. 167.

[11] W.W. Wendlandt, H.G. Hecht, Reflectance Spectroscopy, Plenum Press, New York 1968.

[12] W.W. Wendlandt, Thermal Methods of Analysis, John Wiley, New York, 1964.

[13] C. Duval, R.E. Oesper, Inorganic Thermogravimetric Analysis, Elsevier, Amsterdam, 1963.

[14] S.B. Sharma, B.L. Meyers, D.T. Chen, J. Miller, J.A. Dumesic, Appl. Catal. A 102 (1993) 253.

[15] H.G. Karge, V. Dondur, J. Phy. Chem. 94 (1990) 765.

[16] G.K.S. Prakash, G.A. Olah, in: K. Tanabe, H. Hattori, I. Yamaguchi, I. Tanaka

(Eds.), Acid-Base Catalysis, VCH, New York, 1989, p. 59.

[17] J.L. Falconer, J.A. Schwarz, Catal. Rev. Sci. Eng. 25 (1983) 141.

[18] N.W. Hurst, S.J. Gentry, A. Jones, Catal. Rev. Sci. Eng. 24 (1982) 233.

[19] B. Bhatia, J. Beltramini, D.D. Do, Catal. Today 7 (1990) 309.

[20] B. Dvorak, J. Pasek, J. Catal. 18 (1970) 108.

[21] G. Sengupta, D.K. Gupta, M.L. Kundu, S.P. Sen, J. Catal. 67 (1981) 223.

[22] A. Gervasini, S. Bennici, Appl. Catal. A 281 (2005) 199.

[23] J.W. Niemantsverdriet, Spectroscopic methods in Heterogeneous catalysis, VCH, Weinheim, 1993.

[24] W.N. Delgass, T.R. Hughes, C.S. Fadley, Catal. Rev. 4 (1970) 179.

[25] C.S. Fadley, in: C.R. Brundle, A.D. Baker, (Eds.), Electron Spectroscopy: Theory, Techniques and Applications, Academic Press, New York (1978), Chap. 1

[26] W.F. Egelhoff Jr, Surface Science Reports 6 (1987) 253.

[27] G. Moretti, in: G. Ertl, H. Knozinger, J. Weitkamp, (Eds.), Handbook of Heterogeneous Catalysis, Wiley-VCH, vol.2, 1997, p. 632.

[28] T. Mathew, N.R. Shiju, K. Sreekumar, B.S. Rao, C.S. Gopinath, J. Catal. 210 (2002) 405.

[29] A.K. Datye, D.J. Smith, Catal. Rev. Sci. Eng. 35 (1992) 129.

[30] H. Poppa, Catal. Rev. Sci. Eng. 35 (1993) 359.

[31] M.J. Yacaman, G. Diaz, A. Gomez, Cata. Today 23 (1995) 161.

[32] A. Miller, J. Appl. Phys. 31 (1960) 261 S

[33] F.C.M. Driessens, Inorganica Chimica Acta 1 (1) (1967) 193.

[34] B. Gillot, S. Buguet, E. Kester, J. Mater. Chem., 7(12) (1997) 2513.

[35] A.D.D. Broemme, V.A.M. Brabers, Solid State Ionics 16 (1985) 171.

[36] A.P.B. Sinha, N.R. Sanjana, A.B. Biswas, Acta. Cryst. 10 (1957) 439.

[37] R. Buhl, J. Phys. Chem. Solids 30 (1969) 805.

[38] R.E. Vandenberghe, G.G. Robbrecht, V.A. M. Brabers, Mater. Res. Bull. 8 (1973) 571.

[39] V.S. Escribano, E.F. López, P.S. Huidobro, M. Panizza. C. Resini, J.M. Gallardo-Amores, G. Busca, Solid State Sci. 5 (2003) 1481.

[40] F. Milella, J.M. Gallardo-Amores, M. Baldi, G. Busca, J. Mater. Chem. 8 (11) (1998)

2525.

[41] V.S. Stubican, C. Greskovich, Geochim. Cosmochim. Acta, 39 (1975) 875.

[42] F. Lavalille, D. Gourier, A.M. Lejus, D. Vivian, J. Solid. Stat. Chem. 49 (1983) 180.

[43] N.N. Greenwood, A. Earnshaw, Chemistry of the Elements, Pergamon, Oxford, fifth edn., 1995, p. 1231.

[44] D.M. Sherman, N. Vergo, The American Mineralogist. 73 (1988) 140.

[45] W.S. Kijlstra, E.K. Poels, A. Bliek, B.M. Weckhuysen, R.A. Schoonheydt, J. Phys. Chem. B 101 (1997) 309.

[46] J.M. Gallardo-Amores, T. Armaroli, G. Ramisi, E. Finocchio, G. Busca, Appl. Catal. B: Environ. 22 (1999) 249.

[47] C.M. Julien, M. Massot, C. Poinsignon, Spectrochim. Acta 28A, 60 (2004) 689

[48] S. Velu, K. Suzuki, M. Okazaki, M.P. Kapoor, T. Osaki, F. Ohashi, J. Catal. 194 (2000) 373.

[49] P. Porta, M.C. Campa, G. Fierro, M. Lo Jacono, G. Minelli, G. Moretti, L. Stoppa, J. Mater. Chem. 3 (5) (1993) 505.

[50] T.J. Richardson and P.N. Ross, Jr., Mater. Res. Bull. 31 (1996) 935

[51] S.M. Rodolfo-Baechler, S.L. González-Cortés, J. Orozco, V. Sagredo, B. Fontal, A.J. Morea, G. Delgado, Mater. Lett. 58 (2004) 2447.

[52] V. Koleva, D. Stoilova, D. Mehandjiev, J. Sol. Stat.Chem., 133 (1997) 416.

[53] G. Fierro, S. Morpurgo, M. Lo Jacono, M. Inversi, I. Pettiti, Appl. Catal. A 166 (1998) 407.

[54] J.V. Dubrawski, React. Solids 2 (1987) 315.

[55] S. Guillemet-Fritsch, C. Chanel, J. Sarrias, S. Bayonne, A. Rousset, X. Alcobe, M.L. Martinez Sarrion, Solid State Ionics, 128 (2000) 233.

[56] G. D. Mukherjee, S.N. Vaidya, C. Karunakaran, Phase Transitions, 75 (2002) 557.

[57] Y. Yongnian, H. Ruili, C. Lin, Z. Jiayu, Appl. Catal. A 101 (1993) 233.

[58] F.W. Chang, W.Y. Kuo, H.C. Yang, Appl.Catal. A 288 (2005) 53.

[59] Z.Yi Ma, C. Yang, W. Wei, W.H.Li, Y.H. Sun, J. Mol. Catal. A: Chem. 231 (2005) 75.

[60] Y. Tanaka, T. Utaka, R. Kikuchi, T. Takeguchi, K. Sasaki, K. Eguchi, J. Catal. 215 (2003) 271.

[61] W.C. Choi, J.S. Kim, T.H. Lee, S.I. Woo, Catal. Today 63 (2000) 229.

[62] C.D. Wagner, W.M. Riggs, L.E. Davis, J.F. Moulder, Hand book of X-ray Photoelectron Spectroscopy, Perkin Elmer Corp. Physical Electronics Div. Eden Prairie, MN, (1979).

[63] N.S. Mclntyre, N.S. Cook, M.G. Anal. Chem. 47 (1975) 2208.

[64] M. Oku, K. Hirokawa, S. Ikeda, J. Electron Spectrosc. 7 (1975) 465.

[65] G.C. Allen, S.J. Harris, J.A. Jutson, J.M. Dyke, Appl. Surf. Sci. 37 (1989) 111.

[66] B.L. Yang, S.F. Chan, W.S. Chang, Y.Z, Chen, J. Catal. 130 (1991) 52.

[67] J.J. Yeh, I. Lindau, At. Data Nucl. Data Tables, vol. 32 (1985) 1.

[68] T. Mathew, N.R. Shiju, K. Sreekumar, B.S. Rao, C.S. Gopinath, J. Catal. 210 (2002) 405.

[69] F. Bosi, S. Lucchesi, A. Della Giusta, American Mineralogist 87 (2002) 1121

[70] M. Okeeffe, J. Phys. Chem. Solids, 21 (1961) 172.

[71] D.G. Wickham, W.J. Croft, J. Phys. Chem. Solids 7 (1958) 351.

[72] F.C.M. Driessens and G.D. Rieck, J. Inorg. Nucl. Chem. 28 (1966) 1593.

[73] J.M. Jocobs, R.F. Parton, A.M. Boden, P.A. Jocobs, Stud. Surf. Sci. Catal. 41 (1988) 221.

[74] A.P.B. Sinha, N.R. sanjana, A.B. Biswas, Acta. Crist. 10 (1957) 439. and ref. 72

[75] M. Vijayaraj, C.S. Gopinath, J. Catal. 241 (2006) 83

CHAPTER 3

METHYLATION OF PHENOL ON MIXED OXIDE SPINELS

3.1. Introduction

Structure sensitive catalytic reactions give an opportunity to correlate the performance with the surface and bulk properties of catalysts. The ability to measure the concentration and the dispersion of active species on the catalyst using various characterization techniques helps in specifying active sites that give a desired product in a particular reaction. The extent of product formation in a reaction can be compared with the specific catalytic site densities on the catalyst. Investigation of complex metal oxide systems for their activity has been primarily targeted at monitoring the changes in the oxidation state and nature of the adsorbed species. Identification of active species on oxide catalysts has generally been based on some kind of spectral analysis of an adsorbed species. However, these techniques usually may not always provide the complete information needed to describe the active sites accurately. In case of complex metal oxide systems, drawing definite conclusions on the nature of the active sites under the experimental conditions has not been established adequately [1,2].

Electronic properties of metal oxide catalysts determined by XPS provide information on various oxidation states of the active species and their respective densities. XRD analysis provides information about the active crystalline phases that are responsible for chemical reaction. Infrared data of chemisorbed probe molecules such as CO, CO_2, NH_3 and pyridine etc. reveal the presence of types of active species. Temperature programmed desorption of probe molecules on catalyst surface indicate the presence of active sites differing in their ease of desorption, which can be quantified. TPR and TPO data from metal oxide catalysts provides significant information regarding red-ox nature of the system, particularly if they are to be used in oxidation/reduction reaction. In this chapter, the structural and acid-base properties (obtained by XRD, XPS and TPD etc.) of Cu-Mn-O, Zn-Mn-O and Cu-Zn-Mn-O catalysts have been correlated with their catalytic activity for phenol methylation.

3.2. Methylation of spinels on Cu-Mn spinels

3.2.1. Effect of catalyst composition

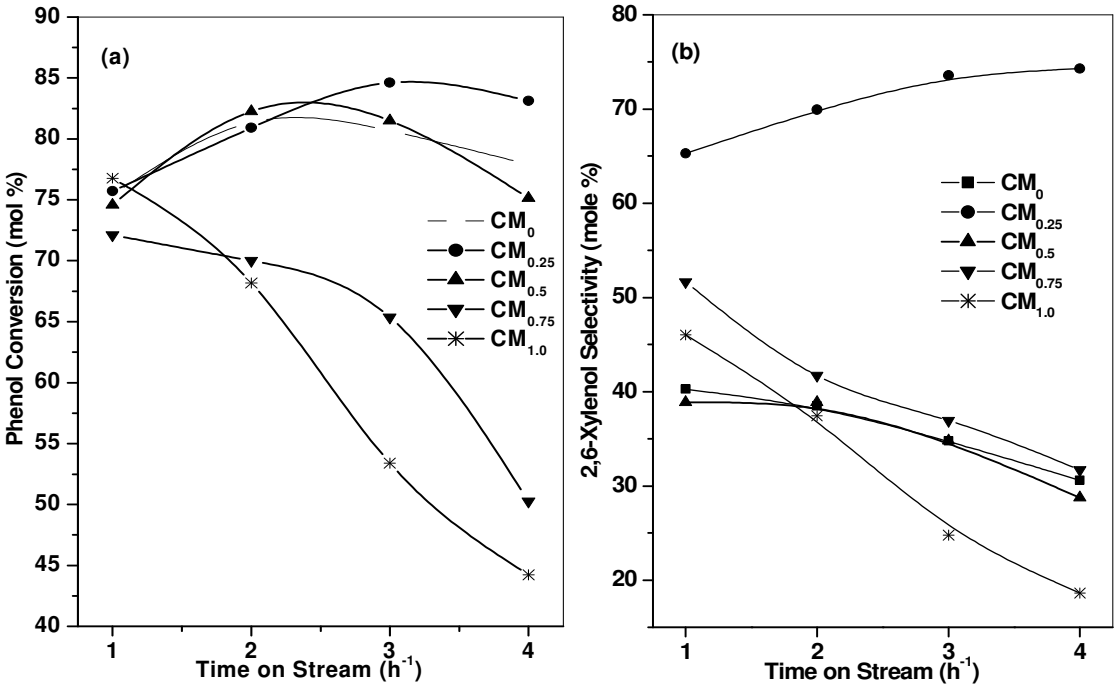

Fig.3.1. *Effect of catalyst composition on (a) phenol conversion and (b) 2,6-xylenol selectivity on copper-manganese spinel oxide catalysts at 673 K. (MeOH/phenol = 5, WHSV 1h^{-1})*

Fig.3.1 shows variation of phenol conversion and 2,6-xylenol selectivity with time on stream (TOS) on copper–manganese oxide spinel catalysts at 673 K. The screening of the catalysts was carried out under identical conditions using a methanol-to-phenol ratio of 5 and at a space velocity of 1 h^{-1}. All the catalysts are active and highly selective for methylation of phenol at the *ortho*-position. Phenol alkylation mainly yielded ortho methylated products such as o-cresol and 2,6-xylenol, with a small amount (<2%) of mesitol. Phenol conversion and *o*-cresol/2,6-xylenol selectivity varied significantly with TOS depending on the catalyst composition. The phenol conversion was comparable (around 75%) on all the catalysts up to 1 h TOS. Nonetheless, phenol conversion decreased more rapidly after 3 h on stream on high copper-containing catalysts ($CM_{0.75}$ and $CM_{1.0}$), than compared to the other compositions. The differences in the activity and 2,6-xylenol selectivity were more apparent after 2 h on stream, particularly for samples with $x \geq 0.5$. Hence, it is perceived that phenol conversion does not differ significantly among the

samples with low copper content and it only varies for catalysts that have high copper content ($x \geq 0.75$). The initial activity was maximum on the sample with x = 1. A clear trend was observed in the deactivation of catalysts with increasing amount of copper, which deactivated more rapidly.

Phenol conversion was increased from 72 to 77-mole % initially with increase of copper content (x = 0 to 1.0). But on $CM_{1.0}$ catalyst, it dropped from 77 to 44% after 4 h TOS. However, the catalyst with x = 0.25 showed relatively stable activity and the highest 2,6-xylenol selectivity (~74%). The total *ortho* selectivity remains stable with variation of copper concentration in the samples. It was also relatively constant over time on stream. The catalysts with high copper content either deactivated rapidly or showed lower selectivity to 2,6-xylenol. Pure manganese oxide catalyst prepared in our laboratory was more active at lower temperatures than the reported catalyst prepared from carbonate precursors [3]. The 2,6-xylenol selectivity fell continuously for catalysts with $x > 0.25$, though the initial selectivity's were higher. The $CM_{0.25}$ catalyst demonstrated good activity and 2,6-xylenol selectivity, without much deactivation for the duration of the experiment.

Fig.3.2 shows comparative performance of copper-manganite spinel catalysts in phenol methylation with the variation of catalysts composition against the reaction time. These results suggest that there is an increase in the selectivity of 2,6-xylenol at the expense of *o*-cresol. It is also observed that $CM_{0.25}$ has yielded more 2,6-xylenol with a concomitant decrease in *o*-cresol. This observation reveals that the formation of 2,6-xylenol in phenol methylation is a consecutive reaction.

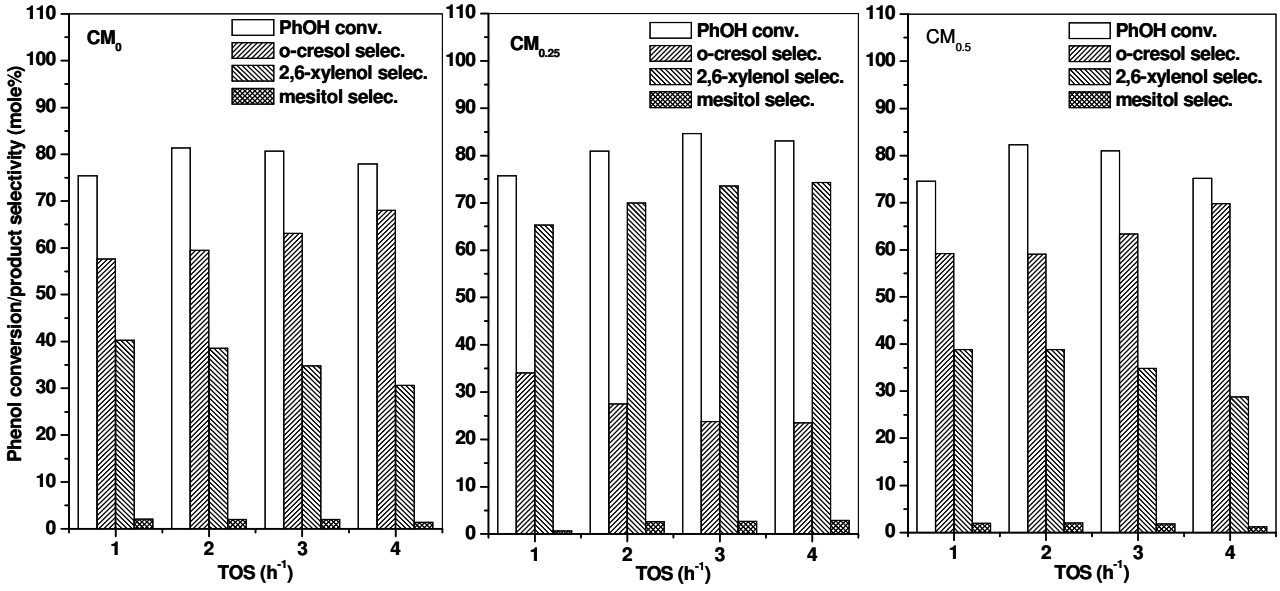

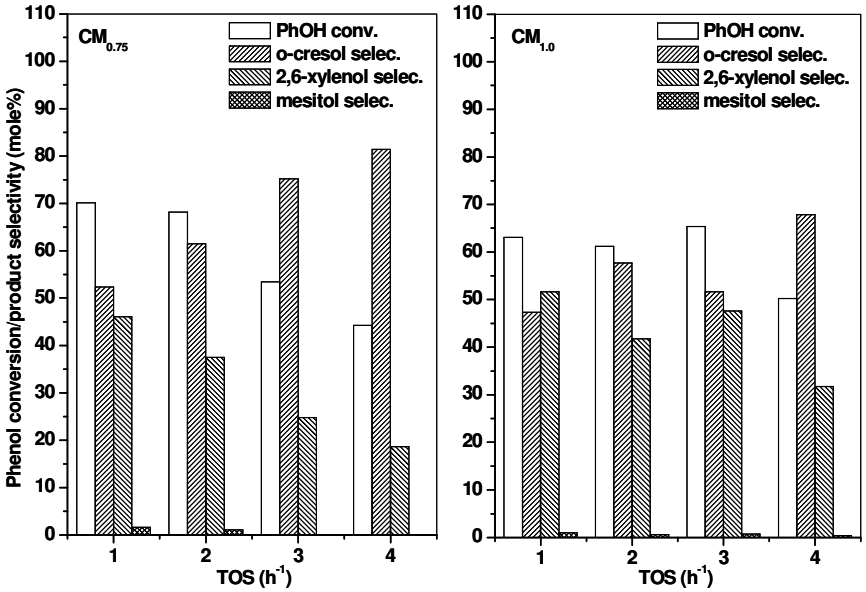

Fig. 3.2. *Phenol conversion and product selectivity's over copper manganese oxide spinel catalysts against time on stream. (WHSV 1h^{-1}, MeOH/phenol = 5, 673K)*

An increase in the concentration of mesitol, which forms on further methylation of 2,6-xylenol, was observed when the concentration of 2,6-xylenol in the products was higher (on $CM_{0.25}$). There was no marked influence of reaction temperature on the product selectivity. .No *O*-alkylated product like anisole was observed during reaction in the temperature range studied in this work. This indicates that methylation occurs directly at the carbon atom at ortho-position of phenol molecule and not *via* anisole isomerization [4]. Hence, these catalysts are claimed to be highly selective to produce ortho-methyl phenols, i.e >98% under optimum conditions.

3.2.2. Effect of reaction temperature

Fig.3.3 shows variation of phenol conversion and selectivity to various ortho-alkyl phenols against the reaction temperature (623-723 K) over $CM_{0.25}$ catalyst, using the feed composition of phenol to methanol mole ratio 1:5 and at WHSV 1h^{-1}. The conversion of phenol increased with temperature, reaching a maximum at 673 K. It remained nearly constant thereafter on further increase in reaction temperature. Similarly, the yield of 2,6-xylenol also reached a maximum at 673 K. An increase in the reaction temperature beyond 673 K led to increased concentration of *o*-cresol, which may be due to de-alkylation of 2,6-

xylenol or non availability of methanol as it undergoes decomposition at higher temperature.

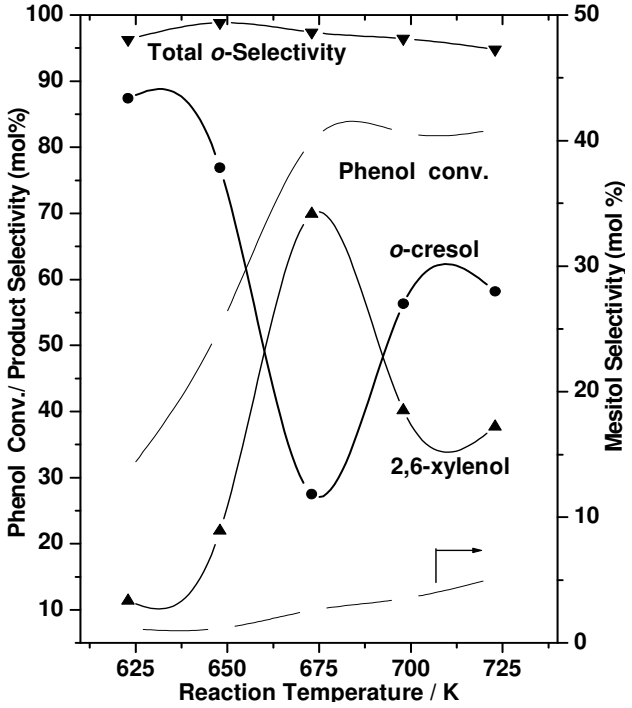

Fig.3.3. *Influence of reaction temperature on phenol conversion and product selectivity on $CM_{0.25}$ catalyst. (MeOH/phenol = 5, WHSV 1h^{-1}, TOS-2)*

The concentration of *o*-cresol was very high at lower temperatures, while it has decreased with increasing reaction temperature, with a concomitant increase in the 2,6-xylenol yield. These findings clearly show that mono-methylation was predominant at lower temperatures, whereas 2,6-xylenol selectivity increased at higher temperatures at the expense of *o*-cresol. Mesitol concentration was also increased with temperature on further alkylation of 2,6-xylenol. Methanol conversion was increased from about 50 to 70% (on the basis of left out MeOH in the product mixture) when the temperature increased from 673 to 723 K. At the same time, no other aliphatic hydrocarbons that can be attributed to oxidative condensation of primary alcohols were observed [5]. No other products formed other than *ortho*-alkyl phenols (except mesitol) over the temperature range studied. The data shows that these catalysts are highly selective in the formation of only *ortho*-methylated products. However, mono-methyl phenol was predominant above 698 K, which may be due to methanol decomposition/reforming that hinders the consecutive methylation of *o*-cresol to 2,6-xylenol.

3.2.3. Effect of phenol to methanol ratio

Alkylation of phenol was carried out using various methanol to phenol molar ratios in the range 2 to 7 over $CM_{0.25}$ at 673 K. Fig.3.4 shows phenol conversion and the product selectivity to various *ortho*-alkylphenols against the feed composition. As may be expected, phenol conversion increased linearly with increasing methanol concentration in the feed, reaching maximum at a phenol to methanol ratio of 1:5. Only a small increase in phenol conversion was observed on further increase of methanol content in the feed. Surprisingly, 2,6-xylenol selectivity also followed a similar trend, while it remained constant for feed ratios grater than 5. In fact, concentration of *o*-cresol in the product dropped from 90 mol% to nearly 24 mol% when methanol-to-phenol mole ratio increased from 7 to 2. Mesitol formation is formed as expected, as result of consecutive alkylation of 2,6-xylenol and its concentration in the product has increased monotonously with the mole ratio. Whereas, 2,6-xylenol selectivity was highest at a ratio of 5, hence this ratio was used for further studies.

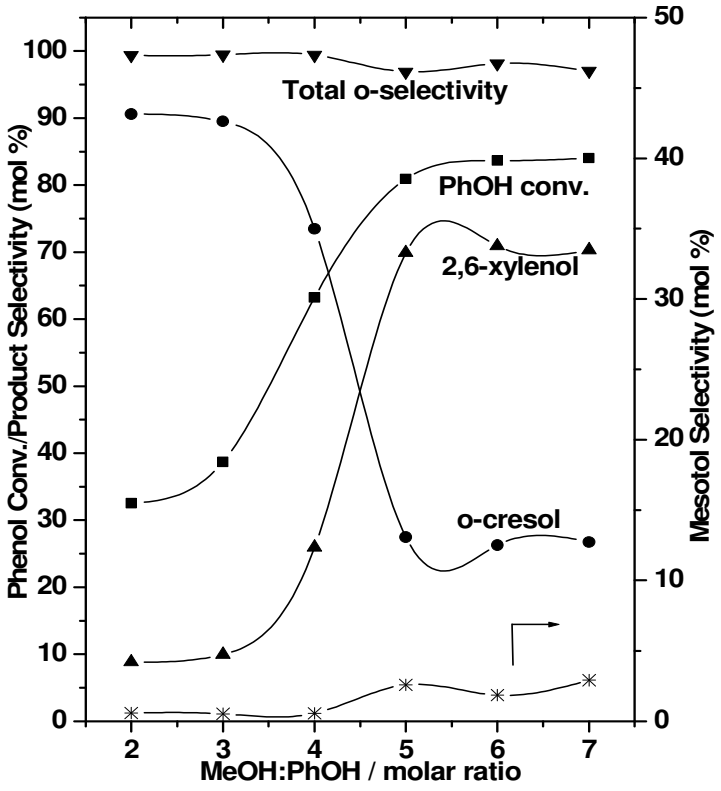

Fig.3.4. *Effect of methanol to phenol mole ratio on phenol conversion and product selectivity. (Catalyst $CM_{0.25,}$ WHSV 1 h^{-1}, 673 K, TOS-2 h)*

The increase in 2,6-xylenol concentration is associated with a concomitant fall in the *o*-cresol concentration. Total *ortho* selectivity of alkylated phenols was nearly 100% at lower methanol to phenol ratio and about 98% at higher ratios. This small reduction in selectivity is attributed to mesitol formation. It is clear that excess methanol is necessary in the reaction feed, though the reaction stoichiometry suggests a MeOH: PhOH ratio of 2 for 2,6-xylenol formation. Since the reaction was carried out at higher temperatures, some amount of methanol may be lost due to undesirable side reactions such as methanol reforming/decomposition.

3.2.4. Effect of space velocity

The effect of space velocity on phenol methylation over $CM_{0.25}$ was studied to obtain optimum space velocity for achieving high 2,6-xylenol selectivity. Reaction was studied at four WHSV values, i.e., 0.5, 1, 1.5 and 2 h^{-1} using 2g of catalyst and methanol to phenol molar ratio of 5 at 673 K. The phenol conversion and selectivity's were dependent on the feed rate shown as shown in Fig.3.5.

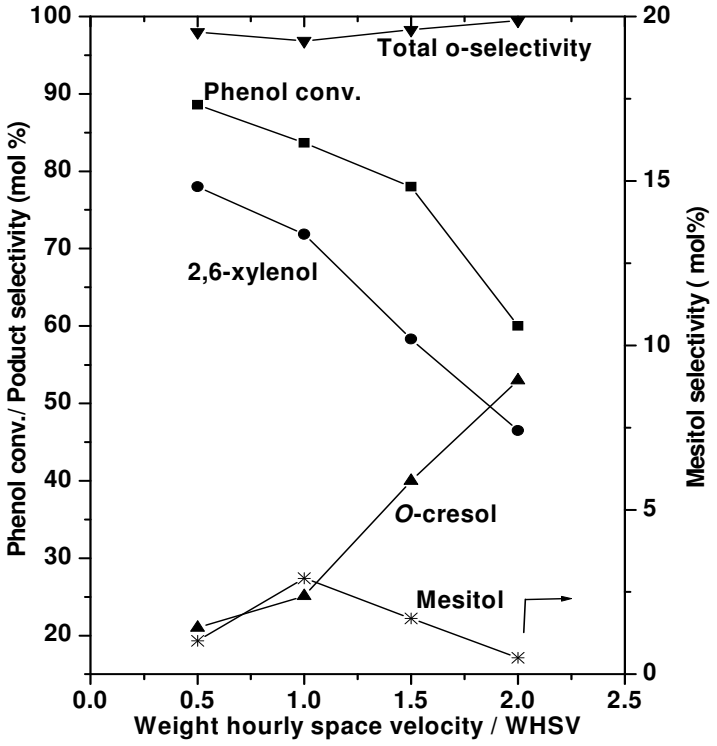

Fig.3.5. *Effect of space velocity (GHSV) on phenol conversion and the product selectivity over* $CM_{0.25}$ *at 673 K. MeOH/ phenol = 5.*

The conversion of phenol and selectivity to 2,6-xylenol decreased as the space velocity was increased, with simultaneous increase in *o*-cresol selectivity. This further shows that *o*-cresol is the primary product and 2,6-xylenol is the secondary product obtained on further alkylation of *o*-cresol. The optimum space velocity to obtain maximum 2,6-xylenol was found to be 1 h^{-1}. Phenol conversion also decreased at higher space velocities and hence further evaluation of the catalysts was carried out at WHSV $1h^{-1}$.

Previous reports show that an increase in contact time (lower space velocity) has always helped in increasing 2,6-xylenol selectivity [6] indicating *o*-cresol is the primary alkylation product. An increase in contact time retains the initially formed *o*-cresol on the catalysts surface and facilitates its consecutive methylation to yield 2,6-xylenol. At high contact times, formation of traces of benzene and toluene were detected on ferrite spinels [7]. However, from our catalyst systems no such compounds were detected in the range of space velocities studied.

3.2.5. Time on stream behavior

Fig.3.6 presents TOS behavior of $CM_{0.25}$ catalyst during phenol methylation at 673 K. $CM_{0.25}$ catalyst was excellent in both conversion of phenol and the selectivity to 2,6-xylenol.

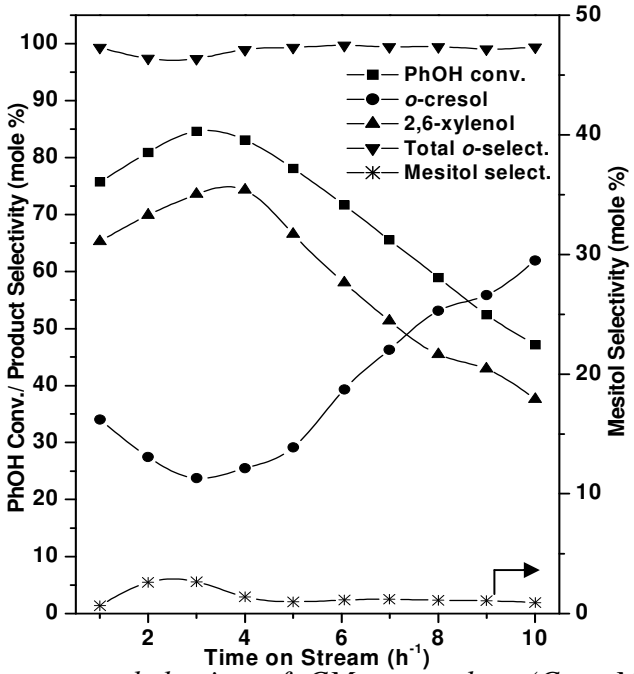

Fig.3.6. *Time on stream behavior of $CM_{0.25}$ catalyst ($Cu_{0.25}Mn_{2.75}O_4$) during phenol methylation. (Temp 673 K, MeOH/Phenol = 5, WHSV 1 h^{-1})*

Nearly stable phenol conversion around 80 mol% was observed on $CM_{0.25}$ catalyst up to 4–5 h, while the conversion decreased continuously with time thereafter. The 2,6-xylenol selectivity was also found to decrease along with phenol conversion while the converse is true for *o*-cresol selectivity. As a result, total ortho-selectivity remained constant while 2,6-xylenol selectivity decreased with a simultaneous increase in *o*-cresol content in the product. Mesitol concentration also decreased to negligible levels with time on stream. Such a decrease in conversion and a change in selectivity might be due to the deactivation of active sites. We address the reasons for the catalyst deactivation and changes in selectivity in the later part of discussion.

3.2.6. Structure- Activity Correlation

Investigation of phenol methylation over a series of $Cu_xMn_{3-x}O_4$ (x = 0-1) catalysts shows that an optimum concentration of copper is required for better activity and high 2,6-xylenol selectivity. $CM_{0.25}$ was found to be the best catalyst at the given reaction conditions (673 K, WHSV $1h^{-1}$, MeOH:phenol = 5) demonstrating its superior activity and high yield of 2,6-xylenol. *O*-cresol concentration was very high at lower reaction temperatures (<673 K), which decreased with increasing reaction temperature, with a concomitant increase in 2,6-xylenol concentration, reaching maximum at 673 K. Increase in phenol conversion is also associated with increase of 2,6-xylenol selectivity up to 673 K. Beyond 673 K phenol conversion has not changed considerably on $CM_{0.25}$ (Fig.3.3), but a fall in 2,6-xylenol selectivity was observed. These observations indicate that the rate of mono-methylation was dominant and dialkylation to 2,6-xylenol increased at higher temperatures. Hence, the reaction temperature significantly influenced the rate of consecutive methylation. The interesting observation is that the total *ortho*-selectivity remained almost same (~98%*)* within the temperature range expected. A reduction in alkyl phenol content in the product at higher temperatures may be due to prevalence of dealkylation reactions. Among the minor products, mesitol was found, at increased concentrations particularly with increasing temperature. This increase could be either due to consecutive alkylation of 2,6-xylenol or disproportionation of xylenols. The concentration of copper in the catalyst also significantly influenced the concentration of

mono-methylated product. CM_0 and $CM_{0.5}$ showed comparable phenol conversion but both are not so selective to produce 2,6-xylenol, when compared to $CM_{0.25}$ at 673 K. The low 2,6-xylenol selectivity of these catalysts (x = 0 and 0.5) may be attributed to their acid-base characteristics. Gasification or decomposition of methanol may also be dominant on these catalysts [8]. Mixed oxides of CuO-Fe_2O_3 and CoO-Fe_2O_3 were reported to catalyze about 68% methanol gasification at 628 K [9,10]. Methanol reforming/decomposition was also dominant on copper rich catalysts (x = 0.75 and 1), which was confirmed by the presence of H_2, CO and CO_2 in the product stream. Tamaru et.al have reported that the methanol adsorbed on zinc oxide decomposes *via* the formate intermediate to form carbon monoxide, carbon dioxide, and hydrogen [11]. The rapid deactivation of these catalysts was mainly due to the structural changes that take place under the reducing atmosphere evolved during the course of reaction. In addition, at higher temperatures, gasification or reforming consumes higher amounts of methanol, thus leading to lower 2,6-xylenol selectivity. However, significant fall in alkyl phenol content at higher temperatures (Fig.3.3) could also be attributed to domination of de-alkylation [12].

A linear relationship between methanol to phenol ratio (up to 5) and phenol conversion was clearly observed. Excess methanol concentration in the feed was required to obtain maximum 2,6-xylenol yielded though the required stoichiometry of methanol to phenol is 2, to obtain 2,6-xylenol. This may partly be due to gasification and reforming of methanol to gaseous products under the present experimental conditions, particularly the reaction temperature. The results presented in Fig.3.6 show that the $CM_{0.25}$ catalyst deactivated with time on stream. Since, no significant carbon deposition was observed, when investigated by thermo-gravimetric analysis of spent catalyst; carbon formation may not be responsible for deactivation of these catalysts. However, the rapid deactivation of catalysts may be ascribed to the acidity of phenol and it was also found that the mole ratio of methanol to phenol lower than 5 caused a rapid deactivation of the catalysts. Though graphitic coke deposition was reported to be the reason for deactivation [13], deactivation of our catalysts after 4-5 h and may be ascribed to structural changes rather than coke deposition. Even when the reaction was carried out in presence of water (MeOH: PhOH: H_2O is 5:1:1), no improvement was observed in the activity or selectivity. On the other

hand, XRD (Fig.3.7) of spent catalysts shows that structural changes occurred during the course of reaction, which may be attributed to the observed deactivation with TOS.

The activity and 2,6-xylenol selectivity on these catalysts may be explained by invoking acid–base and structural properties. Metal oxides are known for their acid–base properties and the respective strengths and acidity/passivity ratios are dependent on their composition [14-16]. The high *ortho*-selectivity during phenol methylation was attributed to presence of acid-base sites on the surface of the catalysts [3,7,8,17]. It has been reported that medium to strong acidity favors C-alkylation, while weak acidity leads to O-alkylation [18]. It has also been reported that the stronger and weaker acid sites are responsible for 2,6-xylenol and *o*-cresol formation, respectively [17]. Tanabe et al. reported that the main active sites on Al_3O_2-ZnO are considered to be of weak acid strength [19], in case of MgO-TiO_2 both acidic and basic sites offered ortho alkylation of phenol [20]. But it is generally accepted that weak acid sites in conjugation with strong basic sites are responsible for the production of 2,6-xylenol during phenol methylation [16]. Phenol adsorbs as phenolate ion on the metal oxides, such that the *ortho* positions are very near to the catalyst surface, hence only *ortho* positions are methylated [12,21]. The TPD of NH_3 and CO_2 (Fig.2.5) results are expected to shed light on acid-base properties of $Cu_xMn_{3-x}O_4$ oxide catalysts that can be correlated with catalytic activity in phenol methylation. Phenol methylation was reported to catalyze by proton acceptor (basic) sites that are present on Mn_3O_4 [3]. TPD of CO_2 on $CM_{0.25}$ shows that the sample had relatively high basicity compared to pure manganese oxide (Fig.2.5a). Addition of a small fraction of copper (x = 0.25) helped to generate relatively high basicity [22,23]. In addition, all the samples had acidity, as observed from TPD of NH_3 (Fig.2.5b). Selectivity to 2,6-xylenol has increased with the addition of copper into the hausmannite Mn_3O_4 structure. At the same time, the total acidity, derived from TPD of NH_3, increased with copper content. High copper containing samples do not show desorption of ammonia at higher temperatures, which `indicates the absence of relatively stronger acidity. Hence, we presume that high basicity along with a matching acidity is responsible for high 2,6-xylenol selectivity. To elucidate the role of Lewis acid-base pair effect; the catalysts were steamed in-situ by taking water in the feed, but it did not influence the activity or selectivity as observed by Gandhe et al. [24]. Presences of water in the feed neither hampered the deactivation of catalyst nor effected a

change in the product selectivity as a result of the generation of Brönsted acidity. Effect of water and generation of Brönsted acid sites on phenol methylation has been reported [24].

Powder X-ray diffraction (Fig.2.1) showed that CM_0, $CM_{0.25}$ and $CM_{0.5}$ samples have hausmannite structure, while the other two catalysts ($CM_{0.75}$ and $CM_{1.0}$) crystallized as $Cu_{1.5}Mn_{1.5}O_4$ phases. This clearly shows that structural changes occurred on subsequent addition of copper to hausmannite spinel. Considering the initial stages (TOS = 1 h^{-1}) of the reaction, catalysts with $Cu_{1.5}Mn_{1.5}O_4$ phase ($CM_{0.75}$ and $CM_{1.0}$) seemed to be good; however they deactivated rapidly after 1 h on stream (Fig.3.1). The high concentration of copper in the sample may have promoted its easy reduction, possibly leading to a loss of catalytic activity over these catalysts. This high copper content may also have shifted the red-ox equilibrium $Cu^{2+} + Mn^{3+} \leftrightarrow Cu^{1+} + Mn^{4+}$ to the right, possibly facilitating easy reduction of copper cations [25-27]. Reduction of copper ions to metallic copper during phenol methylation was reported [8]. The above interpretation is fully supported by our XPS results.

Catalyst $CM_{0.25}$ showed higher activity and selectivity, retaining up to 5 h on stream compared to other catalysts. The rapid deactivation of catalysts with high copper content may be attributed to phase changes that occur during the course of the reaction, leading to the formation of MnO and metallic copper; however, some deactivation, at least in the initial stages, as a result of carbonaceous deposits cannot be ruled out. However, absence of any change in the activity or selectivity of products in the presence of water in the feed indicates carbon deposition was not a determining factor for deactivation. These results show that time on-stream stability is low for oxide phases that are rich in copper, such as the $Cu_{1.5}Mn_{1.5}O_4$ oxide.

Fig.3.7 presents XRD pattern of the spent catalysts that show the formation of MnO, a low valent manganese than the average valence of Mn in a typical hausmannite spinel. Similarly, peaks belonging to Cu metal could be clearly seen in all the samples with higher Cu content ($x \geq 0.5$). Whereas, hardly any metallic Cu was seen in the case of $x = 0.25$, though the presence of MnO could be seen. But, hausmannite phase is not retained even for this sample. It is likely that this sample might contain well-dispersed metallic copper, which is not detected by XRD, in addition to MnO. Compared with other compositions,

$CM_{0.25}$ catalyst appears to be retaining the hausmannite structure for a little longer on stream, delaying its deactivation.

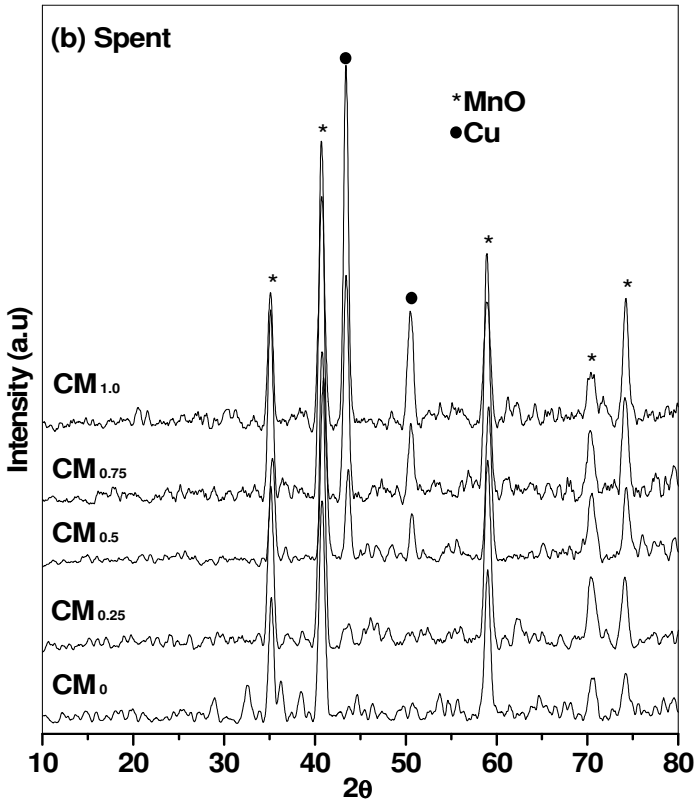

Fig.3.7. *X-ray diffraction pattern of spent copper-manganites after phenol methylation at 673 K. (MeOH: PhOH = 5, WHSV 1h^{-1}, TOS 4 h)*

The control experiment of phenol methylation on MnO, under identical conditions did not show any activity. Decomposition/reforming of methanol on $CM_{0.25}$ under methylation conditions produced CO, CO_2 and H_2. This along with our earlier observation that the sample is reduced to metallic copper and MnO after TPR experiment proves that at high reaction temperatures (673 K) the reduction of catalysts takes place, leading to the formation of MnO and Cu. The later species are not active for phenol methylation. Adding water to the feed did not improve the catalyst life, contrast to that observed by Thomas et al. over Cu-Co ferrite spinels [8]. Hence, it may be concluded that catalysts reported here are prone to irreversible structural changes, under the reaction conditions.

The change in the electronic spectra of the catalysts with variation of copper content could be explained based on the redox reaction. With increasing copper concentration, Cu^{2+}/Cu^{1+} is expected to replace Mn^{2+} in the hausmannite lattice. Cu^{1+} does

not show any *d-d* transitions, as it is a d^{10} system. A shift in the absorption band in UV region to lower wavelengths is attributed to Cu^{2+}/Cu^{1+} incorporation in place of Mn^{2+} (Fig.2.2). This band in the UV region for catalysts with $x \geq 0.5$ could be assigned either to $O^{2-} \rightarrow Cu^{2+}$ or $O^{2-} \rightarrow Mn^{2+}$ charge transfer. Reduction in the intensity of the visible region band, on incorporation of higher amount of copper ($x \geq 0.5$) might be due to change in the oxidation state from Mn^{3+} to Mn^{4+}. Since, no absorption was seen in the visible region at 800 nm, the possibility of Cu^{2+} in octahedral environment can be ruled out. At low concentration, copper may simply replace Mn^{2+} ions in the tetrahedral sites as no absorption bands due to Cu^{2+} in octahedral sites are observed.

FTIR spectra corroborate the UV results as the structural vibrations observed for CM_0 and $CM_{0.25}$ are in good agreement with hausmannite structure [28-31]. Further increase in copper content lead to the transformation of hausmannite to $Cu_{1.5}Mn_{1.5}O_4$ phase, as a result the IR bands at 623 and 516 cm^{-1} disappear from these samples (Fig.2.3). The IR spectra of spent catalysts (Fig.3.8) obtained on phenol methylation reaction showed, identical bands that are characteristic of MnO for all compositions [32,33]. Hence, it is noted that irrespective of the composition all manganese oxide catalysts undergo reduction to MnO.

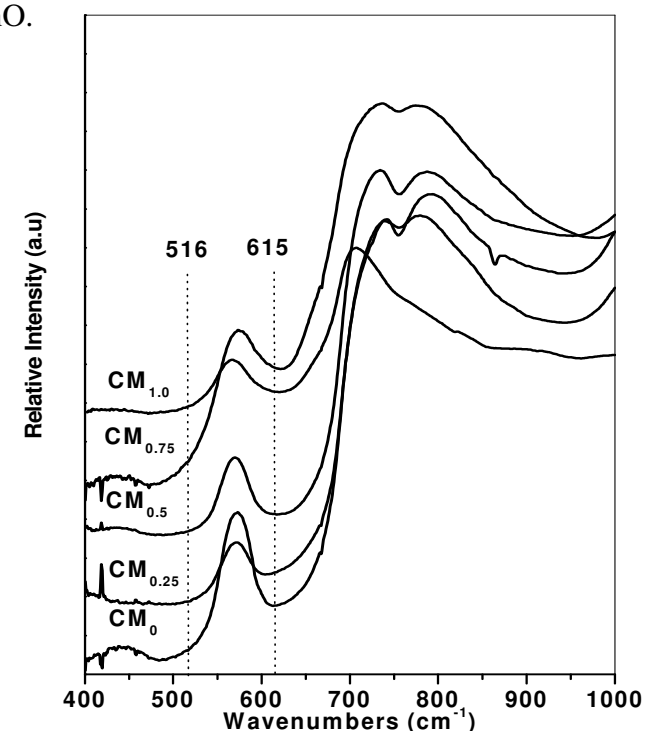

Fig.3.8. *FTIR spectra of spent $Cu_xMn_{3-x}O_4$ catalysts after phenol methylation reaction (Methanol to phenol ratio is 5 and WHSV $1h^{-1}$)*

In the case of TPR (Fig.2.6), it is difficult to interpret profiles of the present copper-manganese oxide system, as they contain various combinations of oxidation states of copper and manganese. It is not possible to attribute individual peaks to any redox species. As discussed in section 2.4.7, for samples with x > 0.25 the low temperature TPR peak at 445 K, is attributed to the reduction of surface Mn^{3+} ions that are present in the manganese oxide spinel. An increase in the intensity of low temperature peak with the increase in copper concentration may be due to the presence of surface copper ions along with Mn^{3+} ions. It has been reported that copper ions are reduced at higher temperatures in mixed oxides compared to bulk CuO [31,34]. TPR of CM_x catalysts that shows low temperature shift of the most intense peak with copper substitution may be due to the enhancement of reduction of $Mn^{3+}/^{4+}$ ions with neighboring Cu ions in the spinel lattice. Similar observations were reported elsewhere [31,34]. Cu^{2+} in copper-manganese spinel may reduce to metallic Cu either in single or two steps i.e. $Cu^{2+} \rightarrow Cu^{1+} \rightarrow Cu^{o}$. On the other hand, reduction of Cu^{2+} in pure CuO occurs at 523 K as reported by Tanaka et al. [35]. The observation of a single reduction peak for this system may be attributed to the formation of copper-manganese oxide solid solution as a result of Cu^{2+}/Cu^{1+}---O---Mn^{3+}/Mn^{4+} bonds. These results are in good agreement with those reported for such spinels [35].

The splitting of Mn_{2p} and the Mn_{3s} in the XPS spectra is often used to determine the manganese oxidation states [36]. One may also expect Mn_{2p} shake up satellite peaks, as all 3*d* configurations of manganese are paramagnetic [37]. But the satellites are clearly observed only for MnO. In the case of Mn_2O_3 and MnO_2, $Mn_{2p1/2}$ peaks are superimposed on the satellites [37]. The BE value of 642.0 eV (Fig.2.8) for CM_0 sample may be attributed to Mn_3O_4 phase, which supports the powder XRD results. The $Mn_{2p3/2}$ B.E of pure Mn_3O_4 is expected to be between the B.E values of Mn^{3+} and Mn^{2+}. But, the impurity present in the sample, i.e., Mn_5O_8, with an average oxidation state of +3.2 might shift the binding energy to slightly higher values. Incorporation of copper (Cu^{+}) into tetrahedral sites of hausmannite is expected to shift in binding energies of Mn_{2p} to higher value, as a result of the formation of Mn^{4+} ($Cu^{2+} + Mn^{3+} \leftrightarrow Cu^{1+} + Mn^{4+}$). These observations are in good agreement with the previous reports [38].

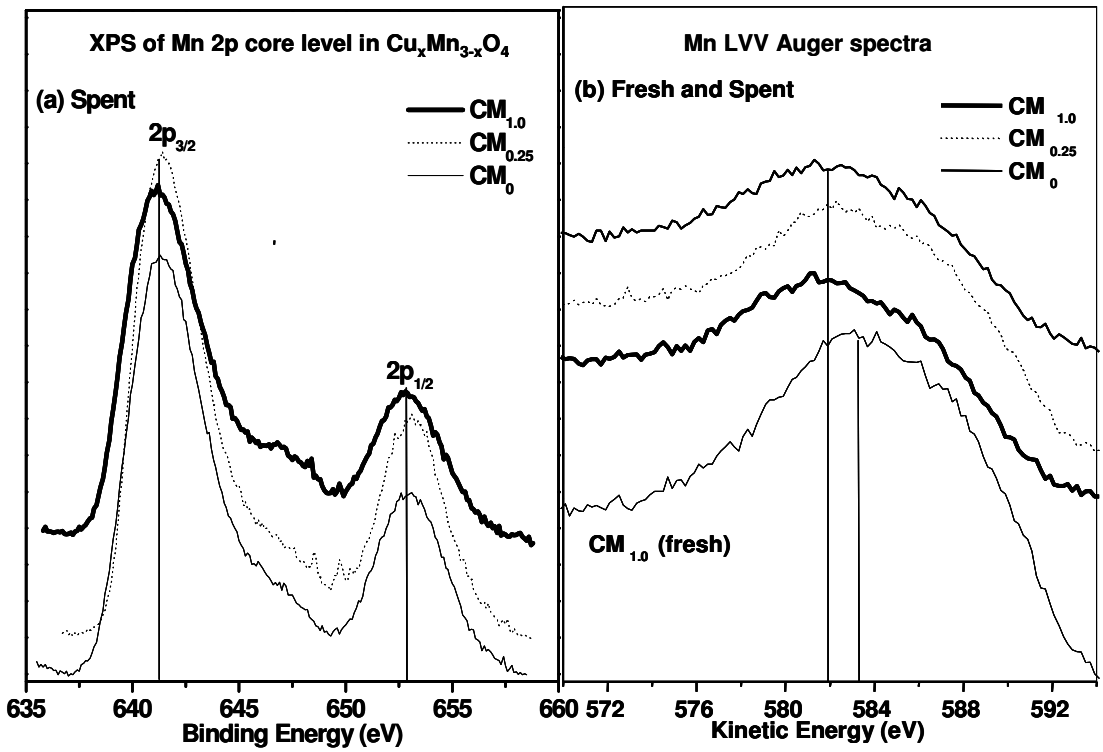

Fig. 3.9. *Mn 2p photoemission spectra of (a) spent catalysts and (b) Mn LVV of fresh and spent catalysts. Spent catalysts are obtained after 4 h of phenol methylation reaction at T = 673 K.*

The B.E of spent catalyst at ~641.4 eV (Fig.3.9) is attributed to the presence of Mn^{2+}, though the presence of some Mn^{3+} cannot be ruled out. The formation of MnO after phenol methylation is also confirmed by XRD. The ratio of Cu to Mn on the surface was reportedly estimated using XPS [8]. We have considered integrated intensities of the Cu (2p) and Mn (2p) peaks to estimate their concentrations. It has been observed that the surface copper has enriched by 1.3 times on $CM_{0.25}$ while in case of $CM_{1.0}$ bulk and surface compositions were nearly same.

From the Fig.3.10 (a) it was observed that the B.E. of $Cu_{2p3/2}$ value for spent catalysts is close to Cu^{1+}, but we presume it to be metallic copper based on the powder XRD results (Fig.2.1). Cation distribution is generally deciphered based on XPS results. Thermodynamic calculations for site preference energy of several bivalent and trivalent cations in spinel structures were reported [28,39].

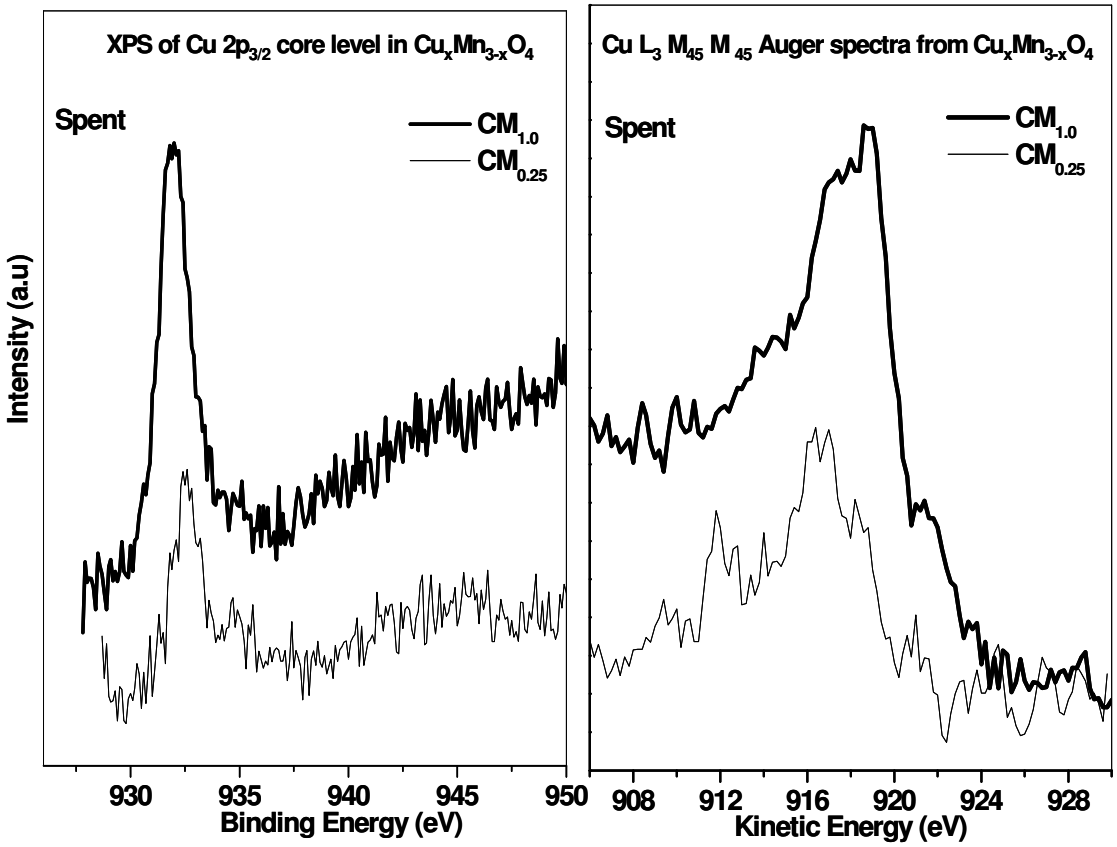

Fig.3.10. (a) *Cu 2p core level XPS spectra and (b) X-ray initiated Augur electron spectra (XAES) from Cu-$M_3M_{45}M_{45}$ of spent $Cu_xMn_{3-x}O_4$ catalysts*

The calculations showed that octahedral site preference energy for Mn^{3+}/Mn^{4+} is higher than that for Cu^{2+}. On the other hand, Mn^{2+} and Cu^{1+} have more preference for tetrahedral sites. However, some reports suggest presence of bivalent copper, at least a part of it, in octahedral sites [40]. In the case of copper containing spinels, most reports agree with the location of monovalent copper in tetrahedral and bivalent copper in octahedral sites [41]. From the literature, it is found that the binding energy values of copper $Cu_{2p3/2}$ peak in spinels follows the order $Cu^+(Oh)<Cu^+(Td)< Cu^{2+}(Oh)<Cu^{2+}(Td)$ [42].

XPS spectra of the valence band (VB) region obtained from spent catalysts are shown in Fig.3.11.The main VB observed below 9 eV had contributions from 3d orbitals of Cu, Mn and 2p bands of O. The high-intensity of VB observed is mainly due to Cu 3d bands and its intensity increased with increasing copper content. This observation clearly suggests that the new features were from Cu 3d bands. The band at low BE (2 eV) can be

attributed to a Cu-$3d^{10}$ band and O 2p bands [8]. An overlap of Mn 3d and Cu 3d was observed at around 4 eV from fresh catalysts (Fig.2.11).

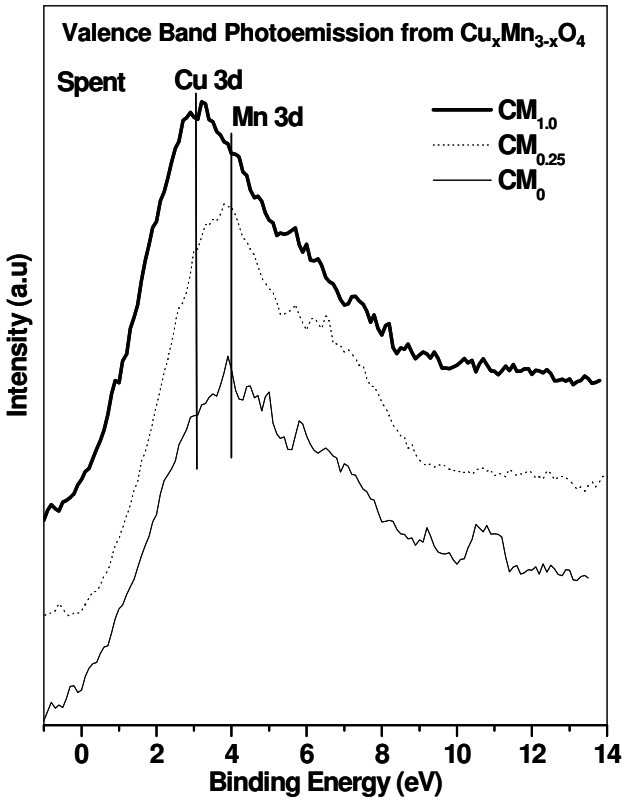

Fig. 3.11. *Valence band XPS spectra of spent copper- manganite catalysts*

The intensity variation observed with increasing copper content is mostly due to the high σ of the Cu 3d bands. The changes observed on spent catalysts from core levels are reflected strongly in the VB spectra: (i) main VB shifting toward lower BE with increasing copper content; (ii) the satellite appearing at around 12 eV on fresh catalysts (Fig.2.10) disappearing on $CM_{0.25}$ and $CM_{1.0}$, and (iii) the disappearing Cu^{1+}-$3d^{10}$ band on $CM^{1.0}$ due to reduction of $^{Cu1+} \rightarrow$ Cu and hence an associated shift in BE of the 3d bands.

3.2.7. Relation between catalytic activity and acid-base character

Previous reports on the correlation of acid-base properties to catalytic methylation of phenol to yield various methyl phenols were not helpful in comparing or generalizing our catalyst system. Hence, we speculate on a possible correlation based on our phenol methylation reaction results. Performance of $CM_{0.25}$ showed that it had higher activity and

also better selectivity towards 2,6-xylenol yield. In general, the Lewis acidity is attributed to the metal ions, while the basicity can be attributed to the presence of oxide anions on the surface of a metal oxide. Obviously, the compositional variation influences the distribution of metal and oxide ions as well as their strengths. It is known that Mn_3O_4 is a basic oxide; addition of copper should further enhance the basicity of the system. But the surface acid-base property of the mixed oxide catalysts strongly depends on the nature and content of the surface cations. Many reports claim that acidity is the determining factor for phenol conversion activity, whereas basicity accounts for high 2,6-xylenol selectivity. It is therefore, the better activity and 2,6-xylenol selectivity. On $CM_{0.25}$ may be attributed to the presence of Cu^{2+} with suitable acidity and basicity as well as greater structural stability. According to Thomas et al. Cu^{2+} is the active species and its synergetic interaction with other metal cations (Co) in the system leads to better 2,6-xylenol yield [8].

3.2.8. Electronic and structural changes

The changes occurring in the electronic properties of the catalysts during the reaction can be explained by XRD, TPR and XPS findings. Reducing atmosphere was created during the phenol methylation reaction, confirmed by the evolution of H_2 and CO, which probably formed by the by steam reforming/decomposition of methanol. These reducing gases H_2 and CO are responsible for the catalyst reduction, resulting in the formation of Cu and MnO. These reduced species are not active for phenol methylation and hence the catalysts deactivate after few hours. This reduction is confirmed by XRD of spent catalysts, which exhibited Cu metal and MnO. XPS findings also corroborate the above observations. The changes observed in case of main peaks, satellites, and Auger features of Mn and Cu provide clearly indicates that partial reduction of these species occurred during the reaction. It is useful to highlight the following features from XPS; (1) Copper reduction was seen for $x > 0.25$, with the extent of reduction increasing linearly with increasing 'x' value; (2) Partial reduction of all metal ions and a consequent increase in the energy overlap of 3d band in the spent catalysts occurred; (3) A comparable activity was observed for $x = 0$ to 0.5 indicating the equal importance of Cu^{2+} and Mn^{3+} for better performance; (4) The complete phase change of the catalysts after reaction, identified from

XRD and XPS results hints the structural collapse; (5) All the above points indicate considerable redistribution of the cations under reaction conditions.

The extent of red-ox interaction that was observed between Mn^{3+} and Cu^{2+} increases with increasing 'x' value. Further, it is confirmed (from XRD) by the formation of $Cu_{1.5}Mn_{1.5}O_4$ phase. The extent of reduction in $CM_{1.0}$ has reached 45% (Reducibility of Cu, calculated as the amount of reduced Cu to Cu^{2+}content). The activity and selectivity were higher on $CM_{0.25}$, because the extent of reduction was minimum (as confirmed by XRD and XPS). Although overlap of 3d bands from Cu and Mn in the fresh catalysts is expected to enhance the activity and selectivity through synergic interaction [8], the increase in the extent of reduction with higher copper content leads to poor activity and selectivity. But the better overlap of 3d bands could not be used in phenol methylation due to reductive atmosphere (structure collapse) and a higher extent of reduction. However, these processes are relatively low in $CM_{0.25}$, contributing to the higher activity for phenol methylation and better 2,6-xylenol selectivity.

3.2.9. Mechanism of C-methylation of phenol

Two pathways are proposed for the formation of 2,6-xylenol by the methylation of phenol. One probable path is through the formation of anisole, which further reacts with methanol to give 2,6-xylenol via isomerization of methyl anisole. The alternate route is through the C-alkylation of phenol to give *o*-cresol followed by its consecutive methylation to give 2,6-xylenol. In either case, for phenol methylation to take place, the first key step is the adsorption of phenol on the catalyst surface. Tanabe et al. [43] supported the second mechanism, wherein C-alkyl phenols are formed through the adsorption of phenolate ion, in the perpendicular orientation to the surface, on MgO catalyst system. This particular orientation of the phenolate ion on the catalyst surface leads to its methylation in the ortho position. Since, we did not observe anisole, at any of the reaction conditions, we feel that the later mechanism proposed by Tanabe et al. could be the most probable and applicable to our catalyst system. To support this, reactions were carried out with only anisole or a mixture of anisole and methanol with $CM_{0.25}$ catalyst, Therefore, the methylation of phenol over the present catalyst cannot be considered to proceed via anisole. An increase in the 2,6-xylenol selectivity at the expense of *o*-cresol

and further methylation of 2,6-xylenol to tri-methyl phenol (mesitol) demonstrates that the reaction is consecutive, giving further credence to the above mechanism. As the O-H bond length of phenol inevitably governs distance between the phenoxide species and the proton, the methyl cation may be at a site neighboring the *ortho*-position of the phenoxide species. Therefore, the proposed mechanism is applicable for this reaction, system on these catalysts.

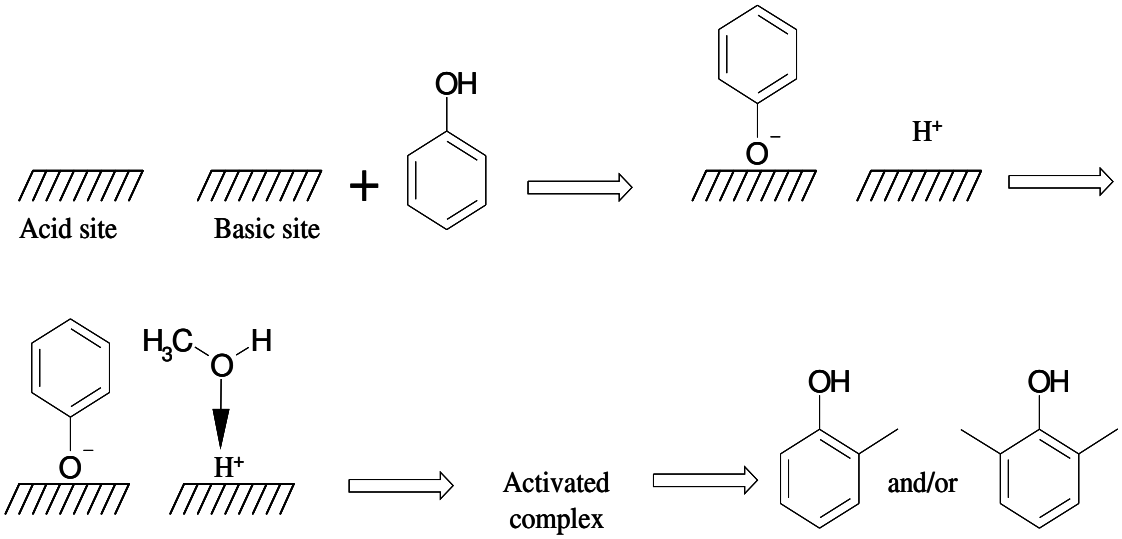

Scheme.1 *Reaction mechanism of phenol methylation on acid base sites on mixed oxide catalysts*

3.3. Methylation of phenol on Zn-Mn spinels

3.3.1. Effect of catalyst composition

Fig.3.12 shows phenol conversion and 2,6-xylenol selectivity in phenol methylation against reaction time over the zinc-manganese spinel catalysts ($Zn_xMn_{3-x}O_4$, x = 0-1) that contain various zinc contents. The comparison of the catalyst performance was carried out under identical conditions (MeOH:PhOH is 5 and WHSV $1h^{-1}$) that were found to be optimum during evaluation of copper-manganese spinel catalysts (Fig.3.4 and Fig.3.5). The reaction results reveal that these systems are highly selective for methylation of phenol at the *ortho*-position of phenol, yielding *o*-cresol and 2,6-xylenol. The catalytic activity significantly varies with the amount of zinc present in the system. The highest phenol conversion and 2,6-xylenol selectivity were observed at low content of zinc (x =

0.25). Further increase in zinc content led to a decrease in the phenol conversion as well as 2,6-xylenol selectivity.

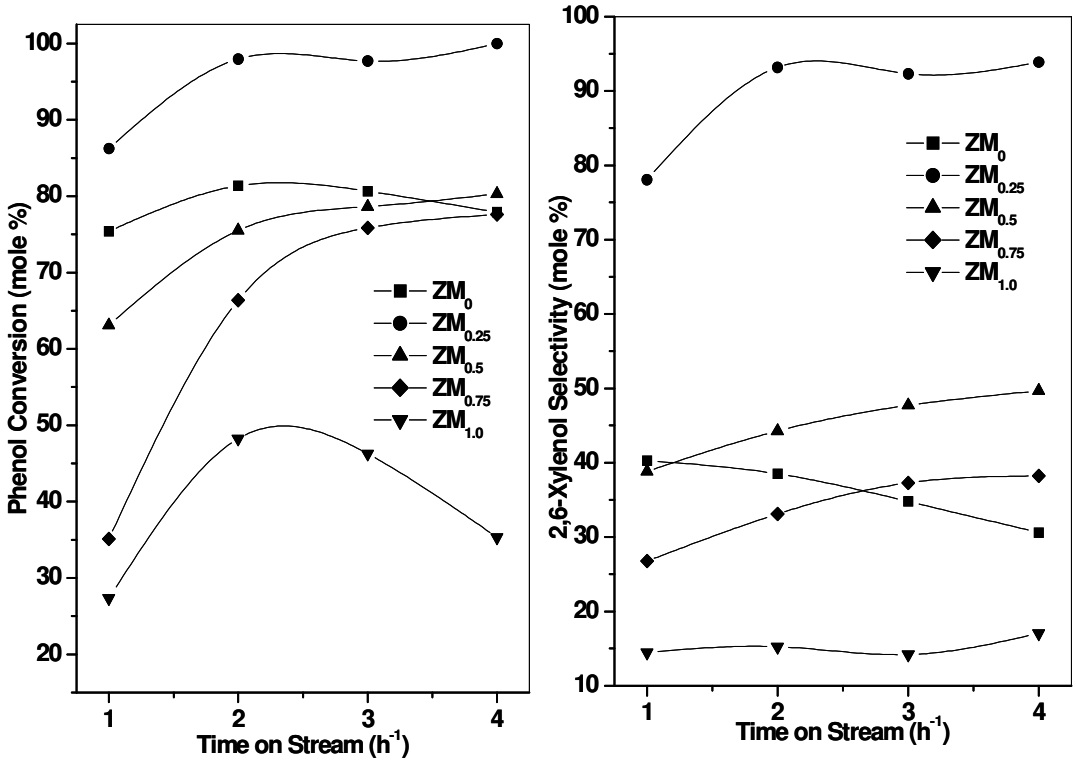

Fig.3.12. *Phenol conversion and 2,6-xylenol selectivity over zinc-manganite spinel catalysts after calcination at 773 K. (methanol to phenol ratio 5, Temp 723K, WHSV 1h^{-1})*

The maximum phenol conversion (100%) and 2,6-xylenol selectivity (94%) were achieved on $ZM_{0.25}$ catalyst at 723 K. The other products formed were *o*-cresol and mesitol (<1%). It may be seen that the catalytic activity progressively decreased at higher substitution of Mn^{2+} by Zn^{2+} ions that follows the order of $ZM_{0.25}$ >ZM_0 >$ZM_{0.5}$ >$ZM_{0.75}$ >$ZM_{1.0}$ (at 3 h of TOS). A rapid fall in the phenol conversion was observed on $ZM_{1.0}$ compared with other catalysts. In terms of selectivity, $ZM_{0.25}$ catalyst offered highest 2,6-xylenol selectivity, while $ZM_{1.0}$ offered the least. The 2,6-xylenol selectivity on these catalysts follow the order $ZM_{0.25}$ >$ZM_{0.5}$ >ZM_0 >$ZM_{0.75}$ >$ZM_{1.0}$ (after 2 h of TOS). Even though the catalytic activity varied considerably with zinc concentration, the total *ortho* selectivity remained >99% as was the case with copper-manganese spinel catalysts, regardless of the composition of catalysts. The phenol conversion was reasonably good on ZM_0 catalyst, but there is a continuous decline in 2,6-xylenol selectivity with reaction time as shown earlier for pure manganese oxide (CM_0). One basic difference between Cu-Mn

and Zn-Mn spinel catalysts is that there is hardly any deactivation on all Zn-manganites at least during the first 4 h on stream.

3.3.2. Effect of the reaction temperature

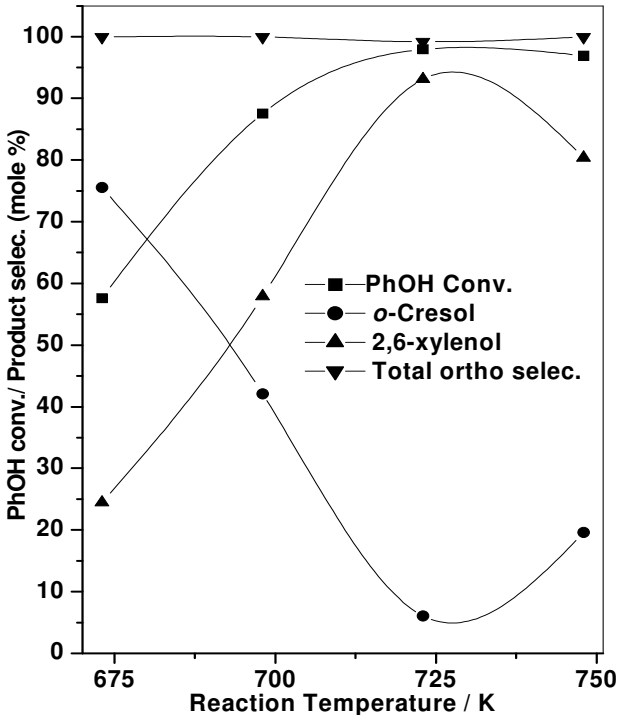

Fig.3.13. Effect of the reaction temperature on phenol methylation over $ZM_{0.25}$ catalysts (WHSV $1h^{-1}$, MeOH: PhOH is 5:1)

Fig.3.13 shows the influence of reaction temperature on phenol conversion and product selectivity over $ZM_{0.25}$ catalyst in the range of 673 to 748 K using feed containing MeOH: PhOH in the ratio of 5 and WHSV $1h^{-1}$. The main products observed in the reaction were 2,6-xylenol and *o*-cresol in addition to gaseous products such as H_2, CO and CO_2. Initially, the phenol conversion increased with reaction temperature that touched a maximum at 723 K, which further increases in the temperature led to a fall in the phenol conversion. Phenol conversion has increased from 57 to 97 mol% and 2,6 xylenol selectivity from 25 to 93 mol% with an increase in temperature from 673 to 723 K. Therefore, optimum temperature for this system was found to be 723 K for obtaining highest phenol conversion and 2,6-xylenol selectivity. At temperatures above 723 K, the concentration of *o*-cresol increased though there was no change in the ortho selectivity. These results suggest that highest phenol conversion and 2,6-xylenol selectivity on zinc-

manganites occurred relatively at higher temperature (723 K) than copper-manganite catalysts (673 K). Another important feature of zinc-manganite catalysts is that the sample with lower zinc (x = 0.25) offered highest selectivity to 2,6-xylenol. $ZM_{0.25}$ exhibited better activity and 2,6-xylenol selectivity than $CM_{0.25}$ under optimum conditions. At high temperatures, methanol decomposition produced CO, H_2 and CO_2 gases.

Activity and selectivity of the catalysts as a function of reaction temperature and zinc content are shown in Fig.3.14. Similar to the observations made earlier for Cu-Mn spinel systems, the reaction temperature as well as concentration of substitute (zinc) in manganite showed a marked influence on the activity and the product selectivity. The phenol conversion increased linearly with reaction temperature over all catalysts, except that change was not linear on $ZM_{0.25}$ catalyst at higher temperatures.

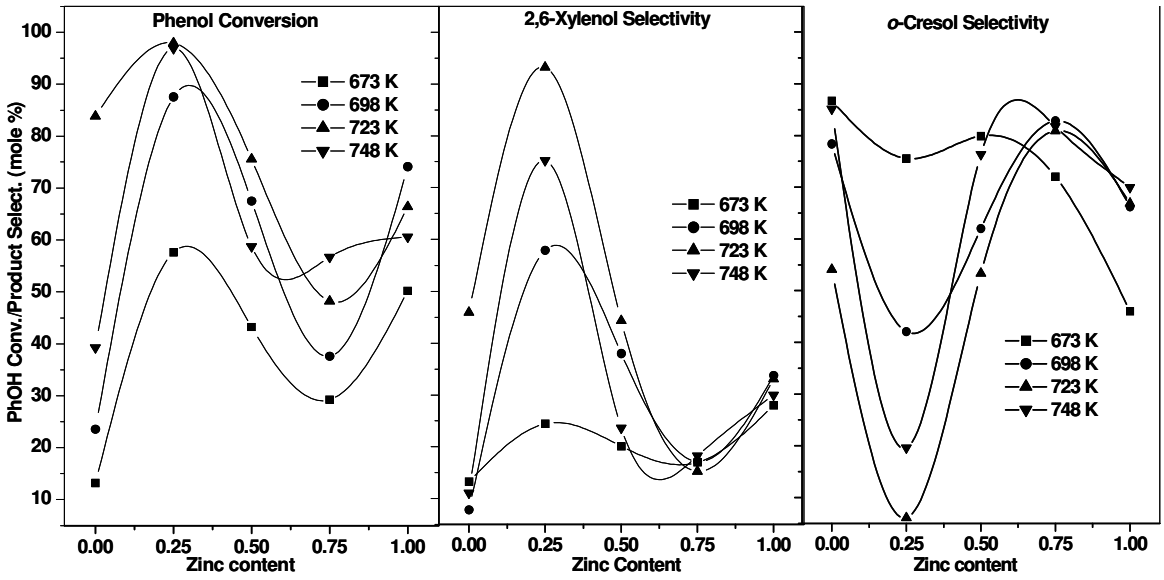

Fig.3.14. Phenol conversion and product selectivity's during phenol methylation at different temperatures on $Zn_xMn_{3-x}O_4$ (x = 0 to 1) catalysts, TOS 2 h.

High temperatures influenced the consecutive methylation of phenol on $ZM_{0.25}$ yielding higher 2,6-xylenol selectivity reaching maximum at 723 K (Fig.3.14). Whereas, further increase in temperature beyond 723 K led to a fall in consecutive methylation of *o*-cresol resulting in the higher concentration of *o*-cresol in the product. An increase in the amount of zinc in manganese oxide enhanced the formation of *o*-cresol; as a result there was a fall in the rate of dimethylation of phenol. In addition, a substantial reduction in the phenol

conversion was observed with increasing zinc content. All the catalysts form exclusively *ortho*-methyl products. In other wards, increase of Zn^{2+} ions, beyond x = 0.25, replacing Mn^{2+} ions in the hausmannite structure, did not help in 2,6-xylenol formation and phenol conversion. As evidenced from these results, the catalysts are highly selective to form *ortho*-methyl phenols giving 100% total *ortho*-selectivity.

3.3.3. Time on stream stability

After arriving at the optimum composition of the catalyst, reactant feed ratio and reaction temperature, the $ZM_{0.25}$ catalyst was investigated further for its on-stream stability.

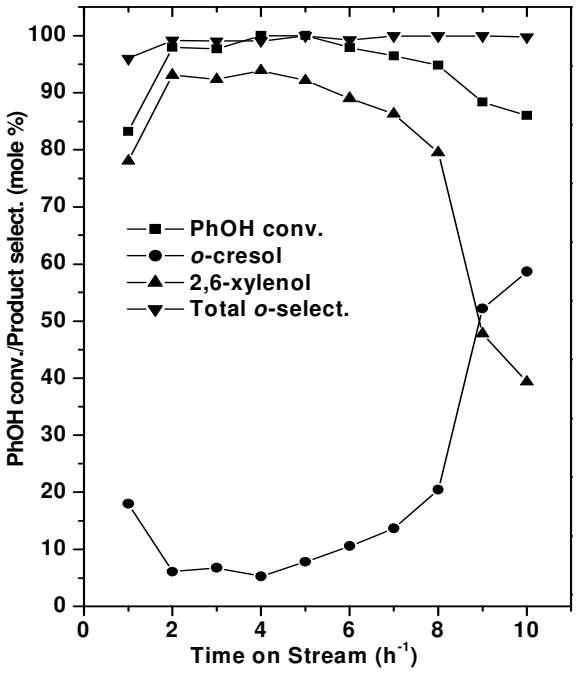

Fig.3.15. *Time on stream behavior of $ZM_{0.25}$ catalyst during phenol methylation at 723K.*

Fig.3.15 presents phenol conversion and product selectivity against TOS on $ZM_{0.25}$ catalyst at 723 K, using methanol to phenol ratio of 5 and at space velocity of 1 h^{-1}. Close to 100% phenol conversion was observed on this catalyst up to 5 h of TOS, while the conversion started declining for further time on stream reaching a value of 88% after 10 hrs on stream. Similarly, the 2,6-xylenol selectivity was almost constant up to 5 h, while it dropped rapidly afterwards producing more *o*-cresol after 8 h. Even after this deactivation with time, 100% total *ortho* selectivity was always observed on these catalysts. To start

with, *o*-cresol selectivity was low, which has increased with TOS with a concomitant decrease in 2,6-xylenol. To find the influence of water in the feed, catalytic performance of $ZM_{0.25}$ with TOS using water-containing feed was investigated. Previous reports [44], suggest that hydroxyl ions are formed on Lewis acid sites on reacting with water that enhanced the product selectivity by horizontal adsorption of phenol to produce a mixture of alkyl phenols [45]. However, no change in either activity (phenol conversion) or 2,6-xylenol selectivity was observed for this system in the presence of water in the feed. Similarly, there was no improvement in the catalyst stability. This finding suggests that the life of the catalysts cannot be improved, similar in the case of Cu-Mn spinels.

3.3.4. Discussion on structure- activity correlation

Methylation of phenol on zinc manganites spinel catalysts was investigated with the variation in zinc content. It was observed that the amount of zinc and the stability of the spinel structure are essential for the better activity and the 2,6-xylenol selectivity. From the previous reports, it has been identified that acid-base bi-functional mechanism operates in phenol methylation on oxide catalysts to yield 2,6-xylenol [46]. In addition, the acidity of the oxides and the nature/strength of the acid sites would also determine the activity and product selectivity. In this study, TPD of CO_2 and NH_3 were used to study and determine the acid-base properties of zinc-manganite catalysts (Fig.2.14). The ratio of acid to basic sites on the catalysts considerably influenced the performance of the catalysts. Although it is very difficult to measure the acid-base properties in absolute values, relative strengths of acid or basic sites obtained by TPD under identical conditions can be correlated. From the TPD of CO_2, it was seen that ZM_x catalysts with x = 0-0.5 showed basic sites of similar strength (T_{max} is same) and relatively higher basicity than ZM_x catalysts with x = 0.75 and 1.0. Similarly, TPD of NH_3 shows that ammonia desorbed at two temperatures on ZMx catalysts with x = 0 and x = 0.25. These desorption peaks (Tmax = 451 and 590 K) may be assigned to sites with weak and moderate acidity. A shift to low temperature of the T_{max} of high temperature peak for catalysts with x > 0.25 was observed. Hence, it is inferred that the catalysts with x > 0.25 are associated with acid sites of lower strength than ZM_0 and $ZM_{0.25}$. However, the total acidity on the catalysts increased gradually with increase in zinc content. This increase may be attributed to the coordination of NH_3 to Lewis Zn^{2+} sites.

Based on these TPD results, we presume that enhanced activity on $ZM_{0.25}$ was mainly due to moderate acidity along with matching basicity. Although, ZM_0 catalyst showed higher acidity it was not so active and selective for 2,6-xylenol compared to $ZM_{0.25}$. It is noted that the addition of a small amount (x = 0.25) of zinc helped in the generation of appropriate acidity that helped in enhancing the phenol methylation activity and 2,6-xylenol selectivity. According to Jacobs [47], appropriate concentration of Zn^{2+} and Mn^{2+}/Mn^{3+} ratio on the catalyst surface is the decisive factor for catalytic activity and selectivity. Hence, in spite of having nearly comparable acidity and basicity on ZM_0 and $ZM_{0.25,}$ the later yielded more 2,6-xylenol. Acid sites of higher strength (absence of high temperature T_{max}), were not observed on the catalysts with x > 0.5, indicating the absence of strong acidity. Hence, we presume that reasonably high acidity along with a matching basicity is responsible for high 2,6-xylenol selectivity on zinc manganites, and the catalyst with optimum composition for methylation of phenol was found to be $ZM_{0.25}$.

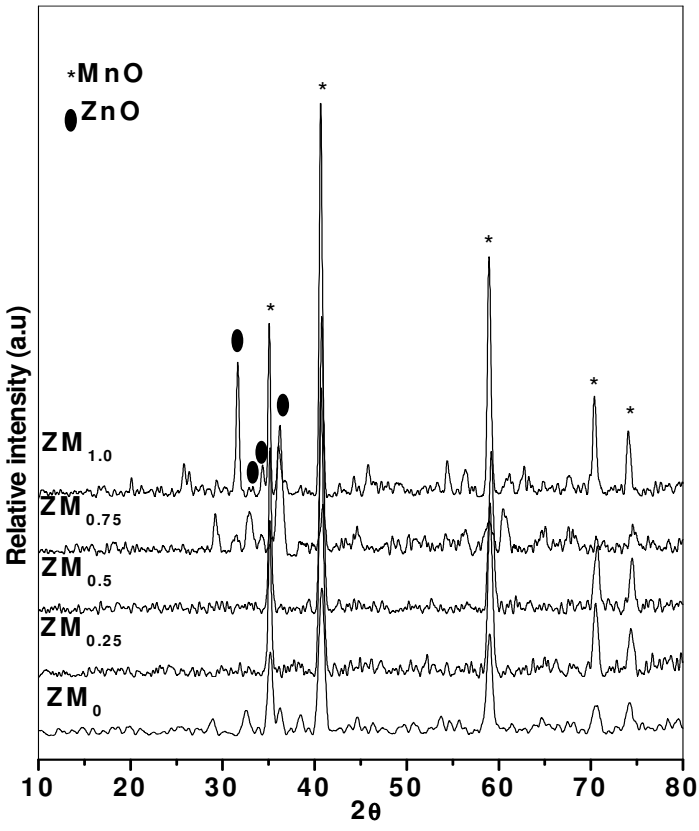

Fig.3.16 *XRD of spent $Zn_xMn_{3-x}O_4$ catalysts after phenol methylation reaction at 723 K (MeOH: PhOH is 5 and WHSV 1 h^{-1})*

Since, phenol methylation reaction is carried out at high temperatures; the reductive conditions developed during the course of the reaction, as a result of methanol decomposition/reforming, can influence the reducibility of these catalysts during the course of the reaction. The TPR data of ZM_0 and $ZM_{0.25}$ catalysts showed two reduction peaks (T_{max}) at 563 and 703 K, whereas the other catalysts showed only a higher temperature reduction peak. As mentioned earlier, the low temperature peak is attributed to the reduction of surface Mn^{3+} ions. This peak was observed only for $ZM_{0.25}$ catalyst (also seen for pure Mn_3O_4), while it was absent for $ZM_{0.5\text{-}1.0}$. These TPR data suggests that Mn^{3+} ions were presented on the surface of the catalyst with x = 0.25 and the concentration of Mn^{3+} ions have decreased with the addition of more zinc i.e., for the catalysts with x > 0.25. It is known that reduction of Zn^{2+} is not feasible under the present reaction conditions. However, incorporation Zn^{2+} in hausmannite structure stabilizes the Mn^{3+}/Mn^{4+} ion in the lattice and hence, the main reduction peak observed for pure manganese oxide (T_{max} ~703 K) has shifted to higher temperature (T_{max} ~735 K) for x > 0.25. The reducibility of Mn^{3+}/Mn^{4+} species further reduced in case of $ZM_{1.0}$ as the T_{max} further increased (~750K) which may be due to stabilization of Mn^{3+} at high concentration of Zn^{2+} in the spinel structure. Thus better activity and selectivity on $ZM_{0.25}$ may be attributed to the presence of appropriate concentration of $Zn^{2+}/Mn^{3+/4+}$.

Heterogeneous surface of the catalysts can be studied by the crystalline phase and surface area. In turn these properties of the catalyst surface can be correlated with the reaction data. The observed crystalline phases, their unit cell parameters and surface areas of fresh and spent catalysts are summarized in Table 2.5. BET surface areas of the catalysts revealed that the amount of zinc in spinels strongly influenced these values. The surface area values initially increased with zinc content (up to x = 0.25) while further incorporation of zinc resulted in the lowering of these values. However, all the spent catalysts (Fig3.16) showed reduction in the surface area after phenol methylation reaction. This influence is also evident in the increased crystallites size of the spent catalysts. XRD of the fresh catalysts (Fig.2.11) showed mainly hausmannite (Mn_3O_4) or hetaerolite ($ZnMn_2O_4$) structures on incorporation of Zn with x > 0.25. On incorporation of zinc into manganese oxide, there was a shift in the XRD peak position to higher 2θ, indicating formation of the solid solution. Any major changes in the spinel structure were not observed with

incorporation of zinc. However, careful study of XRD patterns revealed a gradual phase transformation from hausmannite to hetaerolite. These observations suggest the formation of pure solid solutions of zinc-manganese oxide with increasing zinc content resulting in the formation of hetaerolite phase. UV-visible spectra obtained for ZM_0 (Fig.2.12) is consistent with the reports for hausmannite structures [30]. Where as, $ZnMn_2O_4$ formed a normal spinel with tetragonal structure similar to hausmannite (Mn_3O_4) [30]. The UV-visible and FTIR (Fig.2.13) results corroborated the hausmannite structure after incorporation of higher amount of zinc.

XRD of the spent catalysts (Fig.3.16) obtained after 4 h of the reaction show MnO, with lower oxidation state (Mn^{2+}) due to the reduction of Mn^{3+} ions present in the hausmannite phase under the reaction conditions. Change in the oxidation state of manganese ions induced structural changes in the catalyst that caused deactivation of the catalysts. Formation of MnO and ZnO was identified by the XRD for spent catalysts ($x \geq 0.75$). Hence, it may be concluded based on the above results that activity of zinc manganite catalysts is mainly due to relatively moderate acidity with matching basicity. The surface Zn^{2+} to Mn^{3+} ratio markedly influenced the 2,6-xylenol selectivity. The optimum acid-base property suitable for 100% phenol conversion and highest 2,6-xylenol selectivity was observed on $ZM_{0.25}$. In spite of the having considerable activity, these catalysts did undergo deactivation with TOS. Deactivation of the catalysts was attributed to the structural changes that occurred during the course of reaction. The pure MnO and a physical mixture of MnO and ZnO did not show any activity. Though the carbon deposition can lead to deactivation of catalysts, we attribute structural collapse for deactivation rather than carbon deposition.

3.4. Methylation of phenol on Cu-Zn-Mn spinels

Mixed oxide catalysts that contain cations such as Zn, Cu, Co and Ni have been reported as highly active and selective for *ortho* alkylation in phenol methylation reaction due to the synergic interaction among the constituent metal ions and overlap of 3d bands [48-50]. Hence, ternary oxide spinel catalysts containing copper, zinc and manganese were proposed and investigated for phenol methylation, results of which are reported in this section. The catalytic activity and selectivity in phenol methylation on copper-zinc-

manganite spinel catalysts with various compositions are presented below. Chemical composition and the textural properties of these catalysts are given in Table 2.9.

3.4.1. Effect of catalyst composition

Fig.3.17 shows the comparative performance of the Cu-Zn-Mn spinel catalysts in phenol methylation at 673 and 723 K. These catalysts were evaluated under the optimum reaction conditions (feed ratio and space velocity) that were arrived on the basis of results obtained on Cu-Mn and Zn-Mn spinel catalysts. Ternary mixed oxide catalysts showed good phenol conversions at 723 K than when compared at 673 K. As the atomic ratio of Cu/Zn decreases in these catalysts a clear fall in the phenol conversion was observed. Whereas CZM2 catalyst that has medium ratio of Cu/Mn showed high 2,6-xylenol yield than other catalysts.

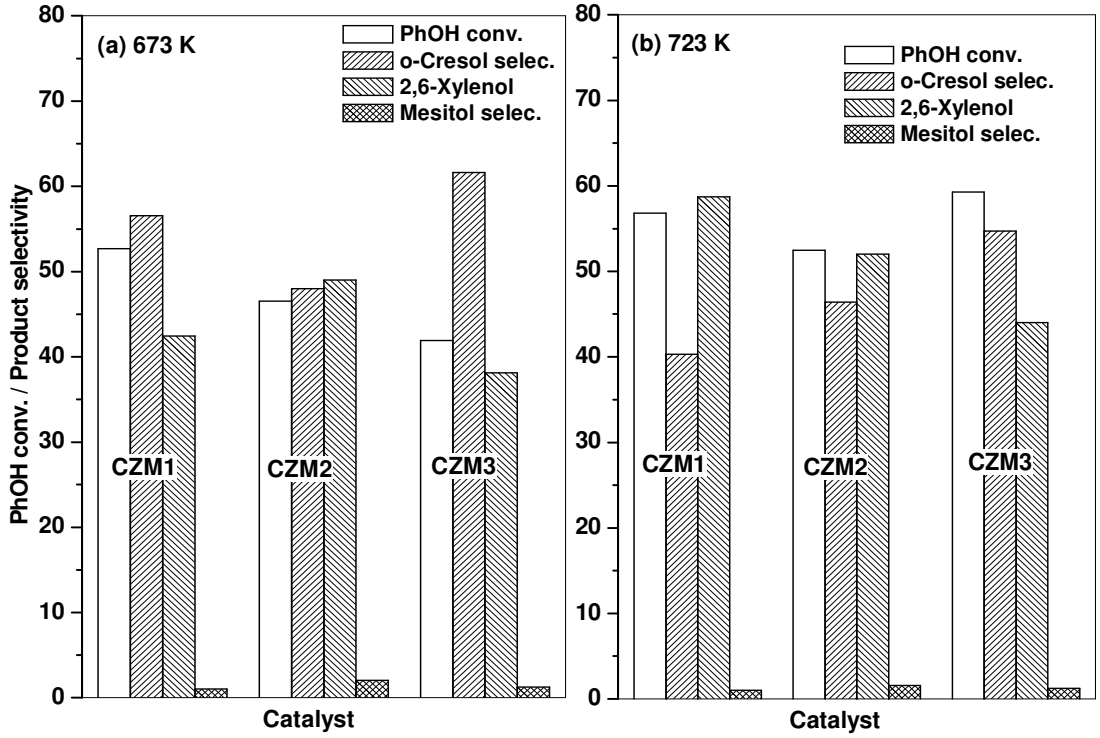

Fig.3.17. *Catalytic performance over copper- zinc- manganites in phenol methylation at 673 and 723 K, (methanol to phenol ratio 5 and WHSV 1h^{-1} TOS 2*)

As was observed in case of CM_x catalysts, CZM2 sample yielded higher mesitol compared to the other catalysts as a result of higher 2,6-xylenol content in the product.

High activity and 2,6-xylenol selectivity were observed at 723 K on all the catalysts compared to the activity at 673K.

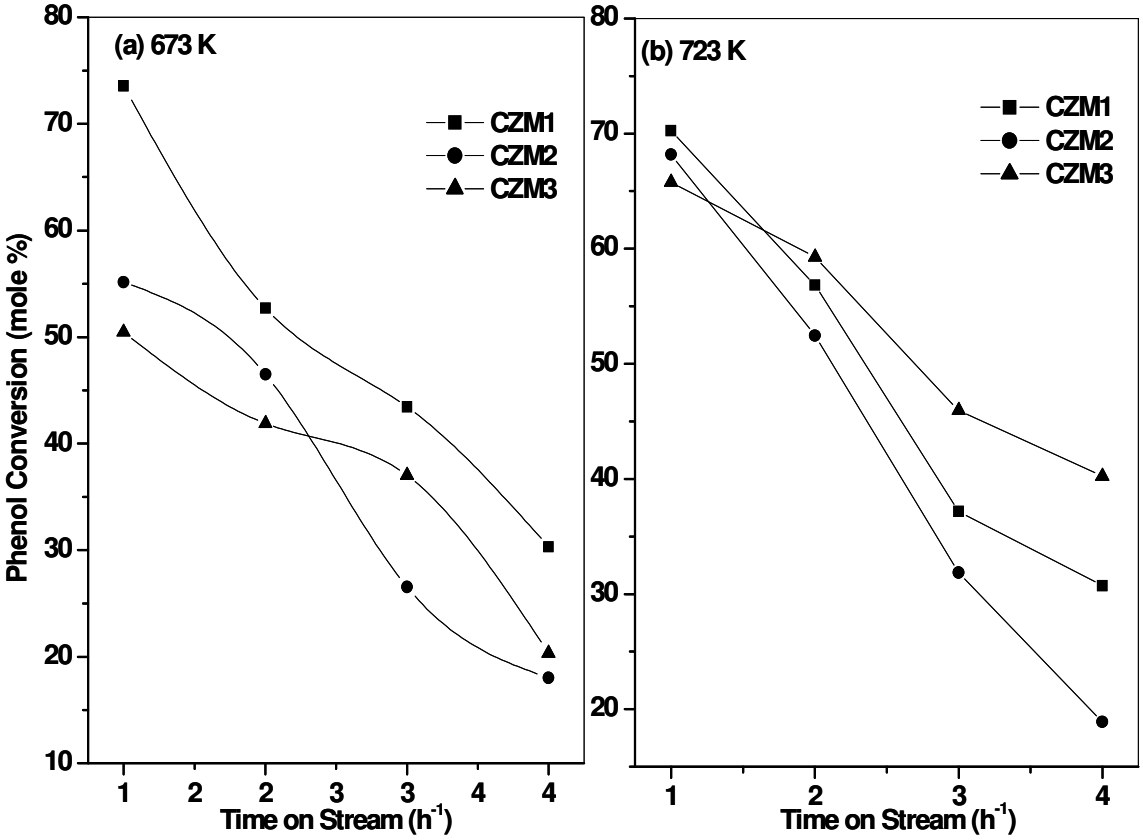

Fig.3.18. *Variation of phenol conversion at two different temperatures with time on stream over copper- zinc-manganite catalysts. (WHSV 1h^{-1}, MeOH: PhOH is 5:1)*

The phenol conversion observed on CZM_x catalysts at two reaction temperatures (673 and 723 K) using MeOH: PhOH 5 and WHSV 1h^{-1} against time on stream are given in Fig.3.18. It may be seen that all the catalysts were active for methylation of phenol, while highest phenol conversion (74-mol %) was obtained at 673 K on CZM1 catalyst. Whereas the conversion decreased with TOS on all catalysts, reaching a value of 32-mol% after 4 h on CZM1 catalyst. Decrease in Cu/Zn ratio in the catalysts decreased the phenol conversion. Though the deactivation was to the same extent when the reaction was carried out at higher temperature (723K), CZM3 catalyst seems to be relatively stable with TOS. From the Fig.3.18 it may be seen that a similar trend at 673 and 723 K was observed in case of 2,6-xylenol selectivity. A rapid fall in phenol conversion on all the catalysts with time on stream was observed even at high temperature. The order of deactivation among

these catalysts is as follows CZM3>CZM2>CZM1 at 673 K and CZM3>CZM1>CM2 at 723 K (at TOS 2 h).

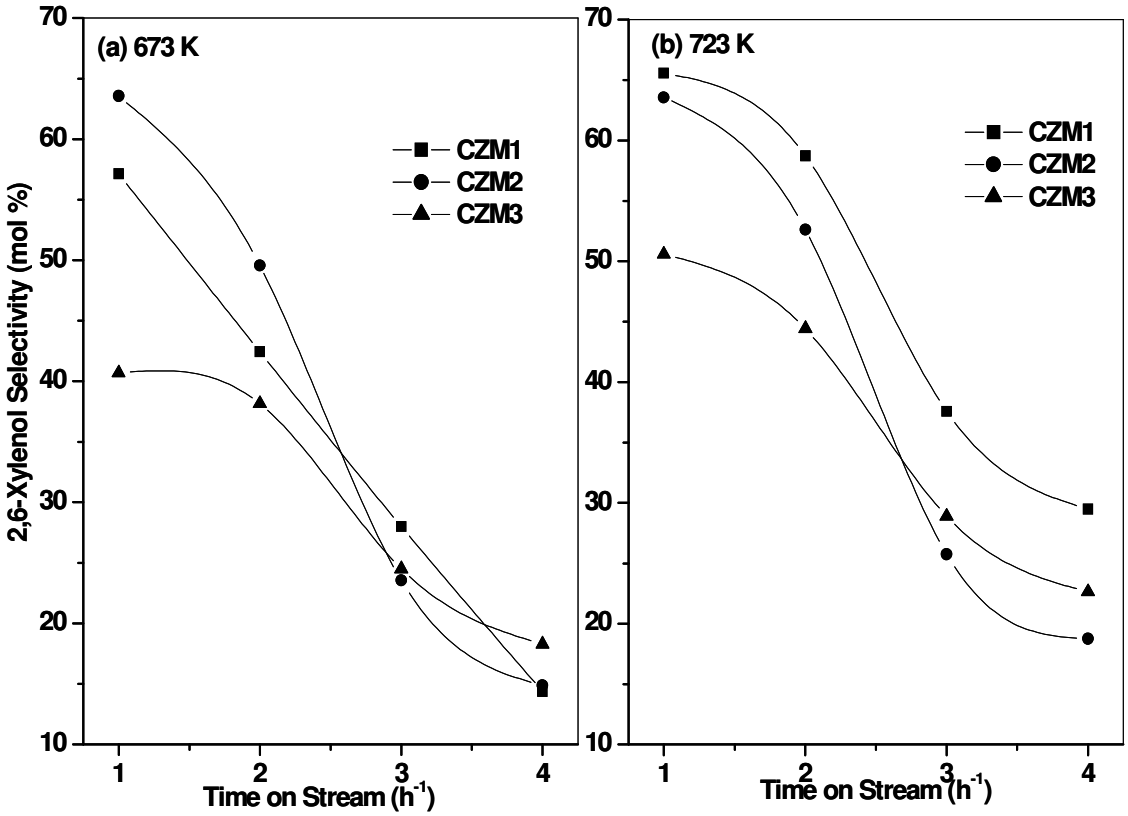

Fig.3.19. *Variation of 2,6-xylenol selectivity with TOS on copper-zinc-manganite catalysts. (a) 673K and (b) 723 K. (WHSV 1h^{-1}, MeOH:PhOH is 5:1)*

Similarly, higher 2,6-xylenol selectivity (64-mol%) was obtained on CZM2 catalyst at 673 K while CZM1 was superior in this respect at 723 K giving 66-mol% (Fig.3.19). Though CZM3 catalyst with relatively low copper content exhibited better phenol conversion at 723 K. Interestingly, CZM1 at 723 K showed better 2,6-xylenol selectivity (~66 mol%), though it too dropped to 28mol% after 4 h on stream. CZM2 was better for 2,6-xylenol selectivity at 673 K, while CZM1 was superior at 723 K. The 2,6-xylenol selectivity values are almost similar on all the catalysts after 2 h TOS at 673 K. With the increase of temperature both phenol conversion (65%) and 2,6-xylenol selectivity increased (58%).

These results show that Cu-Zn-Mn mixed oxide catalysts were no way superior in their activity either compared to Cu-Mn or Cu-Zn mixed oxides. The phenol conversion

values are not comparable. Although the CZM3 catalyst showed high phenol conversion at 723 K, but it was observed that the rate of consecutive methylation of *o*-cresol to 2,6-xylenol was higher CZM1 catalyst. This catalyst with higher Cu/Zn ratio (i.e.20) exhibited high 2,6-xylenol yield at 673 K.

3.4.2. Phenol methylation on copper spinel catalysts: Discussion

The reaction temperature and the variation of Cu and Zn concentrations in the spinel system showed marked influence on their activity and product selectivity in phenol methylation reaction. From the above results, it is observed that the structural changes that occurred during the course of reaction had a major impact on phenol conversion. Apart from this the nature and strength of surface acid-base properties determined the activity. Hence, it is expected that the structural stability could be controlled by incorporation of mixture of other metal ions into the manganese oxide lattice. In other wards, the deactivation of catalysts due to structural changes may be possible to overcome by stabilizing the structures. The catalytic activity on promoted manganese oxides was studied to improve both in terms of phenol conversion as well as 2,6-xylenol selectivity [46]. The catalysts with high Cu/Zn ratio (CZM1) in the mixed oxide composition showed relatively better phenol conversion at 673 K, but consecutive methylation of phenol to 2,6-xylenol was low. CZM2 catalyst containing equal concentration of Cu and Zn (Cu/Zn =1) though relatively showed low activity compared to CZM1, but it was selective towards 2,6-xylenol formation. The disparity in the methylation activity between CZM1 and CZM2 may be due to the acid-base properties and heterogeneous distribution of metals on the surface. Though both the catalysts formed $Cu_{1.5}Mn_{1.5}O_4$ phase, the later exhibited high surface area. These catalysts with cubic crystalline phases that are formed with high concentrations of copper showed inferior activity in phenol methylation than tetragonal hausmannite phases. It was observed that catalysts with high Cu/Zn ratio (CZM1 and CZM2) showed rapid deactivation, which is on expected lines as the high copper containing samples may undergo reduction to metallic copper at high temperature (723 K) as a result of prevailing reduction atmosphere during the course of reaction. The presence of Zn ions did not improve the catalytic activity as was observed on zinc-manganite catalysts. As was reported on Cu/Zn catalysts that the Zn^{2+} ions stabilized the copper

species under redox conditions for water gas shift reaction [27]. But, Catalyst with high zinc content (CZM3) showed high phenol conversion than CZM1 and CZM2 at 723 K after 2h of TOS. Relatively better stability of this catalyst may be due to the lower concentration of copper, which might have reduced the extent of reduction (Fig.2.20). Unlike CM_x catalysts ZM_x catalysts did not transform tetragonal to cubic form at higher Zn contents. In spite of inferior activity of copper-zinc- manganese oxides when compared with CM_x or ZM_x, these catalysts are highly selective for methylating phenol in the *ortho* position leading to o-cresol and 2,6-xylenol. Phenol methylation on these catalysts requires a balanced acidity and basicity. The chemisorbed phenol rings orient themselves vertical to the surface giving preferring an electrophilic attack of alkoxide ions in the ortho positions as only ortho positions are acceceble [51].

Structural changes: According to the previous reports, incorporation of Zn^{2+} ions into manganese oxide does not influence the structure of hausmannite structure [52]. This is mainly due to Zn^{2+} (d^{10} system) that occupies tetrahedral sites in the tetragonal sites of hausmannite structure. As Zn^{2+} does not undergo reduction under the experimental conditions, there will not be any change in the oxidation state of Mn ions. Whereas, Cu^{2+} ions in higher concentration distort the tetragonal structure of hausmannite and lead to formation of cubic phase because of redox equilibrium between the Cu^{2+} and Mn^{3+} ions. Higher concentration of Cu in the ternary metal oxide system also resulted in the cubic phase, $Cu_{1.5}Mn_{1.5}O_4$. The extent of reduction of Cu ions is high in these catalysts, resulting in rapid deactivation. The deactivation of catalysts due to reduction of the catalysts in phenol methylation was reported earlier [45].

3.5. Conclusions

Alkylation of phenol using methanol on Cu and/or Zn manganese oxide spinel catalysts revealed that these systems are highly selective for methylation of phenol at the ortho positions leading to formation of o-cresol and 2,6-xylenol. The product streams were absolutely free from other cresols and xylenol isomers. The *O*-methylated product, anisole was also not observed. A trace amount of tri-methyl phenol was observed on these catalysts. Regardless of the composition of the catalysts, the sum of the *o*-cresol and 2,6-xylenol remained at similar levels (>97%). It is observed that, in phenol methylation

reaction, the ratio of Cu^{2+}/Mn^{3+}, Zn^{2+}/Mn^{3+} and Cu^{2+}/Zn^{2+} play a decisive role in determining the total activity and selectivity for the products. The structural changes that occurred during phenol methylation were identified as the main reason for deactivation of the catalysts. In addition, higher concentration of Cu enhanced the reducibility of manganese ions that resulted in structural collapse.

3.5. References

[1] R.F. Lobo, M. Tsapatsis, C.C Freyhardt, S. Khodabandeh, P. Wagner, C.Y Chen, K.J. Balkus Jr., S.I. Zones, M.E. Davis, J. Am. Chem. Soc. 119 (1997) 8474.

[2] C.C. Freyhardt, M. Tsapatsis, R.F. Lobo, K.J. Balkus Jr., M.E. Davis, Nature, 381, (1996) 295.

[3] C. Bezouhanova, M.A. Al-Zihari, Appl. Catal. A 83 (1992) 45.

[4] T. Nishizaki, H. Hattori, and K. Tanabe, An abstract presented at the 23rd Annual Meeting of the Chemical Society of Japan, Tokyo, Part I, 53, No. 03419, 1970.

[5] H. Grabowska, R. Klimkiewicz, L. Syper, J. Wrzyszcz, Top. Catal. 11/12 (2000) 289.

[6] K. Sreekumar, T. Mathew, R. Rajgopal, R. Vetrivel, B.S. Rao, Catal. Lett. 65 (2000) 99.

[7] K. Sreekumar, S. Sugunan, J. Mol. Catal. A: Chem. 185 (2002) 259.

[8] T. Mathew, N.R. Shiju, K. Sreekumar, B.S. Rao, C.S. Gopinath, J. Catal. 210 (2002) 405.

[9] T. Kotanigawa, M. Yamamoto, K. Shimokawa, Y. Yoshida, Bull. Chem. Soc. Jpn. 44 (1971) 1961.

[10] T. Kotanigawa, K. Shimokawa, Bull. Chem. Soc. Jpn. 47 (1974) 1535.

[11] A. Ueno, T. Onishi, and K. Tamaru, Trans. Faraday Soc., 67 (1971) 3585.

[12] T.F. Tsai, F.L. Wang, Catal. Lett. 73, (2001) 167.

[13] W.C. Choi, J.S. Kim, T.H. Lee, S.I. Woo, Catal. Today 63 (2000) 229.

[14] K. Tanabe, T. Nishizaki, in: F.C. Tompkins, (Eds.), Proceedings of the sixth International Congress on Catalysis, vol. 2, 1977, 863.

[15] K. Tanabe, in: B. Imelik et.al (Eds.), Catalysis by acids and bases, Stud. Surf. Sci. Catal. vol. 20, Elseviers, Amsterdam, 1985, 1.

[16] J.M. Campelo, A. Garcia, D. Luna, J.M. Marinas, M.S. Moreno, Stud. Surf. Sci. catal. 41 (1988) 249.

[17] E. Santacesaria, D. Grasso, Appl. Catal. 64 (1990) 83.

[18] K.R. Reddy, K. Ramesh, K.K. Seela, V.V. Rao, K.V.R. Chary, Catal. Commun. 4 (2003) 112.

[19] K. Tanabe, K. Shimazu, H. Hattori, K. Shimazu, J. Catal. 57 (1979) 35.

[20] K. Tanabe, H. Hattori, T. Sumiyoshi, K. Tamaru, T. Kondo, J. Catal. 53 (1978) 1.

[21] K. Tanabe, Stud. Surf. Sci. Catal. Elsevier, Amsterdam, vol. 20, 1985, Chap. 1.

[22] T. Mathew, B.B. Tope, N.R. Shiju, S.G. Hegde, B.S. Rao, C.S. Gopinath, Phys. Chem. Chem. Phys. 4 (2002) 4260.

[23] T. Mathew, M. Vijayaraj, S. Pai, B.B. Tope, S.G. Hegde, B.S. Rao, C. S. Gopinath, J. Catal. 227 (2004) 175.

[24] A.R. Ghande, S.P. Naik, S.B. Kakodkar, J.B. Fernandes, Catal. Comm. 7 (2006) 285.

[25] A.A. Mirzaei, H.R. Shaterian, M. Kaykhaii, Appl. Surf. Sci. 239 (2005) 246.

[26] B.L. Yang, S.F. Chan, W.S. Chang, Y.Z. Chen, J. Catal. 130 (1991) 52.

[27] P. Porta, G. Moretti, M. Musicanti, A. Nardella, Catal. Today 9 (1991) 211.

[28] V.S. Escribano, E.F. López, P.S. Huidobro, M. Panizza. C. Resini, J.M. Gallardo-Amores, G. Busca, Solid State Sciences 5 (2003) 1481.

[29] J.M. Gallardo-Amores, T. Armaroli, G. Ramis, E. Finocchio, G. Busca, Appl. Catal. B: Environ. 22 (1999) 249.

[30] F. Milella. J.M. Gallardo-Amores, M. Baldi. G. Busca. J. Mater. Chem. 8 (1998) 2525.

[31] A. Wöllner, F. Lange, H. Schmelz, H. Knozinger, Appl. Catal. A 94 (1993) 181

[32] A.K.H. Nohman, M.I. Zaki, S.A.A. Mansour, R.B. Fahim, C. Kappenstein, Thermochimica Acta 210 (1992) 103.

[33] M. LeBlanc and G. Wehner, Z. Phys. Chem., 168 (1934) 59.

[34] C.G. Ramakutty, S. Sugunan, Appl. Catal. A 218 (2001) 39.

[35] Y. Tanaka, T. Utaka, R. Kikuchi, T. Takeguchi, K. Sasaki, K. Eguchi, J. Catal. 215 (2003) 271.

[36] S.M. Rodulfo-Baechler, S.L. Gonzalez-Cortes, J. Orozco, V. Sagredo, B. Fontal, A.J. Mora, G. Delgado, Mater. Lett. 58 (2004) 2447.

[37] L. Yin, I. Adler, T. Tsang, L.J. Matienzo, S.O. Grim, Chem. Phys. Lett. 24

(1974) 81.

[38] G.C. Allen, S.J. Harris, J.A. Jutson, J.M. Dyke, Appl. Surf. Sci. 37 (1989) 111.

[39] F.C.M. Driessens, Inorganica Chimica Acta, 1 (1967) 193

[40] A. Navrotsky, O.J. Kleppa, J. Inorg. Nucl. Chem. 29 (1967) 2701.

[41] J. Topfer, A. Feltz, P. Dordor, J.P. Doumerc, Mat. Res. Bull. 29 (1994) 225.

[42] C. Drouet, C. Laberty, J.L.G. Fierro, P. Alphonse, A. Rousset, Int. J. Inorg. Mater. 2 (2000) 419.

[43] K. Tanabe, K. Shimazu, H. Hattori, K. Shimazu, J. Catal. 57 (1979) 35.

[44] R. Klimkiewicz, H. Grabowska, H. Teterycz, Appl. Catal. A: Gen. 246 (2003) 125.

[45] H. Grabowska, R. Klimkiewicz , W. Tylus , P.J. Godowski, Appl. Catal. A 240 (2003) 111.

[46] K.T. Li, I. Wang, K.R. Chang, Ind. Eng. Chem. Res. 32 (1993) 1007.

[47] J.P. Jacobs, A. Maltha, J.R.H. Reintjes, T. Drimal, V. Ponec, H.H. Brongersma, J. Catal. 147 (1994) 294.

[48] K. Sreekumar, S. Sugunan, Appl. Catal. A 230 (2002) 245.

[49] K. Sreekumar, S. Sugunan, J. Mol. Catal. A (185 (2002) 259.

[50] T. Mathew, S. Shylesh, B.M. Devassy, M. Vijayaraj, C.V.V. Satyanarayana, B. S. Rao, C.S. Gopinath, Appl. Catal. A 273 (2004) 35.

[51] J. Wrzyszcz, H. Grabowska, W. Mista, L. Syper, M. Zawadzki, Appl. Catal. A: Gen. 166 (1998) L249.

[52] S. Guillemet- Fritsch, C. Chanel, J. Sarrias, S. Bayonne, A. Rousset, X. Alcobe, M.L. MartinezSarrion, Solid State Ionics 128 (200) 233.

CHAPTER 4

WATER GAS SHIFT REACTION ON Cu BASED SPINEL CATALYSTS

4.1. Introduction

Water gas shift (WGS) reaction is an important process step in the commercial production of hydrogen [1] via steam reforming of hydrocarbons. It is also important in case of futuristic energy technologies such as fuel cells based on H_2 [2]. In water gas shift reaction, steam and carbon monoxide react to form carbon dioxide and hydrogen (water splitting). Altough WGS reaction was well studied, there has been a renewed interest in view of fuel cell applications that require pure hydrogen. The WGSR is desirable for CO removal from reformed fuels containing high concentrations of CO. Gas composition and operating conditions for the WGS reaction differ significantly between industrial and fuel cell applications. The hydrogen production for PEFCs involves frequent startups and shutdowns. The catalysts used for the shift reaction in case of fuel cell applications are, therefore, sometimes exposed to water at low temperatures and oxygen during shutdown. Hence, efforts are being made to design highly active and stable WGS catalysts that are not only highly active but are also robust for fuel cell applications. Platinum supported on ceria based oxides has been increasingly studied as alternative to the commercially available Cu-ZnO-Al_2O_3 low temeprature shift (LTS) catalyst. The later operates between 453-523 K for bringing CO levels to 0.1 - 0.5 vol %. The higher activity of copper and platinum when supported on ceria, in redox reactions, has been ascribed to their high oxygen storage capacity (OSC) and reducibility [3]. Copper catalysts in combination with ceria have received considerable attention over precious metals due to their advantage interms of cost. Copper based catalysts are generally more active for the CO oxidation reaction but not stable to oxidant gases and sinter above 573 K when compared to precious metals [4,5]. Therefore, formation of highly dispersed copper in combination with reducible support resulted in enhancement of the catalytic activity [6,7]. Hence, development of highly stable Cu-catalysts is important considering their low cost and better WGS activity [5-12]. In this regard, copper based spinel catalysts (Cu/MnO) [6,7] have receieved greater attention due to their higher WGS activity at low temperatures than supported platinum catalysts (Pt/CeO_2) [4]. The equilibrium conversion of CO largely depends on the reaction temperature, lower temperatures being more favorable for higher percent of CO removal. On the other hand, from the kinetic viewpoint, the reactivities are better at high

temperatures. It was reported that spinel type Cu-oxide catalysts showed excellent WGS activity compared to the conventional $Cu/ZnO/Al_2O_3$ catalysts [6,7,13-18]. Hopcalite, a manganese oxide spinel ($CuMnO_4$) is known for its high CO oxidation activity at ambient temperature, is used in gas masks in coal mines for oxidation of CO and other gass [19-21]. Mnganese oxide based spinel catalysts have been claimed for high WGS activity without any by-product formation under wide range of experimental conditions [18]. Knowing the limitations of commercial $Cu/ZnO/Al_2O_3$ catalyst [12,22], which sinters above 573 K leading to deactivation, it also needs high steam to carbon ratio, careful reduction process. It deactivates in presence of oxidants and sulfur. Hence, systematic study of Cu based spinel catalysts were taken up. In the present study, catalytic activity of Cu-Mn and Cu-Zn-Mn spinel-type oxides were evaluated for WGS reaction at high concentration of CO and in presence of CO_2 and H_2. The aim of the present work is to study the influence of (i) the spinel-type Mn mixed oxide (ii) the copper loading (iii) addition of zinc (iv) reaction temperature (v) WGS feed composition and (vi) the space velocity. In this chapter, we report two catalyst systems for WGS reaction, one containing Cu and Mn in various proportions ($Cu_xMn_{3-x}O_4$, x = 0.25, 0.5 and 1.0) designated as $CM_{0.25}$, $CM_{0.5}$ and $CM_{1.0,}$ respectively, (Table 2.1) while the other system contains Zn in addition to Cu and Mn. These Cu-Zn-Mn spinels contain Cu:Zn:Mn in the atomic ratio of 36:18:46, 35:35:30 and 18:36:46 which are designated as CZM1, CZM2 and CZM3, respectively. The activity of Cu catalysts in WGS reaction was discussed and correlated with the structural and red-ox characteristics of the catalysts obtained by employing different characterization techniques such as XRD, TG-DTA and XPS. Even the spent catalysts were charecterized by XPS for obtaining valuble information.

4.2. Activity of Cu- Mn and Cu-Zn-Mn spinel catalysts: Results and Discussion

4.2.1. Effect of catalyst composition

From the literature it is known that certain first-row transition metal oxides have been successfully used as active catalysts or promoters for water gas shift reaction [23,24]. Among the transition metal systems, copper-zinc has been the most promising catalyst for

this reaction. Activities of Cu-Mn and Cu-Zn-Mn spinel catalysts for the water-gas shift reaction at two different reaction temperatures are shown in Fig.4.1. All the catalysts used in this study were reduced in situ at 523 K, unless otherwise stated, using 5%H_2 in nitrogen, before being cooled to the reaction temperature. The reaction data on CO conversion given in Fig.4.1 was obtained at 473 and 523 K after 1 h of TOS.

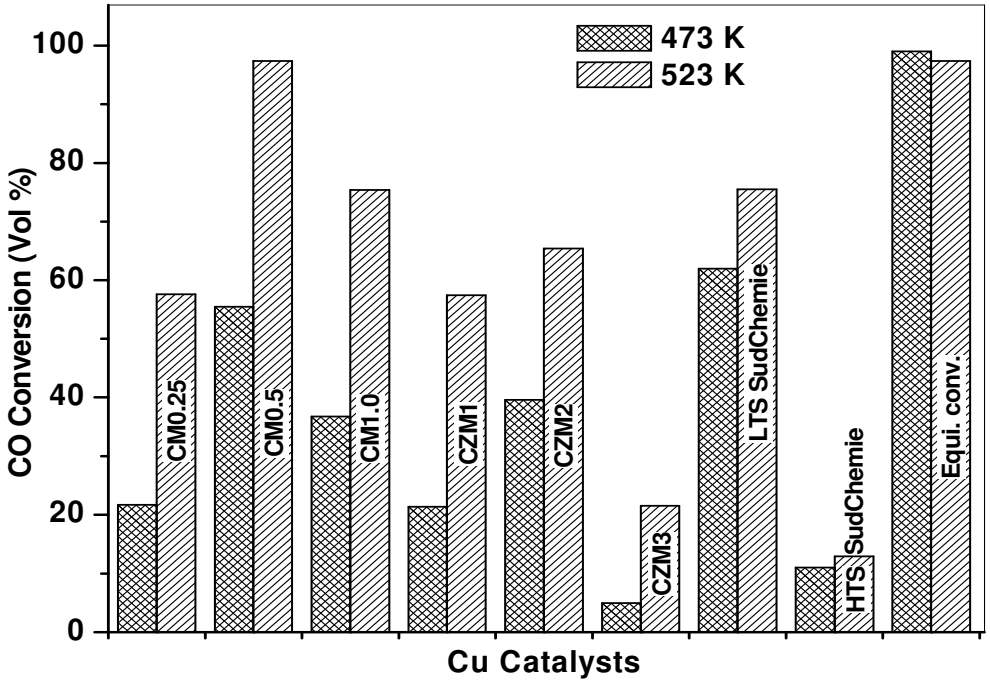

Fig.4.1. *WGS activity over copper-manganese (CM_x) and copper-zinc-manganese oxide spinels (CZM_x) with various compositions at 473 and 523 K.*
*(Feed composition (*24%H_2, 21%N_2, 6% CO, 9%CO_2 and 40% H_2O*), GHSV 5000 h^{-1}, TOS 1 h)*

Results of these catalysts are also compared with the performance of commercial LTS and HTS catalysts (supplied by Sud-Chemie, India) under similar reaction conditions). Activity of the copper-manganese spinel-type oxide catalysts varied considerably with their composition. It is also observed that the copper content in the spinel-system and the reaction temperature has a strong influence on the CO conversion in WGS reaction (Fig.4.1). The catalysts $CM_{0.5}$ and CZM2 showed highest CO conversion among the Cu-Mn and Cu-Zn-Mn series of spinels, respectively, at both the reaction temperatures studied. Where as, activity increased for all the catalysts when the temperature increased from 473 to 523 K. Though both $CM_{0.5}$ and CZM2 catalysts showed relatively lower activity than commercial LTS catalyst (Cu-ZnO-Al_2O_3), at lower temperature (473 K),

$CM_{0.5}$ gave better WGS activity than LTS catalyst at higher temperature (≥523 K). Although LTS showed relatively higher activity (62 mol % CO conversion) at 473 K, it did not reach the required equilibrium CO conversion (98.7%) for the given feed composition (24%H_2, 21%N_2, 6% CO, 9%CO_2, and 40% H_2O). It is known that commercial LTS catalysts are more effective only at lower space velocity (≤3000 h^{-1}) and when the CO concentration is low (≤3%). $CM_{0.5}$ catalyst gave high CO conversion (97%) at 523 K, which is nearly equivalent to the equilibrium CO conversion (97.4%). All the catalysts showed considerable increase in the CO conversion with the increase in reaction temperature. It is known that CO conversion is not kinetically favored at low temperatures. The CO conversion has improved towards equilibrium on $CM_{0.5}$ at 523 K. However, the CO conversion is lower than the equilibrium on all other catalysts. These results show that the concentration of copper in manganite spinels has an important role to achieve high CO conversion at optimum temperature i.e. 523 K. According to Tanaka et al. [7], Cu-Mn spinel-type catalysts calcined at high temperature (1173 K) having low surface area showed excellent CO conversion activity at 523 K. Whereas, our best catalyst, $CM_{0.5}$ calcined at 773 K, which has relatively high surface area showed superior activity under the more vigorous conditions (6% CO, 40% H_2 and 40% H_2O) than that were used (1.25% CO, 37.5% H_2 and 25% H_2O) by Tanaka et.al. The CO conversion has increased initially ($CM_{0.25}$ to $CM_{0.5}$) with the increase in copper in manganese oxide spinel system indicating Cu is the active component in the catalyst. However, on further increase in Cu content ($CM_{1.0}$) the activity decreased, probably due to high copper content in the spinel that led to lower copper dispersion resulting in its agglomeration in reducing atmosphere.

4.2.2. Effect of reaction temperature

Effect of the reaction temperature on CO conversion was investigated in the 473 to 673 K range over Cu-based spinel-type catalysts and the results are shown in Fig.4.2. Significant influence of the temperature on CO conversions was observed for all the catalysts. Highest equilibrium CO conversion that can be achieved for given feed composition is 98.7% at 473 K and 83.14% at 673 K.

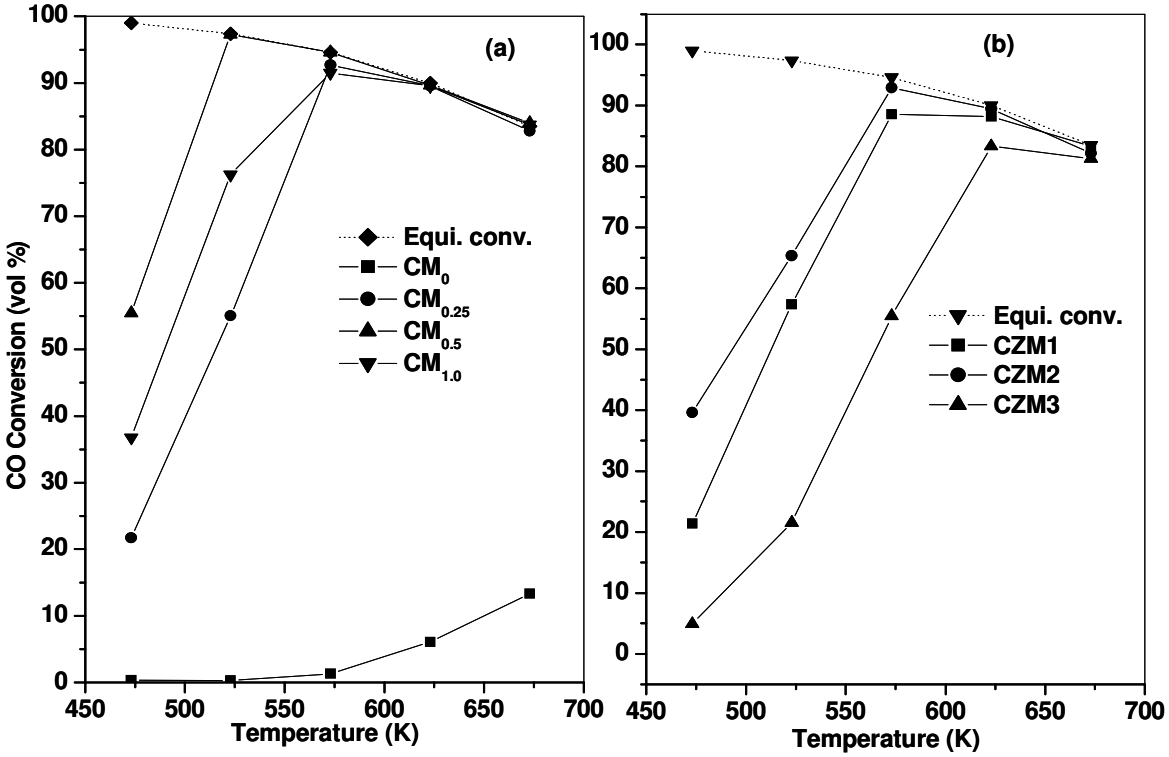

Fig.4.2. *Effect of reaction temperature on WGS activity over (a) Cu-Mn (b) Cu-Zn-Mn catalysts after calcination at 773 K. Feed composition (24%H_2, 21%N_2, 6% CO, 9%CO_2, and 40% H_2O), GHSV 5000 h^{-1}, TOS 1 h*

Catalytic activity gradually increased with the temperature. Equilibrium CO conversion was achieved on $CM_{0.5}$ at relatively lower temperature (~523 K) compared to other catalysts in Cu-Mn and Cu-Zn-Mn series. Pure manganese oxide showed a lower activity for the shift reaction. Since WGS reaction is an exothermic and reversible reaction, the equilibrium conversion of carbon monoxide largely depends on the reaction temperature: lower temperatures favor higher CO removal but not kinetics. Therefore, there exists an optimum temperature (473 and 553 K) for achieving good CO conversion that is suitable for a PEM fuel processor. In addition, CO_2 formed by forward reaction can react with H_2 to form CO according to Le-Chatelier's principle [25,26]. It is inferred from the above result that the increase in Cu loading led to the increase in WGS activity until x = 0.5, but excess Cu loading did not help in further improvement of activity. The concentration of copper in the $CM_{0.5}$ was most appropriate to optimize the kinetic and thermodynamic factors helping to achieve equilibrium CO conversion at relatively low temperature (at 523 K). But, other Cu-Mn catalysts ($CM_{0.25}$ and $CM_{1.0}$) gave equilibrium CO conversions at much higher

temperature (≥573 K). Thus at low temperatures (<523 K) the WGS activity of Cu-Mn catalysts followed the order of $CM_{0.5}$ >$CM_{1.0}$>$CM_{0.25}$>CM_0. At 573 K and above, the WGS activity of Cu-Mn catalysts was nearly comparable though they differ in their chemical composition. Therefore the optimum Cu loading appears to be x = 0.5. The CZM1 and CZM2 catalysts also showed a linear increase in the activity with increasing reaction temperature. CZM1 and CZM2 catalysts showed CO conversions of about 88.6% and 92.7%, respectively at 573 K. At further high temperatures, nearly equilibrium CO conversions were achieved on these catalysts. However, CZM3 showed relatively low activity over the temperature range studied compared to other Cu-Zn-Mn catalysts. This may be attributed to low Cu content among the CZM catalysts. It is also clear from these results that the WGS activity of CZM_x catalysts is not influenced by the zinc content. Although CZM1 and CZM2 catalysts exhibited high CO conversions at 573 K, the temperature is on the higher side compared to $CM_{0.5}$ catalyst.

4.2.3. Effect of space velocity

The effect of space velocity (contact time) on the CO conversion in WGS reaction over Cu-Mn and Cu-Zn-Mn catalysts is shown in Fig.4.3 at two reaction temperatures (573 and 623 K, respectively). It was demonstrated that the activity of the copper based catalysts depends on the surface area and crystalanity [11]. They also, reported that the CO conversion is dependant on the space velocity and that the thermodynamic equilibrium is achieved at a low space velocity. It is observed that among these catalysts, $CM_{0.5}$ showed relatively better performance in terms of high CO conversion even at higher space velocities, where as other Cu-Mn catalysts deactivated rapidly with time at a given space velocity. For better comparison of the catalysts, the effect of space velocity was investigated at 573 K. Catalyst $CM_{0.5}$ gave stable equilibrium CO conversion that was almost constant up to a GHSV of 20 000 h^{-1}.

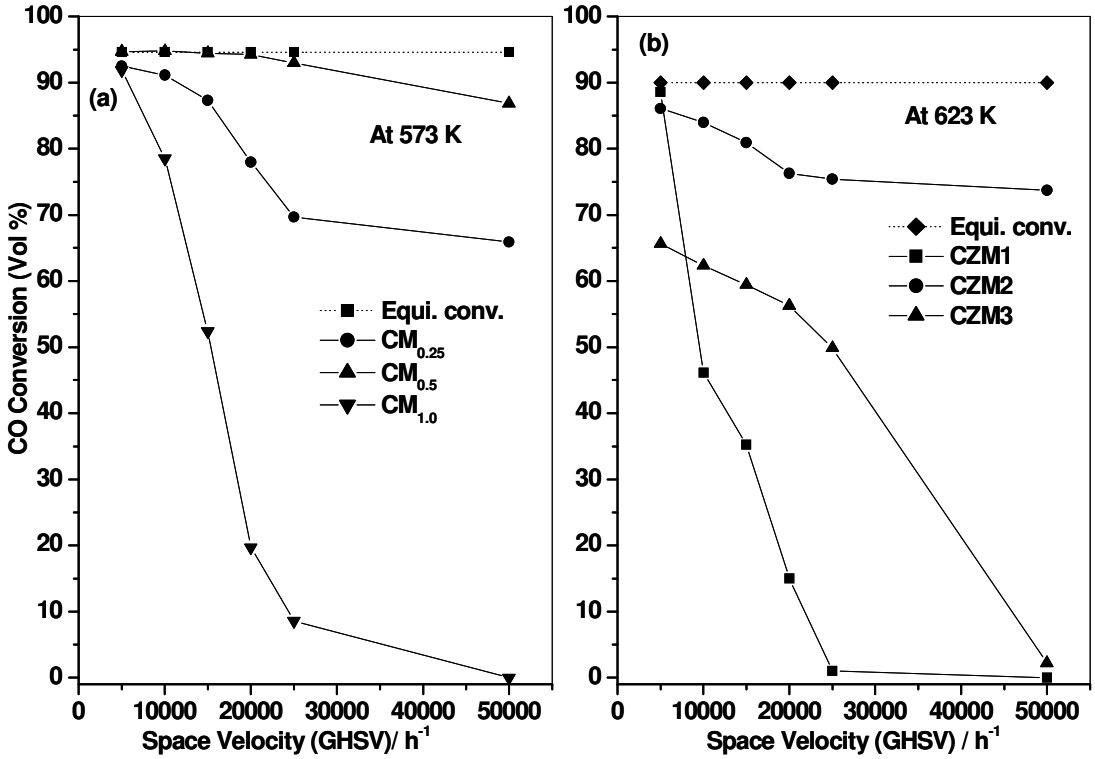

Fig.4.3. *Influence of space velocity (GHSV) on (a) copper manganites at 573 K and (b) copper-zinc-manganite catalysts at 623 K after calcination at 773 K. Feed composition* (24%H_2, 21%N_2, 6% CO, 9%CO_2, and 40% H_2O*).*

But on further increase of space velocity, a fall in the CO conversion from 94 to 86%, when the space velocity increased from 20,000 to 50,000 h^{-1}. Although all Cu-Mn catalysts showed comparable CO conversion at GHSV of 5,000 h^{-1} (≥573 K), at high space velocities only $CM_{0.5}$ catalyst exhibited relatively better performance. $CM_{1.0}$ catalyst with high amount of copper showed poor performance. Even when the space velocity is slightly increased to 10,000 h^{-1}, the differences in activity of various Cu-Mn catalysts became very clear and the activity followed the order $CM_{0.5} > CM_{0.25} > CM_{1.0}$ at 573 K. The highest CO conversion observed at 573 K for a GHSV 50,000 h^{-1} was 86% on $CM_{0.5}$ catalyst.

The addition of zinc to Cu-Mn mixed oxide system did not show any improvement on CO conversion at high space velocities. But it certainly stabilized the catalysts to give better performance when Cu/Zn ratio was appropriate. The catalysts CZM1, CZM2 and CZM3 contain Cu/Zn molar ratio of 2, 1 and 0.5, respectively. Although CZM1 exhibited nearly equilibrium CO conversion initially, it dropped steeply with increasing space velocity; while the performance of CZM2 catalyst was relatively stable at higher space

velocities. It was reported that combination of copper and zinc in commercial mixed oxide catalysts (Cu/ZnO) would lead to better performance in WGS reaction [28]. Among the Cu-Zn-Mn catalysts, CZM2 exhibited highest CO conversion (at 623 K) at a given space velocity. Although this catalyst showed superior activity at high space velocities, the corresponding CO conversion values were relatively low when compared with $CM_{0.5}$. The decrease in the CO conversion at high space velocities is probably because of competitive adsorption of CO over that of H_2O on Cu sites under the CO rich conditions. As a result, the relative abundance of surface hydroxyl groups, which are believed to be the key for the formation of intermediates in the oxidation of adsorbed CO are limited. Regeneration of the Cu sites might be hindered resulting in the lower CO conversion than that expected at equilibrium for the given temperature [13].

4.2.4. Influence of calcination at higher temperature

The WGS activity of CM and CZM catalysts calcined at 973 K was ploted against the reaction temperature in Fig.4.4.

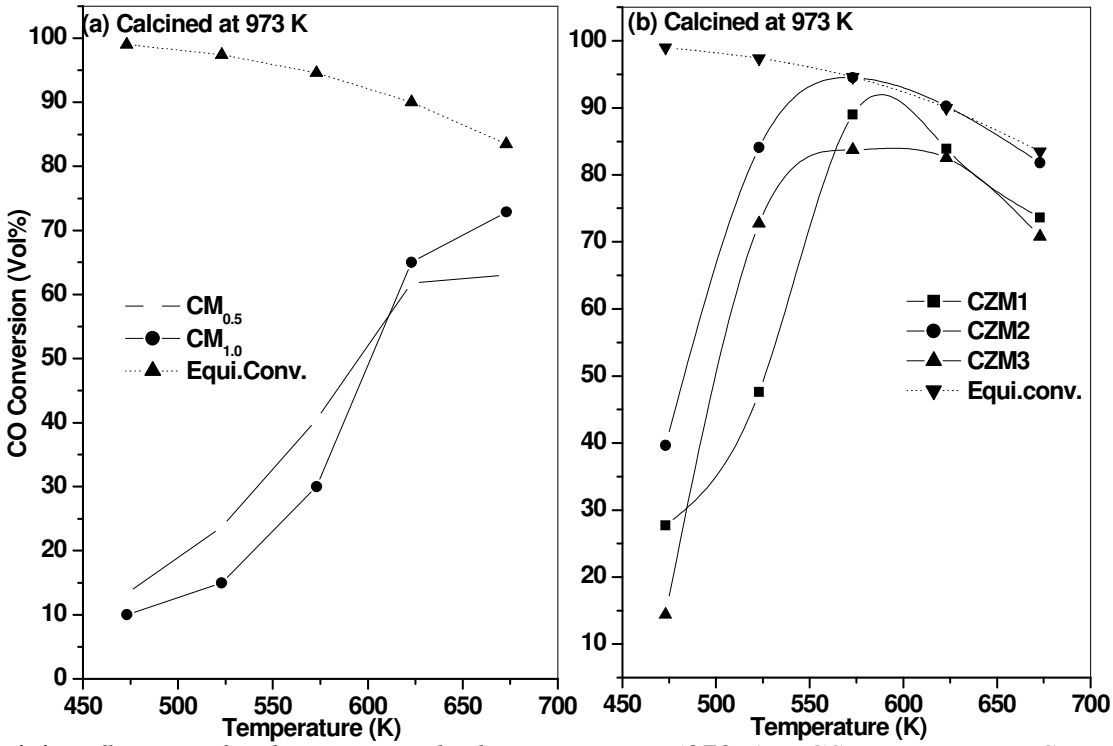

Fig.4.4. *Influence of calcination at high temperature (973K) WGS activity over Cu-Mn catalysts. Feed composition (*24%H_2, 21%N_2, 6% CO, 9%CO_2*, and 40% H_2O), GHSV =5000 h^{-1}*

It was observed that $CM_{0.5}$ gave better performance at lower temperature in terms of CO conversion (Fig.4.4a, up to 573 K), while $CM_{1.0}$ was better at higher temperature. The highest CO conversion achieved on $CM_{0.5}$ was 62% at 623 K at a GHSV of 5 000 h^{-1}. The activity was lower compared to to the same sample calcined at 773 K. It is expected that an increase in calcination temperature would minimize the Cu surface area due to sintering thereby reducing WGS activity. Hence, the calcination temperature has a significant effect on the catalytic activity.

The low activity of catalysts calcined at high temperature may be attributed to sintering of active Cu species. These observations are in contrary to the results reported by Tanaka et al. as they observed excellent WGS activity on Cu-Mn catalysts despite the samples had low surface area [7]. Whereas the zinc containing CZM_x catalysts retained the activity even after calcination at 973 K, probably the presence of zinc hindered the aggregation of copper particles on the surface of the catalysts.

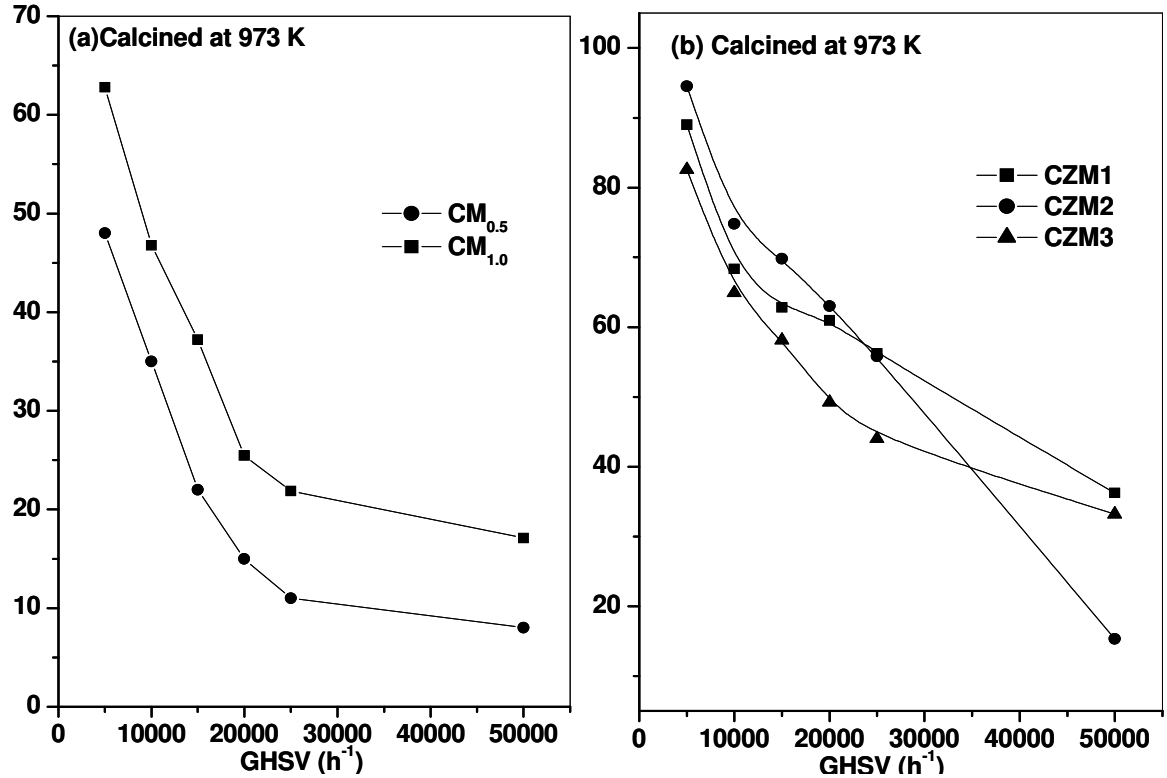

Fig.4.5. *Influence of calcination at high temperature (973 K) on WGS activity over Cu-Mn catalysts at various space velocities at (a) 573 K and (b) 623 K. Feed composition (24%H_2, 21%N_2, 6% CO, 9%CO_2, and 40% H_2O).*

CZM3 that was high amount of zinc showed relatively better activity compared with the sample calcined at 773 K, while CZM2 catalyst showed better performance with in the series. The CZM1 catalyst with high Cu/Zn ratio showed poor WGS activity; this maay be due to sintering at high calcination temperature. Relatively better activity was observed on CZM2 and CZM3 catalysts compared to CZM1.

Effect of space velocity on WGS activity over these catalysts (after calcination at 973 K) is also presented in Fig.4.5. In case of CM_x series of catalysts, $CM_{1.0}$ with higher copper content showed better CO conversion (62%, 5000 h^{-1}) despite of its low surface area. Tanaka et al. made similar observations. There is a continuous decrease in CO conversion with increasing space velocity on all the catalysts. The activity of CZM catalysts in WGS reaction against space velocity was similar as observed in the case of catalysts calcined at 773 K.

4.2.5. Comparison of WGS activity with and without CO_2 in the feed

The presence of H_2 and CO_2 and their concentration in thr feed are known to influence the WGS reaction. Where as, many studies reported in the literature were carried out in absence of either or one of them [25]. This is a serious lacunae as we report in this study that the forward reaction is inhibited by the presence of CO_2 and thus the CO conversion values reported in the absence of CO_2 in the WGS gas feed are always likely to be higher than the values one could have usually obtained in realistic conditions. Although the WGS reaction has been widely investigated, there have been only limited reports on the influence of CO and CO_2 concentrations in the feed [7,29].

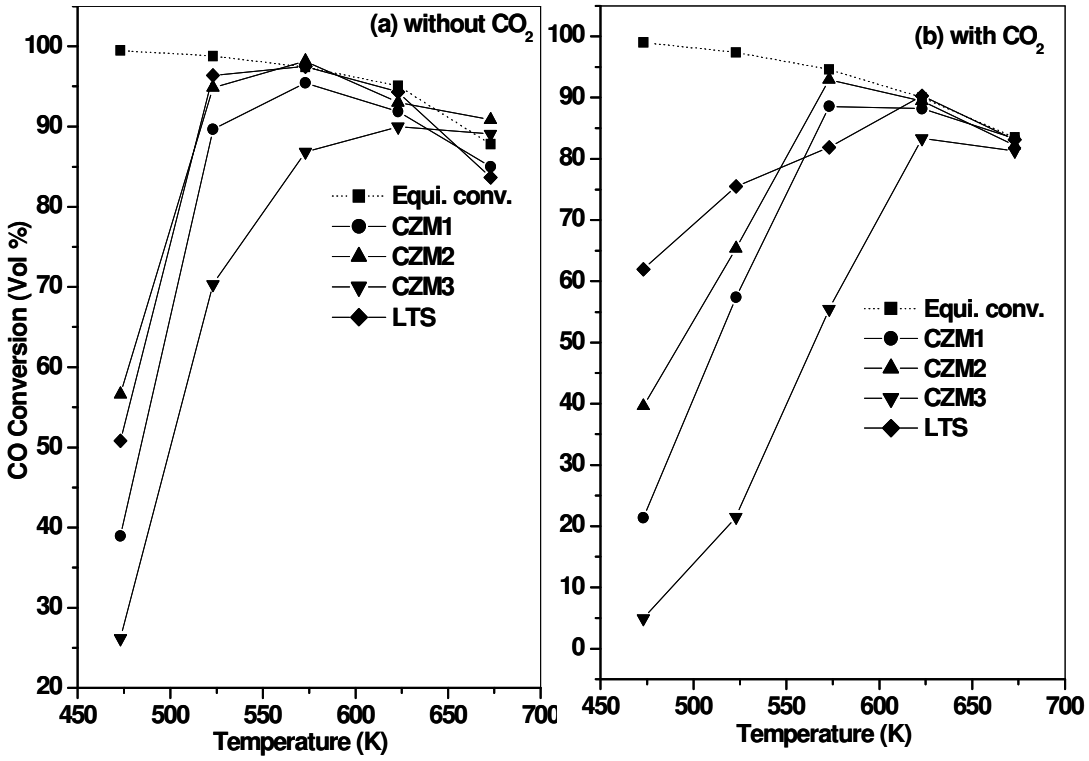

Fig.4.6. *Influence of CO_2 in the WGS gas mixture on the catalytic activity over Cu-Zn-Mn catalysts calcined at 773 K. (Feed composition (a) 30%H_2, 24%N_2, 6% CO and 40% H_2O (b) 24%H_2, 21%N_2, 6% CO, 9%CO_2, and 40% H_2O), GHSV =*

Fig.4.6 presents the CO conversion data on CZM_x catalysts in the presence and absence of CO_2 in the WGS gas feed mix at different reaction temperatures. The results suggest that CO conversion values close to equilibrium were achieved only at higher temperatures in presence of carbon dioxide. The CZM2 catalyst showed slightly better performance at 473 K, compared to commercial LTS catalyst in the absence of carbon dioxide in the feed, while at higher reaction temperatures (>473 K) both gave comparable performance. CZM1 and CZM3 catalysts were relatively less active at any given temperature even in the absence of CO_2 in the feed. In presence of CO_2 in the WGS feed; the performance of commercial LTS catalyst was better at low temperatures (≤523K), whereas at 573 K, CZM2 catalyst appeared to be more active. At still high temperatures, all the catalysts exhibited nearly similar CO conversion. It is also seen that coexistence of CO_2 in the feed reduces the CO conversion at higher temperatures.

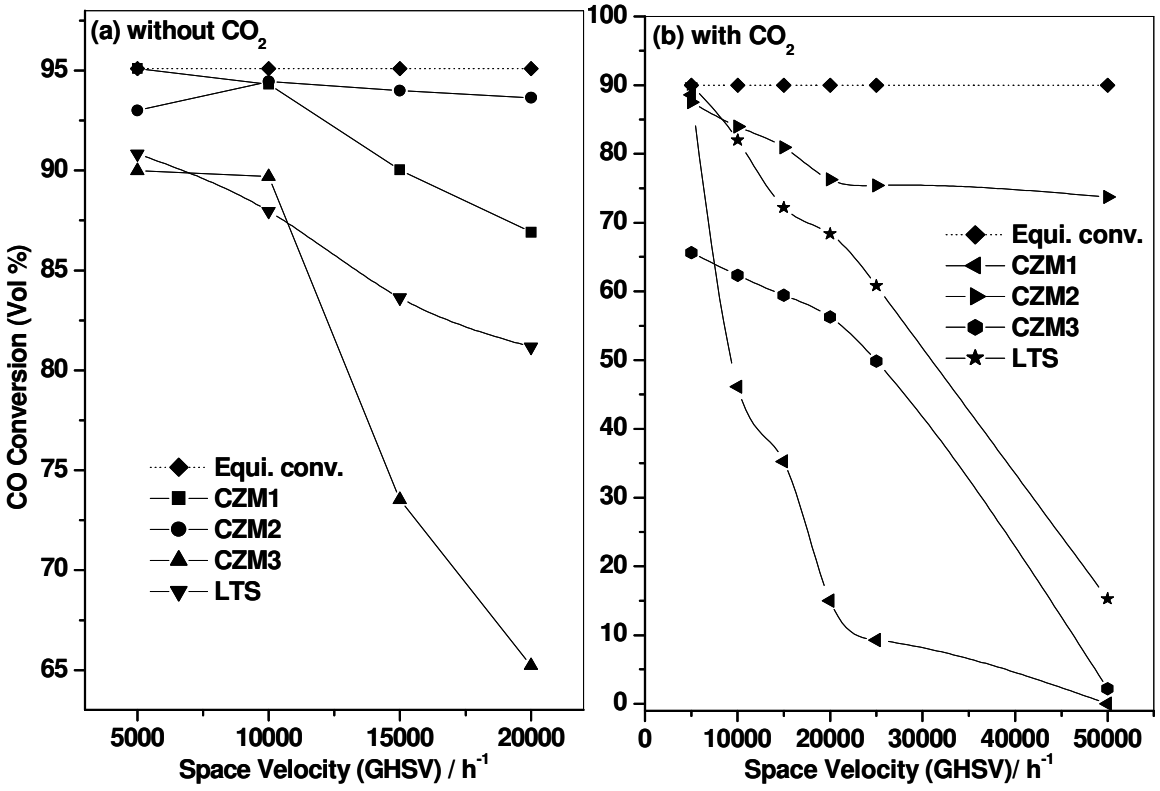

Fig.4.7. *Influence of CO_2 in the WGS gas feed on the catalytic activity at various space velocity over Cu-Zn-Mn calcined at 773 K. Feed composition (a) 30%H_2, 24%N_2, 6% CO and 40% H_2O) (b) (*24%H_2, 21%N_2, 6% CO, 9%CO_2, and 40% H_2O.

These results suggest that the presence of CO_2 in the feed shifts equilibrium towards low CO conversions. Fig.4.7 shows the effect of CO_2 in the feed at various space velocities. It is evident that CZM1 showed better performance in the absence of CO_2 when compared to CZM3, while the presence of CO_2 led to a steep fall in the CO conversion particularly at high at space velocities on the former catalyst. However, the CO conversion at a given space velocity was always higher in the absence of CO_2 in the feed on all the catalysts. It is inferred from these results that at low temperatures, the slow desorption rates of CO_2 or its high surface coverage results in the low CO conversion. Hence, it can be stated that the desorption rates of CO_2 at low temperatures determines the efficiency of a low temperature shift catalyst. Among the series of Cu-Zn-Mn catalysts, CZM2 offered better CO conversion, than commercial low temperature shift catalyst even at relatively higher space velocities. Therefore, it may be stated that this particular catalyst composition enhanced desorption of CO_2 at relatively low temperatures. The zinc content also plays a major role

in achieving high CO conversions; we believe that the percentage of zinc was optimum in CZM2; thus enhancing the rate of CO_2 desorption that resulted in high CO conversion.

4.2.6. Effect of space velocity at various reaction temperatures on $CM_{0.5}$ catalyst

Fig.4.8 presents the effect of space velocity on the WGS activity of $CM_{0.5}$ catalyst at different reaction temperatures. The results show that the activity dropped relatively more rapidly at 523 K with the increase of space velocity, despite showing high initial activity. Where as, at higher reaction temperatures (573 and 623 K), the same catalyst showed relatively much better activity without much fall with increasing space velocity, though CO conversions were low as a result of higher reaction temperatures (equilibrium effect). The better activity at higher temperatures can be attributed to the higher kinetic rates, as the reaction is limited by kinetics at low temperatures. Two different mechanisms have been reported for this reaction; both the mechanisms were supported by various groups of researchers [30-32].

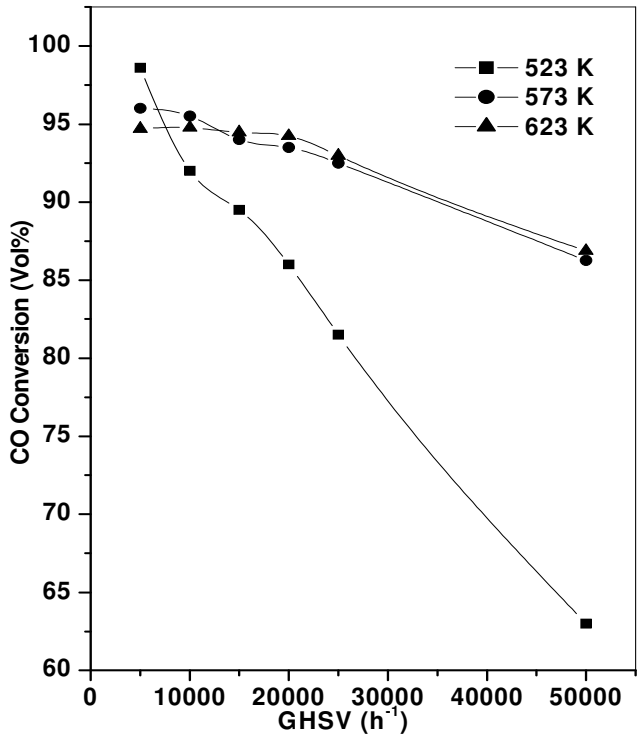

Fig.4.8. Comparision of WGS activity of $CM_{0.5}$ catalyst at different reaction temperatures against variation of space velocity. Feed composition 24%H_2, 21%N_2, 6% CO, 9%CO_2, and 40% H_2O

4.2.7. WGS activity against time on stream over $CM_{0.5}$ catalyst

Fig.4.9 presents the time on stream study of $CM_{0.5}$ catalyst at 573 K. The catalyst was highly stable up to 15 h on stream. The CO conversion was about 94% till 15 h of TOS, which fall thereafter. After 30 h of TOS, the CO conversion reduced to 87%. This decrease in the activity may be attributed either to strongly bound carbonates, whose accumulation might have increased with time or may be because of sintering of Cu. It was observed in these studies that these Cu containing spinels collapse by forming Cu metal and MnO. The Cu metal may sinter with time. Though carbonates could not be identified by power XRD, these were also reported to be responsible for deactivation [33].

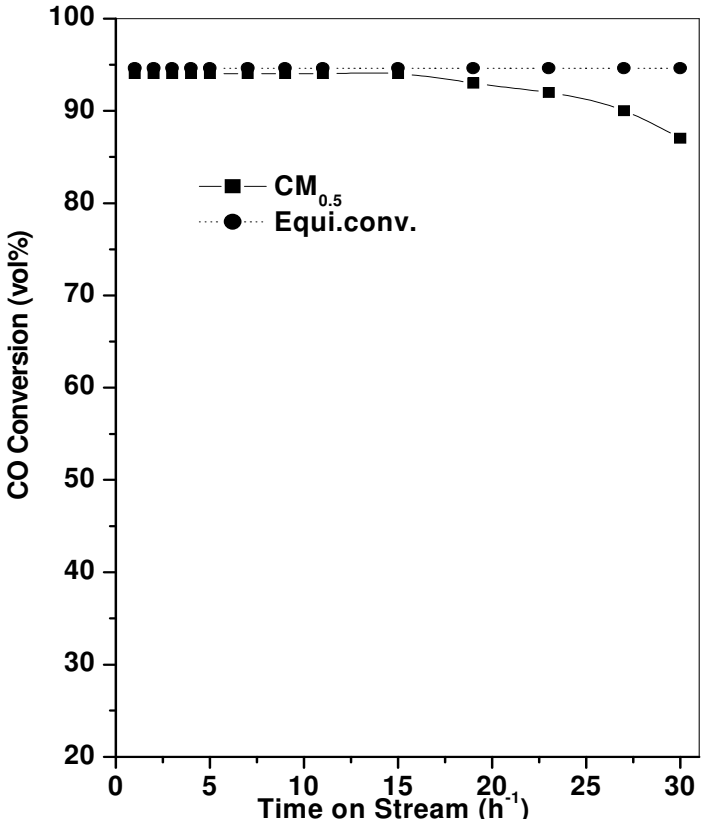

Fig.4.9. *WGS activity of $CM_{0.5}$ catalyst against time on stream studies at 573 K. GHSV 5000 h^{-1}, Feed composition 24%H_2, 21%N_2, 6% CO, 9%CO_2, and 40% H_2O*

4.2.8. Structure- activity correlation and characterization of spent catalysts

It has been reported that the active sites on supported copper catalysts for WGS reaction depend on the crystalline phase of the support or catalyst, active metal surface

area and copper crystallite size [34]. The catalyst composition, crystalline phase(s), crystallite sizes and surface area values for CM_x and CZM_x series catalysts are presented in Table 2.1 and Table 2.8, respectively. The surface areas of zinc containing catalysts were higher when compared to Cu-Mn spinels calcined at 773 K. This could be due to better stabilization of the structure on incorporation of zinc, apart from the influence of composition. After calcination at 993 K, surface areas of all the catalysts reduced as may be expected due to aggregation of the particles. However, high temperature calcined catalysts were not that active as observed for Cu-Mn catalysts [7]. $CM_{0.5}$ was observed to have stoichiometric spinel phase, hausmannite along with Mn_5O_8. Whereas, $CM_{1.0}$, CZM1 and CZM2 formed nonstoichiometric spinel phases ($Cu_{1.5}Mn_{1.5}O_4$). It has been reported that CO conversion depends on the space velocity and the thermodynamic equilibrium can be achieved with much ease at low space velocities [35]. $CM_{0.5}$ and CZM2 catalysts show better activity in terms of CO conversion among Cu-Mn and Cu-Zn-Mn series catalysts, respectively. At low temperature, $CM_{0.5}$ catalyst, which in our view has optimum copper content, gave better CO conversion compared to other CM or CZM series catalysts. However, at high space velocities even this catalyst gave lower than equilibrium CO conversion. It was observed that during the WGS reaction copper oxide has reduced to copper metal, while higher oxides (Mn_3O_4), reduced to corresponding lower oxides (MnO/ZnO) (Fig.4.10b). Water present in the feed acts as oxidant and the active species in the catalysts might undergo redox cycle (in redox mechanism) to yield carbon dioxide when reacted with CO. Hence, it is appropriate to correlate the catalytic activity with crystalline structure, dispersion of copper and red-ox behavior of the catalysts. It was seen that catalyst with high copper content ($CM_{1.0}$), showed aggregation of copper metal resulting in lowering of its catalytic activity (Table.2.4). In the red-ox type reactions, although the reduced species get oxidized (red-ox cycle) in the presence of oxidant (H_2O), high Cu content may have low intimacy with manganese ions resulting in the formation of large aggregates. Similarly, higher calcination temperature may also have led to low surface areas as a result of sintering. XRD of fresh catalysts revealed that $CM_{1.0}$ (Fig.2.13) and Cu-Zn-Mn (Fig.2.14) catalysts formed nonstoichiometric $Cu_{1.5}Mn_{1.5}O_4$ phases. High surface area of these catalysts could be the reason for robust WGS activity even for feeds that contain high concentration of CO (6 vol %). Tanaka et al. reported that Cu/Mn

catalysts with low surface area (1 m^2/g) also showed higher activity [7,36]. Hence, it was claimed that surface area might be not be determining factor for WGS activity on these catalysts. However, our results show that catalysts calcined at low temperatures with high surface area gave better activity. Apart from this, the stability of Cu-Mn spinel phase, which influences the reduction of copper ions and the dispersion of active copper species determine the activity [28]. The XRD of spent catalysts given in Fig.4.10 shows that the constituent metal ions reduced to lower oxidation states (Cu^o, Zn^{2+} and Mn^{2+}). Our TPR results show (Fig.2.15) that reduction occurs even before exposing them to the feed.

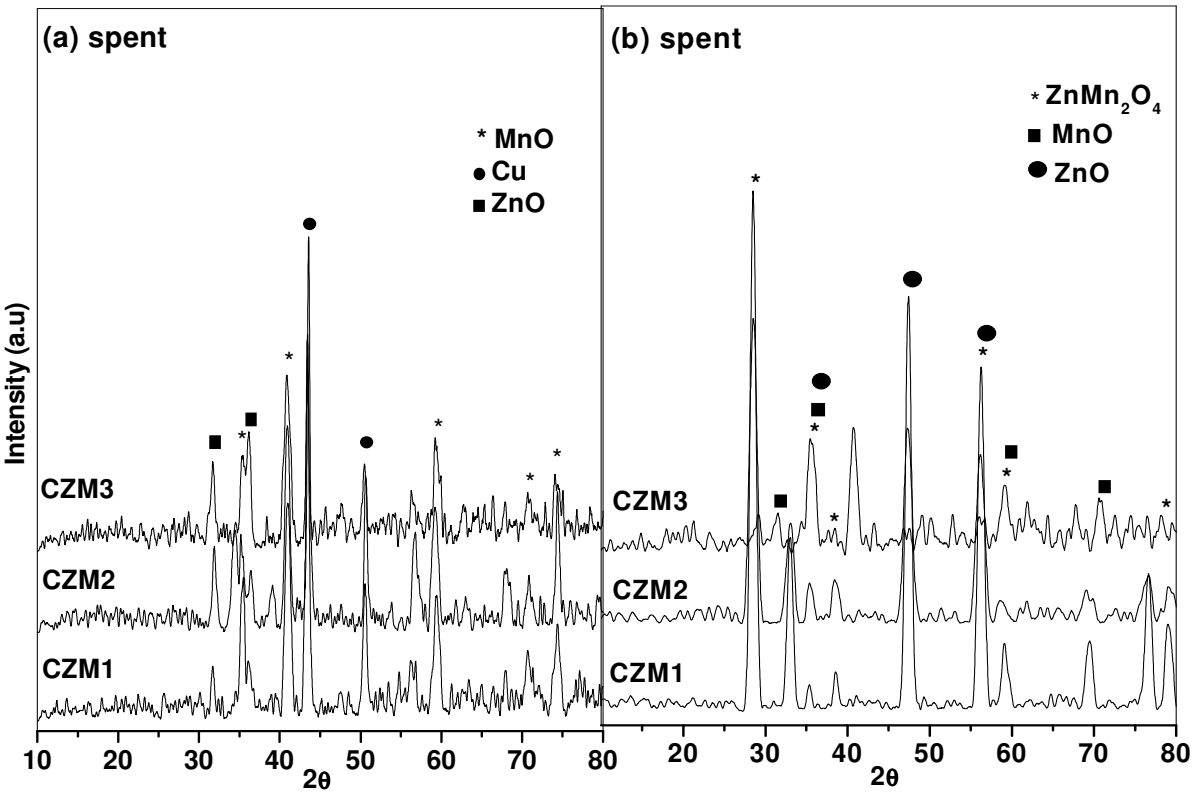

Fig.4.10. *XRD of spent Cu-Zn-Mn spinel-type, fresh catalysts calcined at (a) 773 K (b) 973 K after water gas shift reaction. (Feed composition 24%H_2, 21%N_2, 6% CO, 9%CO_2, and 40% H_2O, temp 673 K, GHSV=50 000 h^{-1}).*

XRD peaks corresponding to Cu metal were seen for samples with higher loading of copper. MnO was formed as a result of the reduction of Mn^{3+} and Mn^{4+} ions in the spinel. As observed in phenol methylation reaction, the spent catalysts (CM_x) after WGS reaction did show complete reduction of metal oxides [37]. However, some reports claimed

presence of Cu_2O or CuO after WGS reaction due to the presence of water or reoxidation in air prior to spectroscopic studies. However, in case of CZM3 catalyst calcined at 993 K, XRD peaks corresponding to $ZnMn_2O_4$ phases were found after WGS reaction (Fig.4.1b). Presence of Zn^{2+} could have hindered the complete reduction of manganese to lower oxidation states under the experimental conditions employed for this study.

It is well known that the properties of supported metal catalysts usually show a strong dependence on both the preparation method and the thermal (activation) treatments [7,11]. The N_2O decomposition on the subsurface of reduced samples was employed to determine the copper metal dispersion and the results are presented in Table 2.4. These results suggest that an increase in the amount of copper led to lowering of dispersion, which in turn is associated with an increase in the copper metal size. It has been reported that the active sites mostly are located at the interface of the active component and the surroundings, i.e the support oxide [38]. It is therefore; expected that the catalytic activity depend upon the metal dispersion, the crystalline phase and copper metal surface area. Although the dispersion of copper species on CZM3 was higher than other ternary catalysts, it showed poor WGS activity. This may be attributed to the presence of $ZnMn_2O_4$ phase, on which copper is dispersed. The reducibility of this catalyst occurred at higher temperature than other CZM catalysts. Hence, we believe that the support on which the metallic copper is dispersed also plays significant role. Decomposition of N_2O on the Cu surface is a widely used and accepted technique for measuring Cu metal surface area of copper based catalysts [34,39]. However, it remains a matter of discussion whether chemisorption results obtained this way can be used to correlate the reaction data. It has been reported that CuO alone showed a poor activity for the shift reaction and the formation of binary system with ZnO resulted in a clear enhancement in the activity [40].

4.2.9. Red-ox properties of Cu-Mn and Cu-Zn-Mn catalysts

The temperature-programmed reduction of copper based spinel catalysts gives information on their red-ox behavior. It also provides information on the oxidation states of copper in various catalyst compositions. It was reported that TPR of Cu/Al_2O_3 or Cu/YSZ catalysts gave three peaks at 433, 483 and 523 K. The two low temperature peaks were ascribed to highly dispersed copper species, which could not be detected by the XRD

otherwise. Where as the peak at 523 K was attributed to the isolated CuO species in the bulk. All the Cu-Mn catalysts showed two reduction peaks (Fig.2.7). Interestingly, $CM_{0.5}$ catalyst exhibited these peaks at relatively lower temperature compared to other Cu-Mn catalysts. It clearly shows that the highly dispersed and bulk copper species reduced at low temperatures for this composition. This easy reducibility also reflected in high WGS activity. As the reducibility of $CM_{1.0}$ occurred at high temperatures both for dispersed and bulk copper, it was not as active as $CM_{0.5}$ for WGS reaction. For copper concentration up to $x \leq 0.5$ in the general formula, $Cu_xMn_{3-x}O_4$, the obtained phase was hausmannite, which gradually changed to non-stoichiometric cubic $Cu_{1.5}Mn_{1.5}O_4$ phase with increasing Cu contents. This observation agrees with the report that the Cu-Mn solid solution forms stoichiometric phases [41]. It was reported that non-stoichimetric $Cu_{1.5}Mn_{1.5}O_4$ phase in the absence of impurities like CuO, MnO or Mn_2O_3 promoted easy reduction of copper resulting in high activity [7]. But, we believe that at low calcination temperature, Cu-Mn catalyst with appropriate copper, i.e., $x = 0.5$ gave high dispersed Cu and reduced with much ease. Among this series of catalysts for WGS activity, $CM_{0.5}$ exhibited highest surface area (36 m^2/g). The micro structural changes induced by the composition might have enhanced the reducibility of copper species. Hence, as may expected the catalyst that is reduced at lower temperature showed better activity in WGS reaction, as it requires easy shuttling of oxidation states of active metal [38]. It is clear from these results that highly dispersed Cu species, formed after reduction of Cu-Mn catalysts with hausmannite structure, which reduced easily, showed better CO conversion activity in WGS reaction. However, calcination of Cu-Mn catalysts at 973 K exhibited low WGS activity compared to catalysts calcined at 773 K, which may be attributed to aggregation of copper species in these catalysts. The addition of zinc to Cu-Mn spinels was expected to show high activity as it was reported that zinc would promote the formation of fine Cu particles on the oxide support [30]. Among the Cu-Zn-Mn catalysts (Fig.2.21), reduction of highly dispersed Cu species occurred at low temperature (at 461 K) for CZM2 than other catalysts. Hence, this catalyst shows better activity in WGS reaction. But, the Cu-Zn-Mn oxides catalysts were unstable and led to the sintering of Cu at higher temperature, whereas stable spinel CZM2 catalyst was moderately active in the shift reaction. At high calcination temperature (at 993 K), these catalysts also showed lower activity.

Therogravimetric analysis of selective CM_x and CZM_x catalysts was carried out in hydrogen atmosphere (5% H_2 in Ar) results of which are illustrated in Fig.4.11. The TG/DTA curves obtained for $CM_{0.5}$ and $CM_{1.0}$ catalysts are presented in Fig.4.11. DTA curves showed that reduction of the catalysts under hydrogen was mostly a two-stage process with corresponding weight loss. The percentage of weight loss and the corresponding reduction temperatures associated with phase changes are presented in Table.4.1. The thermogram of Cu-Mn catalysts shows weight loss in single step below 773 K, while $CM_{1.0}$ showed high weight loss than $CM_{0.5}$. The initial weight loss occurs on removal of physisorbed water on the catalysts, which could not be accounted accurately here; because of onset of reduction process of highly dispersed Cu species started at lower temperatures (< 470 K).

Table. 4.1. *TG-DTA analysis of Cu-Mn and Cu-Zn-Mn spinel-type catalysts in presence of 5% H_2 in Ar*

Catalyst	Wt. Loss (%) (323-700 K)	DTG peak (K)	DTA peaks Reduction temp. (K)
$CM_{0.5}$	12.1	598	380,456,549
$CM_{1.0}$	>14	620	478,620
CZM1	14.3	618,665	457,616
CZM2	14	342,640	443,590
CZM3	11.25	593	450,595

However, the weight loss due to physisorption from $CM_{0.5}$ was less than 0.9 %. The main weight loss occurred for $CM_{0.5}$ and $CM_{1.0}$ was centered at 598 and 620 K. The DTA curve for $CM_{0.5}$ catalyst shows a low temperature broad endothermic peak associated with peaks at 456 and 549 K The high copper containing catalyst ($CM_{1.0}$) showed a broad low temperature endothermic peak at 478 K, which was rather expected due to higher copper content in the catalyst. Chary et al. reported that the finely dispersed copper species undergo reduction simultaneously with rise in temperature [42], The bulk copper species of $CM_{1.0}$ reduced at much higher temperature (549 K vs 620 K) than $CM_{0.5}$; hence the later

exhibited better WGS activity at low temperature (523 K). The Mn^{3+} and Mn^{4+} ions present in spinel system also undergo reduction to form MnO, which was observed by the XRD of catalysts after TPR analysis. However, it is rather difficult to ascribe the endothermic peaks to merely individual metal ions. The high temperature endothermic peak is probably associated with the reduction of manganese ions. TG-DTA profiles of the Cu-Zn-Mn catalysts are presented in Fig.4.12. The nature of all the curves was similar with a two-stage reduction process with endothermic peaks. All these catalysts showed weight loss due to reduction of the metal oxides.

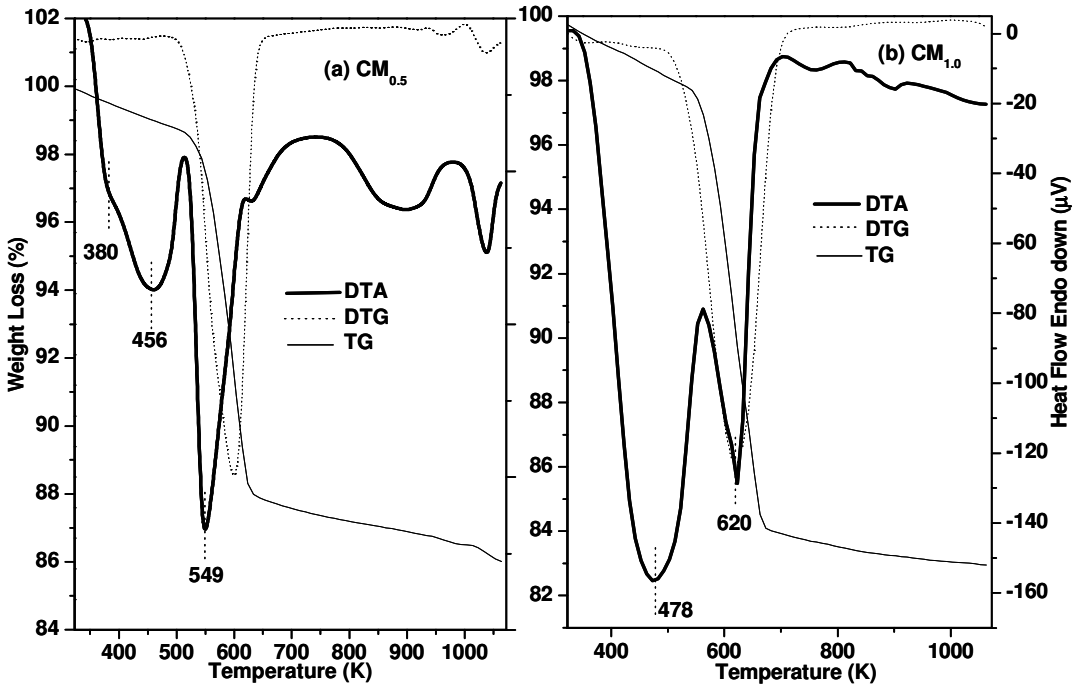

Fig.4.11. Thermo gravimetric analysis (TG-DTA) of Cu-Mn spinel-type catalysts (a) $CM_{0.5}$ (b) $CM_{1.0}$ in presence of 5% H_2 in Ar.

This system also consists of complex series of overlapping processes mainly attributed to the reduction of copper and manganese ions to lower oxidation states. The total weight loss has decreased in the order of CZM1> CZM2>CZM3.

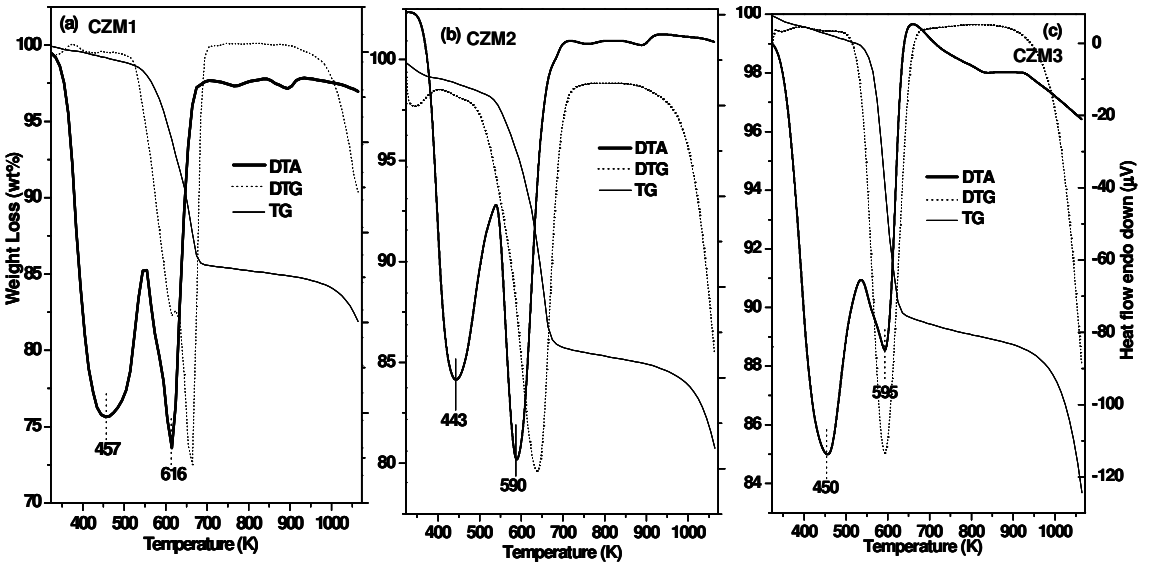

Fig.4.12. Thermo gravimetric analysis (TG-DTA) of Cu-Zn-Mn spinel-type catalysts (a) CZM1 (b) CZM2 (c) CZM3 in presence of 5% H_2 in Ar

The DTG maximum that corresponds to weight loss associated with reduction process also decreased in the order CZM3<CZM2<CZM1, as was observed for weight loss. Thse temperatures were 665, 640 and 593 K for CZM1, CZM2 and CZM3, respectively. The DTA endothermic peaks positions show that among the CZM series catalysts, reduction of CZM2 occurred at relatively lower temperature. This reduction of CZM2 at lower temperatures is in aggrement with TPR results.

4.2.10. XPS analysis of spent catalysts

Cu-Mn and Cu-Zn-Mn spinel series spent catalysts were investigated by XPS after the reaction to determine the oxidation states of the constituent metal ions. XPS spectra of Cu $2p_{3/2}$ core level of spent Cu-Mn and Cu-Zn-Mn catalysts are shown in Fig. 4.13. The main peak due to $2p_{3/2}$ at about 932.3 eV with a satellite peak around 941.5 eV was observed for Cu-Mn catalysts after WGS reaction (573 K, GHSV = 50, 000 h^{-1}). The FWHM of $2p_{3/2}$ peak was found to be about 3.6 eV. The corresponding BE values of $2p_{3/2}$ for fresh Cu-Mn catalysts was found to be in the range of 933.6 eV (Fig.2.10a).

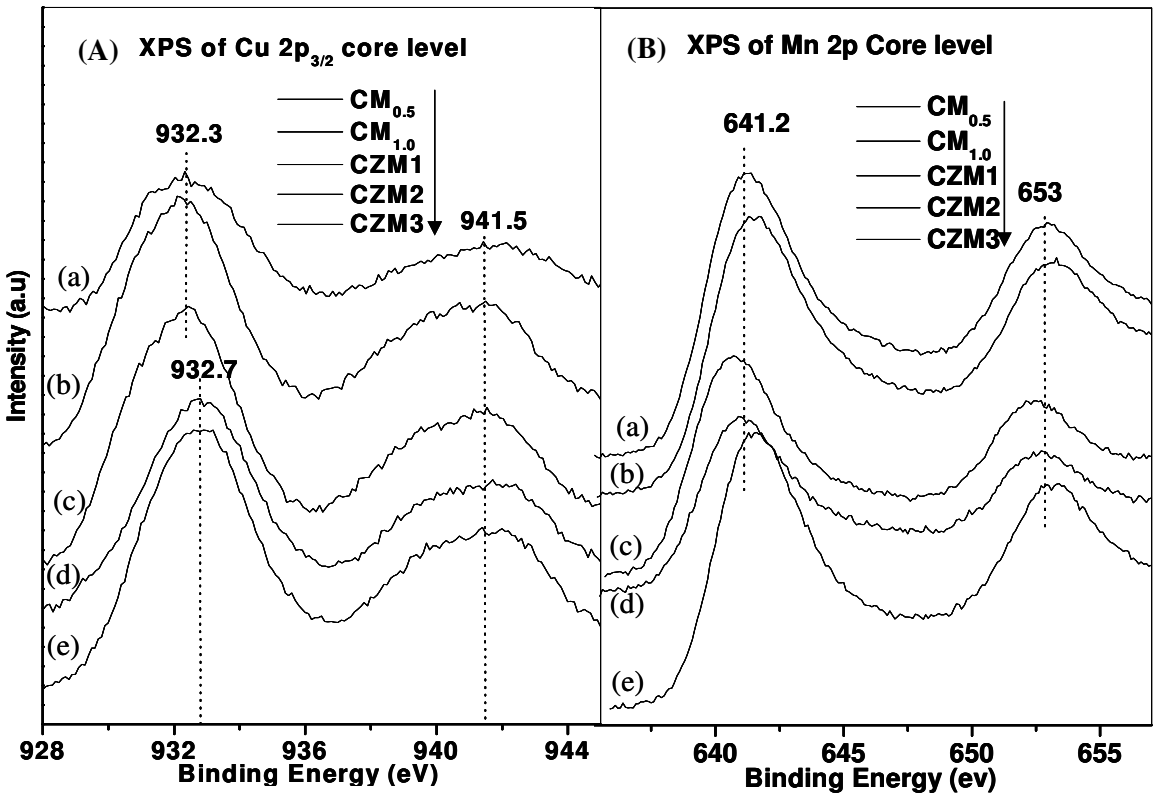

Fig.4.13. XPS spectra of (A) Cu2p and (B) Mn 2p core level of Cu-Mn and Cu-Zn-Mn spinel-type catalysts

The binding energy values of $Cu3p_{3/2}$ peak in CuO are reported to be about 933.6 eV with a shake up satellite at 940-945 eV [43,44]. The BE values of our fresh samples are in good agreement with those reported previously [43,44]. It is seen that all the spent catalysts showed shake up satellites indicating the presence of Cu^{2+} species. The $2p_{3/2}$ peak of Cu^{1+} in Cu_2O is reported to be at 932.2 ± 0.3 eV [45]; While the BE of Cu $2p_{3/2}$ for Cu-Zn-Mn spent catalysts was found to be at 932.3 eV for CZM1 and 932.7 eV for CZM2 and CZM3 with satellite peaks. The broad peak structure indicates these catalysts have combinations of Cu^{1+} and Cu^{2+} ions.

The presence of satellite peaks after the reaction indicates that the catalysts did not reduce completely to form metallic copper unlike in case of phenol methylation reaction. This may be attributed to the presence of oxidant (water) in the WGS feed. High FWHM values [46] observed for these catalysts probably are as a result of more than one peak attributed to the presence of Cu^{o} and Cu^{1+}, resolution of which is rather difficult. The high BE values of $Cu2p_{3/2}$ of CZM2 and CZM3 catalysts indicates that the addition of zinc

hindered the reduction of copper. Alternatively, zinc ions must be promoting the dispersion of Cu on the oxide surface during the reduction process. Although presence of zinc in the ternary oxide enhanced the stability of copper species, the ternary catalysts showed poor WGS activity [42]. The BE values of Mn2p for CZM3 catalysts appears to be at higher compared to other catalysts, which may due to presence of Mn in hetaerolite structure, while other catalysts formed $Cu_{1.5}Mn_{1.5}O_4$.

Mn2p photoemission spectra of the spent catalysts were shown in Fig.4.13. The BE value of 641.4 eV with ΔE of 12.4 eV was observed for all the catalysts, indicating that the oxidation state of manganese in these samples is +2. These BE values for Mn 2p3/2 are in good agreement with those reported earlier [43,44]. Although it is difficult to distinguish various oxidation states of manganese ions as result of their close BE values [47], it is to be noted that the observed value lies between the BE of Mn^{2+} and Mn^{3+} ions. BE values of Mn 2p of all fresh Cu-Zn-Mn catalysts was found to be at 642.4 eV that corresponds to Mn^{3+} ions (Fig.2.22), where as a BE value of 641.5 eV of was observed for fresh $CM_{0.5}$ catalyst. These observations indicate that Zn has stabilized the manganese oxidation state in the ternary system. However, all the catalysts showed similar BE values of Mn2p with a ΔE of 11.6 eV.

Photoemission spectra for Zn $2p_{3/2}$ core level are shown in Fig.4.14(a) for spent CZM catalysts. The BE values were found to be at 1020.8, 1021.2 and 1020.6 ± 0.1 eV with corresponding FWHM of 2.3, 2.4 and 2.3 eV, for CZM1, CZM2, CZM3, respectively. Whereas, all the fresh catalysts exhibited a peak centered at 1021.3 ± 0.1 eV with FWHM values of 2.4, 2.2 and 2.5 for CZM1, CZM2 and CZM3, respectively (Fig.2.23). This value is assigned to Zn^{2+} ions as BE of Zn $2p_{3/2}$ in ZnO was reported to be ~1022 eV [48]. It may be seen that Zn $2p_{3/2}$ peak for spent catalysts appeared at lower BE values. But, for CZM2 the shift in the BE was not significant compared to the fresh catalyst. This change in the BE values of spent catalysts indicate that structural changes occurred during reaction. The shift in BE of Zn 2p might be due to change of environment of Zn in spent catalysts following by the reduction of other constituent metal ions in the catalysts.

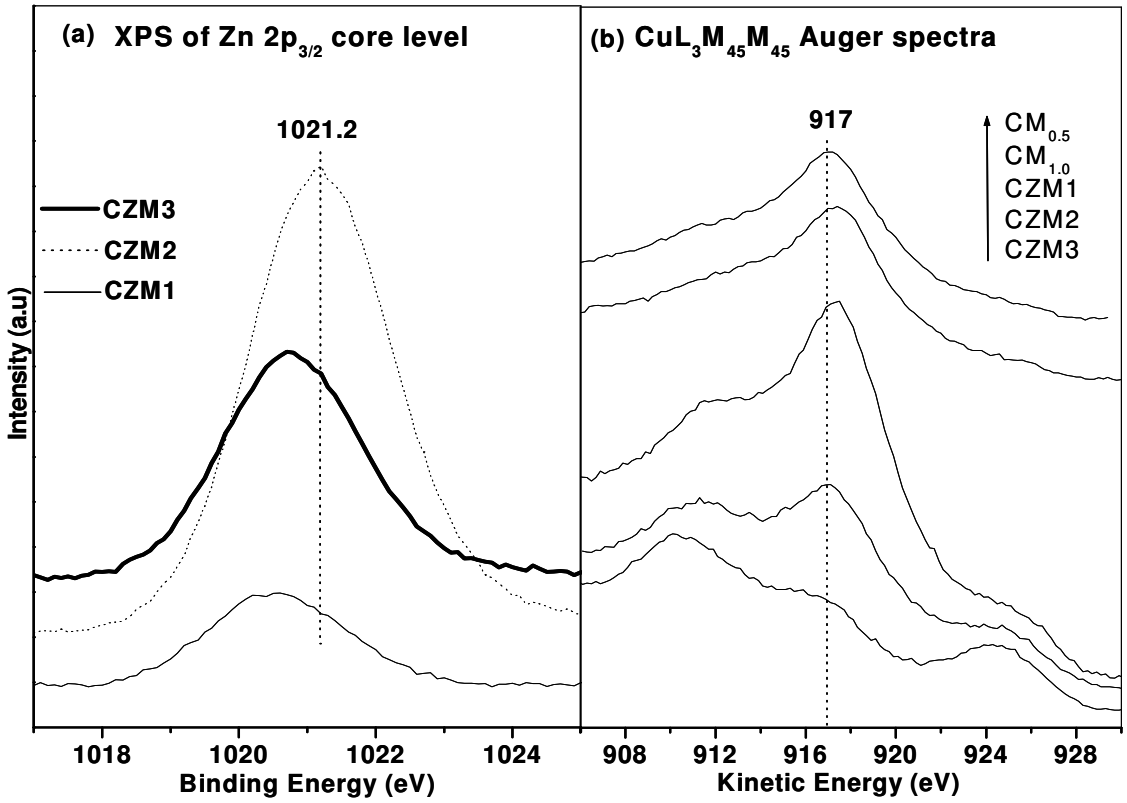

Fig.4.14. XPS spectra of (a) Zn2p and (b) Cu $L_3M_{45}M_{45}$ Auger spectra of Cu-Mn and Cu-Zn-Mn spinel-type catalysts.

The Cu-LMM Auger electron transitions for spent catalysts are shown in Fig. 4.14 (b). The Auger parameter (α^1) distinguishes different oxidation states, as the reduced copper species (Cu^0 and Cu^{1+}) cannot be distinguished by XPS, because they have similar BE values with no satellite features [43,49,50]. Nevertheless, the valance states of reduced Cu species can be easily distinguished using AES, as the Cu^{1+} and Cu^0-LMM appeared at around 916.5 and 918.5 eV, respectively [48]. The Cu-$L_3M_{45}M_{45}$ line for calcined $CM_{0.5}$ and CZM catalysts was 917.6 eV (Fig.2.10 and Fig.2.22), which was reported to be that of CuO at 917.6 eV [48]. In case of all the spent catalysts, the Cu-LMM transition appeared at about 917 eV, which is intermediate in between the values for Cu_2O and CuO. The broad Cu-LMM peak structure seen for CZM1 and CZM2 indicate the contribution of Cu^{1+} and some Cu^0 species at low KE. These results suggest that the reduction of Cu^{2+} ions takes place on all the catalysts. Owing to a large overlap of the Auger transitions with a

significant background in the spectra, making it difficult for reliable estimation of individual Cu species.

4.2.11. Mechanism of the reaction

Although the WGS reaction involves only four simple molecules, the reaction mechanism appears to be quite complex. There are generally two reaction mechanisms proposed in the literature for the WGS reaction, associative and redox. In associative mechanism, a formate species is believed to be formed which then decomposes forming CO_2 and H_2 [51-53]. The redox mechanism consists of a surface oxidation, $H_2O + * \leftrightarrow H_2 + O*$, followed by surface reduction, $CO + O* \leftrightarrow CO_2 + *$. Under conditions of this study, it is predicted that the associative mechanism is probably prevalent. Grenoble et.al [52] proposed a reaction sequence based on an associative mechanism, which includes formate as an intermediate in order to account for the apparent bifunctionality of the supported catalyst system. They concluded that the WGS reaction occurred at two sites with the metal activating carbon monoxide and the support sites as the principle sites for water activation [54]. The surface reduction of the active species as well as the support is crucial for generation of active germinal OH groups on the surface of the catalyst. It has also been reported that the reaction mechanism varies with the reaction temperature [55]. XRD of our spent catalysts (Fig.4.1) shows that manganese is present as MnO, while Cu is present as metallic copper. WGS reaction mechanism over copper based catalysts is the associative mechanism as simple Langmuir- Hinshelwood process [36]. Most of the evidence for the surface adsorbed formate intermediate has been gathered by using infrared spectroscopy [56-58]. XRD after WGS reaction over catalysts in this study showed presence of Cu, MnO and ZnO (CZM_x) without even trace amounts of of CuO or Cu_2O indicating that no oxidation of reduced copper was involved during the reaction. But, redox mechanism cannot be ruled out at high temperatures as reported previously [51-53]. Though it is very difficult to propose and prove a particular mechanism for WGS reaction, from the above observations, we believe that associative mechanism prevails on these catalysts. Addition of CO is expected to yield surface formates by the reaction with geminal OH groups. Then the addition of water decomposes the formates to give the reaction products ($H_2 + CO_2$). It was reported that the reduction of the catalysts at low temperature generates high density

of geminal OH groups and hence exhibit higher WGS activity [54]. The deactivation of the catalysts may be attributed to the formation of carbonates covering active sites at the surface. Therefore in this study, easy reducibility of $CM_{0.5}$ and CZM2 that have porous microstructures showed higher activity among Cu-Mn and Cu-Zn-Mn series catalysts.

4.3. Conclusions

Water gas shift reaction over Cu-Mn and Cu-Zn-Mn spinel type catalysts showed that an optimum concentration of copper was required to obtain high CO conversions, at low reaction temperatures and high space velocities, with desirable stable activity. The important function of the metal is to catalyze the reducibility of the catalyst. The shifting of the reduction temperature to lower levels and a higher extent of reduction of the copper was observed on $CM_{0.5}$ and CZM2 catalysts that showed good WGS activity. It is believed that the formation of carbonate species may be responsible for deactivation of the catalysts. The XRD and XPS of spent catalysts revealed that Cu-Mn catalysts reduced completely into their lower oxidation states Cu^{o} and MnO. Whereas reducibility of Cu-Zn-Mn did not take place to that extent, as the characteristic peaks of their spent catalysts show.

4. 4. References

[1] J.R. Ladebeck, J.P. Wagner, In: W. Vielstich, A. Lamm, H.A. Gasteiger, (Eds.). Handbook of Fuel Cells – Fundamentals, Technology and Applications, John Wiley & Sons, Ltd, Chichester, vol. 3, 2003, p. 190.

[2] A.L. Dicks, J. Power Sources 71 (1998) 111.

[3] A. Trovarelli, Catal .Rev. Sci. Eng. 38 (4) (1996) 439.

[4] P. Bera, S. Malwadkar, A. Gayen, C.V.V. Satyanarayana, B.S. Rao, M.S. Hegde, Catal. Lett. 96 (3-4) (2004) 213.

[5] T. Utaka, T. Takeguchi, R. Kikuchi, K. Eguchi. Appl. Catal. 246 (2003) 117.

[6] Y. Tanaka, T. Utaka, R. Kikuchi, K. Sasaki and K. Eguchi. Appl. Catal. 242 (2003), 287.

[7] Y. Tanaka, T. Utaka, R. Kikuchi, T. Takeguchi, K. Sasaki, K. Eguchi, J. Catal. 215 (2003) 271.

[8] M.J.L. Gines, N. Amadeo, M. Laborde, C.R. Apesteguia, Appl. Catal. A 131 (1995) 283.

[9] K. Sekizawa, S.-I. Yano, K. Eguchi, H. Arai, Appl. Catal. A 169 (1998) 291.

[10] J. Wu, M. Saito, J. Catal. 195 (2000) 420.

[11] T. Utaka, K. Sekizawa, K. Eguchi, Appl. Catal. A 194-195 (2000) 21.

[12] Y. Tanaka, T. Utaka, R. Kikuchi, K. Sasaki, K. Eguchi, Appl. Catal. A 238 (2003) 11.

[13] G.J. Hutchings, R.G. Copperthwaitet, F.M. Gottschalk, R. Hunter, J. Mellor, S.W. Orchard, T. Sangiorgio, J. Catal. 137 (1992) 408.

[14] Y. Tanaka, T. Takeguchi, R. Kikuchi, K. Eguchi, Appl. Catal. A 279 (2005) 59.

[15] B. Solsona, G.H. Hutchings, T. Garcia, S.H. Taylor, New J. Chem, 28 (2004) 708.

[16] F.M. Gottschalk, G.J. Hutchings, J. Chem. Soc. Chem. Comm. (1988) 123.

[17] G.J. Hutchings, F.M. Gottschalk, R. Hunter, S.W. Orchard, J. Chem. Soc. Faraday Trans. I, 85 (2) (1989) 363.

[18] F.M. Gottschalk, G.J. Hutchings, Appl. Catal. 51 (1989) 127.

[19] S. Veprek, D.L. Cocke, S. Kehl, H.R. Oswald, J. Catal. 100 (1986) 250.

[20] P. Porta, G. Moretti, M. Musicanti, A. Nardella, Solid State Ionics 63–65 (1993)

257.

[21] G. Fierro, S. Morpurgo, M. Lo Jacono, M. Inversi, I. Pettiti, Appl. Catal. A 166 (1998) 407.

[22] B.J. Hansen, J.H. Carstensen, A.G. Romeo, PEQUIVEN, Venezuela (1981) 1.

[23] V. Idakiev, D. Mihajlova, B. Kunev, A. Andreev, React. Kinet. Catal. Lett. 33 (1987) 119.

[24] A. Andreev, V. Idakiev, D. Mihajlova, D. Shopov, Appl. Catal. 22 (1986) 385.

[25] Fuel Cell Handbook, seventh ed., US Department of Energy, National Energy Technology Laboratory, West Virginia, 2000, p. 9.

[26] P.W. Atkins, Physical Chemistry, third ed., Oxford University Press, Oxford, 1987, p. 219.

[27] C. Zerva, C.J. Philippopoulos, Appl. Catal. B: Environ. 67 (2006) 105

[28] C.J.G. van der Grift, A. Mulder, J.W. Geus, Appl. Catal. 60 (1990) 181.

[29] Y. Denkwitz, A. Karpenko, V. Plzak, R. Leppelt, B. Schumacher, R.J. Behm, J. Catal. 246 (2007) 74.

[30] C. Rhodes, G.J. Hutchings, A.M. Ward, Catal. Today 23 (1995) 43.

[31] N.A. Koryabkina, A.A. Phatak, W.F. Ruettinger, R.J. Farrauto, F.H. Ribeiro, J. Catal. 217 (2003) 233.

[32] O. Jakdetchai, T. Nakajima, J. Mol. Struct. (Theochem) 619 (2002) 51.

[33] A. Dandekar, R.T.K. Baker, M.A. Vannice, J. Catal. 183 (1999) 131.

[34] T. Shishido , M. Yamamoto, I. Atake , D. Li b, Y. Tian , H. Morioka, M. Hondac, T. Sano, K. Takehira, J. Mol. Catal. A: Chem. 253 (2006) 270.

[35] C. Wheeler, A. Jhalani, E.J. Klein, S. Tummala, L.D. Schmidt, J. Catal. 223 (2004) 191.

[36] P. Panagiotopoulou, A. Christodoulakis, D.L. Kondarides, S. Boghosian, J. Catal. 240 (2006) 114.

[37] A.S. Reddy, C.S. Gopinath, S. Chilukuri, J. Catal. 243 (2006) 278.

[38] C. Zerva, C.J. Philippopoulos, Appl. Catal. B: Environ. 67 (2006) 105.

[39] S. Sato, R. Takahashi, T. Sodesawa, K. Yuma, Y. Obata, J. Catal. 196 (2000) 195.

[40] M.S. Spencer, Top. Catal. 8 (3-4) (1999) 259.

[41] G.J. Hutchings, A.A. Mirzaei, R.W. Joyner, M.R.H. Siddiqui, S.H. Taylor, Appl.

Catal. A: General 166 (1998) 143.

[38] X. Wang, J.A. Rodriguez, J.C. Hanson, D. Gamarra, A. Martinez-Arias, M. Fernandez-Garcya, J. Phys. Chem. B 110 (2006) 428.

[42] K.V.R. Chary, G. Vidya Sagar, D. Naresh, K.K. Seela, B. Sridar, J. Phys. Chem. B 109 (2005) 9444.

[43] C.D. Wagner, W.M. Riggs, L.E. Davis, J.F. Moulder, E. Meilenberg, Handbook of X-ray Photoelectron Spectroscopy, Perkin–Elmer Corp. Physical Electronics Div., Eden Prairie, MN, 1979.

[44] N.S. McIntyre, N.S. Cook, M.G. Anal. Chem. 47 (1975) 2208.

[45] S. Angelov, E. Zhecheva, K. Petrov, D. Mehandjiev, Mat. Res. Bull. 17 (1982) 235

[46] M.R. Morales, B.P. Barbero, L.E. Cadús, Appl. Catal. B: Environ. 67 (2004) 229.

[47] G.C. Allen, S.J. Harris, J.A. Jutson, J.M. Dyke, Appl. Surf. Sci. 37 (1989) 111.

[48] G. Moretti, G. Fierro, M.L. Jacono, P. Porta, Surf. Interface Anal. 14 (1989) 325.

[49] T. Mathew, N.R. Shiju, K. Sreekumar, B.S. Rao, C.S. Gopinath, J. Catal. 210 (2002) 405.

[50] B.L. Yang, S.F. Chan, W.S. Chang, Y.Z. Chen, J. Catal. 130 (1991) 52.

[51] T. Van Herwijnen, W.A. De Jong, J. Catal. 63 (1980) 83.

[52] D.C. Grenoble, M.M. Estadt, D.F. Ollis, J. Catal. 67 (1981) 90.

[53] T. Salmi, R. Hakkarainen, Appl. Catal. Catal. 49 (1989) 285.

[54] Y. Amenomiya, G. Pleizer, J. Catal. 76 (1982) 343.

[55] T.M Yureva, Kinet. Katal., 10 (1969) 862.

[56] Y. Nato, K. Fukuda, T. Onishi, K. Tamaru, Trans. Faraday. Soc. 63 (1967) 2300.

[57] T. Shido, Y. Iwasawa, J. Catal. 129 (1991) 343.

[58] T. Shido, Y. Iwasawa, J. Catal. 140 (1993) 575.

[59] C. Diagne, P.J. Vos, A. Keinneman, M.J. Perez, F.M. Portella, React. Kinet. Catal. Lett. 42 (1990) 25.

CHAPTER 5

SUMMARY AND CONCLUSIONS

5.1. Summary

This thesis describes the preparation, characterization and catalytic evaluation of Cu-Mn, Zn-Mn and Cu-Zn-Mn spinel type oxide catalysts. The catalytic reactions studied were methylation of phenol to obtain 2,6-xylenol selectivity and water gas shift reaction to convert CO to carbon dioxide and H_2 by reacting with water. The later reaction helps in the removal of CO from reformats making it suitable for PEM fuel cell applications. Cu-Mn and Zn-Mn spinel catalysts were found to be highly active for phenol methylation, but Cu-Zn-Mn spinels did not show appreciable activity. For water gas shift reaction, copper containing catalysts were found to be better highly active. This chapter presents a brief summary of the work described in the preceding chapters; general conclusions arrived from the work and suggestions for further research.

Chapter 1 presents a general introduction about heterogeneous catalysts and in particular about metal oxide catalysts. The general classification of heterogeneous catalysts and the bulk structures of metal oxides (spinels) are discussed. The surface chemistry of metal oxides/transition metal oxides and in particular about their acid-base and redox properties are described. Synthesis procedures used for preparation of various catalytic materials and their role in acid-base and redox catalysis is highlighted. This chapter also includes an introduction to methylation of phenol and water gas shift reactions. A review of the literature to date in these areas has been included. At the end, the aim and objectives of the thesis is outlined.

Chapter 2 is divided in to 3 sections. Section A described the preparation of Cu and/or Zn based containing manganese oxide spinel catalysts through co-precipitation ($M_xMn_{3-x}O_4$, M = Cu or Zn, x = 0 to 1 and $Cu_xZn_yMn_{3-(x+y)}O_4$, x and y = 0.5 or 1) followed by calcination at 773 K. Procedures used for catalytic evaluation of these materials in phenol methylation and water gas shift reaction were also described.

Section B deals with the theory and experimental procedures of different characterization techniques employed in this study. The analytical techniques such as powder XRD, surface area (by N_2 sorption), UV-visible, IR spectroscopy, TPD, TPR, XPS-AES and SEM are described.

Section C presents characterization results obtained using above described techniques, followed by discussion on freshly calcined Cu catalysts. All the catalysts that differ in metal ion contents were characterized after calcination at 773 K. The characterization of Cu-Mn spinels revealed that the structure of catalysts strongly depends on the concentration of copper in the composition. The low copper containing catalysts ($x \leq 0.5$) crystallized in tetragonal hausmannite form, while at higher copper contents, (with $x \geq 0.75$) they catalysts formed cubic spinels. XPS results revealed that catalysts with $x \leq 0.25$ predominantly contain Cu^{2+}, while samples $x = 1$ contain both Cu^{1+} and Cu^{2+}. Similarly, Zn-Mn and Cu-Zn-Mn catalysts were also found to form into spinel phases.

Chapter 3 presents the catalytic activity in three sections. Section 3.1 contains results of phenol methylation using methanol as alkylating agent on Cu-Mn spinel catalysts. The influence of various parameters like catalyst composition, reaction temperature, space velocity and composition of reactant feed on the activity and selectivity is reported. The Cu-Mn catalyst with $x = 0.25$ exhibited high phenol conversion (85 mol%) accompanied by high 2,6-xylenol selectivity (74 mol%) at 673 K. The structure-activity correlation based on the analysis of fresh and spent Cu-Mn catalysts after phenol methylation is discussed.

Section 3.3 and 3.4 of chapter 3 describe the evaluation of Zn-Mn and Cu-Zn-Mn catalysts in phenol methylation. The effect of various reaction parameters such as reaction temperature, space velocity and phenol to methanol mole ratio on phenol conversion and 2,6-xylenol selectivity are reported. Among the Zn-Mn catalysts, the one with $x = 0.25$ showed highest phenol conversion (100 mol%) and 2,6-xylenol selectivity (94mol%) at 723 K. Cu-Zn-Mn catalysts did not show high activity or selectivity in the alkylation of phenol with methanol. Equal molar concentrations of Cu and Zn in manganese spinel catalysts showed better activity in Cu-Zn-Mn series catalysts. An important observation was that all these catalysts were highly selective for ortho-alkylation. The correlation between the structure and activity of the catalysts based on the characterization of acid-base and red-ox properties of catalysts is included in this chapter.

Chapter 4 deals with the results of WGS reaction on Cu-Mn and Cu-Zn-Mn catalysts. Effect of various reaction parameters such as temperature, space velocity, and influence of CO_2 in the feed gas mixture was investigated. Only copper containing spinel

catalysts were found to be active for this reaction. Catalysts with highly reducible CuO showed better CO conversion. The $CM_{0.5}$ and CZM2 catalysts were found to be better among the Cu-Mn and Cu-Zn-Mn series spinels calcined at 773 K. The $CM_{0.5}$ catalysts showed higher CO conversion (97 mol%) at 523 K, while CZM2 gave ~93 mol% CO conversion at 573 K. The structure-activity correlation is discussed based on the characterization results obtained for fresh and spent catalysts using techniques like XRD, TPR and XPS etc.

Chapter 5 contains the conclusions arrived at based on the above results and also sums up the entire study. At the end thesis contains suggestions for further research in order to develop the above catalyst materials further and use them for commercially important industrial processes.

5.2. General conclusions

It was observed that the mixed oxide spinel catalysts exhibit acid-base and red-ox properties, which depend on the structure and concentration of constituent metals. In this study, manganese based spinel catalysts that contain copper or zinc gave highly selective ortho-alkyl phenols during phenol methylation. The spinel catalysts at lower concentration (x = 0.25) of copper or zinc showed good phenol conversion and much better 2,6-xylenol selectivity. The better 2,6-xylenol selectivity has been attributed to appropriate combination of acidity and basicity for the given composition. The Lewis acidity of the catalysts is generally attributed to the metal ions, while the basicity is attributed to the presence of oxide anions on the surface of a metal oxide. Obviously, the compositional variation influences the distribution of metal and oxide ions as well as their strengths at the surface, there by influencing the acid-base properties. It is claimed in this study that acidity is the determining factor for phenol conversion activity, whereas basicity accounts for high 2,6-xylenol selectivity. One important observation made in this study was that all catalysts deactivated with time on stream. The reason for deactivation was structural collapse of spinel oxides, during the course of methylation of phenol, in the prevailing reducing atmosphere. It is observed that mixed metal oxide catalysts that have optimum concentration of acidity and basicity along with structural stability under reducing atmosphere are suitable for better activity and ortho-selectivity.

These Cu based spinels showed high CO conversion under robust conditions where in the WGS feed contain high CO concentration (6 mol%) in the presence of carbon dioxide (12 mol%). It is clear from these results that highly dispersed Cu species formed on reduction of Cu-Mn catalysts with hausmannite structure, with relatively better reducibility, showed higher CO conversion activity. Highly dispersed copper was achieved when samples with low concentration of copper were reduced in dilute H_2 flow followed by calcination at 773 K. Calcination at higher temperatures led to aggregation of copper species in these catalysts. Water gas shift reaction over Cu-Mn and Cu-Zn-Mn spinel type catalysts showed that an optimum concentration of copper is required to obtain high CO conversion at low reaction temperatures and at high space velocities. The shifting of the reduction temperature to lower values and a large extent of reduction of the copper was observed on $CM_{0.5}$ and CZM2 catalysts, which inturn showed good WGS activity. It is believed that the formation of carbonate species may be responsible for deactivation of the catalysts.

5.3. Suggestions for further research

Alkyl phenols such as *o*-cresol and 2,6-xylenol are important chemical intermediates in the preparation of agrochemicals and polymers. This work shows that copper based spinels are promising catalysts for higher ortho-selectivity in methylation of phenol. Having done preliminary investigation in laboratory scale, a lot more work need to be carried out for developing a process, keeping in view the current demand for the above-mentioned chemicals.

Though considerable improved activity and selectivity were achieved on Cu-Mn spinels, there is still scope to improve them further by substituting other transition metals partially in to spinel structures. In the present study, catalysts were prepared by co-precipitation method. However, the influence of other preparation methods has to be studied. A method of preparation that improves the surface acid-base properties will help in increasing the activity. Even the co-precipitation can be carried out using different alkylating agents like NaOH, NH_3 and Na_2CO_3 etc., which may influence the heterogeneity of metal ions at the surface [1]. This heterogeneity of metal ions at the surface determines

the acid-base properties [2]. The selectivity of the catalysts has to be still improved, minimizing the amount of by-products.

One significant problem observed with the present series of catalysts is deactivation or lower stability of the catalysts. Further, in depth research has to be carried out to stabilize the spinel structures. Partial replacement with non-reducible metal ions like Mg^{2+}, Al^{3+}, Si^{4+} and Ti^{4+} etc. in to these spinels should be investigated to stabilize these structures under reduced atmosphere.

The nature of active sites may be investigated further, preferably *in situ* since the actual active species in the reaction conditions can be explored by these studies only [3]. *In situ* FTIR using probe molecules may be used to estimate ratios of acid and base sites and their respective strengths, which can compliment TPD results.

Due to recent advances in the development and possible commercialization of polymer electrolyte fuel cells (PEMFC), generation of hydrogen efficiently, in which WGS reaction at low temperature plays a vital role, this work assumes added urgently [4]. Spinel catalysts based on Cu-Mn are active and give high CO conversions in water gas shift reaction. Hence, a detailed investigation is required for development and possible commercialization of these catalysts. Deactivation of Cu catalysts due to presence of sulfur should be overcome, by using promoters. Sulfur tolerance may me improved by using the Cu-Mn spinels with partial substitution of Zn, Co, Mo etc [5,6]. The catalysts have to be modified to work in a wide range of reformate compositions. Evaluation of spinel catalysts should be carried out using different WGS feed mixtures generated by different reforming various fuels such as natural gas, ethanol, methanol, diesel and DME. Detailed kinetic study and validation of the reaction results are required for reactor design and for subsequent commercialization of these catalysts.

5.4. References

[1] G.J. Hutchings, A.A. Mirzaei, R.W. Joynerb, M.R.H. Siddiqui, S.H. Taylor Appl. Catal. A166 (1998) 143.

[2] M.A. Barteau, Chem. Rev. 96 (1996) 1413.

[3] C.J. Dillon, J.H. Holles, R.J. Davis, J.A. Labinger, M.E. Davis, J. Catal. 218 (2003) 54.

[4] Fuel Cell Handbook, Sixth edn. U.S. Department of Energy, West Virginia, 2004, p. 31.

[5] J.R. Mellor, R.G. Copperthwaite, N.J. Coville Appl. Catal. A 164 (1997) 69.

[6] M. Laniecki, M. Ignacik, Catal. Today 116 (2006) 400.

List of publications/posters presented at symposia

1. Selective *Ortho-* methylation of phenol over copper manganese oxide spinel catalysts

A. Satyanarayana Reddy, Chinnakonda S. Gopinath and Satyanarayana Chilukuri, J. Catal. 243 (2006) 278.

2. Water gas shift reaction of reformed fuels over Cu-Mn-O and Cu-Zn-Mn-O mixed oxide spinel Catalysts

A. Satyanarayana Reddy, Sivaram Pradan and Satyanarayana Chilukuri, J. Catal. (Communicated)

3. Efficient Zinc-Manganite Spinel Catalysts for *ortho*-methylation of phenol to produce 2,6-xylenol

A. Satyanarayana Reddy, **S. P. Mirajkar and Satyanarayana Chilukuri, J. Mol. Catal. A (communicated)**

4. Supported Copper catalysts on CeO_2, ZrO_2-CeO_2 and CeO_2-TiO_2 for water gas shift reaction

A. Satyanarayana Reddy, Sivaram Pradhan and Satyanarayana Chilukuri, (under manuscript preparation)

5. Synthesis and Characterization of V_2O_5 / CeO_2-TiO_2 catalysts by sol-gel process: Oxidative Dehydrogenation of ethyl benzene using nitrous oxide

A. Satyanarayana Reddy, N.R.Shiju, S.P. Mirajkar and C.V.V. Satyanarayana (ready for communication)

6. The processing of CdSe/Polymer nanocomposites *via* solution organometallic chemistry

P. K. Khanna, Narendra Singh, Shobit Charan, Sunil P. Lonkar, **A. Satyanarayana Reddy**, Yogesh Patil and A. Kasi Viswanath, Materials Chemistry& physics 97 (2006) 288.

7. Redistribution of cations amongst different lattice sites in $Cu_{1-x}Co_xFe_2O_4$ ferrospinels during alkylation: magnetic study

Thomas Mathew, S. Shylesh, **S. N. Reddy**, C. P. Sebastian, S. K. Date, B. S. Rao and S. D. Kulkarni, Catal. Lett., 93, 3-4 (2004) 155.

8. Morphology of $BaSO_4$ crystals grown at the liquid-liquid interface.

Debabrata R. ray, Ashavani Kumar, **Satyanarayana Reddy,** S. R. Sainkar, N.R. Pavaskar and Murali Sastry, Crst. Eng. Comm. 45 (2001) 1.

9. Morphology of $BaSO_4$ crystals grown on Templates of varying dimensionality: the case of Cysteine-Capped Gold nanoparticles (0-D), DNA (1-D), and Lipid bilayer Stacks (2-D)

Debabrata Rautaray, Ashavani Kumar, **Satyanarayana Reddy**, S. R. Sainkar, N. R. Pavaskar and Murali Sastry, Crystal growth & Design, 2 (2002) 197.

10. Morphology of $SrCO_3$ crystals grown at the liquid-liquid interface

Satyanarayana Reddy, Debabrata R. Ray, Murali Sastry, Bull. Mater. Sci. 26, 3 (2003) 283.

Presentations/Posters

1. Dehydrogenation of Ethylbenzene on V-MgO catalysts, promoting effect of N_2O poster presented at the 1st-Indo-German Conference on catalysis held at IICT, HYD. Feb, 6-8, 2003.

Satyanarayana Reddy, N. R. Shiju, Mettu Anil, B. S. Rao, C. V. V. Satyanarayana

2. Selective *ortho*-methylation of phenol with methanol over copper manganite spinel Catalysts, Oral presentation at the National Symposium on Sustainable Development through Catalysis, Bhavnagar India, 18-20, Jan 2005.

A. Satyanarayana Reddy, S. P. Mirajkar; C. V. V. Satyanarayana